University of Alberta

Fluid characteristics and evolution of porphyry Cu-Au-Mo and Mo systems, Yukon-British Columbia, Canada

By

David Selby ©

A thesis submitted to the Faculty of Graduate Studies and Research in partial fulfilment of the requirements for the degree of Doctor of Philosophy

Department of Earth and Atmospheric Sciences

Edmonton, Alberta
Fall 1999

National Library of Canada
Acquisitions and Bibliographic Services
395 Wellington Street
Ottawa ON K1A 0N4
Canada

Bibliothèque nationale du Canada
Acquisitions et services bibliographiques
395, rue Wellington
Ottawa ON K1A 0N4
Canada

Your file Votre référence

Our file Notre référence

The author has granted a non-exclusive licence allowing the National Library of Canada to reproduce, loan, distribute or sell copies of this thesis in microform, paper or electronic formats.

L'auteur a accordé une licence non exclusive permettant à la Bibliothèque nationale du Canada de reproduire, prêter, distribuer ou vendre des copies de cette thèse sous la forme de microfiche/film, de reproduction sur papier ou sur format électronique.

The author retains ownership of the copyright in this thesis. Neither the thesis nor substantial extracts from it may be printed or otherwise reproduced without the author's permission.

L'auteur conserve la propriété du droit d'auteur qui protège cette thèse. Ni la thèse ni des extraits substantiels de celle-ci ne doivent être imprimés ou autrement reproduits sans son autorisation.

0-612-46917-4

Canada

University of Alberta

Library Release Form

Name of Author: **David Selby**

Title of Thesis: **Fluid characteristics and evolution of porphyry Cu-Au-Mo and Mo systems, Yukon-British Columbia, Canada**

Degree: **Doctor of Philosophy**

Year this Degree Granted: **1999**

Permission is hereby granted to the University of Alberta to reproduce single copies of this thesis and to lend or sell such copies for private, scholarly, or scientific research purposes only.

The author reserves all other publication and other rights in association with the copyright in the thesis, and except as hereinbefore provided, neither the thesis nor any substantial portion thereof may be printed or otherwise reproduced in any material form whatever without the author's prior written permission.

David Selby

184 Kingsland,
Harlow,
Essex,
CM18 6XS
U.K.

September 27th, 1999

University of Alberta

Faculty of Graduate Studies and Research

The undersigned certify that they have read, and recommend to the Faculty of Graduate Studies and Research for acceptance, a thesis entitled Fluid characteristics and evolution of porphyry Cu-Au-Mo and Mo systems, Yukon-British Columbia, Canada submitted by David Selby in partial fulfilment of the requirements for the degree of Doctor of Philosophy.

Dr. R. A. Creaser (Supervisor)

Dr. K. Muehlenbachs (Co-Supervisor)

Dr. J. P. Richards (Committee Member)

Dr. T. Chacko (Committee Member)

Dr. A. H. Clark (External Reader)

Dr. D. B. Tannant (Committee Member)

Date: 27th September '99

To Bruce, friend and advisor

Abstract

Geochemical techniques (isotopic, major, trace, and rare earth elements, fluid inclusion, solute chemistry) have been used to investigate porphyry mineralization of the Canadian Cordillera. Specifically, the Endako porphyry Mo deposit, central British Columbia, and the Casino, Cash, and Mt. Nansen Cu-Au-Mo occurrences of the Yukon were studied with the objective of characterizing the hydrothermal fluids associated with alteration and mineralization and subsequently to produce a more comprehensive understanding of these systems. The crystalline rocks neighboring the porphyry occurrences in the Yukon were also studied with the objective of understanding their protoliths and tectonic setting during formation.

The low fluorine Endako porphyry Mo deposit is characterized by early quartz ± molydenite stockwork veins, with K-feldspar-bearing selvages and paragenetically later quartz-molybdenite ribbon veins, with sericite-bearing selvages. Oxygen isotope, fluid inclusion and solute chemistry studies indicate the involvement of hydrothermal fluids, exsolved from a crystallizing melt, in the formation of the Endako molybdenum deposit. However, hydrogen isotope compositions suggest the early involvement of meteoric water in the ore forming fluids and ore genesis.

The geochemical characteristics of the Devonian-Mississippian rocks of west-central Yukon indicate that the Yukon was a land mass outboard of North America

representing a continental arc during Devonian-Mississippian times. The mid-Cretaceous Dawson Range batholith represents magmas crustally derived of the Precambrian basement of the Yukon. Whereas, the late Cretaceous plutons, genetically related to porphyry Cu mineralization, are associated with magmas that were derived from a mantle source contemporaneous with subduction.

Biotites in granitic rocks altered by mineralizing fluids of the Casino occurrence possess elemental compositions distinct from biotites in neighboring unaltered granitic rocks. The observed chemical trends are similar to those reported from other porphyry Cu deposits; however, the absolute elemental contents are variable between porphyry Cu deposits. Calculated fugacity ratios of the hydrothermal fluids of porphyry Cu deposits suggest that log $fH_2O/fHCl$ and log $fHF/fHCl$ are similar; whereas, log fH_2O/fHF values are variable.

Isotopic compositions (H, Sr, Pb, Ar) of primary mineralizing fluids associated with porphyry Cu-Au-Mo mineralization of the west-central Yukon indicate that fluids are composed of mixed non-magmatic and magmatic fluids. This hypothesis is atypical to the generally accepted thinking of fluid origin of porphyry Cu systems.

Acknowledgements

Acknowledgements. A free hand for the author to express anything he/she wishes and therefore I encourage the reader most forcefully to read on. But if your decision is not to, well be it to your own loss and disappointment. The following may be interpreted to be of emotional, strange, humorous, and/or disgusting nature, nevertheless, that is your interpretation and yours alone.

Acknowledgement. In how many ways can one say thankyou? Thanks can be expressed by, recognition, appreciation, indebtedness, gratefulness, to mention but a few examples in English, and not to forget those of you of foreign tongue, merci, grazie, tack, tak, danke, gracias. Though these words for myself do not fully cut it. Thanks alone is not enough to the many. A thesis has but one author accompanied by a title, but it is the manifestation of countless friends and colleagues.

In compiling my thesis I am reminded of a passage from a Novel by Stephen Fry that I will now relate to you. So here goes. You've presented your Ph.D. thesis to your supervisor and this is your first meeting with him/her since.

So then, have you sought help?"
"I'm sorry?"
"For your drug problem."
"My what?"
"You're all smacked up with joints of heroin, man! You can't deceive me. High on Euphoria or some other fashionable narcotic. I know this a problem for all people your age. I think you should do something about it. And that right urgently."
"Er...are you perhaps confusing me with someone else, Sir?"
"Oh, I don't think so. No indeed. What other explanation could there be?"
"For what?"

"For this, boy. For this!" He waved the thesis with a snarl.
My world began to disintegrate. "You mean you don't like it?"
"Like it? Like it? It's garbage. Offal. It's not a thesis, it's faeces! It's pus, moral slime, ordure."
"But.....but....I thought we agreed that I was working along the right lines?"
"We...we talk about your work, and you give every sign of having all well in hand and then this....this effluent. It's not an academic argument, it's a novel and a perfectly disgusting one at that".
"Are you sure you've been reading the right paper?"
"What do you take me for of course I've been reading the right paper! So, if you aren't doped-out crack fiend hallucinating on comic mushrooms then what is the problem? Oh...ha!...of course it's a joke, isn't it? You have the real thesis tucked away somewhere else! Skh! Honestly".
"But I don't understand what's wrong with it? It's not fit for publication?"
"Published?" I swear to God I thought he was going to explode.
"Published? Great fuck, child, even Mills and Boon would blush at the prospect".

The thought of this kind of conversation with one's supervisor is most certainly nerve racking, and one would most definitely be scared shitless, especially during his/her penultimate stage of their program. We have all probably been there. The critiques from our advisors and reviewers plastered across our work, vague, ????, I don't think so, reword, explain, redundant, No No No!!!!, can all be a little disheartening. But it doesn't beat a paper returned bludgeoned by the blood stained colour of a red pen with the words heading the title page, a few changes, reads well. How the hell can it possibly read well, I can barely see the original printed BLACK text! It's an after thought I think to myself. Hmmm, yes, change this and that and, yes it reads well. But the thought of having four years of one's work discarded as complete drivel and being thought barking mad is surely a little worrying. If you haven't been down this road then you must surely be pig headed or are a genius, but then geniuses are generally barking mad anyway! I say, just imagine the thought of rewriting the whole damn thesis again!

Not on your nellie. It is not quite a simple as Calvin and Hobbes would like you to think.

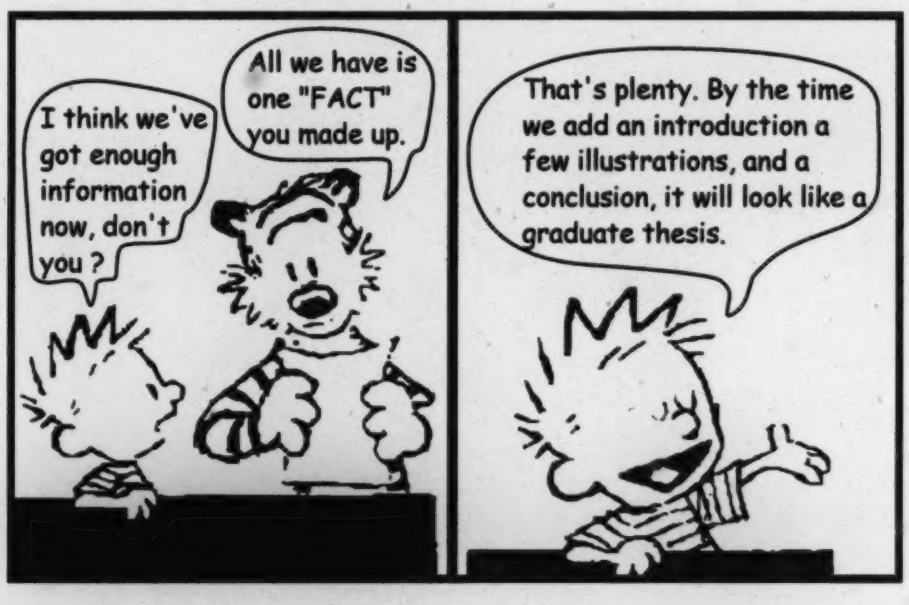
I think we've got enough information now, don't you?
All we have is one "FACT" you made up.
That's plenty. By the time we add an introduction a few illustrations, and a conclusion, it will look like a graduate thesis.

Moving on. If one takes the time to look at this thesis you will see the name Bruce Nesbitt making a frequent appearance. Bruce is the reason I came to the U of A for my Ph.D. program. I started writing to Bruce towards the end of my undergraduate degree after discussions with Bob Foster (undergraduate advisor). Bruce was quick to accept me as a student, and in September 1994 young and freshly graduated from Southampton University I arrived at the U of A. The first few months I found were hard and taxing, and finding Bruce not to be very personable did not help matters. Infact, I found him very unapproachable and uninterested in topics I wished to pursue. It was during these times I almost said sod it and quit. But I am thankful to myself and especially to the encouragement of

Ron Sheets that I did not. As time marched on a research topic was devised and here I am indebted to Karlis Muehlenbachs and his Stable Isotope course. It was then I found Bruce's attitude changed, as if almost overnight, he was suddenly interested it what was going on. But I found Bruce's personality wasn't an oddity towards me. He seemed to behave the same with other new students, as if he was putting you on trial, can this person conduct research? This I feel was the ice-breaking question with Bruce. Once the ice was broken during the following years Bruce was always very encouraging with discussing new ideas, writing papers and presenting at conferences. With his belief of poster competitions at the Annual Round-Up conference always being reserved for the UBC crowd being broken when I returned as a prizewinner, twice! During the later years of my Ph.D. research Bruce became a friend. During August 1998 Bruce passed away. I have a lot to remember and to be thankful to Bruce for, but, if nothing else I will always remember his love of travelling and his strange obsession with Sumo wrestlers.

Rob Creaser became integrated into my research program soon after my candidacy exam. What I am truly thankful to Rob for is his patience to teach, listen and most of all try something new. It takes many hours to teach the methodology of a clean lab and a Mass Spectrometer. Also, cheers for the Friday afternoon squash games. Rob's idea of squash was to play the bastard of all drop shots to the front wall, where I would run like a headless chicken in the search of the tiny green ball, hmmm, is there really any sense in this?

For those at the U of A there are all so many to thank; Bob Luth for numerous quips about the use of equipment and donations to his reference library; Karlis Muehlenbachs for the education on social behaviour at conferences, oh and the introduction to Stable Isotopes; Ron Sheets for numerous discussions on everything and the odd pint of Guinness; Tom Chacko for always having time to help answer a question. For technical help I am grateful to Olga Levner, Don Resultay, James Steer, Diane Caird, Rob Stefeniak, Randy Pakan, Paul Wagner, and Lang Chi. Special thanks to Judith Enarson for dealing with numerous questions.

To those not at the U of A: Walter Prochaska of Institut fur Geowissenschaften for the solute chemistry analysis; Peter Reynolds, Keith Taylor, and Marcos Zentillis of Dalhousie University, Halifax for the encouraging introduction to argon isotopes; Craig Hart of the Yukon Geoscience Program for his continued interest and collaboration (one year we will find the cans of Kokanee); Glenn Johnson at the Endako mine for his hospitality and very dry humour; Jim Mortensen of UBC for use of unpublished data; Mike Villeneuve of the GSC Ottawa for interest and collaboration with the Endako project. To the companies Pacific Sentinel Gold, Placer Dome, Archer Cathro, and BYG for access to the sites Casino, Endako, Cash, and Mt. Nansen, and to the pilots of Alkan Air and Trans North for the transportation in and out of these areas. And last but not least to Fred Flykt-Rosén, my crazy Swedish friend, for his field assistance and continued friendship.

To complete the academic acknowledgements, the research program was supported from funds from the NSERC Grant of Bruce Nesbitt and the Society of Economic Geologists, Geological Society of America and Circumpolar Institute Grants to the author.

To friends, Skids, Jo, Ian, for our vast discussions on the odd and wonderful things of life that one-day will be published in numerous volumes. But will the question be answered? I think not, because the answer and most bloody likely the question will change. Bugger!! To these fellers who are the soundest blokes you could possibly meet, for countless ventures to the Next Act Pub, evenings of watching football (soccer for the North Americans), and several ski trips that no doubt prevented my brain from becoming lime jelly.

For those who know me the acknowledgements would be incomplete without the mention of Matt Perks, Matt, Perky, Boy of Destiny. We were office mates for a couple of years and spent the occasional afternoon reciting quotes from whatever popped into our empty heads, sometimes shouting at each other with hostility. This was only done to freak out the rest of the graduate students in the neighbouring offices who probably thought we were killing each other or that the men in white coats were soon to arrive. Little did they know that we were the men in white coats. How on earth we got any work done or for that fact how Matt finished his M.Sc. I have no idea. The inspiration must lie in the comical genius hidden on the Billy Connelly, Peter Cook and Dudley Moore tapes. There are so many other stories to relate, but for those you will just have to

ask Fred, Mike, Pauline, Tom, Julie, Karen, Leslie, Nancy, Andrea, Steve, George, Tracey, Kerrie-Ann, and of course Rufus, especially try asking Rufus (☆).

Finally to Jan and Chris Selby, yes Mum and Dad, their endless support, not only during my Ph.D., throughout my life that has helped me come this far. A tower of things spring to mind to thank my parents for, but it's things that make a connection, gingerbread from Grasmere, Pic 'n' Mix jellies from Woolworths in Keswick, and Kendal Mint Cake, and of course Marmite (for any Australians we all know it's better than Vegemite!) and Depeche Mode cds.

The author also thanks the following for permission to reproduce text and a comic strip that appear in the acknowledgements.

Making History by Stephen Fry
Copyright 1996 Hutchinson, London.

The Indispensable Calvin and Hobbs. A Calvin and Hobbes Treasury by Bill Watterson
Reprinted with permission of Universal Press Syndicate.
All rights reserved (1992).

Contents

	Page
Chapter I	
Introduction	1
References	6
Figure	8
Chapter II	
Hydrothermal alteration and fluid chemistry of the Endako porphyry molybdenum deposit, British Columbia	
Introduction	9
Geology	11
Structure	12
Mineralization	13
Stockwork Veining	
Ribbon Textured Veins	
Hydrothermal Alteration	15
K-Feldspar Selvages	
Sericite Selvages	
Kaolinite Selvages	
Late Hydrotrhermal and Supergene Alteration	
Analytical Work	18
Fluid Inclusion Study	19
Petrography of Fluid Inclusions	
Salinity and Homogenization Results	
Fluid Inclusion Trapping Conditions	
Stable Isotope Study	26
Considerations of Equilibrium and Hydrothermal Fluid Temperatures	
Isotopic Compositions of the Hydrothermal Fluids	
Post-Ore Fluids	
Solute Chemistry of Fluid Inclusion Waters	31
Discussion	32
Hydrothermal Alteration	
Origin of Low δD Fluids	
Comparisons of Data from Endako and other Hydrothermal Systems	
Summary and Conclusions	39
References	40
Tables	49
Figures	54

Chapter III

Major and trace element compositions and Sr-Nd-Pb Systematics of Crystalline Rocks from the Dawson Range, Yukon, Canada

Introduction 66
Geology of the Dawson Range 68
Results 71
- Wolverine Creek Metamorphic Suite
- Mid Cretaceous Intrusions
- Late Cretaceous Plutons

Discussion 75
- Wolverine Creek Metamorphic Suite
- Mid Cretaceous Intrusions
- Late Cretaceous Plutons

Tectonic Implications 81
- Wolverine Creek Metamorphic Suite
- Mid Cretaceous Intrusions
- Late Cretaceous Plutons

Conclusions 84
References 85
Tables 92
Figures 100

Chapter IV

Biotite chemistry of the Casino porphyry Cu-Au-Mo mineralization, Yukon, Canada: Evaluation of magmatic and hydrothermal fluid chemistry

Introduction 107
Igneous and alteration Petrography 108
Biotite Types at the Casino Occurrence 111
Biotite Analytical Procedures 112
Discussion of Biotite Compositions 113
Comparison of Biotite Chemistry with other Porphyry Cu Deposits 115
Biotite Halogen Chemistry 116
Determination of Hydrothermal Fluid Fugacity Ratios 118
Comparison of Fugacity Values with Values from other Hydrothermal Systems 120
Summary 122
References 123
Figures 127

Chapter V

Evidence for a non-magmatic component in potassic hydrothermal fluids of porphyry Cu-Au-Mo systems, Yukon, Canada

Introduction 137
Mineralization and Hydrothermal Alteration 138
Fluid Inclusions 140
Hydrogen Isotope Study 142
Sr and Pb Isotope Study 142
- Magmatic Isotope Compositions
- Potassic Alteration Isotope Compositions
- Pyllic Alteration Isotope Compositions

Argon Isotope Study 146
Discussion: Potassic Hydrothermal Fluids 148
- Inheritance of Pre-existing Isotope Compositions from the Host Rocks
- Modification of Isotopic Compositions
- Replenishment of the Magma Chamber
- Origins of Isotope Compositions

Phyllic Fluids and Fluid Evolution 155
Implications 156
References 159
Appendices 165
- Appendix 5.A Analytical Procedures
- Appendix 5.B
- Appendix 5.C
- Appendix 5.D

Tables 171
Figures 175

Chapter VI

Summary 185

Appendix I 192

Appendix II 195

Appendix III 196

Appendix IV 208

List of Tables

Page

Chapter II

2.1. First Ice, Halite Melting Temperatures, Salinity and Homogenization Temperatures for Fluid Inclusion Types 49

2.2. P-T trapping conditions for fluids represented by Type 1, 2 and 3 inclusions associated with K-feldspar, sericite and kaolinite alteration assemblages. 50

2.3. Synopsis of Silicate Oxygen, Carbon and Hydrogen Isotope Data from the Endako Porphyry Molybdenum Deposit. 51

2.4. Mineral-Mineral Oxygen Pair Data for Quartz and K-feldspar. 52

2.5. Solute chemistry data. 53

Chapter III

3.1. Description of Rock Types Analyzed. 92

3.2. Major, Trace, and Rare Earth Elements Concentrations. 93

3.3. Rb and Sr concentrations and Isotope Compositions. 96

3.4. Nd and Sm concentrations and Isotope Compositions. 97

3.5. U, Th, and Pb Concentrations, and Pb Isotope Compositions. 98

Chapter V

5.1. δD Compositions of quartz phenocrysts and veins from potassic and phyllic alteration assemblages of the Casino, Cash and Mt. Nansen Porphyry Occurrences. 171

5.2. Rb and Sr Concentrations and Isotope Compositions of the Late Cretaceous Plutons, Apatite, K-feldspar, and Quartz from the Casino, Cash, and Mt. Nansen Porphyry Occurrences. 172

5.3. Pb Isotope Compositions of the Casino Pluton, K-feldspar, Pyrite, Chalcopyrite, and Bornite of the Potassic and Phyllic Alteration Assemblages of the Casino Occurrence. 174

List of Figures

Page

Chapter I

1.1. Location of study areas 8

Chapter II

2.1. Geology of the Endako area 54

2.2. Geology of the Endako porphyry molybdenum deposit. 55

2.3. Hydrothermal alteration map of the Endako deposit, with locations56
of samples analyzed for fluid inclusion studies. 56

2.4. Microthermometry Data of Fluid Inclusions. 57

2.5. Pressure-temperature diagrams to show the conditions of
vein-forming fluids. 58

2.6. Model for Pressure-Temperature Evolution for molybdenum mineralization,
alteration, and post-ore fluids from Endako deposit. 60

2.7. Salinity vs. homogenization temperature plot for inclusions
from sample WD1. 61

2.8. Hydrogen isotope data from mineral separates from the Endako deposit. 62

2.9. Isotopic composition of hydrothermal fluids producing early stockwork
and later ribbon quartz veins. 63

2.10. Isotopic composition of hydrothermal fluids producing late stage calcite
veins. 64

2.11. Solute Chemistry results. 65

Chapter III

3.1. Terrane map of the Yukon showing the Yukon-Tanana terrane. 100

3,2. Geology of the study areas. 101

3.3. Rare earth element plots. 102

3.4. Tectonic setting discrimination diagrams for clastic sediments. 103

3.5. Neodymium isotopic characteristics of the Wolverine Creek Metamorphic Suite. 104

3.6. Pb Isotope composition diagrams. 105

Chapter IV

4.1. Location map of the Casino porphyry Cu-Au-Mo occurrence, Dawson Range, west-central Yukon, Canada 127

4.2. Photomicrographs of biotite from Casino 128

4.3. Biotite chemistry plots for least-altered biotites, plus altered and secondary biotites from propylitic, phyllic and potassic alteration zones. 129

4.4. Chemical data for biotites from the Casino occurrence. 134

4.5. Chemical data for least-altered biotites from the Dawson Range batholith 135

4.6. Log (fH_2O)/($fHCl$), (fH_2O)/(fHF) and (fHF)/($fHCl$) ratios for the Casino occurrence 136

Chapter V

5.1. Location of the Casino, Cash, and Mt. Nansen, porphyry Cu-Au-Mo occurrences of west-central, Yukon, Canada. 175

5.2. δD_{FI} values for fluid inclusion fluids for Casino, Cash, and Mt. Nansen Cu-Au-Mo occurrences. 176

5.3. Plot of the $^{87}Sr/^{86}Sr_{t=70}$ compositions of whole rock samples of the late Cretaceous plutons, magmatic apatite, and hydrothermal K-feldspar of the Casino, Cash, and Mt. Nansen Cu-Au-Mo occurrences.

samples of the Casino occurrence. 177

5.4. Plot of $^{207}Pb/^{204}Pb$ versus $^{87}Sr/^{86}Sr_{t=70}$ compositions of leached K-feldspar. 178

5.5. $^{87}Rb/^{86}Sr$ vs. $^{87}Sr/^{86}Sr$ plot fluid inclusion waters in vein quartz and K-feldspar 180

5.6. $^{40}Ar/^{39}Ar$ age spectrum plot of the hydrothermal K-feldspar samples from the Casino, Cash and Mt. Nansen. 181

5.5. $^{39}Ar/^{40}Ar$ versus $^{36}Ar/^{40}Ar$ isotope correlation plots of the hydrothermal K-feldspar samples from the Casino, Cash and Mt. Nansen 183

Chapter I

Introduction

Investigating and establishing the origin(s) of hydrothermal fluids contributing to the formation of metalliferous mineral occurrences has been a major pursuit of Earth Scientists for hundreds of years. During the 16th Century, Agricola postulated that heated groundwaters of meteoric origin were the source from which ores precipitated; whereas, Descartes during the 17th Century hypothesized the ore-fluids originated from the cooling of the Earth's interior. These philosophies of ore origin were broadly continued with the hypotheses of Werner and Hutton during the 18th Century. With respect to porphyry mineralization, it was not until the early 20th Century that the association of an igneous body and mineralization was implied and the ore-bearing fluids being derived from a magma (Ransome, 1904; Lindgren, 1905). Since that time, scientific developments of the origin of primary hydrothermal fluids associated with porphyry systems have established two schools of thought: (1) fluids are derived from a crystallizing magma (e.g., Burnham, 1979; Hedenquist and Lowenstern, 1994; Hedenquist et al., 1988 and references therein), and (2) fluids are of meteoric origin (e.g., Cathles, 1977; Norton, 1982; 1984).

Presented and discussed in this dissertation is the chemical composition and origin of hydrothermal fluids associated with porphyry Cu and Mo deposits of the Canadian Cordillera. The specific sites of porphyry mineralization studied are the Endako porphyry molybdenum deposit (central British Columbia), and the Casino, Cash, Mt. Nansen porphyry Cu occurrences (west-central Yukon) (Fig. 1.1). The research in this dissertation is presented in paper-format as four chapters, with each chapter comprising a single, complete study. Chapter two presents a study on the Endako

porphyry molybdenum deposit entitled "Hydrothermal alteration and fluid chemistry of the Endako porphyry molybdenum deposit, British Columbia". A version of this chapter has been accepted for publication in the journal Economic Geology and is co-authored by Drs. Nesbitt, Muehlenbachs, and Prochaska. The author formulated all field work, laboratory analysis, data synthesis and wrote the chapter. Co-author Dr. Prochaska contributed to the chapter by conducting solute geochemical analysis in his laboratory at Institut für Geowissenschaften, Leoben, Austria. Helpful editorial comments of the chapter were suggested by co-authors Nesbitt and Muehlenbachs. Chapters three, four and five deal with the porphyry Cu deposits of west-central Yukon. Chapter three presents a study discussing the chemical compositions of the plutons associated with porphyry Cu mineralization, as well as the neighboring country rocks and is entitled "Major and trace element compositions and Sr-Nd-Pb systematics of crystalline rocks from the Dawson Range, Yukon, Canada". A version of this chapter has been accepted for publication in the Canadian Journal of Earth Sciences and is co-authored by Drs. Creaser and Nesbitt. My personal role of this chapter was in the execution of field work, laboratory analysis, data synthesis and writing the chapter. The co-authors contributed to the manuscript thought editorial comments. Chapter four deals with the chemical composition of biotite and is entitled "Chemical composition of biotite of the Casino porphyry Cu-Au-Mo mineralization, Yukon, Canada: Evaluation of magmatic and hydrothermal fluid chemistry". A version of this chapter has been submitted to the journal Chemical Geology and is co-authored by Dr. Nesbitt. I conducted the field work, laboratory analysis, data synthesis, and wrote the chapter. Chapter five presents and discusses the chemical composition of hydrothermal fluids responsible for potassic-stage alteration and is entitled "Evidence for a non-magmatic component in potassic hydrothermal fluids of porphyry Cu-Au-Mo systems, Yukon, Canada". A version of this chapter has been submitted to the journal Geochimica et Cosmochimica Acta and is co-

authored by Drs. Nesbitt, Creaser, Reynolds and Muehlenbachs. I completed field work, laboratory analysis, data synthesis and the formulization of the manuscript. Co-author Dr. Reynolds contributed to the manuscript by conducting argon isotopic analyses in his laboratory at Dalhousie University, Halifax. The co-authors Creaser, Nesbitt, and Muehlenbachs contributed to the manuscript thought editorial comments.

The rationale for the research presented in this thesis was developed from stable isotope studies on the Babine Lake porphyry Cu deposits (Fig. 1.1) (Zaluski et al. 1994; Sheets et al. 1996). This study identified an anomalous hydrogen isotope composition ($\delta D = -100$ to -135 ‰) for the fluids associated with potassic-stage alteration. These values are significantly different from the generally accepted "magmatic" δD values of –40 to –80 ‰ (Taylor, 1979). The hydrogen isotope compositions were interpreted to either represent a meteoric or crustal assimilation of material depleted in deuterium (Sheets et al. 1996). The crucial question from these studies is to what degree are deuterium depleted fluids universal to porphyry Cu-Mo occurrences worldwide. This study was undertaken to test for the presence of deuterium depleted fluids in other porphyry deposits of the Canadian Cordillera and to establish whether the hydrogen isotope signature was developed from either crustal assimilation or meteoric water.

The objectives of Chapter 2 are twofold, to present the geology and geochemistry of the low fluorine Endako porphyry Mo deposit, central British Columbia and to discuss possible origins of the hydrothermal fluids associated with the Mo mineralization and alteration. Previous studies on porphyry Mo systems have typically discussed the geological and geochemical characteristics of high fluorine deposits. However, research on low fluorine systems, such as Endako, is limited. Chapter 2 summarizes the hydrothermal alteration and fluid compositions of the Endako deposit, using petrographic, stable isotope, and fluid inclusion data. An aspect of this research that differs from previous studies on porphyry Mo deposits is a solute chemistry study of fluid

inclusion waters. These results are compared to ore-fluids associated with other hydrothermal systems.

The study of the Endako deposit established the presence of deuterium depleted fluids associated with molybdenum mineralization. However, the question of whether crustal assimilation or meteoric water was the origin of the depleted hydrogen isotope values could not be established. To investigate the latter, three porphyry Cu occurrences (Casino, Cash and Mt. Nansen) of west-central Yukon were examined (Fig. 1.1). These localities were choosen because of the light stable isotope composition of meteoric water at the time (late Cretaceous) of porphyry mineralization and alteration. Also, because the neighboring country rocks are significantly older than the plutons of the porphyry occurrences, and therefore would yield contrasting radiogenic isotopic signatures to the plutons themselves.

In Chapter 3, crystalline rocks from the Dawson Range, west-central Yukon-Tanana terrane are examined with the principal objective of determining the geochemical characteristics and origin of the magmas that generated the plutons associated with porphyry mineralization and alteration. Also presented are the geochemical characteristics of the Devono-Mississippian metaigneous and metasedimentary units, mid-Cretaceous Dawson Range batholith and Casino Plutonic Suite. Major, trace and rare earth element (REE) and Sr, Pb, and Nd isotope composition of crystalline rocks are particularly useful in evaluating the protoliths and the tectonic affinity of these rocks. Presently not constrained are the protoliths of the Devono-Mississippian units of the Yukon-Tanana terrane, especially those of the Dawson Range. The geology of the Dawson Range is dominated by the mid-Cretaceous Dawson Range batholith, which is intruded by late Cretaceous plutons. The origin of the mid- and late Cretaceous granitic bodies and their associated tectonic settings had previously not been evaluated. The research has provided constraints on the protoliths of rocks and tectonic settings of the

Yukon-Tanana terrane during Devono-Mississippian, and mid- and late Cretaceous times. The geochemical data for the crystalline rocks presented in Chapter 3 are further discussed in Chapter 5 with respect to evaluating the geochemical compositions of the porphyry hydrothermal fluids associated with the late Cretaceous porphyry systems.

Numerous porphyry Cu-Au-Mo occurrences are present in the Dawson Range, west-central Yukon. Previous studies only described the mineralization and hydrothermal alteration features of these porphyry occurrences, without evaluating of the origin of hydrothermal fluids associated with these deposits. In Chapters 4 and 5 the geochemical characteristics of the hydrothermal fluids of the Casino, Cash and Mt. Nansen occurrences are reported and discussed.

The goal of Chapter 4 is to present the composition, particularly the halogen contents of biotite from least-altered, propylitic, phyllic and potassic alteration assemblages of the Casino porphyry system. Few studies of the chemical composition of bitoite report the full elemental chemistry (Jacobs and Parry, 1979). The chemical composition of biotite in the Casino occurrence is compared with the few data available for other porphyry systems to evaluate if the chemical trends described at Casino are similar to other porphyry systems. The biotite halogen chemistry is used to determine the log (fHF)/(fHCl), ($f$$H_2O$)/($f$HCl) and ($f$$H_2O$)/($f$HF) ratios of the hydrothermal fluids. The log (fHF)/(fHCl), ($f$$H_2O$)/($f$HCl) and ($f$$H_2O$)/($f$HF) ratios are determined using new formulations derived from the increased knowledge of the F-Cl-OH partitioning in biotite. These data are discussed to show the fugacity evolution in the fluids, with the results compared with the recalculated fugacity values of other porphyry systems.

In Chapter 5, the geochemical compositions of potassic hydrothermal fluids associated with porphyry Cu-Au-Mo mineralization of the west-central Yukon, Canada are presented and discussed. Addressing the geochemical characteristics of hydrothermal fluids of porphyry mineralization is important in understanding the origin and the

processes during ore genesis associated with these systems. Numerous previous studies of porphyry deposits have built the hypothesis that early fluids associated with potassic alteration are of a magmatic origin. This study builds on the previous approaches of techniques used to study hydrothermal fluids of porphyry systems. In addition to stable isotope and fluid inclusion techniques, mineral separates from hydrothermal altertaion zones are analyzed for their radiogenic isotopic compositions. Specifically, the Sr and Pb isotopic compositions of hydrothermal K-feldspar, and the Sr isotope compositions of fluid inclusion waters from the potassic zone are determined. This research program is the first example of such a comprehensive investigation of geochemical compositions of fluids responsible for potassic-stage alteration in the northern Canadian Cordillera and to my knowledge anywhere in the world. The geochemical compositions of potassic-stage fluids and isotopic data on the host plutons and country rocks (discussed in Chapter 3) are used to evaluate the geochemical compositions of the hydrothermal minerals, and subsequently the origin of the fluids. This research shows for the porphyries of the west-central Yukon potassic hydrothermal fluids are derived from the mixing of non-magmatic and magmatic fluids.

References

Burnham, C. W. 1979. Magmas and hydrothermal fluids. *In* Geochemistry of hydrothermal ore deposits. *Edited by* H. L. Barnes, 77-136 p.

Cathles, L. M., II 1977. An analysis of the cooling of intrusions by ground water convection which includes boiling. Economic Geology, **72**: 804-826.

Hedenquist, J. W., Arribas, A., Jr., and Reynolds, T. J. 1998. Evolution of an intrusion-centered hydrothermal system: Far Southeast-Lepanto porphyry and epithermal Cu-Au deposits, Philippines. Economic Geology, **93**: 373-404.

Hedenquist, J. W., and Lowenstern, J. B. 1994. The role of magmas in the formation of hydrothermal ore deposits. Nature, **370**: 519-527.

Lindgren, W. 1905. The copper deposits of the Clifton-Morenci district, Arizona. U. S. Geological Survey Professional Paper 43, 375p.

Norton, D. L. 1982. Fluid and heat transport phenomena typical of copper-bearing pluton envirnoments. *In* Advances in geology of porphyry copper deposits of southwestern North American: Tuscon. University of Arizona Press. *Edited by* S. R. Titley, 59-72.

Norton, D. L. 1984. Theory of hydrothermal systems. Annual Review Earth and Plantary Sciences, **12**: 155-77.

Jacobs, D. C., and Parry, W. T. 1979. Geochemistry of biotite in the Santa Rita porphyry copper deposit, New Mexico. Economic Geology, **74:** 860-887.

Ransome, F. L. 1904. Geology and ore deposits of the Bisbee Quadrangle, Arizona. U. S. Geological Survey Professional Paper 21, 168p.

Sheets, R. W., Nesbitt, B. E., and Muehlenbachs, K. 1996. Meteoric water component in magmatic fluids from porphyry copper mineralization, Babine Lake area, British Columbia. Geology, **24:** 1091-1094.

Taylor, H., Jr. 1979. Oxygen and hydrogen isotope relationships in hydrothermal mineral Deposits. *In* Geochemistry of hydrothermal ore deposits. *Edited by* H. L. Barnes. 236-272.

Zaluski, G., Nesbitt, B. E., and Muchlenbachs, K. 1994. Hydrothermal alteration and stable isotope systematics of the Babine Porphyry Cu deposits, British Columbia: Implications for fluid evolution of porphyry systems. Economic Geology, **89:** 1518-1541.

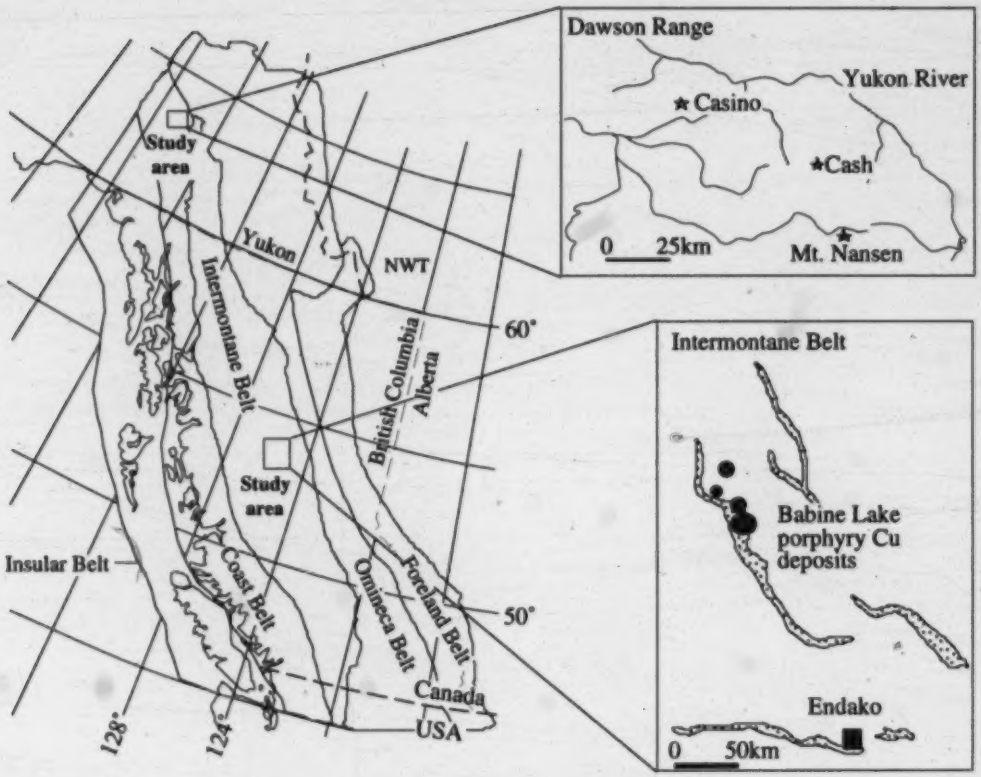

Fig. 1.1. Geological-physiograpgic belt map of the Canadian Cordillera showing the location of the Babine Lake, Endako, Casino, Cash, and Mt. Nansen porphyry deposits.

Chapter II

Hydrothermal alteration and fluid chemistry of the Endako porphyry molybdenum deposit, British Columbia*

*A version of this paper has been accepted for publication in Economic Geology, August 1999, co-authored by Bruce E. Nesbitt and Karlis Muehlenbachs of the Department of Earth and Atmospheric Sciences, University of Alberta, T6G 2E3, Canada, and Walter Prochaska, of the Institut für Geowissenschaften, Montanuniversität, A-8700 Leoben, Austria.

Introduction

The most important source of molybdenum in the world are stockwork porphyry molybdenum deposits. Characteristics of this deposit type have been presented by Clark (1972), Soregaroli and Sutherland Brown (1976), Woodcock and Hollister (1978), Hollister (1978), Westra and Keith (1981), Mutschler et al. (1981), White et al., (1981), and Carten et al. (1993). The classification by Westra and Keith (1981) divides porphyry molybdenum deposits into calc-alkaline, alkali-calcic, and alkalic types. The characteristics of calc-alkaline molybdenum deposits, (which includes Endako and Adanac in British Columbia, Canada, and Buckingham in the United States) include a low fluorine content (0.05 to 0.15 wt. %), minor tungsten, and absence of tin. In constrast, alkali-calcic and alkalic molybdenum deposits are enriched in fluorine (0.5 to 5 wt. %; present as fluorite ± topaz), and tungsten and tin are common. Examples of the latter group include Climax, Urad-Henderson, and Questa in the United States, and are referred to as Climax-type deposits by White et al. (1981). An exception to the alkali-calcic, high fluorine classification of molybdenum deposits is Nogal Peak, which has a low fluorine content (Thompson 1982). Carten et al. (1993) modified the alkalic classification of Westra and Keith (1981) to include grade, tonnage, and tectonic setting.

Numerous studies have documented porphyry molybdenum mineralization (e.g., Soregaroli and Sutherland Brown 1976 and references therein; Sharp 1978; Molling 1989; Wallace et al. 1978; White et al. 1981; Rice et al. 1985; Shaver 1991). However, geochemical studies (e.g., stable isotope and fluid inclusion studies) generally have focused on the high fluorine, alkalic molybdenum deposits (e.g., Hall et al. 1974; Kamilli 1978; Bloom 1981; White et al. 1981; Smith 1983; Rice et al. 1985; Stein and Hannah 1985; Carten 1987; Stein 1988; Carten et al. 1988; Shaver 1991; Cline and Bodnar 1994), with limited research on low fluorine deposits (Dawson 1972; Bloom 1981; Hall et al. 1984; Theodore and Menzie 1984; Theodore et al. 1992). This chapter presents a hydrothermal alteration and fluid chemistry study of the Endako molybdenum deposit, British Columbia based on field work, petrography, microthermometry and geochemistry of fluid inclusions, and stable (oxygen, carbon and hydrogen) isotope compositions of veins, hydrothermal alteration minerals, and the host rock. In addition, this chapter presents the first solute chemistry study of fluid inclusion waters from a porphyry molybdenum deposit. Previous studies of the Endako molybdenum deposit include information on geology, geochronology, and fluid inclusion microthermometry by Drummond and Kimura (1969), Kimura and Drummond (1969), White et al. (1968, 1970), Dawson (1972), Kimura et al. (1976), Bloom (1981), Carter (1981), Bysouth et al. (1995), Enkin et al. (1997), and Anderson et al. (1998b). The Endako deposit is composed of a northwesterly-trending orebody with a length of 3360 m and a width and depth of 370 m. The deposit consists of four open pits: East Endako, West Endako, East Denak and West Denak. Mining commenced in the West and East Endako pits in 1965, with the Denak pits being developed in 1977. Ore reserves at the end of 1998 were 85 million tonnes with an average grade of 0.136 % MoS_2 at a cutoff of 0.07 % MoS_2.

Geology

The Endako granitic phase of the Francois Lake Plutonic Suite of central British Columbia of the Canadian Cordillera hosts the Endako porphyry molybdenum deposit (Fig. 2.1). Geology of the Endako area includes plutonic, volcanic and sedimentary units comprised of the late Triassic Boer plutonic suite, Jurassic Hazelton Group, late Jurassic to early Cretaceous Francois Lake Plutonic Suite, Jurassic to Cretaceous Stellako phase, and the Eocene Ootsa and Endako Groups (Fig. 2.1) (Struik et al. 1997; Anderson and Snyder 1998; Whalen et al. 1998). The Francois Lake Plutonic Suite is divided into younger early Cretaceous (149-145 Ma) and older late Jurassic (159-154 Ma) suites on the basis of field relationships and geochronology (Anderson et al. 1998a, 1998b). The younger suite comprises the Casey phase (aplitic biotite monzogranite and granodiorite, 145 ± 1.5 Ma U-Pb zircon), and the Endako phase, which includes the Francois and Sam Ross Creek subphases (granite to granodiorite, 147 ± 1.5 Ma U-Pb zircon). The older suite comprises the Nithi phase (biotite monzogranite, 158-155 ± 1.5 Ma Ar-Ar biotite), an the Glenannan phase, which includes the Tatin Lake and Hanson subphases (biotite monzonite to monzogranite, 156 Ma Ar-Ar biotite). Contacts between phases of the Francois Lake Plutonic Suite are sharp, widely exhibit chilled margins, and are crosscut by granitic, and basalt and/or andesite dikes (Dawson 1972). The granitic dikes are related to the Francois Lake Plutonic Suite, possibly the Casey phase (Anderson et al. 1998b), and predate both mineralization (Carr 1966; Dawson 1972; Anderson et al. 1998b), and the basalt and/or andesite dikes of Tertiary age (Wanless et al. 1974). Granitic dikes consist of aplite, pegmatite and quartz feldspar porphyry, and are common at the Endako deposit (Fig. 2.2), near intrusive contacts, along the Casey and Tailings Creek faults, and at Nithi mountain (Carr 1966; Dawson 1972). Cross-cutting relations among pre-mineral dikes show the chronological order of aplite (oldest), porphyritic

granite and quartz feldspar porphyry (youngest) (Dawson 1972). Tertiary basaltic and/or andesitic dikes are common at Endako (Fig. 2.2) and along the Casey Fault (Fig. 2.1).

The Endako deposit, hosted by the Endako phase of the Francois Lake Plutonic Suite, is bordered to the north by the Casey phase, and to the south by the Francois subphase of the Francois Lake Plutonic Suite, and to the east by the Jurassic-Cretaceous Stellako phase (Fig. 2.1). Additional molybdenum mineralized rocks are present within the Endako phase to the northwest and southeast of the Endako deposit, and in the Nithi phase on Nithi mountain and at Owl Lake in the Casey phase (Fig. 2.2) (Carr 1966; L'Heureux and Anderson 1997).

Structure

Major structural components of the Endako orebody include pre-mineral dikes, laminated quartz-molybdenite (ribbon-texture) veins, and Tertiary post-mineral dikes and deformation. Pre-mineral granitic dikes strike northeasterly at 40 to 45°, and dip steeply to the west or are vertical. Ribbon-textured veins have north to east–northeasterly strikes of 070 to 350°, with northwesterly dips of 20 to 60°, and westerly strikes, with southerly dips of 50 to 70°. Northwest-dipping veins are crosscut by the south-dipping vein system. These results contrast with previous determinations of age relations between vein sets by Kimura et al. (1976).

Tertiary post-ore deformation of the orebody is defined by three major cross cutting faults associated with Tertiary age basalt and/or andesite dikes (South Basalt, West Basalt and West Denak faults), and other subsidiary faults, as well as faulting and brecciation of ribbon-texture veins. Post-ore faults are marked by extensive gouge. The West Basalt fault has a 180 m dextral offset between the West Denak and East Denak ore zones (Fig. 2.2). Dips of ribbon-textured veins become shallower and possess more northerly strikes across the Endako deposit from east to west, which defines a south-

easterly tilt of the deposit steepening towards the west. These results are consistent with east to west tilts determined from paleomagnetic studies of Tertiary age dikes within the Endako deposit (Enkin et al. 1997).

Mineralized Rocks

Molybdenite is the only ore mineral, and commonly is associated with pyrite, magnetite, and minor amounts of chalcopyrite, bornite, bismuthinite, scheelite, beryl, specularite, and galena (Bysouth and Wong 1995; Dawson 1972). Two types of quartz veins host molybdenite: (1) stockwork and (2) ribbon-textured veins (Kimura et al. 1976). Minor mineralized rocks also are present as molybdenite coating fracture planes, and disseminated throughout the host rocks. Post-ore veining consists of calcite and minor amounts of chalcedony (Dawson 1972).

Stockwork Veins

Stockwork veins (1 to 5 cm wide) are concentrated in the Endako East pit, becoming progressively less common to the west and to the south. Intensity of stockwork veining is greatest on the north wall of the East Endako pit and no change in intensity of stockwork veins with depth was observed during this study. Early stockwork veins with minor molybdenite are associated with intense Type A K-feldspar alteration (see Hydrothermal Alteration Section below). Later stockwork veins, bordered by K-feldspar alteration assemblages (Types B and C) (see Hydrothermal Alteration Section below), contain predominant molybdenite with magnetite and pyrite. Molybdenite in stockwork veins is present as isolated or aggregated flakes typically < 2 mm long with a rosette texture hosted by quartz grains ≤ 4 mm diameter. Quartz grains are typically subhedral and exhibit weak to strong undulose extinction, and minor recovery textures with the presence of sub-grains.

Ribbon-Textured Veins

Laminated quartz-molybdenite (ribbon-textured) veins constitute the much of the molybdenum ore. Molybdenite in the ribbon-textured veins is typically fine-grained (< 2 mm long), silvery-blue, exhibits a platy habit, and commonly is intergrown with sericite. Ribbon veins are commonly > 5 cm wide with five to ten laminations of molybdenite, but veins locally may be as much as 1 m wide with numerous laminations (Dawson, 1972; Kimura et al. 1976). Ribbon veins are mappable, being traced from pit walls in north-south and west-east directions (see above).

Petrographic observations indicate that quartz in the ribbon veins exhibits undulose extinction, as well as recovery and brecciation textures of diverse intensities. Weakly brecciated ribbon veins are characterized by fine-grained (< 2 mm) silvery-blue molybdenite laminated with clear to milky white quartz and are bordered by a 10 to 50 cm selvage of kaolinite-altered wallrock. Quartz grains are commonly > 4 mm in diameter and exhibit strong undulose extinction, with only minor development of sub-grains. Quartz grains adjacent to molybdenite laminations exhibit complete recovery. Further strain in recovered quartz grains has not occurred because quartz grains exhibit flat-field extinction.

Moderately brecciated veins are characterized by finer-grained (1 to 2 mm), dull gray molybdenite associated with cloudy quartz and are bordered by black gouge (1 to 2 cm) and kaolinite-altered wallrock (≥ 20 cm). Quartz grains are commonly > 4 mm in diameter and exhibit minor brecciation, strong undulose extinction, and abundant sub-grain development, with complete recovery and flat-field extinction observed in quartz grains adjacent to molybdenite. Adjacent to wallrock molybdenite is striated and in thin section is characterized by sigmoidal textures.

Strongly brecciated veins are characterized by incomplete recovery of quartz and are bordered by selvages of kaolinite-altered wallrock as much as 2 m wide. The veins

contain fragments of kaolinite- and sericite-altered quartz monzonite and calcite veinlets. Calcite veins also cross cut brecciation and are therefore both syn- and post-brecciation. Molybdenite is very fine-grained (50 to 100 μm), black, exhibits a sooty texture and is supported in a black crypto-crystalline matrix of quartz. The black color may be a product of inclusions of molybdenite and is referred to as black quartz ore (Bysouth and Wong, 1995). The veins contain minor amounts of quartz fragments that have not been recrystallized, which are relics of the early Cretaceous hydrothermal system. Quartz grains are brecciated and exhibit strong undulose extinction. Pyrite grains are also highly brecciated and fragments are slightly rounded.

Hydrothermal Alteration

Three distinct hydrothermal alteration assemblages are present in the Endako deposit: (1) K-feldspar selvages; (2) quartz + sericite + pyrite selvages, and (3) kaolinite selvages (Bysouth and Wong 1995; Dawson 1972; Drummond and Kimura 1969; Kimura et al. 1976).

K-feldspar Selvages

K-feldspar alteration assemblages develop with or without a stockwork quartz vein, and typically show a network of K-feldspar veins with only minor molybdenite mineralization. K-feldspar alteration assemblages are divided into three types: Type A, K-feldspar ± quartz (typically 80 to 90 modal % K-feldspar); Type B, K-feldspar (85 modal %) + biotite (10 modal %) + quartz (5 modal %); and Type C, K-feldspar (> 60 modal %) + quartz + biotite (equal amounts) (Dawson, 1972; Drummond and Kimura, 1969). K-feldspar selvages are typically 2 to 5 cm wide, but maybe as much as 50 cm wide. Cross-cutting relationships between K-feldspar alteration assemblages show a chronological order of Type A (earliest), B and C (latest) (Drummond and Kimura 1969; Dawson 1972).

The intensity of K-feldspar alteration is defined by the abundance of stockwork veins, which are bordered by K-feldspar alteration assemblages, and the presence or absence of magmatic hornblende. K-feldspar-bearing alteration is the dominant alteration assemblage in the northern part of the East Endako pit, becoming progressively weaker to the south and to the west of the East Endako pit (Fig. 2.3). In the West Denak pit, K-feldspar alteration is almost absent (Fig. 2.3). In the East and West Endako pits, petrographic analyses have shown the nearly complete absence of hornblende. In the West Denak pit, away from faults, hornblende is present, and exhibits incomplete replacement by biotite and calcite.

Sericite Selvages

Sericite alteration assemblages are gray to whitish gray, 3 mm to 5 cm wide, and consist of quartz (50 - 60 modal %), sericite (30 - 50 modal %) and disseminated pyrite (1 -5 modal %) bordering quartz-molybdenite ± magnetite, and quartz-pyrite stockwork veins (Drummond and Kimura 1969). Sericite alteration selvages are commonly developed adjacent to quartz-magnetite stockwork veins in the magnetite-pyrite zone and adjacent to quartz-pyrite stockwork veins in the pyrite zone (Fig. 2.3) (Bysouth and Wong 1995).

Petrographic analyses indicate that areas adjacent to ribbon veins have sericite alteration assemblages. Sericite is present as aggregate clusters (typically 0.1 - 0.5 mm wide) adjacent to the ribbon veins and intergrown with the molybdenite. Plagioclase, K-feldspar, and biotite adjacent to ribbon veins are extensively altered to sericite and chlorite, with alteration decreasing in intensity away from the vein. Whole rock sericite alteration of the Endako phase results in the presence of sericite (< 0.1 - 0.5 mm) and chlorite from breakdown of K-feldspar, plagioclase, and biotite. The alteration is pervasive in the eastern part of the deposit (East and West Endako pits), decreasing in intensity to the west, and virtually absent in the West Denak pit.

Kaolinite Selvages

Kaolinite alteration assemblages contain lesser amounts of sericite, chlorite, and pyrophyllite (Drummond and Kimura 1969; Dawson 1972). Based on the extent of alteration of plagioclase, K-feldspar and biotite, the intensity of kaolinite-altered Endako phase is divided into three types, weak, moderate, and intense (Drummond and Kimura 1969).

Moderate to intense kaolinite alteration is related spatially to ribbon veins, overprinting the original sericite alteration assemblages. The intensity of kaolinite alteration is proportional to intensity of brecciation associated with the ribbon veins (see above). The kaolinite alteration bordering highly brecciated ribbon veins is as much as 2 m wide and the intensity of alteration is spatially related to major faults — East and West Endako faults, South Basalt fault, and the West Basalt fault. At increasing distances from these faults, ribbon veins have narrower kaolinite selvages (10 to 50 cm) and are bordered by a fine black gouge consisting of kaolinite and molybdenite. Intensity of kaolinite alteration of the Endako phase also decreases progressively towards the west.

Late Hydrothermal and Supergene Alteration

Post-ore hydrothermal activity is associated with calcite and minor chalcedony veining (Dawson 1972; Drummond and Kimura 1969). Calcite forms pseudomorphs after hornblende and plagioclase, and is present in veins and veinlets. Calcite veins commonly are associated with post-mineral Tertiary basalt and/or andesite dikes as veins, alteration, and amygdules.

Supergene alteration is a product of deep Tertiary weathering, and typically restricted to an oxidation zone of 1 to 20 m over the deposit (Bysouth and Wong, 1995). Supergene minerals consist of hematite, limonite, ferrimolybdite, powellite, pyrolusite, malachite, and wulfenite (Bysouth and Wong 1995; Dawson 1972; Drummond and

Kimura 1969; Kimura et al. 1976). Supergene alteration has not enhanced ore grade and none of the supergene minerals are recovered.

Analytical Work

Samples for the study were collected from the East Endako, West Endako and West Denak pits and drill cores S803, S820 and S822 from the Endako deposit. The East Denak pit was not sampled due to inaccessibility. Samples of whole-rock powders, clay mixtures and mineral separates of quartz, K-feldspar, biotite, clinochlore, sericite, calcite and kaolinite from hydrothermal alteration assemblages were isolated by conventional crushing and separation techniques for stable isotope analysis. The purity of mineral separates was determined to be > 95 % by XRD analysis, with impurities consisting of kaolinite, quartz, pyrite and molybdenite, removed by hand-picking under a microscope.

Fluid inclusion microthermometry data were obtained using a modified USGS gas-flow heating-freezing stage (Werre et al., 1979). The microthermometry stage was calibrated using pure H_2O and CO_2 fluid inclusions for freezing temperatures and the critical point of pure H_2O for heating temperatures. The uncertainties of microthermometric measurements are ± 0.2°C for freezing and ± 2°C for heating to 374°C. Salinities of fluid inclusions were calculated from final ice-melting and halite dissolution temperatures using the equations of Bodnar and Vityk (1995) and Bodnar et al. (1985) for the H_2O-NaCl system.

Oxygen isotope analyses were conducted on powdered ~10 mg aliquots of silicate and carbonate minerals. Silicate samples were loaded into Ni tubes and oxygen was liberated using BrF_5 at 600°C (Clayton and Mayeda, 1963). The oxygen was converted to CO_2 and analyzed on a Finnigan MAT 252 mass spectrometer. Carbon and oxygen isotope values of carbonates were determined from carbon dioxide, which was liberated from the sample using phosphoric acid (McCrea, 1950). Waters for hydrogen isotope analyses of silicates (whole rock and fluid inclusions in quartz) and calcite were extracted by thermal decrepitation at 1100°C (silicates) and 550°C (calcite) for 2 h. Hydrogen from the extracted water in fluid inclusions (quartz, calcite)

and the structural framework of minerals (whole rock) was generated using the zinc reduction method of Coleman et al. (1982).

Stable isotope data are reported relative to SMOW for oxygen and hydrogen (Craig 1961a) and PDB for carbon (Craig 1957), in δ notation for values in per mil (‰) and Δ_{xy} ($\Delta_{xy} = \delta_x - \delta_y$) for measured fractionation of one phase relative to another in per mil. The analytical uncertainty (1σ) is ± 0.2 ‰ for oxygen and carbon, and ± 5 ‰ for hydrogen. Kaolinite and sericite samples were shown to contain minor amounts of quartz (< 5 %); however, because of the minor amount no correction was applied to the $\delta^{18}O$ results.

Chemical analyses of the solute in fluid inclusion waters were conducted at the Institut für Geowissenschaften, Montanuniversität, Leoben, Austria using a crush-leach procedure (cf. Nesbitt and Prochaska, 1998). For the determination of solute chemistry, 1 g 1 mm grain size cleaned samples of ore quartz vein, and post-mineral calcite veins were ground in 5 mL of double-distilled water using an agate mortar and pestle. The sample was centrifuged to separate the ground sample residue and leachate. Anions (Cl, Br, and I) of the leachate were analyzed by ion chromatography using a Dionex DX – 500 system with a micromembrane suppressor, with detection limits of an order of magnitude (0.1 ppb) better than systems without autosuppression. Na and K were analyzed by standard atomic absorption spectrometry. The results presented in Table 2.5 and Figure 2.9 are given as ionic ratios, because the amount of anion and cation dilution is not known.

Fluid Inclusion Study

A fluid inclusion study was undertaken to constrain the P–T–X history of vein-forming fluids of the Endako deposit. Microthermometric analyses were performed on samples of stockwork quartz + molybdenite veins bordered by K-feldspar alteration assemblages, stockwork quartz + magnetite + pyrite + molybdenite veins, ribbon quartz + molybdenite veins bordered by sericite alteration assemblages, and post-mineralization calcite veins. In addition, a detailed study of a single ribbon quartz + molybdenite vein

(sample WD1) was conducted. The locations of the samples analyzed are shown on Figure 3.3.

Petrography of Fluid Inclusions

Fluid inclusions are divided into three populations on the basis of petrography and microthermometry. These types include: Type 1, moderate salinity, typically liquid-rich two phase inclusions, with rare opaque and translucent daughter minerals; Type 2, low salinity, liquid-rich two-phase inclusions, and Type 3, liquid-rich inclusions containing a halite daughter phase. This classification scheme is similar to that of Dawson (1972) and Bloom (1981).

Type 1 fluid inclusions: These fluid inclusions were observed in both stockwork and ribbon veins. Type 1 fluid inclusions are typically isolated, randomly distributed, ranging in size from < 5 μm to a maximum of 15 μm and generally have negative crystal shapes, and are interpreted to be primary. Type 1a fluid inclusions homogenize by vapor bubble disappearance, whereas Type 1b fluid inclusions homogenize by critical behavior. Type 1a fluid inclusions are dominant in all ore vein types, while Type 1b fluid inclusions are more abundant in quartz veins with K-feldspar alteration assemblages than in veins with sericite alteration assemblages. Type 1 fluid inclusions typically do not contain daughter phases. However, observed translucent daughter phases are < 2 μm in size, rhombic to anhedral with a relief greater than halite and quartz, and exhibit high birefringence, and straight extinction along the crystal edges. These daughter phases are possibly sulfate or carbonate minerals.

Type 2 fluid inclusions: These fluid inclusions range in size from < 5 μm to a maximum of 10 μm, have irregular, elongate and oblate shapes, and homogenize by vapor bubble disappearance. Type 2 fluid inclusions typically are secondary, and are present as random oriented trails in stockwork veins or as trails adjacent to molybdenite in ribbon veins and are dominant in brecciated ribbon veins, and are present as primary

fluids inclusions in post-ore calcite veins. Type 2 fluid inclusions in quartz veins are less abundant than Type 1 fluid inclusions, though the abundance may reflect the number of inclusions large enough for microthermometric study. The distinction of Type 2 fluid inclusions from Type 1 inclusions without daughter phases is determined on the basis of degree of fill, salinity and homogenization temperatures (Table 2.1).

Type 3 fluid inclusions: These fluid inclusions are primary, range in size up to a maximum of 10 μm, and have negative crystal shapes. Type 3a fluid inclusions homogenize by vapor bubble disappearance and Type 3b fluid inclusions homogenize by halite dissolution (Bloom 1981). Type 3a fluid inclusions are rare, and only present in stockwork veins bordered by a Type A K-feldspar alteration assemblage. Type 3b fluid inclusions were observed by Bloom (1981), but not in this study. The paragenetic relationship between Type 3 and 1 inclusions is unresolved.

Salinity and Homogenization Results

Type 1 fluid inclusions: Fluid inclusion microthermometry data are reported in Table 1. Eutectic (Te) and final ice-melting (Tfm) temperatures were difficult to determine because of the small size of the fluid inclusions, high degree of fill, and cloudy nature of the quartz. Te values were only obtained for seven Type 1 fluid inclusions and temperatures vary between –50 and –27°C. Te values are below the eutectic for the H_2O-NaCl and H_2O-NaCl-KCl systems (Hall et al. 1988), which suggests the presence of components other than NaCl and KCl.

Tfm values of Type 1 fluid inclusions are between –3.2 and –10.8°C (n = 176), with Tfm values dominantly between –4.4 and –6.7°C. These temperatures indicate salinities between 5.3 and 14.8 wt. percent NaCl eq. (Fig. 2.4A). Type 1a fluid inclusions have a mode in the salinity data occurring at 7 to 9 wt. percent NaCl eq. and the data are skewed to higher salinities. Type 1b fluid inclusions have a mode occurring at 10 to 11

wt. percent NaCl eq. and are skewed to lower salinities. Type 1a and 1b fluid inclusions in K-feldspar (n = 3) have salinities between 6.6 and 7.7 wt. percent NaCl eq.

Homogenization temperatures (Th) for Type 1 fluid inclusions are between 250 and 440°C, with a few at higher temperatures (Fig. 2.4B). These values are similar to those obtained by Dawson (1972) and Bloom (1981). Th values of Type 1a fluid inclusions span almost the entire range of the Th values and have a mode at 360 to 370°C. Type 1b fluid inclusions typically homogenize at temperatures above 360°C (Fig. 2.4B). Type 1a and b fluid inclusions in veins bordered by K-feldspar alteration assemblages predominantly have Th values between 390 and 430°C. Th values of 355, 417 and 425°C from Type 1a fluid inclusions in hydrothermal K-feldspar were determined. Type 1a and b fluid inclusions in veins bordered by sericite alteration assemblages predominantly have Th values between 360 and 400°C.

Type 2 fluid Inclusions: Te values were not observed for Type 2 fluid inclusions. Tfm values for Type 2 fluid inclusions in quartz veins are between –0.1 and –3.1°C, with the majority of Tfm values between –1.8 and –2.7°C. These temperatures indicate a salinity between 0.2 and 5.1 wt. percent NaCl eq. with a mode occurring at 3 to 5 wt. percent NaCl eq. (Fig. 2.4C). Th values of Type 2 fluid inclusions in quartz veins are between 130 and 285°C, with a mode occurring at 190 to 230°C (Fig. 2.4D). Based on two fluid inclusion determinations of a post-mineral calcite vein (sample 3146.12) Type 2 fluid inclusions have salinities of 3.1 to 4.2 wt. percent NaCl eq., and Th values of 208 and 210°C.

Type 3 fluid Inclusions: Dissolution of halite is the first phase transition observed during heating of Type 3a fluid inclusions. Halite dissolution temperatures (ThH) are between 167 and 370°C (n = 5). Assuming a H_2O-NaCl system, these dissolution temperatures indicate salinities between 30 and 45 wt. percent NaCl eq. (Bodnar and Vityk, 1995). Type 3a fluid inclusions homogenize by vapor bubble disappearance

between 375 and 420°C, with a mode occurring at 410 to 420°C. Type 3b fluid inclusions were not observed in this study, but Bloom (1981) only reports final fluid inclusion homogenization ThH values, which are between 380 and 420°C, and a value of 550°C, representing salinities of 45 and 49, and 66 wt. percent NaCl eq., respectively. The homogenization temperatures of Type 3b fluid inclusions are similar to higher than compared to Type 3a fluid inclusions.

Fluid Inclusion Trapping Conditions

Trapping conditions of Type 1, 2 and 3 fluid inclusions were obtained from H_2O-NaCl P-T diagrams, constructed using iso-Th lines (equivalents to constant density isochores) from the data of Bodnar (1994), and Bodnar and Vityk (1995). P-T conditions are constrained using the dry solidus of a granite (Piwinskii and Wyllie 1970) and a fluorine-rich granite (Manning 1981) (Fig. 2.5A and C). The latter is representative of the composition and fluorine content of the Endako granite. P-T estimates for vein-forming fluids are reported in Table 2.2.

Type 1 fluid inclusions: On Figure 2.5A the stippled areas between the 7 and 10 wt. percent NaCl eq. iso-Th lines represent trapping conditions of Type 1 fluid inclusions. P–T conditions of trapping are constrained by the fluorine-rich solidus, yielding pressures between 1.6 and 0.2 kbar and temperatures between 560 and 360°C, respectively. Trapping conditions of Type 1 fluid inclusions of stockwork veins bordered by K-feldspar alteration assemblages are discussed below.

Ribbon veins bordered by sericite alteration assemblages are paragenetically later than stockwork veins bordered by K-feldspar alteration assemblages. Fluids responsible for formation of ribbon veins are represented by Type 1 fluid inclusions and were probably trapped at pressures equal to, or lower than fluids represented by Type 3 (see below) and 1 fluid inclusions in veins bordered by K-feldspar alteration assemblages (Table 2.2; Fig. 2.6).

Ribbon veins were generated by periodic dilation of the vein-hosting fractures (Dawson 1972), with the outer parts of the veins being older than the central parts. The vein-forming fluids possessed a range in salinities between 6 and 13 wt. percent NaCl eq., most commonly between 7 and 8 wt. percent NaCl eq. Fluid inclusions analyzed in a ribbon vein (WD1) at the vein edge; next to the vein edge; next to center of the vein; and at the center of vein show no correlation between salinity and homogenization temperatures (Fig. 2.7). These data suggest that salinities and temperatures of ore forming fluids represented by Type 1 fluid inclusions in ribbon veins were fairly constant throughout the process of mineralization.

Type 2 fluid inclusions: The stippled and horizontally shaded areas on Figure 2.5B represent the P-T conditions for Type 2 inclusions for salinities of 1 and 5 wt. percent NaCl eq., respectively. Type 2 fluid inclusions of quartz veins are secondary, and were most likely trapped at pressures and temperatures lower than those of Type 1 fluid inclusions. Type 2 fluid inclusions of calcite veins represent fluids associated with post-ore fluids. Calcite veins cross cut Tertiary basalt and/or andesite dikes, which exhibit vesicular and glassy textures. These textures suggest a hypabyssal setting of dike intrusion, with pressures $\leq$ 0.5 kbar (Sparks et al. 1994), which suggests that the trapping conditions for Type 2 inclusions were at a pressure $\leq$ 0.5 kbar, and at temperatures between 190 and 300°C. Furthermore, trapping temperatures interpreted for Type 2 fluid inclusions are suggested from the Ar systematics of biotite from the Francois Lake Plutonic Suite of the Endako area (Villeneuve et al. 1999). Kaolinite alteration assemblages overprint sericite alteration assemblages (quartz + sericte + pyrite). Kaolinite will coexist with quartz below 350°C (Thompson 1970), which suggests that fluids represented by Type 2 fluid inclusions probably were responsible for development of kaolinite alteration assemblages.

Type 3 fluid inclusions: Trapping conditions of Type 3a and 3b inclusions with salinities of 30-45 wt. percent NaCl eq. are portrayed respectively by horizontally and vertically shaded areas on Figure 2.5C. These areas yield trapping pressures between 0.3 and 2.8 kbars, and temperatures between 370 and 530°C (Fig. 2.5C). Iso-Th lines, which intersect the dry and fluorine-rich solidi, give an upper pressure limit (~2.8 kbars; Fig. 2.5C), which yields a depth (approximately 10 km assuming lithostatic pressures) greater than generally reported for many other porphyry systems (Nash 1976; Theodore and Menzie 1984; Beane and Bodnar 1995). However, the potential range of trapping conditions for Type 3 fluid inclusions encompass the P–T conditions suggested for porphyry systems (e.g., Nash 1976; Theodore and Menzie 1984; Beane and Bodnar 1995).

The association of Type 3b fluid inclusions with a particular alteration assemblage and paragenetic relationship to Type 3a fluid inclusions is unknown. However, Type 3a fluid inclusions are only present apparently in stockwork quartz veins bordered by the Type A, K-feldspar alteration assemblages, which suggests similar timing for fluids represented by Type 3b fluid inclusions. The absence of low-salinity, vapor-rich fluid inclusions coexisting with saline fluid inclusions (Dawson 1972; Bloom 1981; this study) suggests that Type 3 fluid inclusions were not generated through immiscibility of hydrothermal fluids at any time during evolution of the hydrothermal system at Endako.

Type 3a fluid inclusions coexisting with Type 1 fluid inclusions yield an upper limit of P–T conditions of trapping for stockwork veins bordered by K-feldspar alteration assemblages (Table 2.2; Fig. 2.6). The constrained P–T conditions of fluid inclusion entrapment using the fluorine-rich solidus, and Type 1 fluid inclusions (Fig. 2.5A and 2.6), Type 3b fluid inclusions were most likely trapped at pressures greater than Type 3a fluid inclusions (Fig. 2.5C). Fluids represented by Type 3b fluid inclusions may have

been trapped under lithostatic conditions, whereas Type 3a fluid inclusions may have formed following a pressure-drop from lithostatic to hydrostatic conditions during hydro-fracturing (Burham 1979; Cline and Vanko 1995). The Endako phase contains miarolitic cavities, which suggest that it is an epizonal plutonic body developed at pressures ≤ 2 kbars (Candela and Blevin 1995). To account for the presence of miarolitic cavities in the Endako phase and to yield geologically reasonable depths of mineralization under lithostatic pressures an upper limit of 2 kbars is assumed for the pressure conditions during trapping of Type 3b fluid inclusions.

Stable Isotope Study

The full stable isotope data set is presented in Appendix I. A synopsis of the oxygen isotope data is presented in Table 2.3. Least-altered whole rock samples of the pre-mineral dikes possess $\delta^{18}O$ values between 6.2 and 6.9 per mil (n = 4). Whole rock samples of K-feldspar alteration assemblages yield $\delta^{18}O$ values between 6.3 and 7.5 per mil, with a mean value of 6.8 ± 0.4 per mil (n = 7). Samples of moderate to intensive kaolinite-altered Endako phase yield $\delta^{18}O$ values between 5.5 and 6.6 per mil, with a mean of 5.8 ± 0.6 per mil (n = 3), and between 5.2 and 7.5 per mil, with a mean of 6.2 ± 1.1 per mil (n = 5), respectively. Whole rock samples of post-ore basalts yield $\delta^{18}O$ values between –2.4 and 4.5 per mil, with a mean of 1.3 ± 2.2 per mil (n = 6).

Hydrothermal biotite samples yield $\delta^{18}O$ values between 2.0 and 4.5 per mil, with a mean of 3.5 ± 0.8 per mil (n = 8). Lower $\delta^{18}O$ values (2.0 to 3.0 ‰) are recorded from biotite samples with the host rock exhibiting a greater intensity of kaolinite alteration. The range in $\delta^{18}O$ values exhibited by biotite suggests that oxygen isotope exchange occurred between biotite and a later hydrothermal fluid (see below). A single clinochlore sample from a kaolinite alteration assemblage has an $\delta^{18}O$ value of –2.1 per mil.

Hydrothermal K-feldspar samples possess $\delta^{18}O$ values between 2.5 and 6.6 ‰, with a mean of 5.3 ± 1.4 per mil (n = 8). Lower $\delta^{18}O$ values (4.2 and 5.5 ‰) are recorded from K-feldspar samples with the Endako quartz monzonite exhibiting a greater intenisty of kaolinite alteration, with one sample, with minor sericite alteration, possessing an $\delta^{18}O$ value of 2.5 per mil.

Samples of stockwork quartz veins bordered by K-feldspar alteration assemblages, yield $\delta^{18}O$ values between 8.0 and 8.8 per mil, with a mean value of 8.4 ± 0.2 per mil (n = 9). Samples of ribbon vein quartz with sericite alteration assemblages possess $\delta^{18}O$ values between 6.7 and 9.3 per mil, with a mean of 8.4 ± 0.6 per mil (n = 13). Of the thirteen samples of ribbon vein quartz analyzed, twelve samples yield $\delta^{18}O$ values between 8.0 and 9.3 per mil, and one sample has a $\delta^{18}O$ value of 6.7 per mil. The latter sample is of a highly brecciated ribbon vein bordered by a sericite alteration assemblage, which was overprinted by kaolinite alteration.

Sericite and kaolinite yield $\delta^{18}O$ values of 5.6 per mil, and between 6.6 and 6.8 per mil, respectively. Two clay mixtures, montmorillonite + illite, and montmorillonite + nontronite + illite from the fault gouge of the South Basalt fault have $\delta^{18}O$ values of 2.1 and 5.7 per mil, respectively.

Carbon isotope results are shown in Table 2.3. Samples of carbonate altered whole rock samples have $\delta^{18}O$ values between 5.5 to 11.1 per mil and $\delta^{13}C$ values between –2.5 and –4.9 per mil. Samples of vein calcite have $\delta^{18}O$ values between –3.8 and 12.7 per mil with values commonly between 2.6 and 12.7 per mil, and a mean of 7.3 ± 3.2 per mil (n = 22). The $\delta^{13}C$ values for the samples vary between –2.0 and –6.2 per mil.

Hydrogen isotope data are presented in Table 2.3. Whole rock samples of K-feldspar alteration assemblages, containing between 5 and 10 percent biotite, yield δD values between –134 and –167 per mil, with a mean of –153 ± 17 (n = 3).

The hydrogen isotope compositions of hydrothermal fluids are shown in Figure 2.8. Waters from fluid inclusions of stockwork quartz yield δD values between –125 and –150 per mil, with a mean of –137 ± 10 per mil (n = 6). Fluid inclusion waters extracted from two samples of hydrothermal K-feldspar yield δD values of –146 and –162 per mil. Waters from fluid inclusions of ribbon-textured veins with sericite alteration assemblages yield δD values between –105 and –173 per mil, with a mean of –145 ± 24 ‰ (n = 9). Calculated hydrogen isotope compositions of a hydrothermal fluid associated with kaolinite are between –138 and –141 per mil (see below). Post-ore (Tertiary age) calcite veins have δD values between –105 and –147 per mil, with a mean of –117 ± 20 per mil (n = 4).

Considerations of Equilibrium and Hydrothermal Fluid Temperatures

If oxygen isotope equilibrium is attained and preserved between coexisting minerals of K-feldspar and sericite alteration assemblages, then measured isotopic fractionation values can be used to determine temperatures of the hydrothermal fluid from which they formed (O'Neil 1986). Oxygen isotope fractionations between the mineral pairs: quartz-K-feldspar (Δq-f) and quartz-biotite (Δq-b) are given in Tables 2.4a and 2.4b. The temperatures of mineralizing fluids, calculated using experimentally determined fractionation factors of Chacko (1993) and Chacko et al. (1996) for Δq-f and Δq-b fractionation values, range between 200 and 460°C, and 290 and 490°C, respectively (Table 2.4a and 2.4b). The higher calculated temperatures from the Δq-f (1.7 = 460°C and 1.8 = 440°C) and Δq-b fractionation values (3.7 = 490°C, and 4.2 = 460°C) are in close agreement with primary fluid inclusion trapping temperatures of quartz veins associated with K-feldspar alteration assemblages. The higher calculated temperatures from Δq-f and Δq-b fractionation values overlap trapping temperatures of primary fluid inclusions in quartz veins associated with K-feldspar and sericite alteration assemblages, and suggest that quartz, K-feldspar, and biotite represent oxygen isotope

equilibrium. However, the larger Δq-f (3.5) and Δq-b (6.8) values, which yield temperatures not in agreement with the primary fluid inclusion data suggest that oxygen isotope equilibrium was not maintained. The latter suggests that K-feldspar and biotite exchanged oxygen isotopes with post-ore fluids.

Isotopic Composition of the Hydrothermal Fluids

Alteration Fluids: Measured and calculated $\delta^{18}O$ and δD fluid composition values are given in Table 3 and Figure 2.9. The calculated $\delta^{18}O$ fluid compositions were determined from $\delta^{18}O$ values of quartz, K-feldspar, biotite and kaolinite using the quartz-water fractionation factor of Matsuhisa et al. (1979); the K-feldspar-water fractionation factor of O'Neil and Taylor (1967); the combined K-feldspar-water, and K-feldspar-biotite fractionation factors of O'Neil and Taylor (1967) and Chacko et al. (1993, 1996); and the kaolinite-water fractionation factor of Land and Dutton (1978). The calculated δD fluid compositions for kaolinite were determined using the kaolinite-water fractionation factor of Gilg and Sheppard (1996).

$\delta^{18}O$ values of fluids producing the K-feldspar alteration are calculated using an average temperature (440°C) determined from Δq-f (2.3 to 1.7) and Δq-b (≤ 5.0) fractionation values, which are in close agreement with the interpreted fluid inclusion trapping temperatures for hydrothermal fluids associated with K-feldspar alteration. Calculated $\delta^{18}O$ values for fluids that produced K-feldspar alteration are derived using $\delta^{18}O$ values of stockwork vein quartz, and hydrothermal K-feldspar, and biotite $\delta^{18}O$ values that possess Δq–f and Δq–b values, which yield temperatures similar to those determined for fluid inclusion trapping temperatures. Calculated $\delta^{18}O_{fluid}$ values are 5.2 ± 0.2 per mil for quartz, 4.0 ± 0.5 per mil for hydrothermal biotite, 3.8 ± 0.6 per mil for hydrothermal K-feldspar. Fluids from fluid inclusions of quartz stockwork veins yield δD_{FI} (δD_{FI} = hydrogen isotope composition of fluid inclusion waters) values between –125 and –150 per mil.

The $\delta^{18}O$ values of fluids producing sericite alteration assemblages based on the $\delta^{18}O$ values of ribbon vein quartz and using a temperature of 380°C (determined from fluid inclusion trapping temperatures, and stable isotope thermometry) using the calculations yield 3.9 ± 0.6 per mil. Hydrogen isotope composition of hydrothermal fluids associated with sericite alteration are between –105 and –173 per mil.

The $\delta^{18}O$ and δD fluid compositions determined for kaolinite alteration assemblages were calculated from $\delta^{18}O$ and δD values of kaolinite using temperatures of 190 and 300°C (temperatures determined from fluid inclusion thermometry). The calculations yielded $\delta^{18}O$ fluid compositions between 2.1 and –2.2 per mil, and δD fluid compositions between –138 and –141 per mil.

Post-Ore Fluids: The oxygen, carbon and hydrogen isotope ratios of calcite veins from the Endako deposit are similar to values of equivalent Tertiary-age calcite veins from country rocks in the Endako area (Magaritz and Taylor 1976; R. W. King unpub. data). The $\delta^{13}C$ values of calcite veins from Endako (–2.0 to –6.2 ‰) are higher than typical values for magmatic carbon (–5 to –8 ‰; Taylor et al. 1967) and below the range of marine limestones values (–1 to 2 ‰; Ohmoto 1986).

The $\delta^{18}O$ compositions of fluids, which formed the calcite veins, were determined from $\delta^{18}O$ values of calcite using the fractionation factor of O'Neil et al. (1969), at temperatures of 190 and 300°C. The calculated $\delta^{18}O$ values of the vein forming fluids are between 7.6 and –13.4 per mil, with means of –2.7 per mil at 190°C, and 2.2 per mil at 300°C, which are similar to the $\delta^{18}O_{fluid}$ values for the formation of kaolinite. The range in $\delta^{18}O$ fluid compositions (7.6 to –13.4 ‰, Fig. 2.10) cannot singularly be accounted for by differences in temperatures of vein formation. Mixing of approximately 0 to 50 percent of Tertiary meteoric water ($\delta^{18}O$ = –20 ‰; Zaluski et al. 1994) with magmatic water of basalt and/or andesite composition ($\delta^{18}O$ = 6 ‰; Taylor and Sheppard 1986) could generate the $\delta^{18}O_{fluid}$ values calculated for calcite formation. Alternatively, a single

low ^{18}O fluid underwent oxygen isotope evolution under different water/rock ratios, an interpretation for the formation of calcite veins of equivalent Tertiary-age in the Endako area suggested by Magaritz and Taylor (1976) and R. W. King (pers. comm. 1997).

Solute Chemistry of Fluid Inclusion Waters

In this study, fluid inclusion waters in six samples from Endako were analyzed to determine selected solute chemistry of hydrothermal fluids associated with vein formation. Two quartz vein samples associated with K-feldspar alteration assemblage, two-ribbon quartz vein associated with sericite alteration assemblage and two calcite post-ore veins were analyzed.

Fluid inclusion solute chemistry data are summarized in Table 2.5. Results of solute chemistry analyses of ore-related and post-ore veins of Endako are plotted on Br/Cl vs. Br/Na, Br/Cl vs. Na/K, and I/Br vs. I/Cl diagrams (Fig. 2.11). Solute chemistry of veins associated with K-feldspar and sericite alteration assemblages possesses no distinct differences. The solute chemistry of ore-related quartz veins possess similar I/Br, similar to slightly lower Br/Cl; and similar to higher Br/Na, Na/K, and Cl/Br ratios than post-ore calcite veins (Table 2.5). Using the Na/K ratio determined from solute chemistry analyses of the quartz veins and the Na/K geothermometer of Fournier and Truesdell (1973) similar temperatures to those determined from fluid inclusion and stable isotope thermometry analyses were calculated (Table 2.5 and see above).

The I/Cl ratios of the quartz veins are lower than calcite vein sample EqmL3.Cc, though similar to sample 2706.8Cc. The molar ratios determined from two calcite post-ore vein analyses differ notably from each other and temperatures calculated using the Na/K geothermometer are significantly higher (564 and 1003°C) than those interpreted to represent fluid inclusion trapping temperatures (190 to 300°C). The high temperatures may be generated by non-equilibrium between albite and K-feldspar, suggesting that

either the Na/K ratio of the hydrothermal fluid is controlled by an alternative reaction, and/or hydrothermal fluids are Ca-rich (Fournier and Truesdell 1973). These possibilities are both likely, firstly because the hydrothermal fluids are associated with calcite vein formation. Secondly, Type 2 fluid inclusion waters are interpreted to be related to kaolinite formation, therefore the Na/K ratio of the hydrothermal fluid is controlled by K-feldspar breakdown to kaolinite, which liberates K to the hydrothermal fluid.

Because the ore veins from Endako host more than one generation of fluid inclusions, it is likely that solute chemistry data of fluid inclusion waters may not correspond to the initial primary ore fluid. Secondary fluid inclusions (Type 2) were distinguished from primary fluid inclusions (Type 1) based on microthermetric behaviour (see above). Of the 227 liquid-rich fluid inclusions analyzed, 55 (~24 %) were of Type 2 fluid inclusions. The minor abundance of secondary fluid inclusions and typically smaller than Type 1 fluid inclusions suggests that the solute chemistry values probably reflect values of the primary vein-forming fluids. The secondary fluids are also low in salinity, minimizing their impact on solute studies of the quartz ore veins.

Discussion

Hydrothermal Alteration

Early stockwork quartz veins are bordered by K-feldspar alteration assemblages, and contain only minor molybdenite. The major molybdenum-bearing veins are structurally controlled ribbon-textured quartz veins with sericite-bearing alteration assemblages, which post-date the stockwork veins. The sericite assemblages were overprinted by a kaolinite alteration assemblage.

Dawson (1972) and Kimura et al. (1976) state that kaolinite alteration assemblages bordering ribbon veins from Endako were products of waning stage of the early Cretaceous ore system. This study documents an alteration assemblage of quartz-sericite-pyrite bordering ribbon veins, overprinted by an alteration assemblage of

kaolinite and chlorite. The kaolinite alteration overprint is related spatially to Tertiary basalt dikes, and post-ore faults, with the intensity of alteration being proportional to intensity of brecciated ribbon veins and wallrock, and calcite veins. The spatial relationship between Tertiary basalt dikes, faults and calcite veining suggests a Tertiary age for the kaolinite.

Th values of ribbon veins with sericite alteration assemblages with a kaolinite overprint are greater than 350°C (Dawson 1972; Bloom 1981; and this study). This temperature exceeds the stability of kaolinite coexisting with quartz (Thompson 1970). Temperatures necessary for kaolinite formation are consistent with trapping temperatures of Type 2 fluid inclusions of 190 to 300°C. Thus, the kaolinite overprint on the sericite alteration assemblages formed during a later, low temperature (≤ 350°C) event.

Calculated δD_{fluid} values for fluids in equilibrium with kaolinite from Endako are 20 per mil heavier than δD_{FI} values of Endako ore-bearing quartz veins, and is similar to Tertiary meteoric water (this study, determined from calcite veins and Zaluski et al. 1994). The similarity of these values further suggests a Tertiary age for kaolinite. Furthermore, Tertiary basalt and/or andesite dikes, faults, and calcite veins are not commonly observed outside the Endako mine (Dawson 1972, R.W. King pers. comm., 1997; this study). However, where Tertiary dikes are present, e.g., Casey Fault, calcite veins and kaolinite alteration is also present. This study reports kaolinite alteration to be common near post-ore faults and Tertiary dikes, synchronous with calcite veins, and the intensity of the alteration to be proportional to the intensity of brecciation of ribbon veins and faults. The latter suggests that Tertiary hydrothermal fluids were not pervasive, but focused along faults.

Origins of Low δD Fluids

Hydrogen isotope analyses of vein quartz from K-feldspar and sericite alteration assemblages from the Endako deposit differ markedly from δD values typically reported

from high temperature alteration stages of porphyry deposits (δD = –55 to –100 ‰) (Taylor 1979) and magmatic fluids (δD = –40 to –80 ‰) (Taylor and Sheppard 1986). The low δD_{FI} values from ore–stage quartz may accurately reflect the primary ore fluid, or be a mixture of fluid inclusion populations, a contamination by hydrous phases, or a product of hydrogen diffusion. The minor abundance of small secondary inclusions relative to Type 1 fluid inclusions, and the removal of most visible hydrous phases by handpicking suggest that the δD_{FI} values reflect values of primary vein-forming fluid at Endako. Experimental studies have showed that hydrogen will diffuse between an external medium and the fluid inclusion at temperatures > 600°C (Sterner et al. 1995). However, a temperature necessary for hydrogen diffusion was not recognized at Endako, and therefore, it is unlikely that this process altered the δD values of the quartz veins.

Additional evidence for primary low δD values in the vein-forming fluids at Endako is derived from the geologically similar molybdenum mineralization in the Nithi phase at Nithi Mountain (Dawson 1972; L'Heureux and Anderson 1997). Hydrogen isotope ratios were determined from three veins with K-feldspar alteration assemblages from Nithi Mountain. The veins are dominated by liquid-rich Type 1 fluid inclusions, similar to those observed at Endako (R. L'Heureux pers. comm. 1997). Quartz veins from Nithi Mountain possess δD_{FI} values of –148, –152 and –157 per mil, which are similar to δD_{FI} values of quartz with K-feldspar alteration assemblages from Endako. At Nithi Mountain Tertiary dikes and post-ore calcite veins are absent (R. L'Heureux pers. comm. 1997). Absence of Tertiary hydrothermal activity at Nithi Mountain and correlation of δD values with Endako suggest that low δD fluids are not a product of a Tertiary hydrothermal overprint, but reflect values of the primary hydrothermal fluid associated with molybdenum mineralization.

Ore Fluids

The microthermometric data from the stockwork veins bordered by K-feldspar alteration assemblage show that the early fluids were saline brines (≥ 40 wt. % NaCl eq.) represented by Type 3 fluid inclusions. The interpretation of microthermometry data of Type 3b fluid inclusions of Bloom (1981) yield trapping pressures of 1.4 to 2 kbars. The upper pressure limit of 2 kbars is constrained using stable isotope (~440°C) geothermometry and geologically reasonable depths for emplacement of porphyry systems under lithostatic pressure conditions (Figs. 2.5 and 2.6). To explain trapping conditions of fluids represented by Type 1 and 3a fluid inclusions, without an increase in temperature, which would be above the fluorine-rich solidus, a pressure drop of approximately 0.6 to 0.8 kbars is required (Figs. 2.5 and 2.6). The data suggest that saline fluids (Type 3b fluid inclusions) were trapped at lithostatic conditions, with fluids of Type 3a and 1 fluid inclusions trapped in a system evolving from lithostatic to hydrostatic pressures. Absence of vapor-rich fluid inclusions and the presence of inclusions that homogenize by halite dissolution suggest that the Type 3 fluid inclusions were not a product of fluid immiscibility. Theoretical studies of Cline and Bodnar (1991), and fluid inclusion studies of Cline and Bodnar (1994), and Cline and Vanko (1995) show that saline brines can exsolve directly from a magma during early crystallization in batholithic systems. A similar origin is proposed for saline fluids at Endako. The salinity of aqueous fluids from Endako is compatible with a fluid exsolving from a magma crystallizing at pressures ~2 kbars (Cline and Bodnar 1991). Similar pressures were determined from microthermometry data of the Endako deposit.

Fluids trapped by Type 1 fluid inclusions characterize veins associated with sericite alteration assemblages, representing trapping conditions between 0.3 and 0.8 kbars and 360 and 440°C (Figs. 2.5A and 2.6). A detailed study of one ribbon vein (WD1) shows no correlation between salinity and homogenization temperatures and the

location of Type 1 fluid inclusions within the vein (Fig. 2.6). It is therefore suggested that salinities and temperatures remained relatively constant throughout formation of the ribbon veins.

The high salinity of fluids associated with early stockwork veins and K-feldspar alteration assemblages, and low salinity of fluids which formed the ribbon veins may explain why early veins have minor molybdenite or are barren, whereas ribbon veins are the major ore-bearing veins. Candela and Holland (1984) suggest that molybdenum is transported as a hydroxyl complex, and with increasing fluid salinity the solubility of this complex decreases (Keppler and Wyllie 1991). These data may explain the why the major molybdenum ore at the Endako deposit is hosted by the ribbon veins.

Comparisons of Data from Endako with Other Hydrothermal Systems

Fluid inclusion types commonly reported for porphyry Cu and Mo systems are liquid-rich, vapor-rich, liquid-rich with halite daughter phase, and CO_2-bearing inclusions (Beane and Bodnar 1995). Fluid inclusion studies of molybdenum deposits have mainly been reported on the high fluorine type e.g., Questa, Hudson Bay, Climax, Henderson, Central City, Hall (Hall et al. 1974; Kamilli 1978; Bloom 1981; Smith 1983; Shaver 1991; Rice et al. 1985; Carten et al. 1988; Cline and Vanko 1994), with fewer studies on low fluorine systems (Dawson, 1972; Bloom 1981; Theodore and Menzie 1984; Hall et al. 1984; Theodore et al. 1992 and references therein). Fluid inclusion studies of high fluorine systems emphasize the abundance of coexisting saline (30 to 65 wt. % NaCl eq.) and vapor-rich inclusions, and low to moderate salinity fluid inclusions (1 to 20 wt. % NaCl eq.) and CO_2-bearing fluid inclusions, which have Th values typically between 300 to 450°C. Whereas, coexisting low to moderate salinity (1 to 10 wt. % NaCl eq.) liquid-rich and vapor-rich fluid inclusions, and CO_2-bearing fluid inclusions, with less abundant saline (30 to 60 wt. % NaCl eq.) fluid inclusions, and Th values typically between 250 and 450°C are common fluid inclusion characteristics of low fluorine systems. The fluid

inclusion characteristics of both high and low fluorine systems are similar to those of Endako, though at Endako vapor-rich and CO_2-bearing fluid inclusions are absent (Dawson 1972; Bloom 1981; this study). Further, saline fluid inclusions that homogenize by halite dissolution present at Endako are absent from other low fluorine systems (Theodore et al. 1992). At Endako, the presence of saline fluid inclusions that homogenize by halite dissolution, with vapor-rich fluid inclusions absent, the process of fluid immisciblity generating the high saline hydrothermal fluids represented by these fluid inclusions may be precluded. Cline and Vanko (1995) report saline fluids at Questa trapped by fluid inclusions that do not coexist with vapor-rich inclusions, and interpret these fluids to have been exsolved directly from the crystallizing melt, which is also suggested for the saline hydrothermal fluids of Endako.

Low δD values of early fluids of porphyry Cu ± Mo deposits relative to the δD values typically reported from early stage high temperature fluids of porphyry deposits and magmatic fluids have been reported by few other studies (Batchelder 1977; Theodore et al. 1992; Sheets et al. 1996). The Latter report δD values between –76 and –138 ‰. Sheets et al. (1996) explained the deuterium depleted hydrogen isotope ratios by the incorporation of external low deuterium material into the crystallizing magma, either from the incorporation of chemically evolved meteoric fluids or crustal rock assimilation. The ability to identify crustal assimilation using rubidium and strontium isotopic compositions in the Endako area is difficult based on the uniformity of initial strontium isotope values of country rocks (Armstrong unpub. data). The $^{18}O_{fluid}$ values of quartz ore-bearing veins (5.2 ± 0.2) from Endako are relatively depleted in ^{18}O in comparison to those typically of porphyry deposits and magmatic fluids (7 to 9 ‰, Taylor and Sheppard 1986; Taylor 1979), and those of low fluorine deposits (Theodore et al. 1992). Oxygen and hydrogen isotope data suggest the involvement of meteoric fluids mixing with the magmatic fluids over the crustal assimilation of low deuterium material at Endako.

The solute chemistry of the ore-related fluids at Endako have been determined; however, solute chemistry for other porphyry Mo deposits is absent and comparison of these data is limited to studies from other ore-related magmatic systems (St. Austell, Cornwall, Botrell and Yardley 1988; Babine Lake, British Columbia, R. W. Sheets unpub. data; Porgera, Papua New Guinea, Richards et al. 1997; Capitan Pluton, USA, Campbell et al. 1995). The ore-related fluids at Endako have lower Br/Cl and Br/Na values in comparison to ore fluids of St. Austell, Porgera and Babine Lake, and higher values compared with fluids from Capitan Pluton (Fig. 2.11). The I/Cl vs. I/Br values of ore fluids of Endako and Porgera are high relative to the fluids from Capitan Pluton, early stage fluids from Babine Lake, and St. Austell (Fig. 2.11). The low Br/Na, Br/Cl, and I/Cl values of Capitan Pluton, which are similar to those of seawater, are explained to be the product of Na and Cl being derived from evaporites (Campbell et al. 1995). In contrast, the differences in Br/Cl, Br/Na, and I/Br values from Endako, Babine Lake, Porgera, and St. Austell may reflect the individual composition and/or fractionation of a melt, which is associated with a specific ore-related magmatic system as the removal or addition of Br between the hydrothermal fluid and the wallrock is minimal (Böhlke and Irwin, 1992).

The latter suggests that the solute chemistry of the hydrothermal ore fluids of molybdenum mineralization at Endako were derived from a melt with low Br/Cl, Br/Na; or a melt which halogens had fractionated differently relative to other ore-related magmatic systems. In contrast, the oxygen and hydrogen isotopes of ore-related fluids at Endako suggest the involvement of meteoric fluids with magmatic fluids. Porphyry systems studied in areas where local meteoric water δD is similar to the accepted magmatic water δD values hydrothermal fluids possess typical magmatic δD values. However, porphyry systems in settings were the δD value of local meteoric water is significantly different from magmatic water at the time of mineralization possess

hydrothermal fluids with δD values lower than magmatic values (Batchelder 1977; Theodore et al. 1992; Sheets et al. 1996; this study). Porphyry systems studied in areas where local meteoric water δD is similar to the accepted magmatic water δD values hydrothermal fluids possess typical magmatic δD values. However, porphyry systems in settings were the δD value of local meteoric water is significantly different from magmatic water at the time of mineralization possess hydrothermal fluids with δD values lower than magmatic values (Batchelder 1977; Theodore et al. 1992; Sheets et al. 1996; this study).

Summary and Conclusions

Petrographic studies from Endako indicate that early stockwork veins are bordered by K-feldspar alteration assemblages and contain only minor molybdenite. Ribbon-textured veins bordered by sericite host the greater part of the molybdenum ore. The kaolinite alteration assemblages are focused around Tertiary basalts and faults, which indicate a post-ore Tertiary age for this event.

Stable isotope studies of mineral pairs indicate isotopic equilibrium between quartz, K-feldspar and biotite with the primary ore-forming hydrothermal fluids, and that K-feldspar and biotite have re-equilibrated at lower temperatures. Temperatures derived from isotope geothermometry are in good agreement with determined fluid inclusion trapping temperatures, and indicate that ore formation occurred between 360 and 460°C. Low δD values characterize the ore-forming fluids at Endako and related molybdenum mineralization of Nithi Mountain.

Fluid inclusion studies of stockwork quartz veins document trapping of primary high-salinity fluids without coexisting vapor-rich inclusions. The fluids were exsolved directly from the crystallizing melt under lithostatic pressures possibly as high as approximately 2 kbars.

Ore-forming fluids from Endako have lower Br/Cl and Br/Na values in comparison to St. Austell, Porgera, and Babine Lake, and higher Br/Cl and Br/Na values in contrast to Capitan Pluton. The I/Cl and I/Br ratios of ore-fluids from Endako are higher in comparison to Capitan Pluton, Babine Lake and St. Austell. The compositions of the hydrothermal fluids may reflect composition and fractionation behavior directly related to the melt producing the ore fluids, or the interaction between the melt and the crust (e.g., Capitan Pluton, Campbell et al. 1995).

References

Anderson, R. G., and Snyder, L. D. 1998. Jurassic to Tertairy volcanic, sedimentary, and intrusive rocks in the Hallet Lake area, central British Columbia: Current Research 1998-A. Geological Survey of Canada, 1-10.

Anderson, R. G., Snyder, L. D., Wetherup, S., Struik, L. C., Villeneuve, M. E., and Haskin, M. 1998a. Mesozoic to Tertiary volcanism and plutonism in southern Nechako NATMAP area. Part 1: Influence of Eocene tectonics and magmatism on the Mesozoic arc and orogenic collapse. *In* New developments in the Nechako River map area: New Geological Constraints on Mesozoic to Tertiary Metallogenesis and Mineral Exploration in central British Columbia. *Edited by* L. C. Struik, and D. G. MacIntyre, Nechako NATMAP Project; Geological Association of Canada, Cordilleran Section, March 27, 1998, Short Course Notes.

Anderson, R. G., Whalen, J. B., and Villeneuve, M. E. 1998b. Mesozoic to Tertairy volcanism and plutonism in southern Nechako NATMAP area. Part 2: Triassic to Eocene composite intrusions and molybdenum metallogeny: the Endako batholith redefined. *In* New Geological Constraints on Mesozoic to Tertiary Metallogenesis and Mineral Exploration in central British Columbia. *Edited by* L. C. Struik, and D. G. MacIntyre, Nechako NATMAP Project; Geological Association of Canada, Cordilleran Section, March 27, 1998, Short Course Notes.

Batchelder, J. 1977. Light stable isotope and fluid inclusion study of the porphyry Cu deposit at Copper Canyon, Nevada. Economic Geology, **72**: 60-70.

Beane, R. E., and Bodnar, R. J. 1995. Hydrothermal fluids and hydrothermal alteration in porphyry copper deposits. *In* Porphyry copper deposits of the American Cordillera. *Edited by* F. W. Pierce, and J. G. Bohm. Arizona Geological Society Digest 20, Tucson, AZ, 83-93.

Bloom, M. S. 1981. Chemistry of inclusion fluids: stockwork Molybdenum deposits from Questa, New Mexico, and Hudson Bay Mountain and Endako, British Columbia. Econmic Geology, **76**: 1906-1920.

Bodnar, R. J. 1994. Synthetic fluid inclusions: XII. The system H_2O-NaCl. Experimental determination of the halite liquidus and isochores for a 40 wt. % NaCl solution. Geochimica et Cosmochimica Acta, **58**: 1053-1063.

Bodnar, R. J., Burnham, C. W., and Sterner, S. M. 1985. Synthetic fluid inclusions in natural quartz. III. Determinations of phase equilibrium properties in the system H_2O-NaCl to 1000°C and 1500 bars. Geochimica et Cosmochimica Acta, **49**: 1861-1873.

Bodnar, R. J., and Vityk, M. O. 1995. Intrepretation of microthermometric data for H_2O-NaCl fluid inclusions. *In* Fluid inclusions in minerals: methods and applications. *Edited by* Benedetto De Vivo and M. L. Frezzotti, M.L., 117-131.

Böhlke, J. K., and Irwin, J. J. 1991. Laser microprobe analyses of Cl, Br, I, and K in fluid inclusions: Implications for sources of salinity in some ancient hydrothermal fluids. Geochimica et Cosmochimica Acta, **56**: 203-225.

Bottrell, S. H., and Yardley, B. W. D. 1988. The composition of a primary granite-derived ore fluid from S.W. England, determined by fluid inclusion analysis: Geochimica et Cosmochimica Acta, **52**: 585-588.

Burnham, C. W. 1979. Magmas and hydrothermal fluids. *In* Geochemistry of Hydrothermal Ore Deposits. *Edited by* H. L. Barnes, New York, John Wiley, 77-136.

Bysouth, G. D., and Wong, G. Y. 1995. The Endako molybdenum Mine, central British Columbia: An update. *In* Porphyry Deposits of the Northwestern Cordillera of North America. *Edited by* T. G. Schroeter, Canadian Institute of Mining, Metallurgy and Petroleum, Special Volume **46**: 697-703.

Campbell, A. R., Banks, D. A., Phillips, R. S., and Yardley, B. W. D. 1995. Geochemistry of Th-U-REE mineralizing magmatic fluids, Capitan Mountains, New Mexico. Economic Geology, **90**: 1271-1287.

Candela, P. A., and Blevin, P. L. 1995. Do some miarolitic granites preserve evidence of magmatic volatile phase permeability? Economic Geology, **90**: 2310-2316.

Candela, P. A., and Holland, H. D. 1984. The partitioning of copper and molybdenum between silicate melts and aqueous fluids. Geochimica et Cosmochimica Acta, **48**: 373-380.

Carr, J. M. 1966. Geology of the Endako area, British Columbia: Minister of Mines and Petroleum Resources, Annual Report, 114-135.

Carten, R. B., Geraghty, E. P., and Walker, B. M. 1988. Cyclic development of igneous features and their relationship to high-temperature hydrothermal features in the Henderson porphyry molybdenum deposit, Colorado. Economic Geology, **83**: 266-296.

Carten, R. B., White, W. H., and Stein, H. J. 1993. High-grade granite-related molybdenum systems: Classification and Origin. *In* Mineral Deposit Modelling. *Edited by* R. V. Kirkman, W. D. Sinclair, R. I. Thorpe, and J. M. Duke. Geological Association of Canada, Special Paper **40**: 521-554.

Carter, N. C. 1981. Porphyry copper and molybdenum deposits west-central British Columbia: British Columbia Ministry of Energy, Mines and Petroleum Resources Bulletin, **64**: 150.

Chacko, T. 1993. Experimental studies of equilibrium oxygen and carbon isotopic fractionation factors between phases. *In* Short Course Handbook on Experiments at High Pressure and Applications to the Earth's Mantle. *Edited by* R. W. Luth. Mineralogical Association of Canada Short Course **21**: 357-384.

Chacko, T., Hu, X., Mayeda, T. K., Clayton, R. N., and Goldsmith, J. R. 1996 Oxygen isotope fractionation in muscovite, phlogopite, and rutile. Geochimica et Cosdmochimica Acta, **60**: 2595-2608.

Clark, K. F. 1972. Stockwork molybdenum deposits in western Cordillera of North America: Economic Geology, **67**: 731-758.

Clayton, R. N., and Mayeda, T. K. 1963. The use of bromine pentafluoride in the extraxtion of oxygen from oxides and silicates for isotopic analysis. Geochimica et Cosmochimica Acta, **27**: 43-52.

Cline, J. C., and Bodnar, R. J. 1991. Can economic porphyry copper mineralization be generated by a typical calc-alkaline melt? Journal of Geophysical Research, **96**: 8113-8126.

Cline, J. S., and Bodnar, R. J. 1994. Direct evolution of brine from a crystallizing silicic melt at the Questa, New Mexico, Molybdenum deposit. Economic Geology, **89**: 1780-1802.

Cline, J. S., and Vanko, D. 1995. Magmatically generated saline brines related to molybdenum at Questa, New Mexico. *In* Magmas, Fluids, and Ore Deposits. *Edited by* J. F. H. Thompson. Mineralogical Association of Canada Short Course Volume **23**: 153-175

Craig, H. 1957. Isotopic standards for carbon and oxygen and correction factors for mass-spectrometers analysis of carbon dioxide. Geochimica et Cosmochimica Acta, **12**: 133-149.

Craig, H. 1961a. Standards for reporting concentration of deuterium and oxygen- 18 in natural waters. Science, **133**: 1833-1834.

Dawson, K. M. 1972. Geology of the Endako mine: unpublished Ph.D. thesis, University of British Columbia, Vancouver, p. 337.

Drummond, A. D., and Kimura, E. T. 1969. Hydrothermal alteration at the Endako—a comparison to experimental studies: Canadian Mining Metallurgical Bulletin, **62**: 709-714.

Enkin, R., Struik, B., Wetherup, S., and Selby, D. 1997. Paleomagnetic determination of post-Eocene tilts in the Nechako Region: GAC MAC Annual Meeting, Ottawa 1997, p. 46.

Fournier, R. O., and Truesdell, A. H. 1973. An empirical Na-K-Ca geothermometer for natural waters: Geochimica et Cosmochimica Acta, **37**: 1255-1275.

Gilg, H. A., and Sheppard, S. M. F. 1996. Hydrogen isotope fractionation between kaolinite and water revisited: Geochimica et Cosmochmica Acta, **60**: 529-533.

Hall, D. L., Sterner, S. M., and Bodnar, R. J. 1988. Freezing point depression of NaCl-KCl-H_2O solution: Economic Geology, **83**: 197-202.

Hall, W. E., Friedman, I., and Nash, J. T. 1974. Fluid inclusion and light stable isotope study of the Climax molybdenum deposits, Colorado: Economic Geology, **69**: 804-901.

Hall, W. E., Schmidt, E. A., Howe, S. S., and Broch, M. J. 1984. The Thompson Creek, Idaho, porphyry molybdenum deposit—an example of a fluorine-deficient molydenum granodiorite system. *In*, International Association on the Genesis of Ore Deposits. *Edited by* T. V. Janelidze, and A. G. Tvalchrelidze. Symposium, 6th, Tbilisi 1982, Proceedings, 349-357.

Hollister, V. F. 1978. Porphyry molybdenum deposits. *In* International Molybdenum Encyclopaedia. *Edited by* A. Sutulov. Santiago, Chile, Intermet Publications, **1**: 270-283.

Kamilli, R. J. 1978. The genesis of stockwork molybdenite deposits: Implications from fluid inclusion studies at Henderson mine: Geological Society of America Abstracts with Programs, **10**: 431.

Keppler, H., and Wyllie, P. J. 1991. Partitioning of Cu, Sn, Mo, W, U, and Th between melt and aqueous fluid in systems halpogranite-H_2O-HCl and halogranite-H_2O-HF: Contributions to Mineralogy and Petrology, **109**: 139-150.

Kimura, E. T., Bysouth, G. D., and Drummond, A. D. 1976. Endako. *In* Porphyry deposits of the Canadian Cordillera. *Edited by* A. Sutherland Brown. Canadian Institute of Mining and Metallurgy Special Volume **15**: 444-454.

Kimura, E. T., and Drummond, A. D. 1969. Geology of the Endako Molybdenum Deposit. Canadian Institute of Mining and Metallurgy, CIM Bulletin, **62**: 699-708.

L'Heureux, R., and Anderson, R. G. 1997. Early Cretaceous plutonic rocks and molybdenite showings in the Nithi Mountain area (NTS 93F/15 and K/02), central British Columbia. Current Research 1997-A; Geological Survey of Canada, 117-124.

Land, L. S., and Dutton, S. P. 1978. Cementation of a Pennsylvanian deltaic sandstone: isotopic data. Journal of Sedimentary Petrology, **48**: 1167-1176.

Magaritz, M., and Taylor, H. P., Jr. 1976. $^{18}O/^{16}O$ and D/H studies along a 500 km traverse across the coast range batholith and its country rocks, central British Columbia. Canadian Journal Earth Sciences, **13**: 1514-1536.

Manning, D. A. C. 1981. The effect of fluorine on liquidus phase relationships in the system Qz-Ab-Or with excess water at 1 kb. Contributions to Mineralogy and Petrology, **76**: 206-215.

Matsuhia, Y, Goldsmith, J. R., and Clayton, R. N. 1979. Oxygen isotopic fractionation in the system quartz-albite-anothorite-water. Geochimica et Cosmochimica Acta, **43**: 1131-1140.

McCrea, J. M., 1950, On the isotopic chemistry of carbonates and a paleotemperature scale. Journal of Chemical Physics, **18**: 849-857.

Molling, P. A. 1989. Applications of the reaction progress variable to hydrothermal alteration associated with the deposition of the Questa molybdenite deposit, NM. Unpublished Ph.D. dissertation, Baltimore, Maryland, Johns Hopkins University, 229p.

Mutschler, F. E., Wright, E. G., Ludington, S., and Abbott, J. T. 1981 Granite molybenite systems. Economic Geology, **76**: 874-897.

Nash, J. T. 1976. Fluid-inclusion petrology—Data from porphyry copper deposits and applications to exploration: U.S. Geological Survey Professional Paper 907D, 16p.

Nesbitt, B. E., and Prochaska, W. 1998. Solute chemistry of inclusion fluids from sparry dolomites and magnesites in Middle Cambrian carbonate rocks of the southern Canadian Rocky Mountains. Canadian Journal of Earth Sciences, **35**: 546-555.

O'Neil, J. R. 1986. Theoretical and experimental aspects of isotopic fractionation. Reviews in Mineralogy. Mineralogcal Society of America, **16**: 1-37.

O'Neil, J. R., and Taylor, H. P., Jr. 1967. The oxygen isotope and cation exchange of feldspars. American Mineralogist, **52**: 1414-1437.

O'Neil, J. R., Clayton, R. N., and Mayeda, T. K. 1969. Oxygen isotope fractionation in divalent metal carbonates. Journal of Chemical Physics, **51**: 5547-5558.

Ohmoto, H. 1986. Stable isotope geochemistry of ore deposits: Reviews in Mineralogy. Mineralogcal Society of America, **16**: 491-559.

Piwinskii, A. J. and Wyllie, P. J. 1970. Experimental studies of igneous rock series: Felsic body suite from the Needle Point Pluton, Wallowa Batholith, Oregon. Journal of Geology, **78**: 52-76.

Rice, C. M., Harmon, R. S., and Shepherd, T. J. 1985. Central City, Colorado: The upper part of an alkaline porphyry molybdenum system. Economic Geology, **80**: 1769-1796.

Richards, J. P., Bray, C. J., Channer, D. M. D., and Spooner, E. T. C. 1997. Fluid chemistry and processes at the Porgera gold deposit, Papua New Guinea. Mineralium Deposita, **32**: 119-132.

Sharp, J. E. 1978. A molybdenum mineralized breccia pipe complex, Redwell Basin, Colorado. Economic Geology, **73**: 369-382.

Shaver, S. A. 1991. Geology, alteration, mineralization and trace element geochemistry of the Hall (Nevada Moly) deposit, Nye Country, Nevada. *In* Geology and ore deposits of the Great Basin. *Edited by* G. L. Raines, R. E.. Lisle, R. W., Schafer, and W. H. Wilkinson. Geological Society and U. S. Geological Survey, Symposium, Reno/Sparks, April 1990, Proceedings, **1**: 303-332.

Sheets, R. W., Nesbitt, B. E., and Muehlenbachs, K. 1996. A meteoric water component in magmatic fluids from porphyry copper mineralization, Babine lake area, British Columbia. Geology, **24**: 1091-1094.

Smith, R. W. 1983. Aqueous chemistry of molybdenum at elevated temperatures and pressures with applications to porphyry molybdenum deposits. Unpublished Ph.D. dissertation, Socorro, New Mexico, New Mexico Institute of Mining and Technology, 311p.

Soregaroli, A. E., and Sutherland Brown, A. 1976. Characteristics of Canadian Cordilleran molybdenum deposits. *In* Porphyry deposits of the Canadian Cordillera. *Edited by* A. Sutherland Brown. Canadian Institute of Mining and Metallurgy Special Volume **15**: 417-431.

Sparks, R. S. J., Barclay, J., Jaupart, C., Mader, H. M., and Phillips, J. C. 1994. Physical aspects of magmatic degassing 1. Experimental and theorectical constraints on vesiculation. Reviews in Mineralogy, **30**: 413-445.

Stein, H. J. 1988. Genetic traits of Climax-type granites and molybdenum minerlaization, Colorado mineral belt, Canadian Institute of Mining and Metallurgy Special Volume **39**: 394-401.

Stein, H. J., and Hannah, J. L. 1985. Movement and origin of ore fluids in Climax-type systems. Geology, **13**: 469-474.

Sterner, S., Hall, D., and Keppler, H. 1995. Compositional re-equilibration of fluid inclusions in quartz. Contributions to Mineralogy and Petrology, **119**: 1-15.

Struik, L. C., Whalen, J. B., Letwin, J. M., and L'Heureux, R.,1997. General geology of the southeast Fort Fraser map area; central British Columbia: Current Research 1997-A. Geological Survey of Canada, 65-75.

Taylor, H., Jr. 1979. Oxygen and hydrogen isotope relationships in hydrothermal minerals deposits: In: Geochemistry of hydrothermal ore deposits. *In* Geochemistry of Hydrothermal Ore Deposits. *Edited by* H. L. Barnes. New York Wiley Interscience, 501-567.

Taylor, H. P., Jr., Frechen, J., and Degens, E. T. 1967. Oxygen and carbon isotope studies of carbonatites from the Laacher See district, West Germany and the Alno district, Sweden: Geochimica et Cosmochimica Acta, **31**: 401-430.

Taylor, H. P., Jr., and Sheppard, S. 1986. Igneous rocks 1. Processes of isotopic fractionation and isotope systematics: Reviews in Mineralogy. Mineralogcal Society of America, **16**: 227-271.

Taylor, S. R., and McLennan, S. M. 1985. The continental crust: its composition and evolution. Blackwell Scientific Publications, Oxford, 312p.

Theodore, T. G., Blake, D. W., Loucks, T. A., and Johnson, C. A. 1992. Geology of the Buckingham stockwork molybdenum deposit and surrounding area, Lander County, Nevada. U. S. Geological Survey Professional Paper 798-D, 307p.

Theodore, T. G., and Menzie, W. D. 1984. Fluorine-deficient porphyry molybdenum deposits in the western North American Cordillera. *In* International Association on the Genesis of Ore Deposits. *Edited by* T. V. Janelidze and A. G. Tvalchrelidze. Symposium, 6th, Tbilisi 1982, Proceedings, p. 463-470.

Thompson, A. B., 1970, A note on the Kaolinite-pyrophyllite equilibrium. American Journal of Science, **268**: 454-458.

Thompson, T. B., 1982, Classification and genesis of stockwork molybdenum deposits—A discussion. Economic Geology, **77**: 709-714.

Villeneuve, M. E., Struik, L. C., Lowe, C., Whalen, J. B., Anderson, R. G., Enkin, R. J., Shives, R., and Selby, D. 1999. Geochronology, Structure and Genetics of the Endako Molybdenum Camp. *In* Vancouver: Where Discoveries Start 16th Annual Cordilleran Exploration Roundup (Abstr.), p. 5-7.

Wallace, S. R., Mackenzie, W. B., Blair, R. G., and Muncaster, N. K. 1978. Geology of the Urad and Henderson molybdenite deposits, Clear Creek County, Colorado, with a section on a comparison of these deposits with those at Climax, Colorado. Economic Geology, **73**: 325-368.

Wanless, R. K., Stevens, R. D., Lachance, G. R., and Delabrio, R. N. D. 1974. Age determination and geological studies: K-Ar isotopic ages, report 12. Geological Survey of Canada Paper, p. 72-74.

Werre, R. W., Jr., Bodnar, R. J., Bethke, P. M., and Barton, P. B., Jr. 1979. A novel gas-flow fluid inclusion heating/freezing stage. Geological Society of America Abstracts and Programs, **11**: 539.

Westra, G., and Keith, S. B., 1981, Classification and genesis of stockwork molybdenum deposits. Economic Geology, **76**: 844-873.

Whalen, J. B., Struik, L. C., and Hrudey, M. 1998. Bedrock geology of the Endako map area, central British Columbia. Current Research 1998-A; Geological Survey of Canada, 113-123.

White, W. H., Bookstrom, A. A., Kamilli, R. J., Ganster, M. W., Smith, R. P., Ranta, D. E., and Steininger, R. C. 1981. Character and origin of Climax-Type molybdenum deposits: Economic Geology 75th Anniversary Volume, 270-316.

White, W. H., Harakàl, J. E., and Carter, N. C. 1968. Potassium-argon ages of some ore deposits in British columbia. Canadian Institute of Mining and Metallurgy Bulletin, **61**: 1326-1334.

White, W. H., Sinclair, A. J., Harakal, J. E., and Dawson, K. M. 1970. Potassium-argon ages of Topley intrusions near Endako, British Columbia. Canadian Journal of Earth Sciences, **7**: 1172-1178.

Woodcock, J. R., and Hollister, V. F. 1978. Porphyry molybdenite deposits of the North American Cordillera. Minerals Science and Engineering (Johannesburg), **10**: 3-18.

Yardley, B. W. D., and Banks, D. A. 1994. The ligand chemistry of crustal fluids. Mineralogical magazine, **10**: 3-18.

Zaluski, G., Nesbitt, B., and Muchlenbachs, K. 1994. Hydrothermal alteration and stable isotope systematics of the Babine Porphyry Cu deposits, British Columbia: Implications for fluid evolution of porphyry systems. Economic Geology, **89**: 1518-1541.

Table 2.1. First ice, halite melting temperatures, salinity and homogenization temperatures for fluid inclusion types.

Inclusion Type	Te (°C)	Tm NaCl (°C)	Salinity wt. percent NaCl eq.	Th L-V (L) (°C)	Th L-V (H) (°C)
Type 1					
1a	–27 to –45		5.3 to 14.8	290 to 546	
1b	–33 to –50		9.5 to 12.7	328 to 445	
Type 2					
2a		–0.1 to –3.1	0.2 to 5.1	130 to 285	
2b		–1.8 to –2.5	3.1 to 4.2	210 to 210	
Type 3					
3a		167 to 370	30 to 45	375 to 420	
3b*			45 to 60		380 to 550

*Fluid inclusion data from Bloom (1981)

Table 2.2. P-T trapping conditions for hydrothermal fluids recoreded by Type 1, 2, and 3 fluid inclusions associated with K-feldspar, sericite and kaolinite alteration assemblages.

Fluid type/ P-T Conditions	K-feldspar alteration fluids	Sericite alteration fluids	Kaolinite alteration and Post ore fluids
Pressure (kbars)	> 0.3 to 2.0	>0.3 to 0.8	≤ 0.5
Temperature (°C)	360 to 460	360 to 440	190 to 300

Table 2.3. Synopsis of oxygen, carbon and hydrogen isotope data from the Endako porphyry molybdenum deposit.

Mineral/Rock	$\delta^{18}O$ (per mil) (SMOW)	δD (per mil) (SMOW)	$\delta^{13}C$ (per mil) (PDB)	H_2O Calc T°C[1]	$\delta^{18}OH_2O$ (per mil)	δDH_2O (per mil)
Pre-Mineral Dikes						
Porphyritic granite	2.7 to 6.9					
Qz-fsp porphyry	6.2 to 6.9					
K-feldspar Alteration						
Whole-rock[2]	6.3 to 7.5	–134 to –167				
K-feldspar	2.5 to 6.6	–146 to –162		440[1]	3.8 ± 0.6	–146 to –162
Biotite	2.0 to 4.5			440[1]	4.0 ± 0.5	
Stockwork quartz	8.0 to 8.8	–125 to –150		440[1]	5.2 ± 0.2	–125 to –150
Sericite Alteration						
Quartz	6.7 to 9.5	–105 to –170		380[1]	3.9 ± 0.6	–105 to –173
Sericite	5.6					
Kaolinite Alteration						
Whole-rock[3]	5.5 to 6.6					
Whole-rock[4]	5.2 to 7.2					
Clinochore	–2.1					
Kaolinite	6.6 to 6.8	–156		190 - 300[1]	2.1 to –2.2	–138 to –141
Post Mineralization						
Calcite vein	–3.8 to 12.7	–105 to –147	–2.0 to –6.2	190 - 300[1]	7.6 to –13.4	–105 to –147
WR+calcite	5.5 to 11.1		–2.5 to –4.9			
Chalcedony	7.3 to 8.7					
Basalt	–2.4 to 4.5					
Biotite	3.6					
Mont+Nont+illite	2.1 to 5.7					

[1]δH_2O calcualted using stable isotope and fluid inclusion thermometry, [2, 3, 4]Whole-rock samples of potassic zone are exhibit weak, moderate and intense kaolinite alteration, respectively.

Table 2.4a. Mineral-mineral oxygen pair data for quartz and K-feldspar.

Sample #	$\delta^{18}O$ Qtz (per mil)	$\delta^{18}O$ K-fsp (per mil)	Δq-f	Temperature (°C)[1]
3267.8	8.0	6.2	1.8	440
3146.1B	8.8	2.5	6.3	*
3102.11	8.2	5.5	2.7	310
2794.1	8.2	6.5	1.7	460
2706.7	8.8	5.3	3.5	200
RB857	8.4	6.1	2.3	360

Table 2.4b. Mineral-mineral oxygen pair data for quartz and biotite.

Sample #	$\delta^{18}O$ Qtz (per mil)	$\delta^{18}O$ Biotite (per mil)	Δq-b	Temperature (°C)[1]
3146.1B	8.8	3.9	4.9	400
RB857	8.4	4.2	4.2	460
2794.1	8.2	4.5	3.7	490
2706.7	8.8	4.2	4.6	410
2706.7	8.8	2.0	6.8	290
2794.2	8.2	3.2	5.0	390
S820.207.8	8.6	3.0	5.6	350

[1]Temperatures calculated using fractionation expressions of Chacko (1993) and Chacko et al. (1996). *Δq-f value yields temperature outside the range of expressions from Chacko (1993).

Table 2.5. Solute chemistry data.

sample#	3267.8Q	3267.AQ	3267.SQ	3102.2Q	2706.8Cc	EqmL3.Cc
mineral	quartz	quartz	quartz	quartz	calcite	calcite
Alteration	K-feldspar		Sericite		Post-ore	
anion/cation (molar ratios)						
Br/Cl (*10^3)	1.0000	0.4466	0.2770	0.4922	0.5135	1.4444
I/Cl (*10^6)	63.041	56.064	19.314	86.189	42.595	175.115
Na/Br (*10^2)	1070	1622	1166	1599	301	1529
Cl/Br	995	2248	3624	2048	1974	699
I/Br	0.0630	0.1255	0.0697	0.1751	0.0829	0.1212
Br/Na	0.933	0.617	0.863	0.630	11.538	2.273
Na/K	6.894	4.160	4.198	3.008	0.929	0.297
log(Na/K)	0.61	0.39	0.39	0.25	–0.03	–0.53
log(Na/K) T°C[1]	308	376	376	429	564	1003
δD	–135	–125	–140	–130	–147	–112
$\delta^{18}O$	8.0	8.5	8.2	8.7	4.6	4.5
$\delta^{13}C$					–4.6	–5.2
Salinity (wt. % NaCl)	10		10	8		

[1]Temperatures calculated using fractionation expression of Fournier and Truesdell (1973).

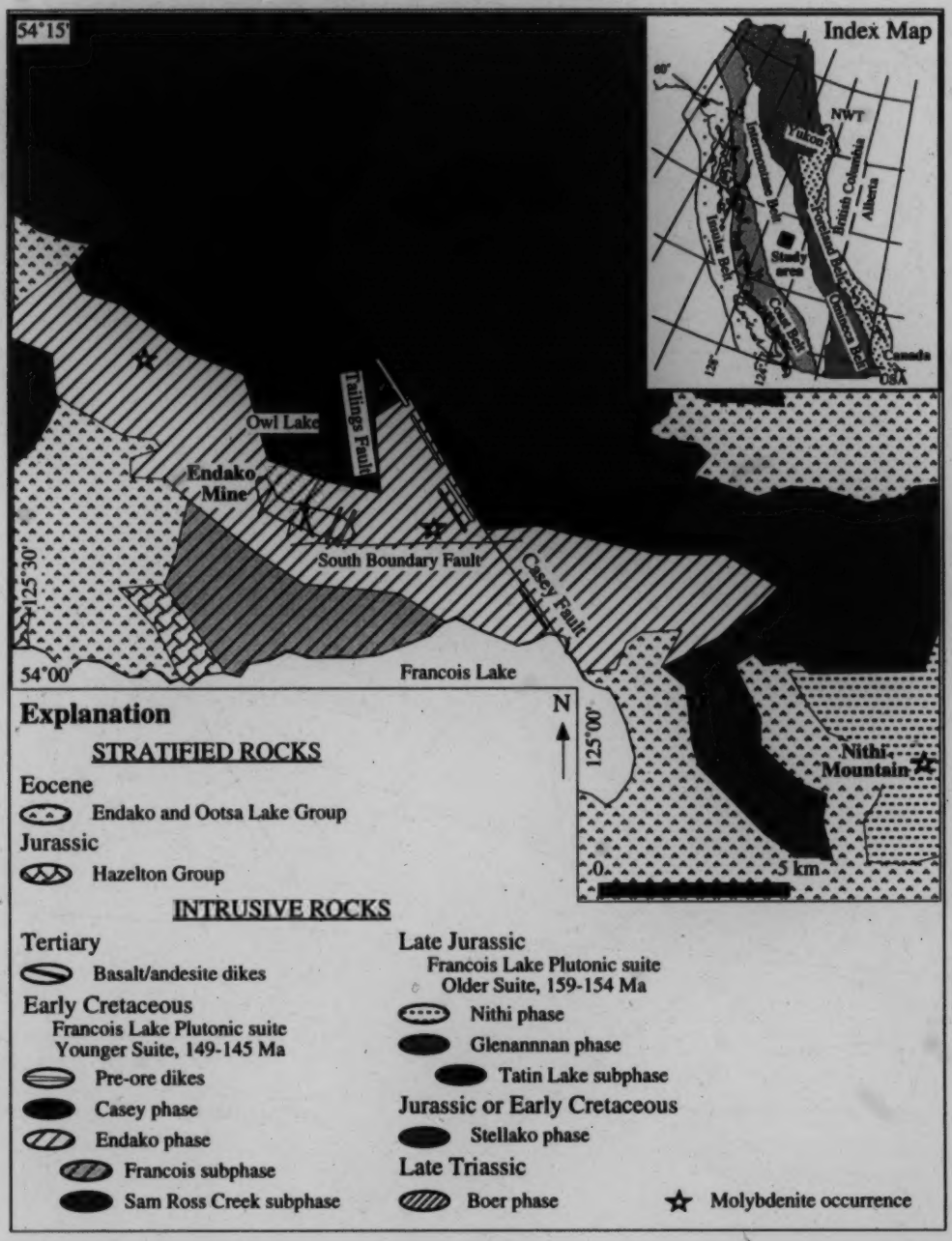

Fig. 2.1. Geology of the Endako area. Modified after Struik et al. (1997), Anderson and Snyder (1998), and Whalen et al. (1998).

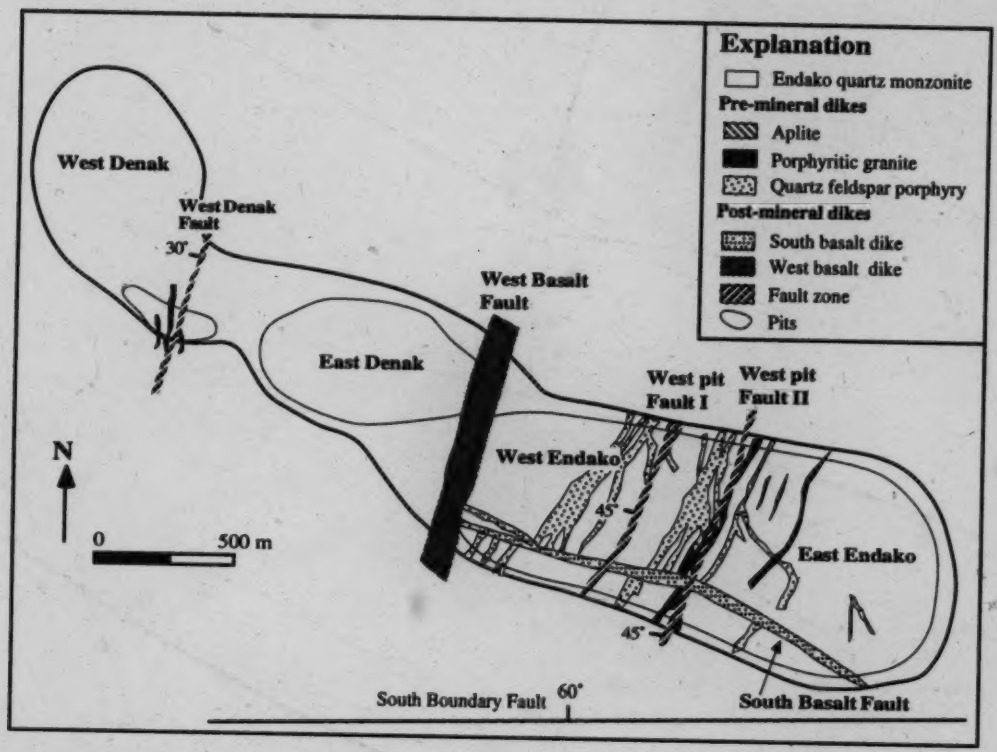

Fig. 2.2. Geology of the Endako porphyry molybdenum deposit. Modified after Dawson (1972) and Kimura et al (1976).

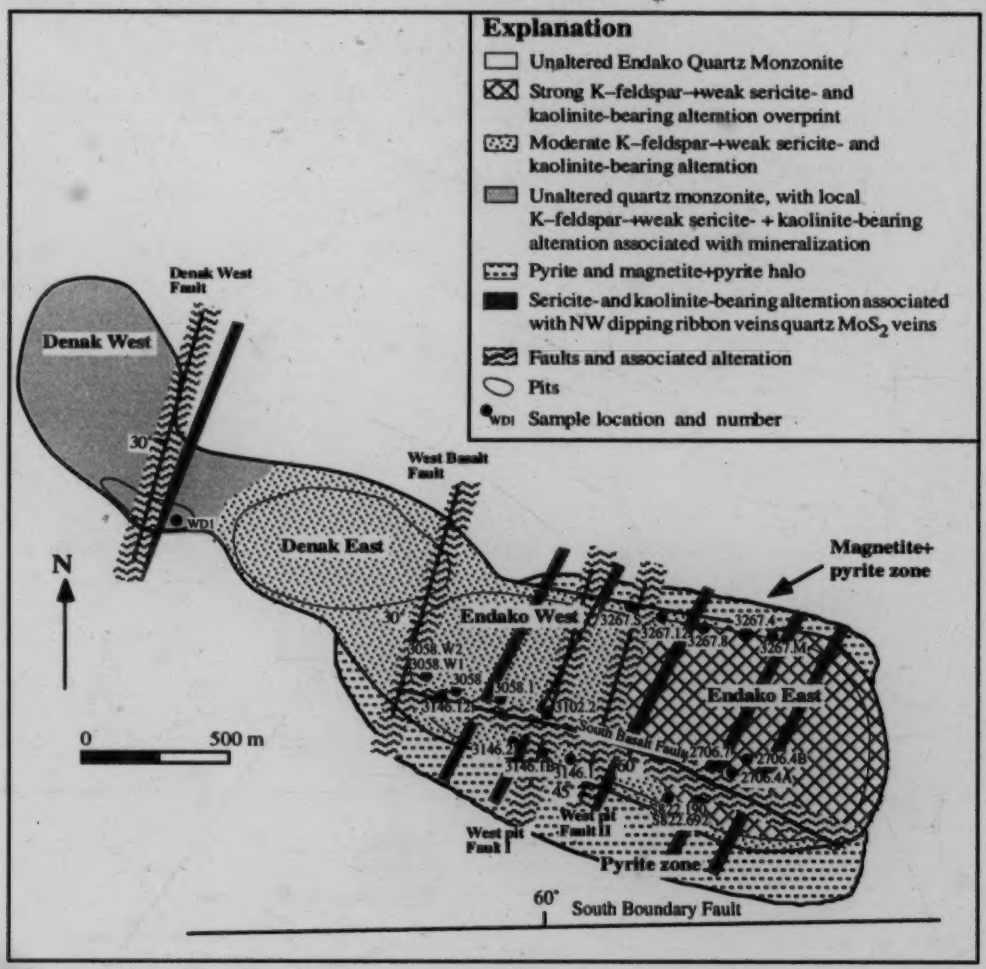

Fig. 2.3. Hydrothermal alteration map of the Endako deposit, with locations of samples analyzed for fluid inclusion studies.

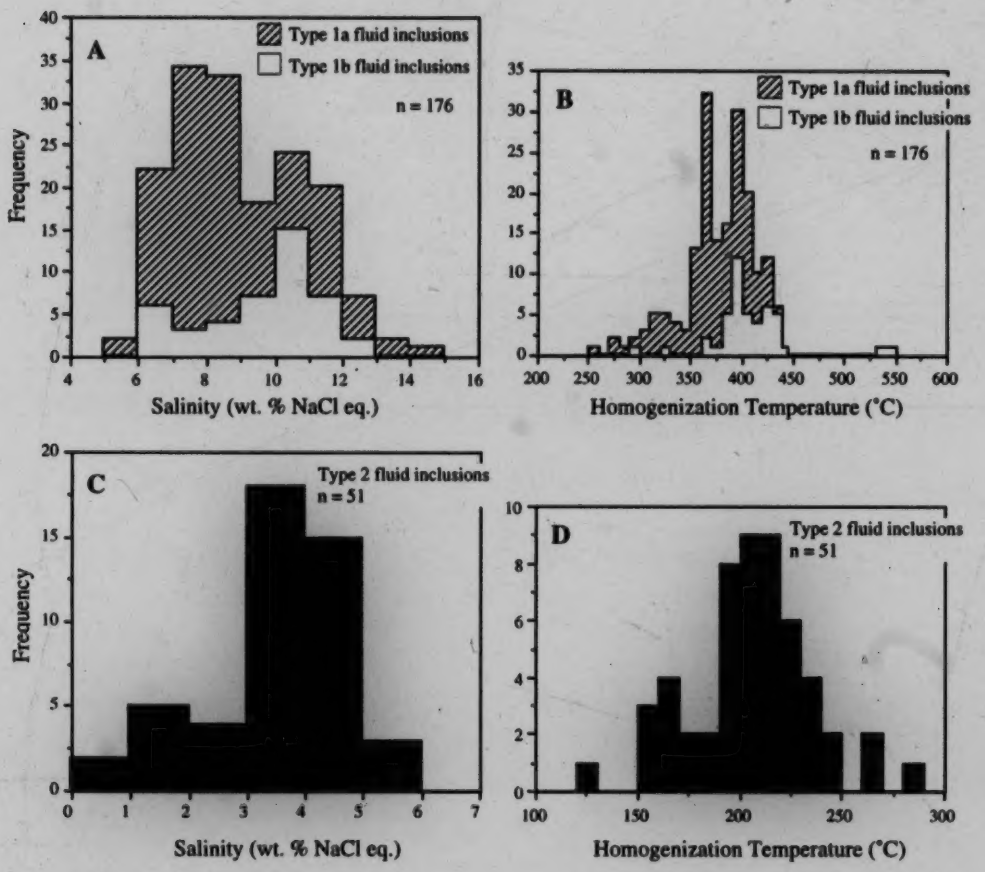

Fig. 2.4. A: Histogram of salinity values (wt. % NaCl eq.) for different sub-populations of Type 1 fluid inclusions, B: Th (°C) plot for the different sub-populations of Type 1 fluid inclusions, C: Salinity (wt. % NaCl eq.) plot for Type 2 fluid inclusions, D: Th (°C) plot for Type 2 fluid inclusions.

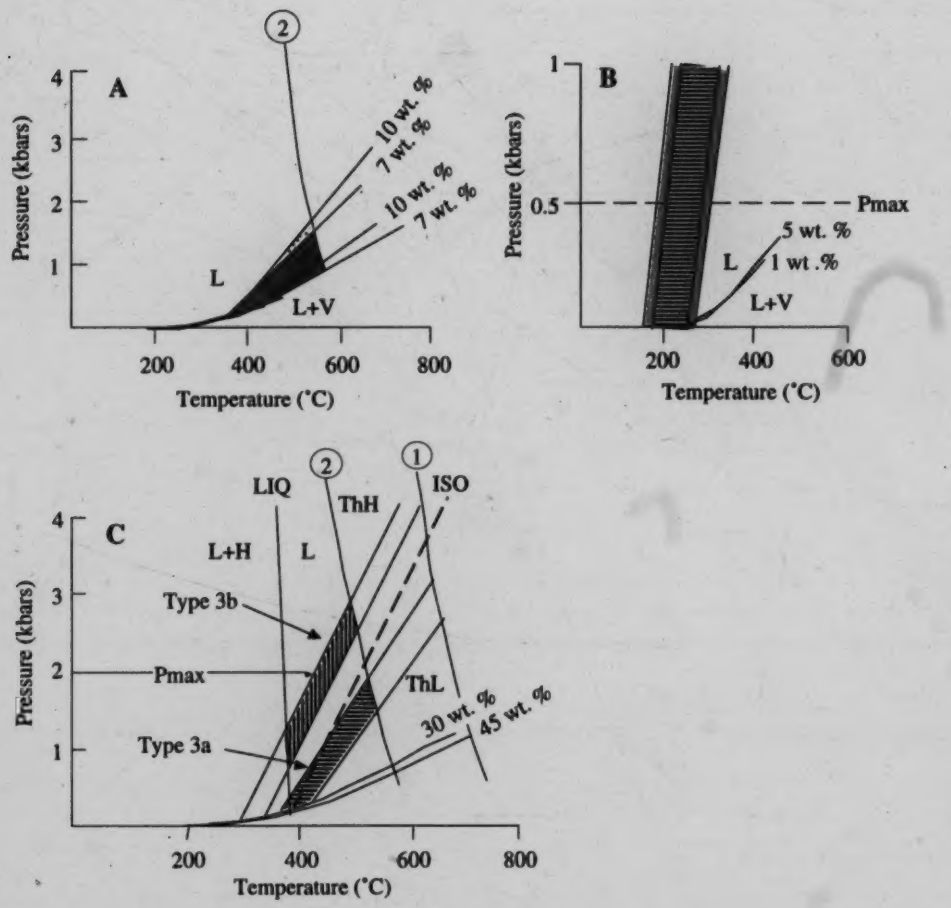

Fig. 2.5. Pressure-temperature diagrams to show the conditions of vein-forming fluids. Curved lines labelled 1 and 2 represent the dry solidus of a quartz monzonite and the solidus of a granite-bearing 2 wt. % fluorine, respectively. A: shows the P-T conditions of trapping of 10 and 7 wt. % NaCl eq. fluids contained within Type 1 fluid inclusions. Isochores demarking the fields are constructed for 7 and 10 wt. % NaCl and temperatures of homogenization of 360 and 440°C. B: shows the P-T conditions of trapping of low saline fluids contained within Type 2 fluid inclusions. The stippled and horizontal shaded areas represent the trapping conditions of 1 and 5 wt. % NaCl eq., respectively. C: depicts the trapping conditions of fluids in Type 3a and 3b fluid

inclusions. The LIQ line indicates the halite liquidus, separating two stability fields, liquid + halite (L + H) and liquid (L). Drawn from the intersection of the liquidus with the three phase curve is the isochore ISO, which divides the liquid stable field into two sub-fields. Fluid inclusion that homogenize by halite dissolution (ThH) and those that homogenize by vapor bubble disapperance (ThL). Vertical and horizontal shaded areas represent the trapping conditions of Type 3b and 3a fluid inclusions of 30 - 45 wt. % NaCl eq., respectively.

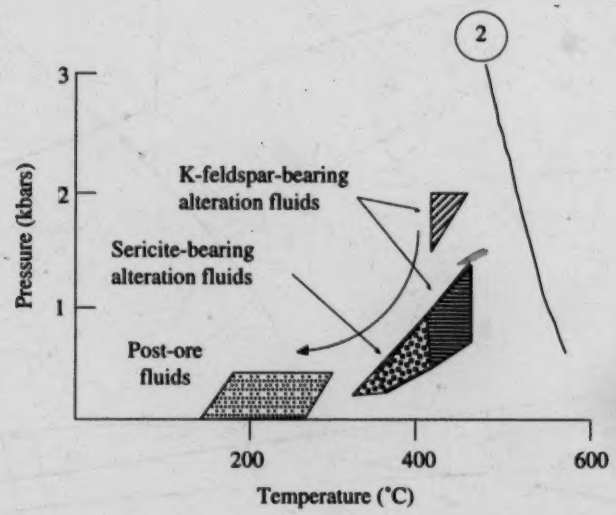

Fig. 2.6. Pressure-temperature evolution model for hydrothermal alteration, and post-ore fluids from the Endako deposit. Curved line labelled 2 represents a solidus of a granite-bearing 2 wt. fluorine. Fluid conditions of K-feldspar alteration are represented by diagonal and horizontal shaded areas, which represent Type 3b and 3a, and 1 fluid inclusions, respectively. Conditions of formation for sericite alteration are represented by Type 1 fluid inclusions, hatched shading. Further decreases in pressure and temperature of the fluids are represented by Type 2 fluids were trapped, gray shaded area.

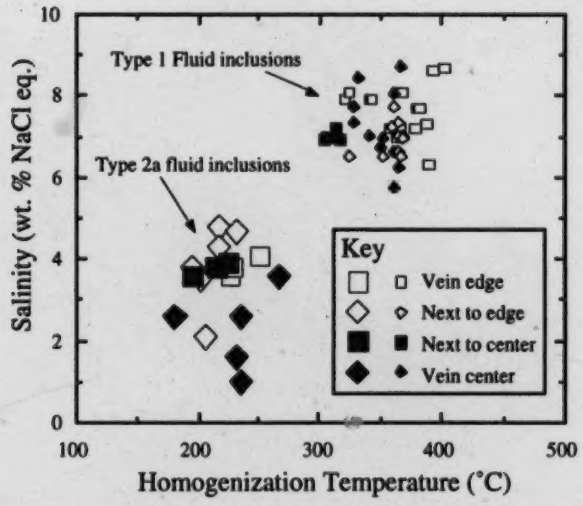

Fig. 2.7. Salinity vs. homogenization temperature (Th) plot for fluid inclusions from sample WD1. Smaller sized symbols represent primary Type 1 inclusions, and larger symbols represent Type 2 fluid inclusions.

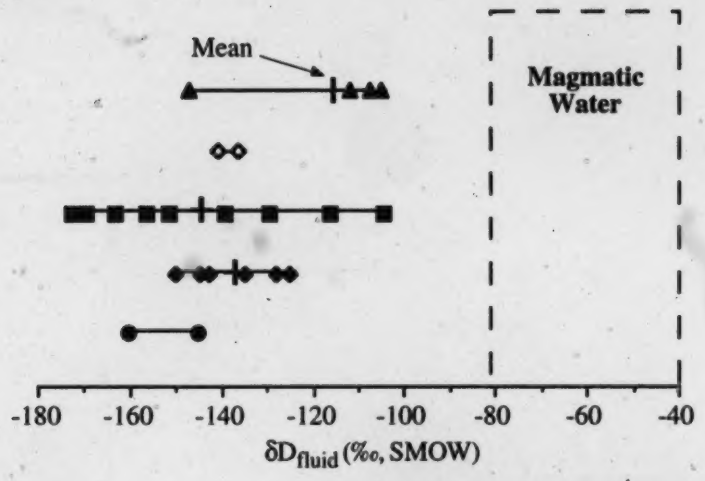

K–feldspar alteration	}	◆ stockwork quartz fluid inclusion waters ● K-feldspar inclusion waters
Sericite alteration	}	■ ribbon vein quartz fluid inclusion waters
Kaolinite alteration	}	◇ kaolinite – calculated δD_{fluid}
Post-ore minerals	}	▲ calcite fluid inclusion waters

Fig. 2.8. Hydrogen isotope data from mineral separates from the Endako deposit. The field that defines magmatic water is from Taylor (1979).

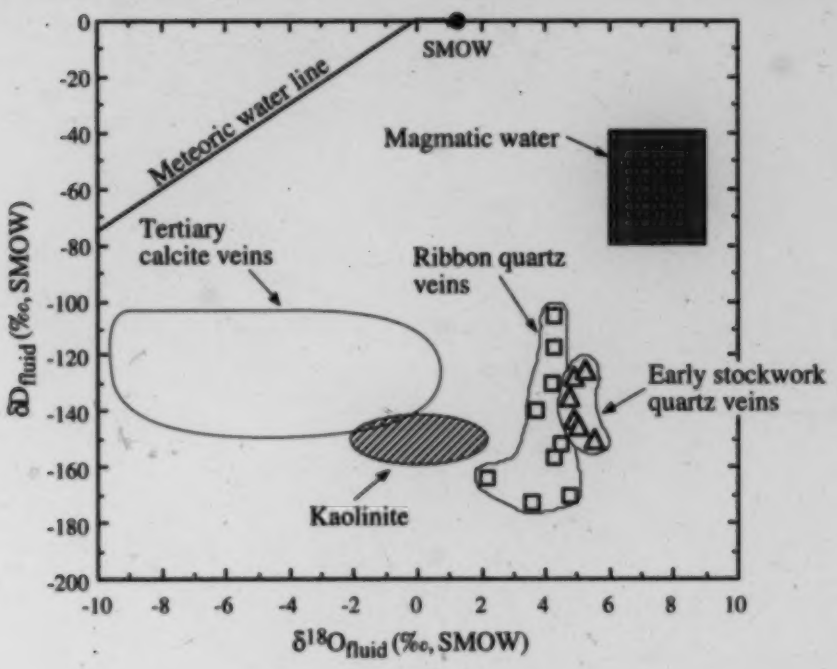

Figure 2.9. Isotopic compositions of hydrothermal fluids producing early stockwork quartz veins with K-feldspar alteration and later ribbon quartz veins with sericite alteration. Also shown are the calculated isotopic compositions of fluids associated with producing kaolinite and calcite veins. Magmatic water is derived from the data of Taylor (1979). Also shown is standard mean ocean water (SMOW).

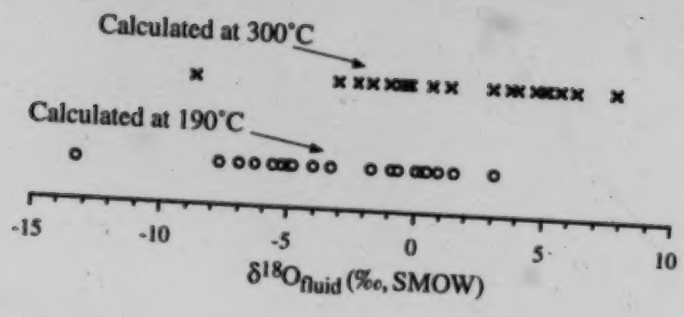

Figure 210. Isotopic compositions of hydrothermal fluids producing late stage calcite veins. Values calculated at 190 and 300°C using the fractionation factor of O'Neil et al. (1969).

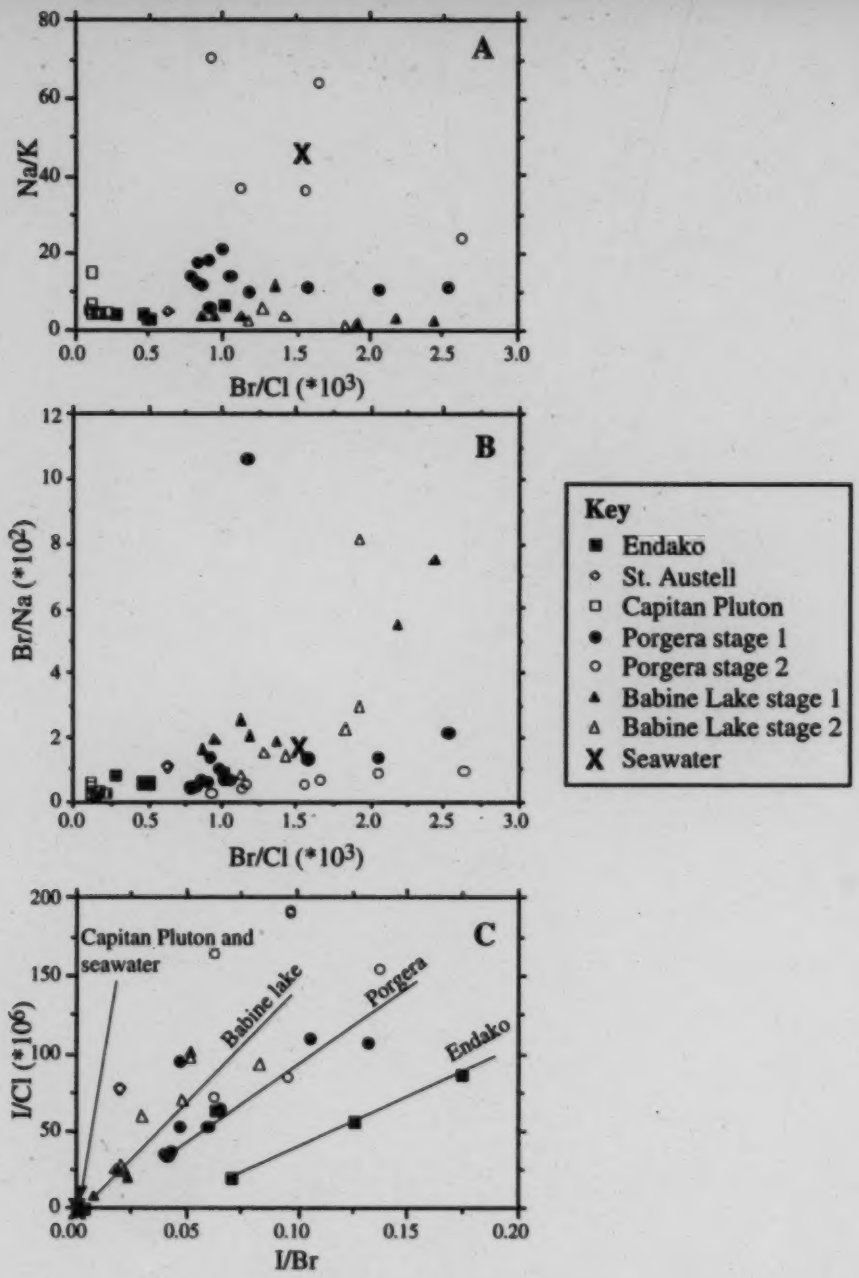

Fig. 2.11. Solute chemistry results for fluid inclusion waters from quartz ore veins from Endako, plotted together with data from Capitan Pluton (Campbell et al. 1995), St. Austell (Bottrell and Yardley 1988; Böhlke and Irwin 1992), Babine Lake (R. W. Sheets unpub. data), Porgera (Richards et al. 1997), and seawater (Taylor and McLennan 1985).

Chapter III

Major and trace element compositons and Sr-Nd-Pb systematics of crystalline rocks from the Dawson Range, Yukon, Canada*

*A version of this paper has been accepted for publication in the Canadian Journal of Earth Sciences, January 1999, co-authored by Robert A. Creaser and Bruce E. Nesbitt of the Department of Earth and Atmospheric Sciences, University of Alberta, T6G 2E3, Canada.

Introduction

The Dawson Range, a west-central portion of the Yukon-Tanana terrane, comprises dominantly metamorphic rocks inferred to be of Devonian-Mississippian age, Mesozoic granitic bodies, and plutons associated with porphyry Cu and epithermal Au mineralization (Figs. 3.1, 3.2). Previous studies of the Dawson Range are limited to reconnaissance scale mapping (Payne et al. 1987; Carlson 1987; Johnston 1995), geological documentation of mineralized areas (e.g., Sinclair et al. 1981; Bower et al. 1995; Hart and Langdon 1998), and K-Ar and Rb-Sr isotopic investigations (Godwin 1975; Tempelman-Kluit and Wanless 1975; Le Couteur and Tempelman-Kluit 1976; Morrison et al. 1979). Studies utilizing techniques such as geochemical (major, trace, rare earth element) and isotopic (Nd, Sr, Pb) analysis that can yield information regarding the origin and the tectonic environment in which rock units are formed are absent for the Dawson Range. Hitherto, tectonic models for the origin of the Dawson Range area were based largely on the data from Devonian-Mississippian rocks of the southern Yukon and eastern Alaska (Mortensen 1992 and references therein; Stevens et al. 1996; Creaser et al. 1997; Grant 1997).

This paper summarizes the geology and the geochemical characteristics of the rock units (Devono-Mississippian Wolverine Creek Metamorphic Suite, mid-Cretaceous Dawson Range batholith, mid-Cretaceous Casino Plutonic Suite, and late Cretaceous plutons) from the Dawson Range in the areas surrounding the Casino, Cash, and Mt. Nansen porphyry copper, molybdenum, gold mineral occurrences. The principal objective of this study is to establish the provenance of detritus in sedimentary units and the origin of the igneous rocks and their tectonic settings of formation.

The data presented for the metasedimentary rocks of the Wolverine Creek Metamorphic Suite are consistent with correlative rock units of the Yukon-Tanana terrane, with the detritus derived from two sources, North American craton to the east and magmatic arc to the west (Creaser et al. 1997; Grant 1997). The geochemistry of meta-igneous rocks of the Wolverine Creek Metamorphic Suite indicate a continental-arc setting for the Yukon-Tanana terrane during Devonian-Mississippian times, which is in agreement with the conclusions of Mortensen (1992) and Stevens et al. (1996).

In addition, major, trace, and rare earth element, and Nd, Sr, and Pb isotopic data presented for the Dawson Range batholith, Casino Plutonic Suite, and late Cretaceous plutons place constraints on the origin of magmas and tectonic settings of the Yukon-Tanana terrane during mid and late Cretaceous time. Evaluation of the data indicates that the Yukon-Tanana terrane is underlain by Precambrian basement or rock units derived from Precambrian crust. The thickening of the basement during the mid-Cretaceous resulted in partial melting, which generated crustal magmas that formed the Dawson Range batholith. Subsequently, during the late Cretaceous, subduction resulted in the production of magmas containing a significant mantle component.

Geology of the Dawson Range

The Yukon-Tanana terrane expands from a narrow region in south-central Yukon (tectonic zone of Stevens et al. 1996; suture zone of Tempelman-Kluit 1979) to encompass much of west-central Yukon and east-central Alaska (Fig. 3.1). The terrane is bordered by Proterozoic to Paleozoic, miogeoclinal strata of continental North America to the north and east and by allochthonous terranes of the Canadian Cordillera to the west and south (Fig. 3.1). The nomenclature of units within the Yukon-Tanana terrane is variable and inconsistent (cf. Hanson 1990; Mortensen 1992). The terminology used in this study is adopted from local names used for the rock units of the Dawson Range (Johnston 1995). The study areas are situated in the Dawson Range of the Yukon-Tanana terrane, which is a northwesterly-trending interior mountain belt that extends northwest of Carmacks to the Alaska border, west-central Yukon (Fig. 3.1).

In the study areas, the Dawson Range is comprised of the Wolverine Creek Metamorphic Suite, Dawson Range batholith, Casino Plutonic Suite, and the Prospector Mountain Plutonic Suite (Carlson 1987; Payne et al. 1987; Johnston 1995) (Fig. 3.2). The Wolverine Creek Metamorphic Suite consists of metasedimentary and meta-igneous rock units (Tempelman-Kluit 1974; Carlson 1987; Payne et al. 1987; Johnston 1995), which are interpreted to be of Devono-Mississippian age based on comparison to the geology of the Dawson area (Wheeler and McFeely 1991). The age of Dawson Range meta-igneous rocks in the study areas is not accurately known, though they are assigned to the Devono-Mississippian Wolverine Creek Metamorphic Suite (Johnston 1995).

The Wolverine Creek Metamorphic Suite is intruded by the mid-Cretaceous (104.0 ± 0.5 Ma, U-Pb zircon, J. K. Mortensen pers. comm. 1997) Dawson Range batholith. The Dawson Range batholith is approximately 300 km long and 60 km wide extending northwest of Carmacks to the Alaskan border, and dominates the geology of the Dawson Range. The rock types hornblende>biotite quartz diorite, hornblende-biotite

diorite, and biotite>hornblende granodiorite characterize this batholith. Associated with the Dawson Range batholith are phases of the Casino Plutonic Suite, which are represented by fine- to medium-grained leucocratic granite, quartz monzonite, and alaskite with associated aplite phases (Carlson 1987; Payne et al. 1987; Johnston 1995; Hart and Selby 1998). The Casino Plutonic Suite is composed of stocks up to 18 km in diameter (Hart and Selby 1998), and is only exposed in the Colorado Creek (NTS 115J/9) and Selwyn River (NTS 115J/10) map areas (Payne et al. 1987; Johnston 1995). Field relationships indicate that the Casino Plutonic Suite intrudes the Dawson Range batholith (Payne et al. 1987), although its age is indistinguishable (104.2 ± 0.5 Ma, U-Pb zircon, J. K. Mortensen pers. comm. 1997; 105 Ma, Ar-Ar muscovite, C. J. R. Hart pers. comm. 1998). Johnston (1995) grouped the Casino Plutonic Suite with the late Cretaceous (70 Ma) Prospector Mountain Plutonic Suite (see below). However, based on geochronology, and geochemical and isotopic data for the Casino Plutonic Suite presented here, suggests a closer association with the mid-Cretaceous Dawson Range batholith. Late Cretaceous igneous activity produced the Prospector Mountain Plutonic Suite (Johnston 1995). This plutonism is represented by small stocks (200 by 500 m) and is commonly associated with porphyry Cu-Au-Mo mineralization, which occurs in a northwest-trending belt defining the Dawson Range mineral region. The late Cretaceous plutons discussed in this paper include the Casino (Patton porphyry), Cash (Cash porphyry), and Mt. Nansen occurrences (Mt. Nansen porphyry). The Big Creek and Klotassin Suite and the Mt. Nansen andesite also comprise the geology at the Cash and Mt. Nansen areas (Fig. 3.2).

Analytical Procedures

A total of 24 samples representing the Wolverine Creek Metamorphic Suite, Dawson Range batholith, Casino Plutonic Suite, and late Cretaceous plutons (Table 3.1) were analyzed for

their Nd, Sr, and Pb isotopic compositions and Sm, Nd, Rb, and Sr contents by isotope dilution mass spectrometry at the University of Alberta in the Earth and Atmospheric Sciences Radiogenic Isotope Facility. Samples were ground to ≤ 35 μm with all surface weathering removed prior to crushing. Major, trace, and rare earth element (REE) compositions were determined on selected samples at Washington State University by x-ray fluorescence (XRF) and inductively coupled plasma mass spectrometric (ICPMS) techniques, using the procedure given in Johnson et al. (1998) and Knaack et al. (1994).

Whole rock powdered samples for Nd analysis were weighed and totally spiked with tracer solutions of ^{150}Nd plus ^{149}Sm. Samples for Sr analysis were totally spiked with ^{84}Sr plus ^{87}Rb tracer solutions. Spiked whole rock samples for Nd and Sr analysis were dissolved in a 5:2 mix of vapor-distilled concentrated HF and HNO_3 in sealed PFA Teflon vials at 160°C for ≈72 and 120 hours, respectively. The resultant fluoride solutions of all samples were evaporated to dryness, then converted to chloride solutions by the addition of 6N HCl to the residue and heated at 160°C for ≈24 hours. The resultant chloride solutions were evaporated to dryness, and 0.75N HCl was added to the residue and heated at 160°C for ≈2 hours. Rb, Sr, and the REE were separated from the dissolved samples using BioRad AG50-X8 200-400 mesh cation exchange resin in PFA Teflon columns. Nd and Sm were separated from REE and each other by using Di (2-ethylhexyl phosphate) -based chromatography (HDEHP). Chemical processing blanks are < 400 pg for Nd, Sm, Sr and < 100 pg for Rb.

Powdered whole rock samples for Pb analysis were weighed and dissolved in a 5:2 mix of vapor-distilled concentrated HF and HNO_3 in sealed PFA Teflon vials at 160°C for ≈72 hours. The fluoride solutions were evaporated to dryness and converted to chlorides by addition of 6N HCl, and then to bromides by the addition of 0.5N HBr. Pb was separated from the cooled solutes using HBr-HNO_3-based chromatography with a BioRad AG1-X8 200-400 mesh anion exchange resin in heatshrink FEP Teflon columns. Pb processing blanks are ≈150 pg.

The isotopic composition of the purified Sr, Nd, and Rb, Sm, and Pb fractions were analyzed using a VG354 5-collector and MM30 mass spectrometers, respectively. The measured isotopic ratios were corrected for mass fractionation and discrimination by normalizing to the

following ratios: $^{146}Nd/^{144}Nd$ = 0.7219, $^{152}Sm/^{154}Sm$ = 1.17537, $^{86}Sr/^{88}Sr$ = 0.1194. Isotopic reference standards measured at the time of the isotopic measurements are as follows: $^{146}Nd/^{144}Nd$ = 0.511848 ± 0.000008 (La Jolla Nd standard), and is in close agreement with previous determined values of Thirlwall (1991); $^{87}Sr/^{86}Sr$ = 0.710238 ± 0.000012, 0.710215 ± 0.000035 and 0.710230 ± 0.00002 (SRM 987 standard). Mass fractionation for measured Pb ratios were corrected by the following factors: $^{206}Pb/^{204}Pb$ = 0.13%. a.m.u.$^{-1}$; $^{207}Pb/^{204}Pb$ = 0.14%. a.m.u.$^{-1}$; and $^{208}Pb/^{204}Pb$ = 0.11%. a.m.u.$^{-1}$, which were established by repeated measurement of the standard NBS 981 using the reference isotopic values of Todt et al. (1996).

Results

The Wolverine Creek Metamorphic Suite

Three metasedimentary rocks representative of the Casino, Cash, and Mt. Nansen areas were analyzed for their trace element and REE compositions with the objective to evaluate the protolith types, which are presently not constrained. The major, trace, and REE values are given in Table 3.2. The rock types (quartz-mica schists, DS192, DS97-49, and calc-silicate, DS97-50) are characterized by transposed layering, are quartz-rich, and contain muscovite, biotite, graphite, microcline, garnet, and clinozoisite. The high quartz content of these rocks is shown by the range in SiO_2 (69 to 84 wt. %), which correlates with a overall higher sediment maturity relative to shales (Taylor and McLennan 1985). The SiO_2/Al_2O_3 (4.7 to 29) and K_2O/Na_2O (1.49 to 1.62) ratios show that the rocks have a graywacke to lithic arenite composition (Pettijohn et al. 1988).

The REE data for the metasedimentary rocks show flat heavy rare earth element (HREE) profiles, with moderate negative Eu anomalies (Eu/Eu* = 0.5 to 0.8) (Fig. 3.3A). The light rare earth element (LREE) profiles vary between samples with least LREE enrichment (La_N/Yb_N = 3.8) for DS192, with higher enrichment (La_N/Yb_N = 4.4 to 10.3) shown for samples DS97-49 and 50. Sample DS97-50 also possesses the highest Th/Sc

(1.77) and La/Sc (5.72) values, with samples DS192 and DS97-49 possessing low Th/Sc (0.1 to 0.4), and La/Sc (1.2 to 1.7) ratios.

The remaining three rock units of the Wolverine Creek Metamorphic Suite (DS194, 218 and DS97-84) were analyzed for major, trace, and REE contents. The protoliths of these rock units are not fully understood, though these rocks are homogeneous in appearance, quartzofeldspathic in composition, and are non-graphite-bearing. They possess chemical compositions compatible with the rocks being meta-igneous. On this basis, the following igneous precursors to the meta-igneous rocks are proposed; granite (DS194), granodiorite (DS97-84), and basalt (DS218), based on the SiO_2 vs. alkali classification of Middlemost (1985). The felsic rocks straddle the peraluminous and metaluminous boundary on the alumina saturation plot (Shand 1947). The inferred meta-igneous rocks possess very similar HREE patterns (Fig. 3.3B). Sample DS194 possesses the largest negative anomaly (Eu/Eu* = 0.47) and LREE enrichment (La_N/Yb_N = 8.62). Smaller Eu anomalies and LREE enrichments are shown for DS97-84 (Eu/Eu* = 0.69, La_N/Yb_N = 1.10) and DS218 (Eu/Eu* = 0.80, La_N/Yb_N = 5.46).

The Nd, Sr, and Pb radiogenic isotope compositions were also determined for rocks of the Wolverine Creek Metamorphic Suite assemblage. The isotopic data are given in Tables 3.3, 3.4, and 3.5. The Nd, Sr, and Pb isotopic compositions are described in epsilon and initial notations, respectively, with εNd, $^{87}Sr/^{86}Sr$, $^{208}Pb/^{204}Pb$, $^{207}Pb/^{204}Pb$, and $^{206}Pb/^{204}Pb$ calculated at the minimum age of 350 Ma. The metasedimentary rocks of the Wolverine Creek Metamorphic Suite possess εNd_{350} values between -3.6 and -8.3, $^{147}Sm/^{144}Nd$ values from 0.1095 to 0.1734, and depleted mantle model ages (T_{DM}, or crustal residence ages) of 1.56 to 1.91 Ga. The $^{87}Sr/^{86}Sr_{350}$ values for the same rocks are between 0.69398 and 0.70472; the very low values clearly indicate disturbance to the Rb-Sr isotopic system by loss of ^{87}Sr. The inferred meta-igneous rocks possess εNd_{350} values

of -0.8 to -11.6, $^{147}Sm/^{144}Nd$ values of 0.1157 to 0.1276, and T_{DM} ages of 1.80 to 2.02 Ga, and $^{87}Sr/^{86}Sr_{350}$ values of 0.70475 to 0.71550. Samples DS193, 194, and 218 were analyzed for their Pb isotopic compositions, and show a narrow range for $^{207}Pb/^{204}Pb_{350}$ (from 15.781 to 15.787) and $^{206}Pb/^{204}Pb_{350}$ (from 18.328 to 18.728), but a wider range in $^{208}Pb/^{204}Pb_{350}$ compositions (from 38.607 to 39.052).

Mid-Cretaceous Intrusions

The major element data (SiO_2, Na_2O, K_2O, and FeO) classify the Dawson Range batholith as calc-alkaline (after the classification of Irvine and Baragar 1971). Based on the SiO_2 vs. alkali plot of Middlemost (1985) for plutonic rocks, the Dawson Range batholith is composed of quartz monzodiorite (Casino area samples DS190, 211), and granodiorite lithologies (Mt. Nansen area sample DS97-63). The extended REE profiles for all samples are virtually identical, showing positive anomalies for Ba and Th, and a pronounced negative Nb anomaly (Fig. 3.3C). Sample DS190 shows slight differences in its REE profile with positive Sr and Eu ($Eu/Eu^* = 1.44$) anomalies, and lower HREE values (Fig. 3.3C). The positive Sr and Eu anomalies coincide with the greater abundance of plagioclase in the sample. The εNd and $^{87}Sr/^{86}Sr$ values for the Dawson Range batholith are calculated at a crystallization age of 104 Ma, yielding εNd_{104} values from -4.5 to -7.4, and $^{87}Sr/^{86}Sr_{104}$ values between 0.70663 and 0.70746. The $^{147}Sm/^{144}Nd$ values range from 0.0958 to 0.1270, with T_{DM} ages of 1.13 to 1.53 Ga. The samples possess very similar $^{206}Pb/^{204}Pb_{104}$ (19.044 to 19.212), $^{207}Pb/^{204}Pb_{104}$ (15.659 to 15.684), and $^{208}Pb/^{204}Pb_{104}$ (38.832 to 39.039) ratios.

The major element data characterize the Casino Plutonic Suite as calc-alkaline, with granite (samples DS185, 230) and alkali feldspar granite (samples DS208, 224) lithologies. The Casino Plutonic Suite intrudes the Dawson Range batholith and although contemporaneous, possesses distinctly different REE profiles (Figs. 3.3C, D). The alkali

feldspar granitic phases of the Casino Plutonic Suite have pronounced Sr and Eu anomalies (Eu/Eu* = 0.64 and 0.71), with slightly higher Th contents. The granitic phases of the Casino Plutonic Suite show pronounced Sr and Eu anomalies (Eu/Eu* = 0.14 and 0.69), and lower Ba contents than the alkali feldspar granitic phases. The Sr and Eu anomalies coincide with the low abundance (≈10%) of plagioclase in these samples. Though the REE profiles for the different lithologies of the Casino Plutonic Suite are distinctly different, the isotope compositions are broadly similar, εNd_{104} values from -3.7 to -6.6, $^{147}Sm/^{144}Nd$ values from 0.0952 to 0.1673, and T_{DM} ages of 1.16 to 1.20 Ga, $^{87}Sr/^{86}Sr_{104}$ values of 0.70592 to 0.70739, and $^{206}Pb/^{204}Pb_{104}$ (19.002 to 19.333), $^{207}Pb/^{204}Pb_{104}$ (15.667 to 15.698), and $^{208}Pb/^{204}Pb_{104}$ (38.741 to 38.996). All these values are similar to those of the Dawson Range batholith.

Late Cretaceous Plutons

These plutons are calc-alkaline, with the major element ratios indicating a classification of the Patton porphyry (samples DS64, 113) as a granodiorite, and the Cash (sample DS97-7) and Mt. Nansen (sample DS97-86) porphyries as granite (classification after Middlemost 1985). The SiO_2 vs. K_2O data classify the Cash and Mt. Nansen porphyries as shoshonitic (K_2O = 3.75 to 4.14), and the Patton porphyry (K_2O = 2.07 to 2.77) as high K (based on the classification of Peccerillo and Taylor 1976). The REE profiles for the late Cretaceous plutons show that they possess slightly higher Th, no Eu anomalies, and greater LREE enrichment (La_N/Yb_N = 15.38 to 17.82) than the Dawson Range batholith (La_N/Yb_N = 7.03 to 10.66) (Fig. 3.3E). The REE profiles for the late Cretaceous plutons are very similar to each other. The slight differences between the late Cretaceous plutons are as follows: Pr to Er are slightly higher for the Mt. Nansen porphyry (DS97-86, Fig. 3.3E); the Patton porphyry has a positive Sr anomaly (DS64, 113, Fig. 3.3E); and the Cash porphyry has slightly higher Th values (DS97-7, Fig. 3E).

The εNd and $^{87}Sr/^{86}Sr$ values are determined for the crystallization age of 70 Ma, show relatively juvenile εNd_{70} (+2.2 to -0.2) and $^{87}Sr/^{86}Sr_{70}$ values (0.70487 to 0.70553), with T_{DM} values between 0.71 and 0.82 Ga. The Pb isotopic compositions were determined only for the Patton Porphyry (Table 3.5), which possesses more radiogenic isotopic ratios than that of a hydrothermal K-feldspar from the potassic zone of the Casino occurrence (Table 3.5), likely indicating some introduction of radiogenic Pb to the whole rock as a result of hydrothermal alteration.

Discussion

The Wolverine Creek Metamorphic Suite

The geochemistry and isotope systematics of metasedimentary rocks of elsewhere in Yukon-Tanana terrane have been investigated by Creaser et al. (1997) and Grant (1997), and correlated late Paleozoic metamorphic rocks of the Tracy Arm, Endicott Arm, Port Houghton, and Ruth assemblages between the Stikine and Peninsular-Alexander-Wrangellia terranes studied by Samson et al. (1991) (≈400 km SW of the study area). Creaser et al. (1997) reported a threefold grouping of geochemical and isotopic data (i.e., Nd isotope data: Type I, εNd_{350} = -3.9 to +3.4, $^{147}Sm/^{144}Nd$ = 0.124 to 0.139, T_{DM} = 0.9 to 1.3 Ga; Type II, εNd_{350} = -4.6 to -14.7, $^{147}Sm/^{144}Nd$ = 0.114 to 0.126, T_{DM} = 1.5 to 2.3 Ga; Type III, εNd_{350} = -20.0 to -24.3, $^{147}Sm/^{144}Nd$= 0.098 to 0.112, T_{DM} = 2.5 to 2.8 Ga). The data of Samson et al. (1991) and Grant (1997) are broadly similar to these populations (Fig. 3.4). Two distinct provenances are proposed for the sedimentary precursors of metamorphic rocks, one bearing the characteristics of a felsic upper crust with a long crustal residence age, and the other with attributes of a primitive crust (basaltic to andesitic) with a short crustal residence history (Creaser et al. 1997). Rocks of intermediate composition (Type II of Creaser et al. 1997) of the two provenances are proposed to represent a mixed sediment of juvenile and ancient crustal lithologies

(Samson et al. 1991; Creaser et al. 1997; Grant 1997). The geochemical and isotopic data of the Wolverine Creek Metamorphic Suite of this study possess similar characteristics to the metamorphic rocks from other regions of the Yukon-Tanana terrane (Fig. 3.4), and suggest that the provenance includes a mixed input of primitive mafic material and geochemically evolved felsic crust with a significant crustal residence history.

The La/Sc and Th/Sc ratios of metasedimentary rocks are useful provenance discrimators (Bhatia and Crook 1986; Taylor and McLennan 1985), with low Th/Sc and La/Sc values being indicative of a source region of dominantly mafic rock types, and high Th/Sc and La/Sc values indicating a source area of felsic compostion. The high Th/Sc (1.77) and La/Sc (5.72) values of sample DS97-50 indicate a source material of upper crustal compositon; with the low Th/Sc (0.1 to 0.4), and La/Sc (1.2 to 1.7) ratios of samples DS192 and DS97-49 suggesting a protolith of an andesitic to average upper continental crust composition (Taylor and McLennan 1985). The increased felsic component shown by the higher Th/Sc values (0.1 to 1.7) is mirrored in the LREE enrichment (La_N/Yb_N = 3.8 to 10.3). The discrimination plots for inferring the tectonic setting of sedimentation (Bhatia and Crook 1986) indicate that the Wolverine Creek Metamorphic Suite assemblage is allied to an oceanic island arc and to passive and active continental margins (Fig. 3.5). These inferred tectonic settings again correlate with those indicated for the metamorphic rocks from other areas of the Yukon-Tanana terrane (Fig. 3.5) (Creaser et al. 1997; Grant 1997), and further illustrate that both a provenance of primitive mafic material and an evolved felsic crust is a widespread characteristic of metasedimentary rocks in the Yukon-Tanana terrane.

Meta-igneous rocks of the Wolverine Creek Metamorphic Suite from the Casino area possess similar εNd_{350} (-6.6 to -11.6) and $^{87}Sr/^{86}Sr_{350}$ (0.70788 to 0.7155) ratios, and suggest that the magmas contained a component of isotopically evolved continental material. The meta-igneous sample DS97-84 from the Mt. Nansen area, shows a more

juvenile composition (εNd_{350} = -0.8, $^{87}Sr/^{86}Sr_{350}$ = 0.70475). These data may suggest either different processes of magma generation or a heterogeneity in the basement of the Yukon-Tanana terrane. Compositional discrimination plots such as Nb vs. Y and Rb vs. Nb + Y (Pearce et al. 1984) indicate a volcanic arc and syn-collisional tectonic setting for the meta-igneous rocks of the Wolverine Creek Metamorphic Suite. A continental calc-alkalic arc tectonic setting is also suggested by the Zr, Ti, Y data based on tectonic discrimination plots of Pearce and Cann (1973) and Pearce (1983), which is consistent with the tectonic environment proposed by Mortensen (1992) for the Yukon-Tanana terrane during the Devonian and Mississippian times.

The precise ages of the meta-igneous rocks of the Wolverine Creek Metamorphic Suite are not known. However, the meta-igneous rocks of the study area may represent magmatism of comparable age to orthogneisses of the Selwyn gneiss and Fiftymile Batholith (50 to 200 km NW of the study area), which possess early Mississippian ages (Mortensen 1986). The meta-igneous rocks in the Yukon-Tanana terrane (e.g., Fiftymile Batholith, Selwyn gneiss, Simpson Range Plutonic Suite, meta-igneous rocks of the Telsin tectonic zone, Lake George, and Macomb subterranes) have been correlated largely on the basis of their U-Pb zircon ages, which are Devonian to early Mississippian (Mortensen 1986; Mortensen 1992; Grant 1997). Radiogenic isotope data from the Simpson Range Plutonic Suite ($^{87}Sr/^{86}Sr_{350}$ = 0.707 to 0.712, εNd_{350} = -1.7 to -12.8, T_{DM} = 1.67 to 2.10 Ga, Grant 1997) and the meta-igneous rocks of the Telsin tectonic zone (εNd_{350} = -2.5 to -6.2, T_{DM} = 1.50 to 1.79 Ga, Stevens et al. 1996) are broadly similar to those reported in this study from the Casino area, whereas the sample from the Mt. Nansen area (DS97-84) has more juvenile values ($^{87}Sr/^{86}Sr_{350}$ = 0.70475, εNd_{350} = -0.8). The meta-igneous rocks of the Wolverine Creek Metamorphic Suite possess similar to less radiogenic initial Pb compositions to the K-feldspars of Simpson Range Plutonic Suite (Grant 1997) and the Alaskan granitoids (Aleinikoff et al. 1987), but are more

radiogenic than model Pb crustal evolution curves of Stacey and Kramers (1975), Zartman and Doe (1981) and Godwin and Sinclair (1982) (Figs. 3.6A-B). The higher Pb isotopic ratios of the meta-igneous rocks of Alaska, Simpson Range Plutonic Suite, and the Wolverine Creek Metamorphic Suite relative to the model evolution of the upper crust suggests that the granitoids were derived from similar crustal material with higher U/Pb and Th/Pb ratios than these models. This is shown on Figs. 3.6A and B in which Pb evolution curves deriving from different $^{238}U/^{204}Pb$ (μ) and $^{232}Th/^{204}Pb$ (ω) ratios are determined from 2 Ga (T_{DM} age given from Nd isotopic data of the Wolverine Creek Metamorphic Suite) model crust of the Stacey and Kramers (1975) curve.

Mid-Cretaceous Intrusions

The REE profiles shown for the Dawson Range batholith, enriched in LILEs (Ba, Sr, K, Th, Rb), Nb anomaly, would typically be ascribed to magmas being derived from a mantle source associated with subduction (Peccerillo and Manetti 1985; Peccerillo et al. 1988). However, a trace element subduction signature may be produced from partial melting of material previously related to subduction processes (Johnston and Wyllie 1988; Morris and Hooper 1997). The Dawson Range batholith was emplaced into the Wolverine Creek Metamorphic Suite of the Yukon-Tanana terrane during the mid-Cretaceous. The high $^{87}Sr/^{86}Sr_{104}$, negative εNd_{104}, early Proterozoic T_{DM} values (Table 3.3 and 3.4), and initial Pb isotopic compositions, which are similar to upper crust evolution of ≈100 Ma (Figs. 3.6C and D) indicate a dominant crustal contribution to the magma of the Dawson Range batholith.

Using the equations of Langmiur et al. (1978), along with the average εNd_{104} and Sr_{104} compositions of the Wolverine Creek Metamorphic Suite (Sr = 0.7112, εNd = -8.5) and a basalt (Sr = 0.70362, εNd = +6.8, Carlson et al. 1981) to represent a mantle component, 60 to 80% contribution of the Wolverine Creek Metamorphic Suite to the

Dawson Range batholith magma would have been necessary to produce the Nd and Sr isotopic composition of the Dawson Range batholith. Relative crustal contributions to the magmas of the Dawson Range batholith are also shown by the Nd crustal index (NCI) (DePaolo et al. 1992) (NCI = 0 means the rock has no crustal Nd and the εNd is equal to the mantle value; NCI = 1 means the rock has a crustal origin and the εNd equals the crustal value). The Dawson Range batholith possesses ~80% crustal Nd (NCI = 0.8). The isotope data suggest that the magmas of Dawson Range batholith was either a mantle-derived melt possibly related to subduction and subsequently strongly contaminated by crustal material, or a magma resulting from partial melting of an isotopically evolved crust. The NCI value for the Dawson Range batholith suggests that the magmas were formed under conditions of high crustal temperature and low mantle-derived melt contribution (DePaolo et al. 1991). However, if the magma of the Dawson Range batholith were mantle-derived from a subduction process, as suggested by the Nb data (Fig. 3.3C), then a large negative Eu anomaly resulting from the generation of magma by fractionation of mantle-derived basalt, and the presence of mafic-intermediate lithologies might be observed. The absence of the latter suggests that the Dawson Range batholith magmas may be the product of partial melting of an isotopically evolved crust, with the subduction signature inherited from the source rocks.

The Casino Plutonic Suite possesses virtually identical Sr and εNd compositions to the Dawson Range batholith. However, the Pb compositions approach those of the Wolverine Creek Metamorphic Suite. The negative Eu anomalies and greater U and Th contents suggest that the Casino Plutonic Suite is a highly fractionated magma. The geochemical and isotopic data of the contemporaneous Casino Plutonic Suite suggest that the magmas were generated as a late-stage, fractionated magma of the Dawson Range batholith, a conclusion consistent with the geochronology and isotopic data.

Late Cretaceous Plutons

The late Cretaceous plutons are enriched in LILEs and possess a Nb anomaly (Fig. 3.3E), similar to the Dawson Range batholith, which suggests that the magmas may be mantle-derived and related to subduction processes (Peccerillo and Manetti 1985; Peccerillo et al. 1988), or have inherited these characteristics from crustal sources. However, unlike the Dawson Range batholith, the late Cretaceous intrusions have much more primitive εNd and Sr isotopic values, younger T_{DM} ages, and greater LREE enrichment. The crustal component in these magmas is ≈20% as determined from the formulation of Langmiur et al. (1978), the average isotope compositions of the Wolverine Creek Metamorphic Suite and the Dawson Range batholith, combined compositions of the latter at 70 Ma, and a mantle component (Sr = 0.70362, εNd = +6.8, Carlson et al. 1981). The isotopic and REE data suggest that the magmas of the late Cretaceous plutons were ultimately generated through subduction processes, and melt generation within the mantle, with subsequent minor crustal inheritance.

Figures 3.6E and F display the initial Pb isotopic ratios of the whole rock Patton porphyry and a hydrothermal K-feldspar, and mantle-derived magmas defined by the Northern Hemisphere Reference Line (NHRL) of Hart (1984). The more radiogenic Pb isotopic ratios of the Patton porphyry relative to the hydrothermal K-feldspar (Table 3.5; Figs. 3.6E-F) likely represent modification of the Patton porphyry with hydrothermally precipitated sulfides, which have a more radiogenic Pb composition than hydrothermal K-feldspar (Selby, unpub. data). Pb isotopic ratios of the hydrothermal K-feldspar are the most likely representative of the magmatic composition of the Patton porphyry, as whole rock samples can not be analyzed which have not been hydrothermally overprinted. The hydrothermal K-feldspar Pb isotopic ratios plot near to the $^{207}Pb/^{204}Pb$ vs. $^{206}Pb/^{204}Pb$ and the $^{208}Pb/^{204}Pb$ vs. $^{206}Pb/^{204}Pb$ NHRLs (Figs. 3.6E-F), which are compatible with mantle-derived magma for the Patton Porphyry. The Pb isotope values are in accord with the

εNd and Sr isotopic data suggesting that the late Cretaceous magmas were mantle-derived, with minimal crustal contamination.

Tectonic Implications

The Wolverine Creek Metamorphic Suite

The geochemical and isotopic data presented for metasedimentary units of the Wolverine Creek Metamorphic Suite from the Dawson Range indicate a mixed provenance of detritus, which is also interpreted for the metasedimentary rocks from the Telsin tectonic zone (Creaser et al. 1997), the Money Klippe (Grant 1997), and correlated metasedimentary rocks located between the Peninsular-Alexander-Wrangellia and Stikine terranes (Samson et al. 1991). The rock units are composed of detritus derived from isotopically evolved and juvenile crustal material. Creaser et al. (1997) proposed that the detritus was shed from Precambrian rocks of North America to the east and mafic-intermediate magmatism of the Yukon-Tanana terrane, which was situated outboard of or distal to ancestral North America during the pre-early Mississippian times. This tectonic model is consistent with the data from the Wolverine Creek Metamorphic Suite of the Dawson Range. A possible source of juvenile sediment in the Dawson Range is the in situ intrusions of ultramafic bodies that occur north of the Casino area (Godwin 1975). These ultramafic bodies may correlate with the in situ intrusions of meta-mafic rocks of the Finlayson Lake area (Murphy 1998).

The Devonian-Mississippian magmatism of the Yukon-Tanana terrane is comprised of mafic to felsic and peraluminous igneous units (Mortensen 1992; Stevens et al. 1996; Grant 1997; Murphy 1998; this study). The meta-mafic-intermediate igneous rocks of the Yukon-Tanana terrane are interpreted to represent magmatism and not allochthonous portions of an oceanic floor (Stevens et al. 1996; Creaser et al. 1997; Grant 1997; Murphy 1998) suggesting an active continental margin setting during Devonian-

Mississippian times. The geochemical affinity of the igneous rocks suggests a volcanic arc setting (Stevens et al. 1996; Grant 1997; this study), which is consistent with previous tectonic interpretations (Mortensen and Jilson 1985; Rubin et al. 1990; Mortensen 1992). The peraluminous orthogneisses are characterized by a greater crustal component (εNd = -14 to -16; Sr = 0.716 to 0.738; Bennett and Hansen 1988; Mortensen 1992; Aleinikoff et al. 1986; Hansen et al. 1989) than those of the felsic meta-igneous units (εNd = -2.5 to -12.8; Sr = 0.7079 to 0.7155; Samson et al. 1991; Stevens et al. 1996; Grant 1997; this study). The peraluminous orthogneisses may represent overthickening of the Yukon-Tanana terrane basement in the magmatic arc promoting anatexis and/or assimilation, which generated these magmas with a strong crustal signature.

Mid-Cretaceous Intrusions

Granitic bodies of mid-Cretaceous age occur throughout the Yukon-Tanana terrane, Intermontane Belt, and the Omineca Belt of the Northern Cordillera (Gabrielse 1985; Wheeler et al. 1991). The isotope systematics of the mid-Cretaceous intrusions (Dawson Range batholith and Casino Plutonic Suite) of the Dawson Range indicate a significant component of crustal material with long crustal residence ages (≈1.1 to 1.5 Ga). The available radiogenic isotope data for other mid-Cretaceous granites suggest that the granites of the Yukon-Tanana terrane and the Omineca Belt have a significant Precambrian crustal signature (Le Couteur and Tempelman-Kluit 1976; Morrison et al. 1979; Driver et al. 1997, 1998; this study). However, mid-Cretaceous granitic plutonism in the Intermontane Belt possesses Sr isotope signatures that are typically more juvenile, and are documented to reflect the emplacement through Phanerozoic crust (Morrison et al. 1979).

The evaluation of the geochemical and isotope data of the mid-Cretaceous intrusions of the Dawson Range indicates that the magmas are most likely not derived from a mantle source contemporaneous with subduction but are a product of partial

melting of the Yukon-Tanana terrane basement. A similar interpretation is given for the mid-Cretaceous Cassiar Batholith, northern British Columbia (Driver et al. 1997, 1998). The emplacement of the Dawson Range batholith is associated with strike-slip faults as indicated by strong, primary-foliation defined by hornblende and feldspar crystals at the margins at the batholith (Payne et al. 1987). Dextral strike-slip motion during the Cretaceous resulted from east-oblique subduction of the Peninsular-Alexander-Wrangellia terrane beneath the margin of North America (Hansen 1990). The generation of the Dawson Range batholith magmas was probably the result of partial melting of the crust caused by overthickening of North America, which is also advocated for the Cassiar batholith (Driver et al. 1998). The contemporaneous strike-slip faults of the Dawson Range batholith may have provided a path for the magma, being emplaced, as observed, as an elongate body.

Late Cretaceous Plutons

These plutons of the Dawson Range are typically associated with porphyry-type mineralization, occurring in a northwest-trending belt, which broadly coincides with the Big Creek Fault (Sinclair et al. 1981). In relation to the mid-Cretaceous intrusions, late Cretaceous plutons have primitive isotopic signatures and geochemical affinities to magmas derived from subduction-related processes. East-oblique subduction beneath the Yukon-Tanana terrane during the late Cretaceous (Hanson 1990) generated mantle-derived magmas with minor crustal inheritance that were emplaced into the Yukon-Tanana terrane of west-central Yukon. Subsequent crystallization and exsolution of hydrothermal fluids from the magmas produced porphyry style Cu-Au-Mo mineralization (Selby et al. 1997).

Conclusions

The metasedimentary rocks of the Wolverine Creek Metamorphic Suite of the Dawson Range are quartz-rich (schists, calc-silicate), with detritus derived from North America to the east and a mafic-intermediate arc to the west. The provenance of the sediments is consistent with similar age metasedimentary rocks of the Yukon-Tanana terrane (Creaser et al. 1997; Grant 1997) and late Paleozoic metamorphic rocks of the Tracy Arm, Endicott Arm, Port Houghton, and Ruth assemblages between the Stikine and Alexander-Wrangellia terranes (Samson et al. 1991). The meta-igneous rocks of the Wolverine Creek Metamorphic Suite represent mafic to felsic Devonian-Mississippian magmatism of continental arc. The magmas inherited a component of Precambrian crustal material.

Isotope studies of the Dawson Range batholith and Casino Plutonic Suite indicate that the Yukon-Tanana terrane is underlain by rocks of a Precambrian provenance, which is in agreement with studies by Le Couteur and Tempelman-Kluit (1975); Morrison et al. (1979); Aleinikoff et al. (1981); Bennet and Hanson (1988); Hanson et al. (1989); Mortensen (1992); Grant (1997). The magmas of the Dawson Range batholith were generated from partial melting of the Yukon-Tanana terrane basement, resulting from overthickening of the crust as a result of subduction, though a component of subduction-derived magma cannot be precluded. Coeval strike-slip faulting produced a pathway for the magmas, producing an elongate batholith. Isotopic ages of Mortensen J. K. (pers. comm. 1997) and Hart C. J. R. (pers. comm. 1998), and REE indicate that the magmas of the Casino Plutonic Suite are a late stage fractionated magma derived from the Dawson Range batholith. It is therefore suggested that the Casino Plutonic Suite should be grouped with the Dawson Range batholith and not the late Cretaceous Prospector Mountain Plutonic Suite as has been done hitherto.

Geochemical data for the late Cretaceous plutons indicate that the magmas were derived from a mantle source during subduction. The data for the Dawson Range batholith and the late Cretaceous plutons indicate that these magmas were generated through significantly different processes (partial melting of the basement and mantle-derived, respectively), though associated with subduction. Changes in the crustal thickness of North America may be the control mechanism for the partial melting of crustal material above the subducting plate, and the processes generating magmas between mid and late Cretaceous times.

References

Aleinikoff, J. N., Dusel-Bacon, C., and Foster, H. L. 1986. Geochronology of augen gneiss and related rocks, Yukon-Tanana Terrane, east-central Alaska. Geological Society of America Bulletin, **97**: 626-637.

Aleinikoff, J. N., Dusel-Bacon, C., Foster, H. L., and Futa, K. 1981. Proterozoic zircon from augen gneiss, Yukon-Tanana upland, east-central Alaska. Geology, **9**: 469-473.

Aleinikoff, J. N., Dusel-Bacon, C., Foster, H. L., and Nokleberg, W. J. 1987. Lead isotopic fingerprinting of tectono-stratigraphic terranes, east-central Alaska. Canadian Journal of Earth Sciences, **24**: 2089-2098.

Bennett, V. C., and Hansen, V. L. 1988. Neodymium isotope similarities between the Yukon-Tanana terrane, Yukon Territory and Continental North America. Geological Society of America Abstracts with Programs, **20**: A111.

Bhatia, M. R., and Crook, K. A. W. 1986. Trace element characteristics of graywackes and tectonic setting discrimination of sedimentary basins. Contributions to Mineralogy and Petrology, **92**: 181-193.

Bower, B., Payne, J., Delong, C., and Rebagliati, C. M. 1995. The oxide-gold supergene and hypogene zones at the Casino gold-copper-molybdenite deposit west-central Yukon. In: Porphyry

Deposits of the Northwestern Cordillera of North America, T. G. Schroeter (ed.), Canadian Institute of Mining, Metallurgy and Petroleum, Special Volume **46**: 352-366.

Boynton, S. A. 1984. Cosmochemistry of the Rare Earth Elements: Meteorite studies. *In* Rare Earth Element Geochemistry, Developments in Geochemistry, **2**. *Edited* by P. Henderson. Elsevier, New York, pp. 90-114.

Carlson, G. G. 1987. Geology of the Mt. Nansen (115-I/3) and Stoddart Creek (115-I/6) map areas, Dawson Range, central Yukon. Indian and Northern Affairs Canada, Northern Affairs: Yukon Region Open File 1987-2.

Carlson, R. W., Lugmair, G. W., and MacDougall, J. D. 1981. Columbia river volcanism: The question of mantle heterogeneity or crustal contamination. Geochimica Cosmochimica et Acta, **45**: 2483-2499.

Creaser, R. A., Erdmer, P. E., Stevens, R. A., and Grant, S. G. 1997. Tectonic affinity of Nisultin and Anvil assemblages strata from the Telsin tectonic zone, northern Canadian Cordillera: constraints from neodymium isotope and geochemical evidence. Tectonics, **16**: 107-121.

DePaolo, D. J., Perry, F. V., and Baldridge, W. S. 1992. Crustal versus mantle sources of granitic magmas; A two-parameter model based on Nd isotopic studies. Royal Society of Edinburgh Transactions: Earth Sciences, **83**: 439-446.

Driver, L. A., Creaser, R. A., Chacko, T., and Erdmer, P. 1997. Isotope geochemistry of the Cretaceous Cassiar batholith, Yukon-B.C., Canada. Abstract with programs, Geological Society of America, A445.

Driver, L. A., Creaser, R. A., Chacko, T., and Erdmer, P. 1998. Petrogenesis of the Cretaceous Cassiar batholith, Yukon-B.C., Canada. Compiled by F. Cook and P. Erdmer. *In* 1998, Slave-northern Cordillera Lithospheric Evolution (SNORCLE) Transect and Cordilleran Tectonics Workshop Meeting (March 6-8), Simon Fraser University, Lithoprobe Report **64**: 158-164.

Gabrielse, H. 1985. Major dextral transcurrent displacement along the northern rocky mountain trench and related lineaments in north-central British Columbia. Geological Society of America Bulletin, **96**: 1-14.

Godwin, C. I. 1975. Alternative interpretations for the Casino complex and Klotassin batholith in the Yukon Crystalline Terrane. Canadian Journal of Earth Sciences, **12**: 1910-1916.

Godwin, C. I., and Sinclair, A. J. 1982. Average lead isotope growth curves for shale-hosted zinc-lead deposits, Canadian Cordillera. Economic Geology, **77**: 675-690.

Goldstein, S. L., O'Nions, R. K., and Hamilton, P. J. 1984. A Sm-Nd isotopic study of atmospheric dusts and particulates from major river systems. Earth and Planetary Science Letters, **70**: 221-236.

Grant, S. L. 1997. Geochemical, radiogenic tracer isotopic, and U-Pb geochronological studies of Yukon Tanana terrane rocks from the Money Klippe, southeastern Yukon, Canada. M.Sc. Thesis, University of Alberta, Edmonton.

Hansen, V. L. 1990. Yukon-Tanana terrane: a partial aquital. Geology, **18**: 365-369.

Hansen, V. L., Mortensen, J. K., and Armstrong, R. L. 1989. Pre-Jurassic ductile deformation Yukon-Tanana terrane: geochronologic constraints from the Telsin suture zone, Yukon. Canadian Journal of Earth Sciences, **26**: 2224-2235.

Hart, C. J. R., and Langdon, M. 1998. Geology and mineral deposits of the Mount Nansen camp Yukon. *In* Yukon Exploration and Geology 1997 Exploration and Geological Services Division, Yukon, Indian and Northern Affairs Canada, pp. 129-138.

Hart, C. J. R., and Selby, D. 1998. The Pattison Creek pluton - a mineralized Casino intrusion made bigger with gamma rays. *In* Yukon Exploration and Geology 1997 Exploration and Geological Services Division, Yukon, Indian and Northern Affairs Canada, pp. 89-96.

Hart, S. R. 1984. A large-scale isotope anomaly in the Southern Hemisphere mantle. Nature, **209**: 753-757.

Irvine, T. N., and Baragar, W. R. A. 1971. A guide to the chemical classification of common volcanic rocks. Canadian Journal of Earth Sciences, **8**: 523-546.

Johnson, D. M., Hooper, P. R., and Conrey, R. M. 1998. XRF analysis of rocks and minerals for major and trace element on a single low dilution Li-tetraborate fused bead. Advances in X-ray Analysis, **41**: In press.

Johnston, A. D., and Wyllie, P. J. 1988. Constraints on the origin of Archean trondhjemites based on phase relations of Nûk gneiss with H_2O at 15 kbar. Contributions to Mineralogy and Petrology, **100**: 35-46.

Johnston, S. T. 1995. Geological compilation with interpretation from geophysical surveys of the northern Dawson Range, central Yukon (115-J/9 and 115-J/10, 115-I/12, 1:100 000 scale map). Exploration and Geological Services Division, Yukon, Indian and Northern Affairs Canada, Open File 1995-2(G).

Knaack, C., Cornelius, S., and Hooper, P. 1994. Trace element analyses of rocks and minerals by ICP-MS. Geoanalytical laboratory, Washington State University, Pullman, Washington.

Langmuir, C. H. R. D., Vocke, J., Hanson, G. N., and Hart, S. R. 1978. A general mixing equation with applications to icelandic basalts. Earth and Planetary Science Letters, **37**: 380-392.

Le Couteur, P. C., and Tempelman-Kluit, D. J. 1976. Rb/Sr ages and a profile of initial Sr^{87}/Sr^{86} ratios for plutonic rocks across the Yukon Crystalline terrane. Canadian Journal of Earth Sciences, **13**: 319-330.

Middlemost, E. A. K. 1985. Magmas and Magmatic Rocks. Longman Group Limited, Essex.

Morris, G. A., and Hooper, P. R. 1997. Petrogenesis of the Colville igneous complex, northeast Washington: Implications for Eocene tectonics in the northern U.S. Cordillera. Geology, **25**: 831-834.

Morrison, G. W., Godwin, C. I., and Armstrong, R. L. 1979. Interpretation of isotopic ages and $^{87}Sr/^{86}Sr$ initial ratios for plutonic rocks in the Whitehorse map area, Yukon. Canadian Journal of Earth Sciences, **16**: 1988-1997.

Mortensen, J. K. 1986. U-Pb ages for granitic orthogneiss from western Yukon Territory: Selwyn Gneiss and Fiftymile batholith revisited. *In* Current Research, Part B Geological Survey of Canada, Paper, 86-1B, pp. 141-146.

Mortensen, J. K. 1992. Pre-mid-Mesozoic tectonic evolution of the Yukon-Tanana terrane, Yukon and Alaska. Tectonics, **11**: 836-853.

Mortensen, J. K., and Jilson, G. A. 1985. Evolution of the Yukon-Tanana terrane: evidence from southeastern Yukon Territory. Geology, **13**: 806-810.

Murphy, D. C. 1998. Mafic and ultramafic meta-plutonic rocks south of Finlayson Lake, Yukon: Setting and implications for the early geological and metallogenic evolution of the Yukon-Tanana terrane. Compiled by F. Cook and P. Erdmer. *In* 1998, Slave-northern Cordillera Lithospheric Evolution (SNORCLE) Transect and Cordilleran Tectonics Workshop Meeting (March 6-8), Simon Fraser University, Lithoprobe Report **64**: 120-129.

Payne, J. G., Gonzalez, R. A., Akhurst, K., and Sisson, W. G. 1987. Geology of the Colorado Creek (115-J/9), and Prospector Mountain (115-I/5) map areas, western Dawson Range, west-central Yukon. Exploration and Geological Services Division, Yukon, Indian and Northern Affairs Canada, Open File 1987-3.

Pearce, J. A. 1983. Role of sub-continental lithosphere in magma genesis at active continental margin. *In* Continental Basalts and Mantle Xenoliths. *Editted by* C. J. Hawkesworth and M. J. Norry. Shiva Published Limited, Nantwich, U.K., pp. 230-249.

Pearce, J. A., and Cann, J. R. 1973. Tectonic setting of basic rocks determined using trace elements analyses. Earth and Planetary Science Letters, **19**: 290-300.

Pearce, J. A., Harris, N. B. W., and Tindle, A. G. 1984. Trace element discrimination diagrams for the tectonic interpretation of granitic rocks. Journal of Petrology, **25**: 956-983.

Peccerillo, A., and Manetti, P. 1985. The potassic alkaline volcanism of central southern Italy; a review of data relevant to petrogenesis and geodynamic significance. Transactions Geological Society of South Africa, **88**: 379-394.

Peccerillo, A., Poli, G., and Serri, G. 1988. Petrogenesis of arenditic and kamafugitic rocks from central Italy. Canadian Mineralogist, **26**: 45-65.

Peccerillo, J. G., and Taylor, S. R. 1976. Geochemistry of some calc-alkaline volcanic rocks from the Kastamonu area, northern Turkey. Contribution to Mineralogy and Petrology, **58**: 63-81.

Pettijohn, F. J., Potter, P. E., and Siever, R. 1988. Sand and sandstone. Spinger-Verlag, New York.

Rubin, C. M., Miller, M. M., and Smith, G. M. 1990. Tectonic development of Cordilleran mid-Paleozoic volcano-plutonic complexes: Evidence for convergent margin tectonism. *In* Paleozoic and Early Mesozoic Paleographic relations; Sierra Nevada, Klamath Mountains, and Related

Terranes. *Edited by* D. S. Harwood and M. M. Miller Special Paper Geological Survey of America, **255**: 1-16.

Samson, S. D., Patchett, J. P., McClelland, W. C., and Gehrels, G. E. 1991. Nd isotopic characterization of metamorphic rocks in the Coast Mountains, Alaskan and Canadian Cordillera: ancient crust bounded by juvenile terranes. Tectonics, **10**: 770-780.

Selby, D., Nesbitt, B. E., Creaser, R. A., and Muehlenbachs, K. 1997. Primary magmatic ore fluids in porphyry deposits: A crustal component? Geological Society of America Annual Meeting, Salt Lake City, 1997, p. 127.

Shand, S. J. 1947. Eruptive rocks, their genesis, composition, classification and their relation to Ore-deposits 3rd ed. J. Wiley and Sons, New York.

Sinclair, W. D., Cathro, R. J., and Jensen, E. M. 1981. The Cash porphyry copper-molybdenum deposit, Dawson Range, Yukon Territory. Canadian Institute of Mining and Metallurgy Bulletin, **74**: 67-75.

Stacey, J. S., and Kramers, J. D. 1975. Approximation of terrestrial lead isotope evolution by two-stage model. Earth and Planetary Science Letters, **26**: 207-221.

Stevens, R. A., Erdmer, P. E., Creaser, R. A., and Grant, S. G. 1996. Mississippian assembly of the Nisultin assemblage: evidence from primary contact relationships and Mississippian magmatism in the Telsin tectonic zone, part of the Yukon-Tanana terrane of the south-central Yukon. Canadian Journal of Earth Sciences, **33**: 103-116.

Taylor, S. R., and McLennan, S. M. 1985. The continental crust: its composition and evolution. Blackwell Scientific Publications, Oxford.

Tempelman-Kluit, D. J. 1974. Reconnaissance geology of Aishihik Lake, Snag and part of the Stewart river map areas, west-central Yukon Territory. Geological Survey of Canada, Paper 73-14, p. 93.

Tempelman-Kluit, D. J. 1979. Transported cataclasite, ophiolite and granodiorite in Yukon: Evidence of arc-continent collision. Paper Geological Survey of Canada, Paper 79-14, pp. 1-28.

Tempelman-Kluit, D. J., and Wanless, R. K. 1975. Potassium-argon age determinations of metamorphic and plutonic rocks in the Yukon Crystalline Terrane. Canadian Journal of Earth Sciences, **12**: 1895-1909.

Thirlwall, M. F. 1991. Long-term reproducibility of multicollector Sr and Nd isotope ratio analyses. Chemical Geology, **94**: 85-104.

Todt, W., Cliff. A., Hanser, A., and Hofmann, A. W. 1996. Evaluation of ^{202}Pb-^{205}Pb double spike for high-precision lead isotope analysis. *In* Earth process: Reading the isotopic code. *Edited by* A. I. Basu and S. R. Hart. Geophysical Monograph **95**: 429-437.

Wheeler, J. O., Brookfield, A. J., Gabrielse, H., Monger, J. W. H., Tipper, H. W., and Woodsworth, G. J. 1991. Terrane map of the Canadian Cordillera. Geological Survey of Canada, Map 1713A.

Wheeler, J. O., and McFeely, P. *(Compilers)*. 1991. Tectonic assemblage map of the Canadian Cordilleran and adjacent parts of the United States of America. Geological Survey of Canada, Map 1712A, scale 1:2,000,000.

Zartman, R. E., and Doe, B. R., 1981. Plumbotectonics - The Model. Tectonophysics, **75**: 135-162.

Table 3.1. Description of rock types analyzed.

late Cretaceous Plutons	
DS64	Plagioclase-biotite porphyry* (Patton porphyry)
DS113	Plagioclase-biotite porphyry* (Patton porphyry)
DS97-7	K-feldspar porphyry* (Cash porphyry)
DS97-12	K-feldspar porphyry (Cash porphyry)
DS97-86	Quartz-plagioclase porphyry* (Mt. Nansen porphyry)
Casino Plutonic Suite	
DS185	Fine grained quartz-monzonite*
DS208	Fine grained quartz-monzonite*
DS210	Fine grained quartz-monzonite
DS221	Medium grained quartz-monzonite
DS224	Fine grained quartz-monzonite*
DS230	Aplitic quartz-monzonite*
Dawson Range Batholith	
DS189	Hornblende>biotite quartz diorite
DS190	Hornblende>biotite quartz diorite*
DS209	Hornblende>biotite quartz diorite*
DS211	Biotite>hornblende diorite
DS97-63	Hornblende>biotite granodiorite*
Wolverine Creek Metamorphic Suite	
Metasedimentary	
DS103	Biotite-quartz schist
DS192	Graphitic-micaeous quartzite*
DS232	Micaeous-quartzite
DS97-49	Microcline-muscovite-quartz schist*
DS97-50	Calc-silicate*
Meta-igneous	
DS193	Quartz-biotite-plagioclase-microcline gneiss
DS194	K-feldpsar-quartz-biotite gneiss*
DS218	Amphibolite*
DS97-84	Quartz-biotite-garnet gneiss*

*Samples analyzed for their major, trace and rare earth element compositions

Table 3.2. Major, trace, and rare earth element concentrations.

Sample	DS64	DS113	DS97-7	DS97-86	DS185	DS208	DS224	DS230	DS190	DS211	DS97-63
	PP	PP	CP	MNP	CPS	CPS	CPS	CPS	DRB	DRB	DRB
					Major elements, wt. %						
SiO_2	65.65	66.37	69.00	64.56	77.43	74.25	74.10	78.60	60.97	59.58	66.54
Al_2O_3	16.49	16.83	15.30	15.61	13.11	13.94	14.21	13.20	19.34	17.93	16.12
TiO_2	0.502	0.482	0.392	0.786	0.038	0.215	0.212	0.015	0.565	0.817	0.517
FeO	4.51	3.29	3.31	5.01	0.60	1.64	1.59	0.44	4.37	6.40	4.13
MnO	0.020	0.015	0.032	0.038	0.010	0.043	0.040	0.003	0.088	0.135	0.093
CaO	3.16	3.72	2.77	3.58	0.69	1.56	1.56	0.11	6.82	6.31	4.42
MgO	2.70	2.56	1.49	2.62	0.04	0.47	0.36	0.02	2.01	3.05	2.10
K_2O	2.77	2.07	4.14	3.75	4.93	5.12	4.79	3.48	2.13	2.18	2.69
Na_2O	3.99	4.46	3.41	3.50	3.14	2.70	3.07	4.11	3.54	3.28	3.26
P_2O_5	0.214	0.193	0.165	0.554	0.020	0.056	0.063	0.029	0.153	0.318	0.135
					Trace elements, ppm						
Ba	922	843	1218	1684	231	2555	2334	391	2454	2414	1446
Rb	97.7	64.4	85.7	111.9	213.8	175.2	178.6	145.2	62.6	60.3	100.9
Cs	2.18	4.17	1.93	4.85	11.69	2.66	3.19	1.75	1.57	3.21	5.64
Sr*	752	962	513	727	68	205	219	37	653	530	405
Pb	9.00	9.78	14.37	14.96	42.97	29.75	33.15	35.47	17.10	15.06	14.04
Th	6.70	7.12	17.94	9.66	25.79	25.06	22.10	8.45	6.77	7.46	10.90
U	2.72	4.38	3.94	5.31	3.10	5.27	7.42	5.25	1.96	2.03	1.95
Zr*	148	156	157	302	40	141	147	55	202	131	128
Nb	8.38	8.11	10.57	15.03	7.77	10.33	13.22	5.96	5.82	8.28	10.72
Hf	3.24	3.32	4.15	7.52	2.17	4.46	4.50	2.75	4.38	2.99	3.34
Y	14.54	14.74	13.60	19.45	13.44	13.00	17.87	36.03	15.93	23.66	23.10
La	28.29	30.59	32.25	36.30	6.21	29.64	41.78	10.35	21.63	22.84	35.14
Ce	52.21	56.74	53.34	71.68	12.68	56.86	70.00	19.46	37.08	42.08	59.44
Pr	5.89	6.34	5.46	8.07	1.40	4.90	6.79	2.08	4.05	4.87	6.09
Nd	23.41	24.05	19.93	32.86	5.38	16.15	23.48	7.56	16.14	20.72	22.10
Sm	4.49	4.59	3.78	6.92	1.50	3.09	4.38	2.33	3.24	4.85	4.54
Eu	1.11	1.25	0.97	2.05	0.33	0.64	0.81	0.12	1.46	1.50	1.20
Gd	3.42	3.53	3.07	5.50	1.45	2.43	3.41	3.13	2.95	4.63	4.04
Tb	0.47	0.50	0.44	0.76	0.29	0.40	0.54	0.73	0.46	0.70	0.66
Dy	2.59	2.71	2.38	3.78	1.89	2.35	3.10	5.08	2.70	4.12	3.82
Ho	0.50	0.53	0.47	0.67	0.41	0.47	0.61	1.08	0.58	0.84	0.82
Er	1.32	1.41	1.25	1.67	1.31	1.37	1.65	3.14	1.60	2.31	2.25
Tm	0.20	0.21	0.19	0.23	0.23	0.22	0.27	0.49	0.24	0.34	0.34
Yb	1.24	1.27	1.22	1.42	1.67	1.46	1.80	3.20	1.51	2.19	2.20
Lu	0.20	0.21	0.20	0.22	0.29	0.25	0.30	0.48	0.25	0.36	0.36
Sc*	10	8	6	11	2	4	5	4	20	17	17
V*	70	72	58	111	7	20	14	0	97	152	152
Cr*	42	37	21	16	0	3	1	0	15	6	6
Ni*	19	19	14	9	7	7	5	7	5	5	5
Cu*	230	252	62	84	2	3	14	8	9	3	3
Zn*	24	21	33	61	32	63	28	0	64	77	77
Ga*	18	23	17	21	12	13	17	16	20	19	19

Table 3.2 continued.

Sample	DS192 WMS	DS194 WMS	DS218 WMS	DS97-49 WMS	DS97-50 WMS	DS97-84 WMS
			Major elements, wt. %			
SiO_2	83.93	72.53	55.33	69.93	76.77	72.00
Al_2O_3	2.80	14.29	17.14	14.90	12.66	14.11
TiO_2	0.154	0.416	0.972	0.509	0.167	0.281
FeO	1.70	2.38	6.92	3.87	1.60	2.87
MnO	0.025	0.046	0.135	0.108	0.053	0.055
CaO	5.85	2.39	8.77	1.75	2.53	3.85
MgO	0.71	0.90	5.13	2.30	0.35	1.10
K_2O	0.58	3.85	2.19	4.01	3.48	2.77
Na_2O	0.00	3.09	3.19	2.47	2.34	2.90
P_2O_5	4.25	0.101	0.227	0.158	0.037	0.066
			Trace elements, ppm			
Ba	60	870	665	1307	903	1214
Rb	32.4	135.2	100.7	110.3	123.3	47.5
Cs	0.74	3.36	5.71	8.96	7.37	0.87
Sr*	29	223	438	216	187	324
Pb	1.25	31.40	16.18	46.91	15.83	11.50
Th	1.55	25.70	6.83	4.28	10.60	4.76
U	5.99	5.07	2.18	1.33	1.73	1.48
Zr*	40	175	108	154	114	209
Nb	2.57	14.41	8.01	9.03	9.33	8.10
Hf	0.83	5.40	3.04	3.97	3.19	5.80
Y	39.79	33.99	28.68	31.27	22.45	30.37
La	13.44	39.23	20.15	21.31	34.34	9.15
Ce	18.21	69.47	44.46	39.42	56.01	22.06
Pr	3.07	7.73	5.69	4.48	5.77	2.77
Nd	13.57	28.84	24.32	17.69	20.38	12.74
Sm	3.38	6.23	5.72	4.30	4.03	3.90
Eu	0.81	0.90	1.46	1.16	0.69	0.92
Gd	4.19	5.49	5.43	4.39	3.64	4.25
Tb	0.66	0.93	0.88	0.77	0.60	0.80
Dy	4.40	5.70	5.18	4.99	3.58	5.29
Ho	1.02	1.17	1.07	1.11	0.75	1.14
Er	2.82	3.27	2.81	3.29	2.20	3.28
Tm	0.40	0.50	0.40	0.51	0.34	0.50
Yb	2.37	3.07	2.49	3.27	2.24	3.35
Lu	0.39	0.43	0.39	0.53	0.36	0.53
Sc*	11	9	28	13	6	14
V*	465	28	175	56	9	47
Cr*	168	12	25	5	3	7
Ni*	59	7	2	4	6	5
Cu*	31	5	6	2	4	10
Zn*	9	44	69	213	34	47
Ga*	5	17	21	17	12	16

Table 3.2 Footnote.

Major element concentrations determined by XRF and normalized to 100% (volatile free). Trace elements determined by ICP-MS, * = trace element analyses by XRF. PP = Patton porphyry; CP = Cash porphyry; MNP = Mt. Nansen porphyry; CPS = Casino Plutonic Suite; DRB = Dawson Range batholith; WMS = Wolverine Creek Metamorphic Suite.

Table 3.3. Rb and Sr concentrations and isotope compositions.

Sample	Rock type	Rb (ppm)	Sr (ppm)	$^{87}Rb/^{86}Sr$	$^{87}Sr/^{86}Sr$ t=350	$^{87}Sr/^{86}Sr$ t=104	$^{87}Sr/^{86}Sr$ t=70	$^{87}Sr/^{86}Sr$ t=0
late Cretaceous Plutons[1]								
DS64	PP	102.37	767.92	0.378			0.70551	0.70588
DS113	PP	66.40	956.47	0.197			0.70541	0.70561
DS97-7	CP	89.00	494.11	0.511			0.70553	0.70604
DS97-12	CP	104.16	488.28	0.605			0.70552	0.70613
DS97-86	MNP	119.93	716.90	0.475			0.70487	0.70534
Casino Plutonic Suite								
DS185	CPS	217.63	69.86	8.840		0.70725	0.71152	0.72031
DS208	CPS	193.70	203.58	2.700		0.70716	0.70846	0.71115
DS210	CPS	172.75	230.02	2.131		0.70730	0.70833	0.71045
DS221	CPS	172.35	204.58	2.391		0.70726	0.70842	0.71080
DS224	CPS	177.62	215.96	2.334		0.70739	0.70852	0.71084
DS230	CPS	148.00	36.88	11.389		0.70592	0.71142	0.72275
Dawson Range Batholith								
DS189	DRB	72.05	381.74	0.536		0.70725	0.70751	0.70804
DS190	DRB	64.79	654.06	0.281		0.70724	0.70737	0.70765
DS209	DRB	79.40	444.95	0.506		0.70706	0.70730	0.70780
DS211	DRB	60.70	558.03	0.309		0.70663	0.70678	0.70709
DS97-63	DRB	74.42	405.73	0.520		0.70746	0.70772	0.70823
Wolverine Creek Metamorphic Suite								
DS103	WMS	157.94	478.92	0.936	0.70296	0.70624	0.70669	0.70762
DS192	WMS	32.13	26.97	3.381	0.70075	0.71260	0.71423	0.71760
DS193	WMS	141.60	365.05	1.101	0.70788	0.71173	0.71227	0.71336
DS194	WMS	138.07	221.98	1.765	0.71550	0.72168	0.72254	0.72429
DS218	WMS	106.31	438.03	0.689	0.70902	0.71144	0.71177	0.71246
DS232	WMS	36.64	24.34	4.272	0.69398	0.70895	0.71102	0.71527
DS97-49	WMS	120.26	209.74	1.627	0.70472	0.71042	0.71121	0.71283
DS97-50	WMS	129.63	183.09	2.009	0.70470	0.71174	0.71271	0.71471
DS97-84	WMS	51.01	319.25	0.453	0.70475	0.70634	0.70656	0.70701

WMS=Wolverine Creek Metamorphic Suite; CPS=Casino Plutonic Suite; DRB=Dawson Range batholith.

[1]late Cretaceous plutons, PP = Patton porphyry; CP = Cash porphyry; MNP = Mt. Nansen porphyry.

$^{87}Sr/^{86}Sr$ errors are quoted as 2σ mean.

Table 3.4. Nd and Sm concentrations and isotope compositions.

Sample	Rock type	Nd (ppm)	Sm (ppm)	$^{147}Sm/^{144}Nd$	$^{143}Nd/^{144}Nd$	εNd t=350	εNd t=104	εNd t=70	εNd t=0	T_{DM}^2 (Ga)
late Cretaceous Plutons[1]										
DS64	PP	25.31	4.5	0.1075	0.512633±9			0.7	-0.1	0.76
DS113	PP	26.24	4.11	0.0947	0.512612±6			0.4	-0.5	0.71
DS97-7	CP	22.01	3.79	0.1043	0.512616±8			0.4	-0.4	0.76
DS97-12	CP	19.68	3.44	0.1059	0.512584±10			-0.2	-1.1	0.82
DS97-86	MNP	35.81	7.27	0.1227	0.512699±10			2.2	1.6	0.74
Casino Plutonic Suite										
DS185	CPS	3.71	1.03	0.1673	0.512304±10		-6.1	-6.3	-6.5	2.81
DS208	CPS	18.06	2.96	0.0992	0.512264±14		-6.0	-6.4	-7.3	1.20
DS210	CPS	18.89	2.97	0.0952	0.512232±9		-6.6	-7.0	-7.9	1.20
DS221	CPS		4.96		0.512198±13					
DS224	CPS	24.07	4.02	0.1011	0.512307±10		-5.2	-5.6	-6.5	1.16
DS230	CPS	8.23	2.01	0.1473	0.512417±13		-3.7	-3.9	-4.3	1.71
Dawson Range Batholith										
DS189	DRB	20.7	3.28	0.0958	0.512286±8		-5.5	-6.0	-6.9	1.13
DS190	DRB	17.15	3.19	0.1125	0.512294±6		-5.6	-6.0	-6.7	1.31
DS209	DRB	17.23	3.62	0.1270	0.512294±10		-5.8	-6.1	-6.7	1.53
DS211	DRB	23.65	4.96	0.1268	0.512362±9		-4.5	-4.8	-5.4	1.40
DS97-63	DRB	19.51	3.62	0.1123	0.512199±7		-7.4	-7.8	-8.6	1.45
Wolverine Creek Metamorphic Suite										
DS103	WMS	21.55	4.52	0.1269	0.512258±6	-4.3	-6.5	-6.8	-7.4	1.59
DS192	WMS	14.93	3.36	0.1363	0.512156±16	-6.7	-8.6	-8.9	-9.4	1.91
DS193	WMS	6.47	1.29	0.1207	0.511956±9	-9.9	-12.3	-12.6	-13.3	1.97
DS194	WMS	30.79	5.89	0.1157	0.511858±8	-11.6	-14.1	-14.5	-15.9	2.02
DS218	WMS	27.62	5.83	0.1276	0.512141±9	-6.6	-8.8	-9.1	-9.7	1.80
DS232	WMS	8.54	1.52	0.1079	0.512150±10	-5.6	-8.3	-8.7	-9.5	1.46
DS97-49	WMS	19.92	4.26	0.1294	0.512298±11	-3.6	-5.7	-6.0	-6.6	1.56
DS97-50	WMS	21.61	3.91	0.1095	0.512015±9	-8.3	-11.0	-11.4	-12.2	1.68
DS97-84	WMS	14.50	4.16	0.1734	0.512542±9	-0.8	-1.6	-1.7	-1.9	2.34

WMS = Wolverine Creek Metamorphic Suite; CPS = Casino Plutonic Suite; DRB = Dawson Range batholith; [1]late Cretaceous plutons, PP = Patton porphyry; CP = Cash porphyry; MNP = Mt. Nansen porphyry. $^{143}Nd/^{144}Nd$ errors are quoted as 2σ mean. [2]T_{DM} depleted mantle age based on the model of Goldstein et al. (1984).

Table 3.5. U, Th, and Pb concentrations, and Pb isotope compositions.

Sample	Rock type	U (ppm)	Th (ppm)	Pb (ppm)	$^{206}Pb/^{204}Pb$ t=0	$^{207}Pb/^{204}Pb$ t=0	$^{208}Pb/^{204}Pb$ t=0	$^{206}Pb/^{204}Pb$ t=350	$^{207}Pb/^{204}Pb$ t=350	$^{208}Pb/^{204}Pb$ t=350
late Cretaceous Plutons										
DS64	PP	2.72	6.7	9	19.550	15.639	39.003			
DS113	PP	4.38	7.12	9.78	19.595	15.639	39.011			
DS65	KSP[1]				19.254	15.605	38.770			
Casino Plutonic Suite										
DS185	CPS	6.2	25	34.5	19.524	15.680	39.245			
DS208	CPS	6.4	24.2	23.3	19.581	15.699	39.358			
DS210	CPS	8.7	28.3	18.8	19.664	15.682	39.393			
DS221	CPS	8.5	24.1	22.9	19.630	15.688	39.319			
Dawson Range Batholith										
DS189	DRB	5.4	14.1	12.1	19.518	15.678	39.342			
DS190	DRB	3.5	8	13.8	19.481	15.738	39.241			
DS209	DRB	4.7	4.8	10.9	19.540	15.685	39.141			
DS211	DRB	4.4	10.9	13.8	19.393	15.669	38.801			
Wolverine Creek Metamorphic Suite										
DS193	WMS	5	6	18.7	19.673	15.790	39.431	18.695	15.786	39.052
DS194	WMS	5.07	25.70	31.40	19.745	15.794	39.579	18.728	15.787	38.607
DS218	WMS	2.18	6.83	16.18	19.570	15.785	39.404	18.328	15.781	38.906

Table 3.5 continued.

Sample	Rock type	$^{206}Pb/^{204}Pb$ t=104	$^{207}Pb/^{204}Pb$ t=104	$^{208}Pb/^{204}Pb$ t=104	$^{206}Pb/^{204}Pb$ t=70	$^{207}Pb/^{204}Pb$ t=70	$^{208}Pb/^{204}Pb$ t=70
late Cretaceous Plutons							
DS64	PP				19.336	15.638	38.829
DS113	PP				19.277	15.638	38.829
DS65	KSP[1]				19.254	15.605	38.770
Casino Plutonic Suite							
DS185	CPS	19.333	15.679	38.993	19.396	15.679	39.075
DS208	CPS	19.289	15.698	38.996	19.385	15.699	39.114
DS210	CPS	19.172	15.680	38.868	19.334	15.681	39.040
DS221	CPS	19.002	15.667	38.741	19.131	15.667	38.859
Dawson Range Batholith							
DS189	DRB	19.044	15.677	38.936	19.199	15.677	39.069
DS190	DRB	19.212	15.677	39.039	19.301	15.738	39.105
DS209	DRB	19.059	15.684	38.988	19.234	15.685	39.034
DS211	DRB	19.083	15.659	38.832	19.171	15.659	38.922
Wolverine Creek Metamorphic Suite							
DS193	WMS	19.388	15.789	39.319	19.482	15.789	39.355
DS194	WMS	19.572	15.792	39.292	19.629	15.793	39.386
DS218	WMS	19.427	15.785	39.257	19.474	15.785	39.305

Table 3.5 Footnote.

WMS = Wolverine Creek Metamorphic Suite; CPS = Casino Plutonic Suite; DRB = Dawson Range batholith; PP = Patton Porphyry. [1]Hydrothermal K-feldspar from the potassic zone of the Casino occurrence.

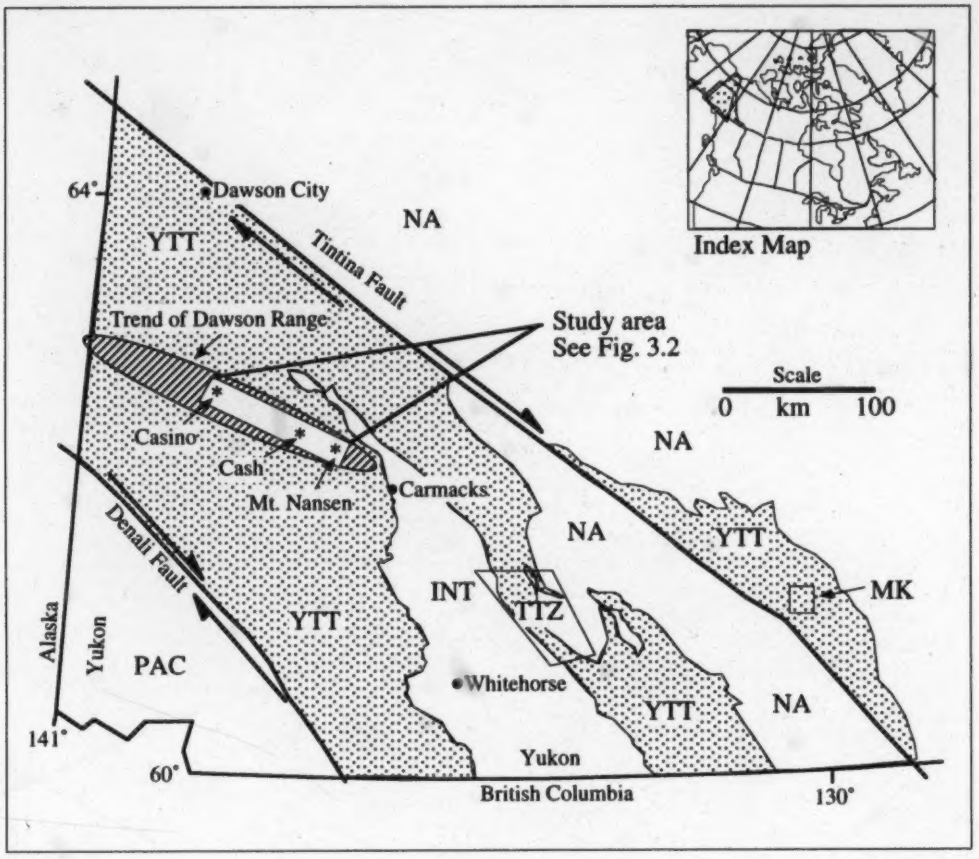

Fig. 3.1. Terrane map of the Yukon showing the Yukon-Tanana terrane modified after Wheeler and Mcfeely 1991. The location of the study is shown by the open box. The annotations, Casino, Cash, and Mt. Nansen, show the localities of the porphyry Cu-Au-Mo occurrences. Terranes: NA (North America), YTT (Yukon-Tanana terrane), TTZ (Telsin tectonic zone, study area of Stevens et al. 1996, Creaser et al. 1997); MK, Money klippe (study area of Grant 1997); INT, Intermontane Belt; PAC, Phanerozoic accreted crust.

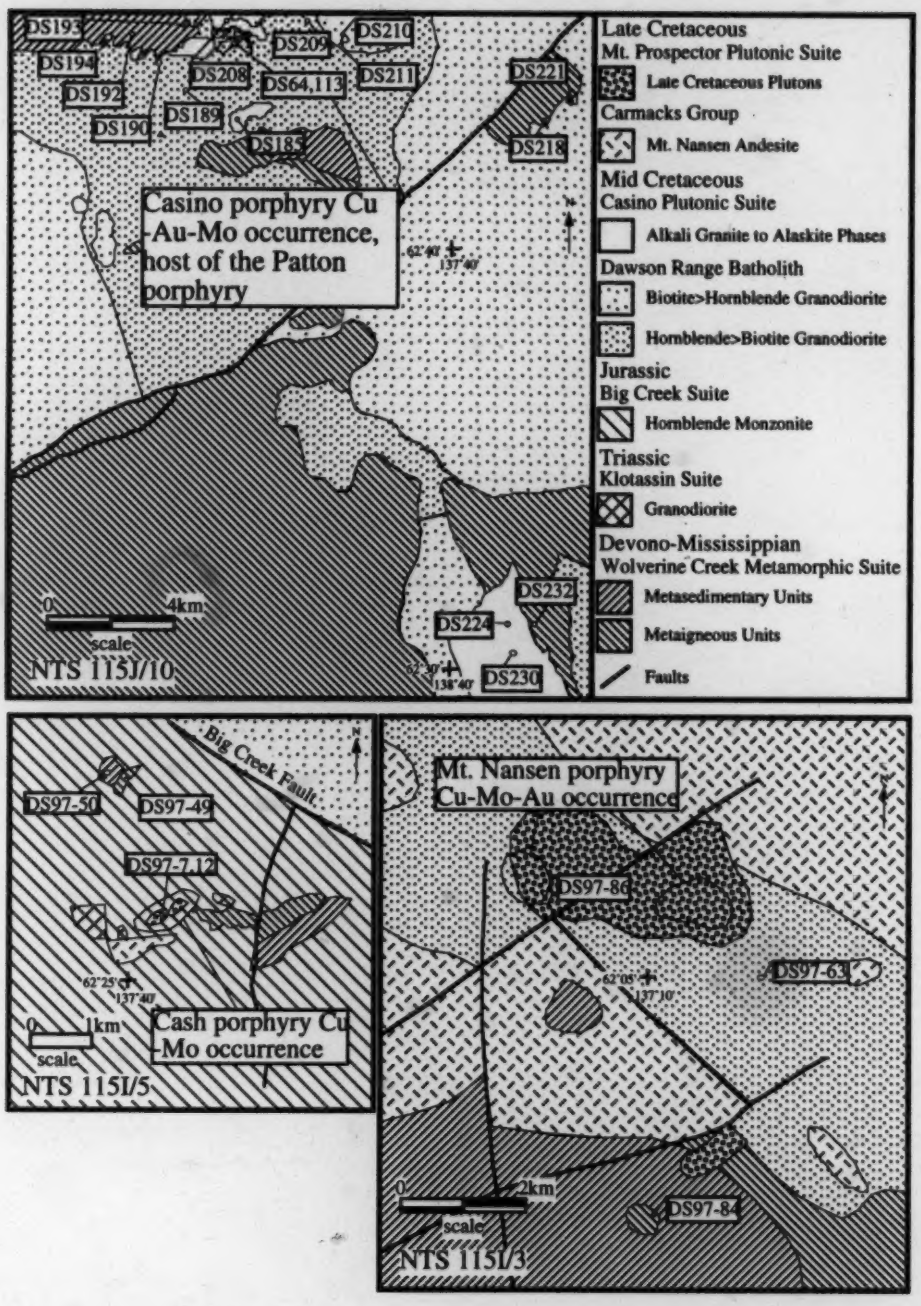

Fig. 3.2. Geology of the study areas showing location of samples (after Payne et al. 1987; Carlson 1987; Johnston 1995; Hart and Selby 1998).

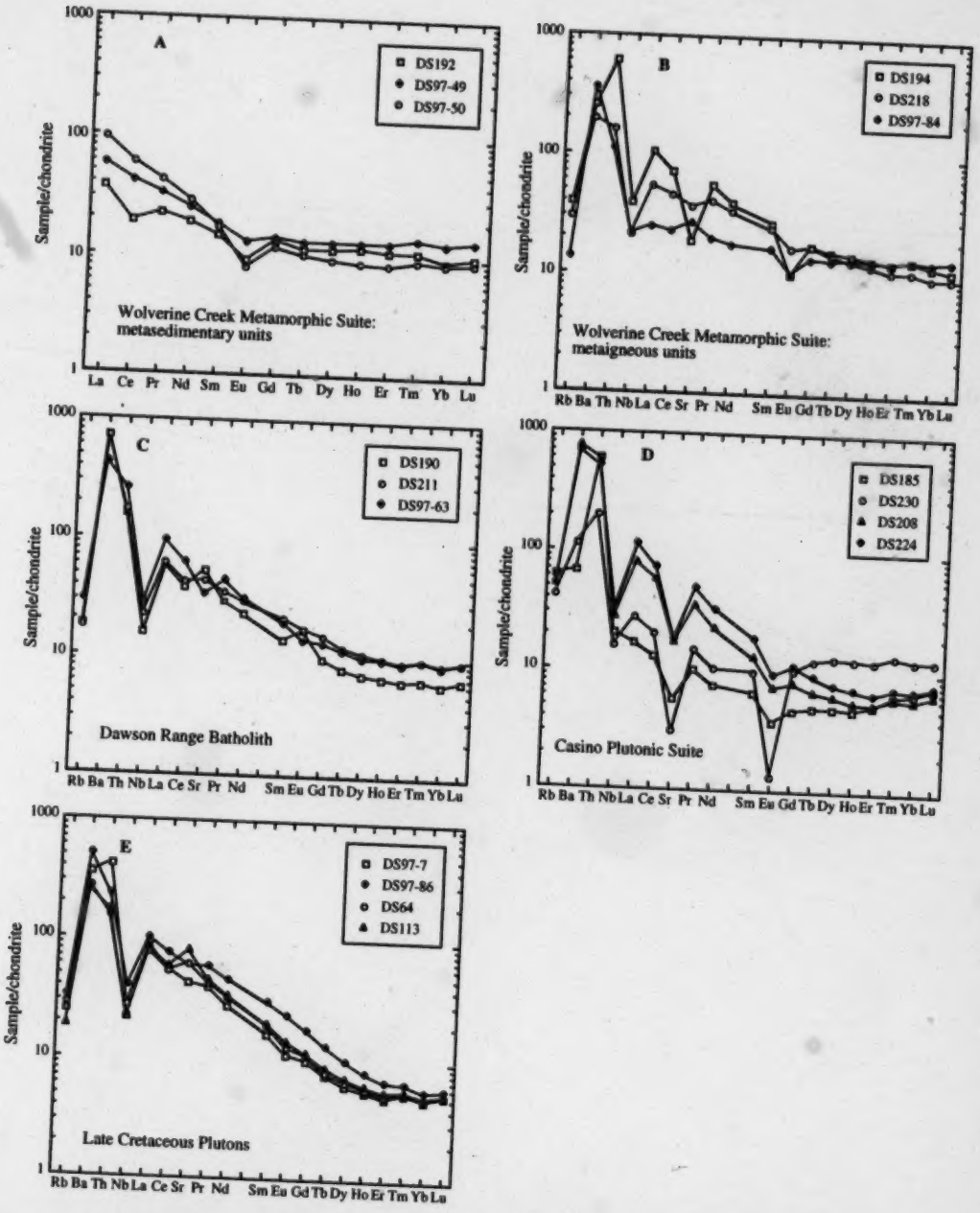

Fig. 3.3. Rare earth element plots for the Wolverine Creek Metamorphic Suite metasedimentary units (A), meta-igneous units (B), Dawson Range batholith (C), Casino Plutonic Suite (D), and the late Cretaceous plutons (E). Chrondrite normalizing values are from Boynton (1984).

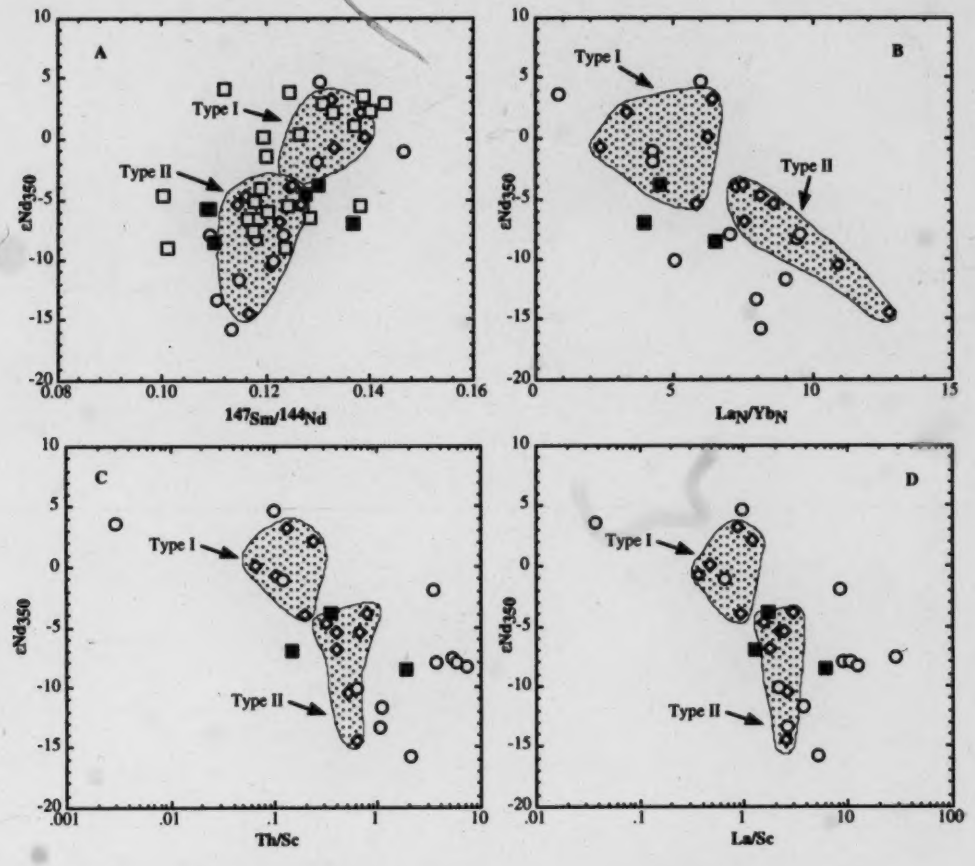

Fig. 3.4. Neodymium isotopic characteristics of the Wolverine Creek Metamorphic Suite. For all plots the shaded areas characterize the generalized fields defined by Creaser et al. (1997) for Type I and II metasediments of the Telsin tectonic zone. A = εNd_{350} vs. $^{147}Sm/^{144}Nd$; B = εNd_{350} vs. La_N/Yb_N; C = εNd_{350} vs. Th/Sc and D = εNd_{350} vs. La/Sc. Plotted for comparison are the data of Creaser et al. (1997), open diamonds, Grant (1997), open circles and shown on plot A only Samson et al. (1991), open squares. Data of this study are shown by black squares.

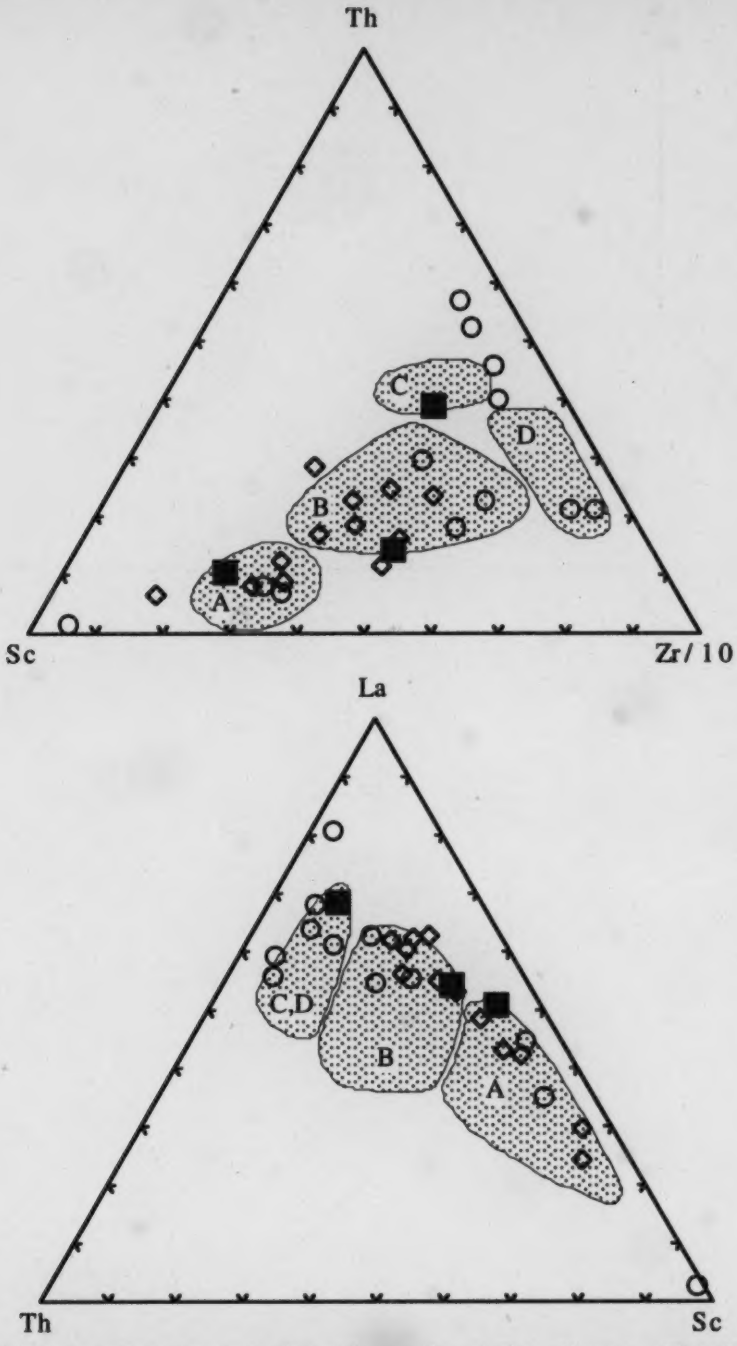

Fig. 3.5. Tectonic setting discrimination diagrams for clastic sediments of Bhatia and Crook (1986). Shaded areas are the generalized fields defined by Bhatia and Crook (1986) where: A = oceanic island arc, B = continental island arc, C = active continental margin, and D = passive margins. Data of this study are shown by black squares. Plotted for comparison are the data of Creaser et al. (1997; open diamonds), and Grant (1997; open circles).

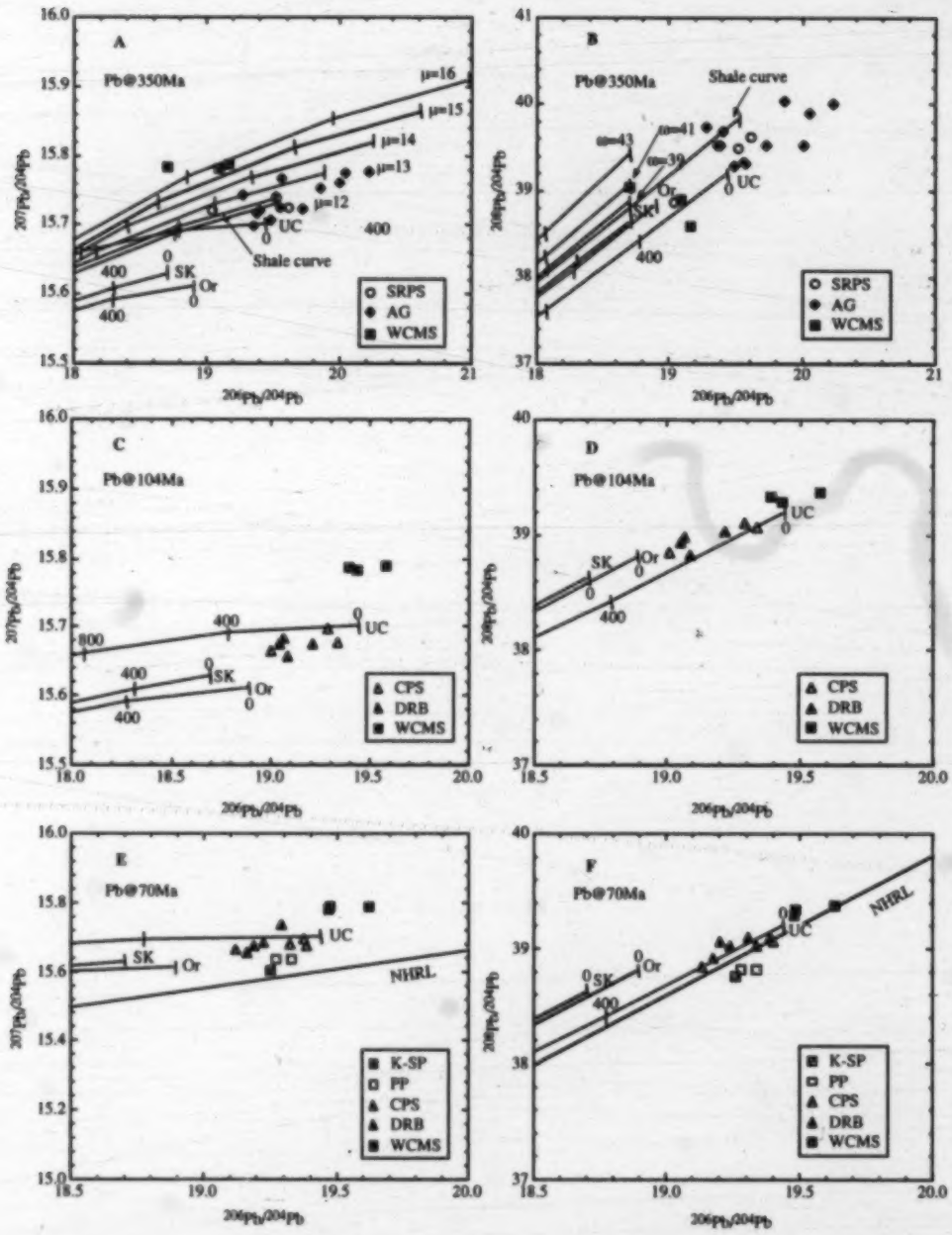

Fig. 3.6. $^{207}Pb/^{204}Pb$ vs. $^{206}Pb/^{204}Pb$ and $^{208}Pb/^{204}Pb$ vs. $^{206}Pb/^{204}Pb$ composition diagrams, with Pb evolution curves of Stacey and Karmers (SK) (1975), Zartman and Doe (UC = upper crust, Or = orogene) (1981), and Godwin and Sinclair (Shale curve) (1982). A, B: whole rock compositions of the meta-igneous rocks of the Wolverine Creek Metamorphic Suite calculated for 350 Ma (black squares). Plotted for comparison are the Pb compositions of K-feldspar from the Simpson

Range Plutonic Suite (SRPS, open circles; Grant 1997) and east Alaskan granitoids (AG, black diamonds; Aleinikoff et al. 1987). Also plotted are Pb evolution curves for model crust of different $^{238}U/^{204}Pb$ (μ) and $^{232}Th/^{204}Pb$ (ω) extracted at 2 Ga from the Stacey and Kramers crustal model. C, D: Whole rock compositions of the Wolverine Creek Metamorphic Suite (black squares), Dawson Range batholith (black triangles) and Casino Plutonic Suite (open triangle) calculated at 104 Ma. E, F: Whole rock compositions of the Wolverine Creek Metamorphic Suite (black squares), Dawson Range batholith (black triangles), Casino Plutonic Suite (open triangle), Patton Porphyry (open squares) and K-feldspar (divided square) calculated at 70 Ma, and Northern Hemisphere Reference Line (NHRL) of Hart (1984) for mantle compositions.

Chapter IV

Chemical Composition of Biotite from the Casino Porphyry Cu-Au-Mo Mineralization, Yukon, Canada: Evaluation of Magmatic and Hydrothermal Fluid Chemistry

*A version of this paper has been submitted for publication to Chemical Geology, October 1998, co-authored by Bruce E. Nesbitt of the Department of Earth and Atmospheric Sciences, University of Alberta, T6G 2E3, Canada.

Introduction

The majority of previous studies of biotite chemical composition in porphyry Cu deposits have concentrated on determinations of the F and Cl contents, with the objective of distinguishing between mineralized and barren plutons (Stollery et al., 1971; Kesler et al., 1975; Parry and Jacobs, 1975), with few studies of porphyry Cu deposits reporting the full elemental chemistry (Jacobs and Parry, 1979). Jacobs and Parry (1979) reported the variations of biotite chemistry from potassic, phyllic, propylitic, and argillic alteration zones, and estimated the HF, HCl, and H_2O fugacity of the hydrothermal fluids. Hitherto, the knowledge of the HF, HCl, and H_2O fugacity of hydrothermal fluids associated with porphyry Cu mineralization and hydrothermal alteration has been limited by the available thermodynamic data (Parry et al., 1978; Jacobs and Parry, 1979; Munoz and Swenson, 1981; Munoz, 1984; Loferski and Ayuso, 1995). However, recent thermodynamic determination of F-Cl-OH partitioning between biotite and a hydrothermal fluid (Zhu and Sverjensky, 1991, 1992), and new equations formulated to determine log $(f\mathrm{HF})/(f\mathrm{HCl})$, $(f\mathrm{H_2O})/(f\mathrm{HCl})$, and $(f\mathrm{H_2O})/(f\mathrm{HF})$ fugacity ratios of fluids

(Munoz, 1992) from biotite compositions, allow a more detailed evaluation of the chemistry of hydrothermal fluids and their evolution within porphyry Cu systems.

This chapter presents data on the chemical composition of biotites from the Casino porphyry Cu-Au-Mo occurrence and the Dawson Range batholith of central-west Yukon (Fig. 4.1). At Casino, mineralization and alteration are superimposed on the associated porphyritic body (Patton porphyry) and the surrounding country rock (Dawson Range batholith). The oxide and halogen contents in biotite are determined from least-altered Dawson Range batholith, and from the propylitic, phyllic and potassic altered rocks of the Casino porphyry system. The halogen data are used to determine the log (fHF)/(fHCl), ($f$$H_2O$)/($f$HCl), and ($f$$H_2O$)/($f$HF) ratios of the hydrothermal fluid associated with the Casino porphyry Cu-Mo-Au occurrence. Further, we report the calculated log (fHF/fHCl), ($f$$H_2O$)/($f$HCl), ($f$$H_2O$)/($f$HF) ratios for hydrothermal fluids associated with other porphyry Cu mineralization using the new formulations of Munoz (1992). These data are compared with the results from the Casino porphyry system.

Igneous and Alteration Petrography

Hydrothermal alteration and Cu-Au-Mo mineralization of the Casino porphyry occurrence is focused on a pluton (Patton porphyry) of late Cretaceous age and the neighboring country rock (Dawson Range batholith) of mid Cretaceous-age. The igneous and alteration petrography of the Dawson Range batholith and Patton porphyry discussed below is based upon descriptions by Godwin (1976), Payne et al. (1987), Bower et al. (1995), and observations of this study.

Dawson Range batholith: The batholith is the dominant country rock in the Casino area, characterized typically by hornblende>biotite potassic quartz diorite, hornblende-biotite diorite, and biotite>hornblende granodiorite. The least-altered Dawson Range batholith is composed of equigranular, medium- to coarse-grained

crystals of hornblende and biotite, and subhedral to euhedral, oscillatory-zoned plagioclase with andesine cores and oligoclase rims. Quartz and K-feldspar are interstitial to plagioclase and mafic minerals. Quartz forms interlocking aggregates, with grains exhibiting slight to moderate strain. A myrmekitic texture occurs between plagioclase and adjacent K-feldspar grains. Zircon, apatite, and sphene are accessory minerals. Alteration is present as minor kaolinite replacing plagioclase, minor chlorite along mineral edges and cleavage planes of biotite, and very small grains (~ 0.1 mm) of epidote. Alteration of the Dawson Range batholith is prominent on the outer margin of the alteration zone associated with the Casino occurrence. Increasing intensity of alteration is shown by the greater abundance and slightly larger (0.5 to 1 mm) epidote grains, which are alteration products of biotite, hornblende, and plagioclase. Chlorite partially replaces hornblende and biotite along mineral rims and cleavage planes.

Patton porphyry: This intrusion is genetically related to mineralization and hydrothermal alteration of the Casino occurrence (Godwin, 1976; Bower et al., 1995). The Patton porphyry is a small, dike-like body (500 by 700 m in diameter) of granodioritic composition, with a mineral assemblage of plagioclase and biotite phenocrysts in an aphanitic matrix of quartz, biotite, and K-feldspar. Plagioclase phenocrysts are the dominant textural characteristic of this rock body. Quartz phenocrysts are present, but rare. Apatite and zircon are accessory minerals.

Potassic alteration: This alteration assemblage is represented by K-feldspar (orthoclase), biotite, quartz, and magnetite, and is spatially associated with small quartz veins (typically 2 to 5 mm) containing pyrite, chalcopyrite, and molybdenite. The most visible evidence of potassic alteration is the presence of secondary K-feldspar and secondary biotite. The grain size is fine to very fine (1 to 2 mm). Magmatic biotite grains subjected to potassic alteration are either partially chloritized or completely

recrystallized to secondary biotite; the latter are observed as small aggregate clusters (typically 10 to 100 μm).

Phyllic alteration: Quartz, sericite, pyrite, and tourmaline (var. dravite) constitutes the phyllic alteration assemblage at Casino. This alteration is associated with quartz veins and also as a pervasive replacement of the preexisting mineral phases. Plagioclase is altered to sericite, and biotite and hornblende to chlorite. Tourmaline occurs as acicular radiating crystals intergrown with sericite, pyrite, and quartz. Phyllic alteration in the Dawson Range batholith and the Patton porphyry is highly destructive, commonly showing complete replacement of the original mineral assemblage. In a few samples of the Dawson Range batholith and Patton porphyry, partially chloritized, relic magmatic biotite is present. However, in many samples biotite was highly chloritized, and unsuitable for microprobe analysis.

Propylitic alteration: This alteration assemblage is characterized by epidote, chlorite, calcite, sericite and quartz, which are alteration products of plagioclase and mafic minerals. Biotite phenocrysts are partially altered to epidote, chlorite and sericite. Propylitic alteration is only observed in the Dawson Range batholith.

Argillic alteration: Kaolinite, sericite and montmorillonite characterize this alteration assemblage, which is locally recognized, associated typically with late faults and sporadically developed overprinted phyllic and potassic alteration assemblages. The argillic alteration is highly destructive, completely replacing the original mineral phases. No samples of argillic alteration provided biotite suitable for microprobe analysis.

Although biotite is present in the potassic, phyllic and propylitic zones at Casino, mineral stability data indicate that biotite is unstable in the chemical conditions that prevail during phyllic and propylitic alteration (Beane, 1994; Beane and Bodnar, 1995). Thus, biotite in these zones at Casino is unlikely to be in mineralogical equilibrium with the alteration assemblage. The latter is evident from the presence of chlorite and epidote

replacement of biotite in the phyllic and propylitic alteration zones, which suggest that permeability was sufficient to allow hydrothermal fluids to interact with biotite (Fig. 4.2C and F). The greater exchangeability of elements residing in the hydroxyl site relative to those in the tetrahedral and octahedral sites of biotite (Fortier and Giletti, 1991), suggest the possibility that this metastable biotite will undergo F-Cl-OH exchange with the fluids responsible for forming the alteration assemblage. Further, K, Rb, Ar and oxygen have similar diffusion rates between 500 to 400°C (Fortier and Giletti 1991), and considering Fe and Mg have similar diffusion rates to oxygen in garnet (Freer and Dennis, 1982; Chakraborty and Ganguly 1991), it is likely that they would behave in a similar fashion in biotite. Also, Mg and Fe content in biotite are directly related to F-Cl-OH exchange between biotite and hydrothermal fluid (Munoz 1984; Volfinger et al. 1985; Zhu and Sverjensky 1992). Therefore in the present study, as in previous studies, we assume F-Cl-OH exchange is associated with the fluids responsible for forming the alteration assemblage, and use biotite compositions to evaluate the composition of the coexisting fluid (cf. Parry et al., 1978; Jacobs and Parry, 1979; Munoz and Swenson, 1981; Munoz, 1984).

Biotite Types at the Casino Occurrence

This study separates biotite into magmatic and secondary types (Fig. 4.2). The term "magmatic" indicates biotite inferred to have crystallized directly from a silicate melt. These grains are further subdivided into least-altered and altered varieties. The least-altered magmatic biotite typically occur outside the alteration zones of the Casino deposit in the least-altered Dawson Range batholith, and texturally as euhedral to subhedral phenocrysts and microphenocrysts, and as subhedral to anhedral flakes (Fig. 4.2A and B). In contrast, the term "altered" biotite denotes magmatic biotite that occurs in either the Dawson Range batholith or the Patton porphyry, in a hydrothermal alteration

assemblage (e.g., potassic, phyllic and propylitic) (Fig. 4.2C, E and F). Altered biotite of the Patton porphyry and the Dawson Range batholith commonly occurs as euhedral phenocrysts, with biotite of the Dawson Range batholith commonly being frayed, ragged, splintery, kinked, and partially chloritized (Fig. 4.2C, E and F).

The term "secondary" describes biotite inferred to have precipitated from a hydrothermal fluid associated with the formation of the potassic alteration assemblage. Secondary biotite is petrographically distinct from magmatic biotite, occurring as aggregates of fine-grained flakes (typically 10 to 100 μm) (Fig. 4.2D). Secondary biotite partially or completely replaces magmatic hornblende or biotite, occurs throughout the rock, and as part of the potassic alteration envelopes bordering quartz veins.

Samples from the potassic zone of the Patton porphyry contain altered and secondary biotite. In contrast, the Dawson Range batholith from the potassic-zone contain only secondary biotite. The Patton porphyry from the phyllic-zone, and the Dawson Range batholith from the phyllic- and propylitic-zones contain only altered biotite.

Biotite Analytical Procedures

All elemental analyses of biotites were obtained from polished thin sections using the JEOL JXA-8900R electron microprobe in the Electron Microprobe Laboratory at the University of Alberta. Element determinations (Si, Al, Fe_{Total}, Mg, Ti, Mn, Ba, Na, K, F and Cl) were carried out using a beam size of 3 μm, an accelerating potential voltage of 15 kV, a probe current of 15 nA, and a counting time of 20 seconds for each element analyzed. Natural biotite, amphibole, sandine, tugtupite, and willemite standards were used in the analytical procedure for F, Si, Al, Fe, Mg, Ti, Cl, Ba, and Mn. Matrix effects were corrected using the ZAF software provided by JEOL. The accuracy of the reported values for the analyses are 1 - 5 % relative (1σ) depending on the abundance of the

element. A microprobe analysis is defined as the arithmetic mean of five spot analyses of a biotite grain. The OH values are calculated on the basis of 11 oxygen formula units. The X_{Mg} and X_{Fe} values are determined from cation fractions and are defined as Mg/(Fe+Mg) and $(Fe+Al^{VI})/(Mg+Fe+Al^{VI})$, respectively (Zhu and Sverjensky, 1992). The X_F, X_{Cl}, and X_{OH} are the mole fractions of F, Cl, and OH in the hydroxyl site.

Discussion of Biotite Compositions

A total of 835 microprobe analyses of 167 biotite grains from the Casino occurrence were obtained. The complete biotite microprobe data set are presented in Appendix III. Compositional trends between different biotite types from different alteration zones, as well as different rock types, are shown graphically on Figure 4.3.

The least-altered biotite grains possess X_{Mg} values between 0.40 and 0.47, significantly lower than biotite from all alteration zones at Casino (0.59 to 0.76) (Fig. 4.3). Least-altered biotite is also characterized by higher FeO and MnO contents, and typically lower F and Cl contents (Fig. 4.3E, F, I, J). However, least-altered biotite and biotite in alteration zones have similar K_2O, Na_2O, TiO_2, Al_2O_3, SiO_2, and BaO contents (Figs. 4.3A, B, C, D, G, H).

The F content is the lowest in the least-altered biotite with the higher X_{Mg} values (Fig. 4.3I). Biotite with high X_{Mg} incorporates more F in comparison to biotite with lower X_{Mg} values, a crystal-chemical effect referred to as the Fe-F avoidance principle (Munoz 1984). The negative correlation shown by the least-altered biotites suggest either that Fe-F avoidance principle does not apply to these biotites or that the lower X_{Mg} biotite coexisted with a more F-rich fluid. The F content of the biotite from the propylitic alteration zone is virtually identical to that of the least-altered biotite. Biotite from the potassic zone possesses a F content significantly higher than in least-altered biotite and biotite in the propylitic zone. The F content of potassic zone biotite in the Dawson Range

batholith is typically higher than biotite of the Patton porphyry. Biotites from the phyllic zone have amongst the highest F contents and X_{Mg} values.

The least-altered biotite possessing X_{Mg} values ~ 0.45 typically possess lower Cl contents in comparison to least-altered biotites with X_{Mg} values < 0.45 (Fig. 4.3J). Biotite with high X_{Mg} values incorporates less Cl than biotite with lower X_{Mg} values, an effect referred to as the Mg-Cl avoidance principle (Munoz 1984). Least-altered biotite with lower Cl contents and higher X_{Mg} values are in agreement with the Mg-Cl avoidance principal. The Cl content of biotite from all alteration zones is typically ≥ 0.2 wt. % (Fig. 4.3J). Biotite from all alteration zones possess similar Cl contents and show no systematic differences between alteration types (Fig. 4.3J). Biotite from the phyllic alteration zone displays a negative correlation with X_{Mg}, in agreement with the Mg-Cl avoidance principle.

The TiO_2 content of least-altered biotite and biotite from all alteration zones is similar (Fig. 4.3A). Secondary biotite of the Dawson Range batholith and the Patton porphyry typically contain lower TiO_2 contents than altered biotite of the Patton porphyry (Fig. 4.3A). Biotite of the phyllic alteration zone have variable TiO_2 contents.

Biotite from the propylitic zone contains approximately 2 wt. % more SiO_2 than from biotite from least-altered rock, however, biotite from all alteration zones contain similar SiO_2 contents (Fig. 4.3D). All biotite from the potassic zone are virtually identical with respect to SiO_2 content, with slightly higher contents in secondary biotite. Biotite in the phyllic zone from the Patton porphyry shows a slight increase in SiO_2 content in comparison to biotite of the Dawson Range batholith.

Secondary biotite from the Patton porphyry and the Dawson Range batholith typically possess slightly higher Al_2O_3 contents than altered biotite of the Patton porphyry. Biotite of the Patton porphyry from the phyllic zone has concentrations of

Al_2O_3 similar to those of secondary biotite, with biotite in the phyllic zone from the Dawson Range batholith having slightly higher Al_2O_3 contents.

The BaO contents of least-altered biotite are variable (0.5 to 1.8 wt. %), with most lying between 0.5 and 1 wt. % (Fig. 4.3C). The BaO content of biotite from alteration assemblages are similar to the BaO compositions of the least-altered biotites, and show no systematic differences between alteration types (Fig. 4.3C). The latter is also the case for the K_2O and Na_2O contents of biotite.

Comparison of Biotite Chemical Compositions with other Porphyry Cu Deposits

Previous studies of biotite chemical compositions in porphyry Cu deposits have examined deposits of the southwestern United States (Jacobs and Parry 1976; Parry et al. 1978; Lanier et al. 1978; Jacobs and Parry 1979 and references therein; Bowman et al. 1987), Canada (Kesler et al. 1975; Sheets and Nesbitt, submitted), Chile and Turkey (Taylor 1983), western Highland deposits, Papua New Guinea (Mason 1978), and plutons associated with porphyry Cu mineralization in the Deboullie pluton, northern Maine, U.S.A (Loferski and Ayuso 1995). At Casino, the X_{Mg} value is the most significant chemical factor that distinguishes least-altered from secondary biotite, consistent with results from other porphyry Cu deposits (Roberts 1973; Parry and Jacobs 1976; Mason, 1978; Jacobs and Parry 1979; Taylor 1983; Brimhall and Crerar 1994). The observation of lower MnO and higher SiO_2, F, and Cl contents in biotite from alteration zones in comparison to biotites in least-altered rock correlate with those of Santa Rita (Jacobs and Parry 1979) and Bingham (Parry et al. 1978; Lanier et al. 1978; and Bowman et al. 1987). However, the BaO, TiO_2, and Al_2O_3 content in biotite from Casino does not provide criteria to distinguish least-altered biotites from biotites in alteration zones as proposed for the Santa Rita and Hanover deposits (Parry and Jacobs 1976; Jacobs and Parry 1979).

The Fe-F and Mg-Cl avoidance principles shown by the biotite data from Casino are also shown for Santa Rita (Jacobs and Parry 1979; Munoz 1990), Los Pelambres and Bakircay (Taylor 1983), Deboullie (Loferski and Ayuso 1995), Bingham (Bowman et al. 1987) and Babine Lake deposits (Sheets and Nesbitt, submitted). The higher SiO_2 content in biotites from alteration zones observed from Casino are also noted for the Ely and Hanover (Jacobs and Parry 1976), Bagdad (Anderson, 1950), Butte (Roberts 1973; Brimhall 1977), Copper Canyon (Batchelder et al. 1977), Bingham (Moore and Czamanske 1973), Los Pelambres and Bakircay (Taylor 1983), Babine Lake (Sheets and Nesbitt, submitted), and the Western Highland deposits (Mason, 1978). In addition, higher F and Cl contents of biotite from alteration zones illustrated at Casino have been reported for Ely, Bingham (Jacobs and Parry 1976), Ray (Banks, 1976), Copper Mountain, (Kesler et al. 1975), Los Pelambres, Bakircay (Taylor 1983), Deboullie (Loferski and Ayuso 1995) and Babine Lake deposits (Kesler et al. 1975; Sheets and Nesbitt, submitted). The biotite chemical compositions from all porphyry Cu deposits typically exhibits the same trends; however, the decreasing TiO2 and increasing Al2O3 content in biotite from alteration zones in comparison to biotite in least-altered rock was not observed at Casino. Further, the absolute concentration of the oxides, halogens, and the X_{Mg} value differ greatly between deposits. However, X_{Mg} values equal to or greater than 0.55 are generally indicative of altered magmatic and secondary hydrothermal biotite.

Biotite Halogen Chemistry

The halogen content in biotite from the potassic and phyllic zones is shown on Figure 4. Zhu and Sverjensky (1992) have shown that the composition of biotite formed under similar physiochemical conditions define linear trends on the log (X_F/X_{OH}) vs. X_{Fe} and log (X_{Cl}/X_{OH}) vs. X_{Mg} plots. The slope defined by the biotite compositions is a

function of temperature, and is independent of pressure and fluid composition, whereas the intercept value is a function of all these parameters (Zhu and Sverjensky 1992). Using the median fluid inclusion homogenization temperatures of Casino established from microthermometric studies of potassic and phyllic stage quartz veins (420 and 390°C, respectively; Selby, unpub. data), the slopes for the log (X_F/X_{OH}) vs. X_{Fe} and log (X_{Cl}/X_{OH}) vs. X_{Mg} plots are derived from equations 23 and 24 of Zhu and Sverjensky (1992). These calculated slopes are passed through the majority of the data points from the potassic and phyllic zones from Casino (Fig. 4.4). However, the data, especially for biotites from the potassic zone do not define linear trends, neither do the data define a broad scatter as shown for biotites from least-altered rock (Fig. 4.5A-B, below). The narrow scatter shown in the data from the alteration zones may suggest that the biotites formed under broadly similar temperature conditions. The biotite data that are scattered with respect to the calculated slopes may suggest a fluid of different temperature and/or composition effected the biotite halogen composition.

Biotite from the potassic and phyllic zones at Casino possess log (X_{Cl}/X_{OH}) values of ~ –1.7 and –1.8, and log (X_F/X_{OH}) values of ~ –1.1 and –0.9, respectively (Fig. 4.4). The y-intercept on the log (X_{Cl}/X_{OH}) vs. X_{Mg} and the log (X_F/X_{OH}) vs. X_{Fe} plots for biotite from the potassic zone is –1.35 and –0.4, respectively, similar to the values for biotite from the phyllic zone (–1.25; –0.4) (Fig. 4). The similarity of intercepts for potassic and phyllic zones suggests that X_F/X_{OH} and X_{Cl}/X_{OH} values of the hydrothermal fluid were fairly constant during the formation of both potassic and phyllic alteration.

Least-altered biotite from the Dawson Range batholith show considerable scatter in log (X_{Cl}/X_{OH}) values (Fig. 4.5A), with less scatter in log (X_F/X_{OH}) values (Fig. 4.5B). Biotite from granitic rocks of Japan (analytical data by Nedachi 1980), the Sierra Nevada batholith (analytical data by Dodge et al. 1969), and the Coast and Transverse Ranges (analytical data by Dodge and Ross 1971) also shows a large scatter on the biotite

compositional diagrams (Figs. 4.5C and D). The scatter shown on the biotite composition plots (Figs. 4.5C and D) suggests that the biotite did not form under similar temperature conditions. This scatter also suggests either the avoidance of the Fe-F and Mg-Cl principles, which would be contradictory to experimental studies of Munoz and Ludington (1974), Munoz and Swenson (1981), and Volfinger et al. (1995), or the low X_{Mg} biotites have coexisted with a more F-rich/Cl-poor fluid. The latter suggests that the least-altered biotite chemistry of the Dawson Range batholith, and granitic rocks from Japan, Sierra Nevada, and the Coast and Transverse Ranges record the change in fluid composition during the crystallization history of the magma.

Determination of Hydrothermal Fluid Fugacity Ratios

Fluorine and chlorine biotite data were used to calculate the log $(fH_2O)/(fHF)$, $(fH_2O)/(fHCl)$, and $(fHF)/(fHCl)$ ratios for hydrothermal fluids associated with mineralization and hydrothermal alteration (Munoz 1992). The fugacity ratios were calculated using the equations of Munoz (1992), that are based on the revised coefficients for F-Cl-OH partitioning between biotite and hydrothermal fluid (Zhu and Sverjensky 1991, 1992). These equations are:

$$\log (fH_2O)/(fHF)^{fluid} = 1000/T\,(2.37 + 1.1(X_{Mg})^{bio}) + 0.43 - \log (X_F/X_{OH})^{bio}$$

$$\log (fH_2O)/(fHCl)^{fluid} = 1000/T\,(1.15 + 0.55(X_{Mg})^{bio}) + 0.68 - \log (X_{Cl}/X_{OH})^{bio}$$

$$\log (fHF)/(fHCl)^{fluid} = -1000/T\,(1.22 + 1.65(X_{Mg})^{bio}) + 0.25 + \log (X_F/X_{Cl})^{bio}$$

Where X_F, X_{Cl}, and X_{OH} are the mole fractions of F, Cl, and OH in the hydroxyl site of the biotite, $(X_{Mg})^{bio}$ here is the sum of Mg/sum octahedral cations, and T is the temperature in Kelvin of the halogen exchange.

Fugacity ratios for hydrothermal fluids associated with potassic and phyllic alteration were calculated for 420°C and 390°C, respectively (see above). Phyllic hydrothermal fluids have similar or slightly higher log $(fH_2O)/(fHCl)$, similar to more

negative log (fHF)/($fHCl$), and similar to higher log (fH_2O)/(fHF) values than those established for fluids associated with the potassic alteration (Fig. 4.6A and B). Fugacity ratios for potassic-zone biotite calculated at 390°C (temperature associated with phyllic alteration) yield values like those determined for the phyllic alteration fluids. However, the log (fH_2O)/($fHCl$), and (fH_2O)/(fHF) ratios for potassic alteration fluids are still lower. The last statement suggests that hydrothermal fluids associated with phyllic alteration are slightly different from fluids related to potassic alteration, and that the biotite halogen chemistry is not representative of a single fluid chemistry. However, the scatter in the few fugacity ratios for potassic and phyllic alteration is suggestive of minor overprinting of the biotite halogen chemistry by late-stage hydrothermal fluids.

Fugacity ratios for hydrothermal fluids associated with propylitic alteration are speculative because temperatures are not accurately known. However, hydrothermal fluids associated within this alteration zone were most likely cooler than those of potassic and phyllic zones, and the fugacity ratios are calculated at 350°C. Calculated log (fH_2O)/($fHCl$) values for the propylitic zone are similar to those established for potassic and phyllic alteration assemblages. In contrast to potassic hydrothermal fluids, those for propylitic alteration had higher log (fH_2O)/(fHF), more negative log (fHF)/($fHCl$) values. The log (fH_2O)/(fHF) and (fHF)/($fHCl$) values for propylitic alteration are within the range of phyllic alteration, however, the log (fH_2O)/(fHF) and (fHF)/($fHCl$) values for propylitic zone are typically higher and more negative (Fig. 5.6A-B). If halogen exchange occurred at lower temperatures higher log (fH_2O)/(fHF) and (fH_2O)/($fHCl$) values, and more negative log (fHF)/($fHCl$) values would characterized the hydrothermal fluids associated with the propylitic alteration (Fig. 4.6A-B). The distinct fugacity ratios determined for the propylitic-stage hydrothermal fluids relative to those for potassic and phyllic alteration also indicate that the biotite halogen chemistry are not representative of a single fluid chemistry.

Comparison of Fugacity Ratios with other Porphyry Cu Systems

Figures 4.6C and D shows the recalculated fugacity ratios determined from biotite associated with potassic alteration for the Bingham (analytical data, Parry et al. 1978; Lanier et al. 1978; Bowman et al. 1987), Santa Rita (analytical data; Parry et al. 1979), Los Pelambres, Bakircay (analytical data, Taylor 1983), and Babine Lake (analytical data, Sheets and Nesbitt, submitted) deposits, and associated with porphyry copper mineralization for the Hanover (analytical data, Jacobs and Parry 1979) and Deboullie plutons (analytical data, Loferski and Ayuso 1995) using the equations of Munoz (1992), and temperatures established from fluid inclusion or mineral pair geothermometry, e.g., 350°C for Santa Rita, Hanover, Los Pelambres, Bakricay and Deboullie, and 400°C for Bingham and the Babine Lake deposits. In comparison to the previous determined fugacity ratios for hydrothermal fluids at Santa Rita, Bingham, and Deboullie (Parry et al. 1978; Jacobs and Parry 1979; Munoz and Swenson 1981, Munoz 1984; Loferski and Ayuso 1995), the recalculated fugacity ratios equate to higher log (fH_2O)/(fHF) and (fHF)/(fHCl) values, and more negative log (fHF)/(fHCl) values.

Hydrothermal fluids associated with potassic and phyllic alteration at Casino possessed log (fH_2O)/(fHCl) and (fH_2O)/(fHF) values similar to or lower than those determined for Santa Rita, Bingham, Babine Lake, Los Pelambres, Bakircay, Hanover and Deboullie (Fig. 4.6C and D). Furthermore, except for Deboullie which yields typically more negative log (fHF)/(fHCl) values, the values determined for potassic and phyllic alteration at Casino are similar, though less negative than those of Santa Rita, Bingham, Babine Lake, Los Pelambres, Bakircay and Hanover (Fig. 4.6C and D). The log (fH_2O)/(fHF) values determined for hydrothermal fluids associated with potassic and phyllic alteration at Casino contrast greatly from those of other porphyry Cu deposits, which yield log (fH_2O)/(fHF) values nearly one order of magnitude higher (Fig. 4.6D).

The fugacity ratios determined for potassic alteration at Bingham describe a large range of values (Fig. 4.6C and D). However, within the spread of the values two distinct fugacity ratios are shown for log (fHF)/(fHCl) and (fH$_2$O)/(fHF), and are denoted by the circled areas in the field for Bingham (Fig. 4.6C and D). The fluids associated with potassic alteration at Bingham possess the highest log (fH$_2$O)/(fHCl) values, similar to higher log (fHF)/(fHCl) values, and similar log (fH$_2$O)/(fHF) values in comparison to Casino and other porphyry Cu deposits (Fig. 4.6C and D). The spread in the fugacity ratios at Bingham may suggest that post potassic hydrothermal fluids have modified the biotite halogen chemistry. However, the distinct fugacity ratios suggest that two different hydrothermal fluids existed at Bingham.

The determined fugacity ratios from biotite microprobe data and the equations of Munoz (1992) suggest that hydrothermal fluids associated with porphyry Cu mineralization possess similar log (fH$_2$O)/(fHCl) and (fHF)/(fHCl) values; however, the log (fH$_2$O)/(fHF) values vary from deposit to deposit (Fig. 4.6C and D). The highest log (fH$_2$O)/(fHF) values are for porphyry Cu mineralization at Bakircay and Los Pelambres, with lower fugacity ratios for Deboullie, Babine Lake, Santa Rita, Hanover, Bingham, and Casino, respectively (Fig. 4.6D). The log (fH$_2$O)/(fHF) ratio for fluids associated with porphyry Cu mineralization are significantly higher than those for porphyry Mo mineralization (log (fH$_2$O)/(fHF) = 4.3 – 4.6 for Henderson, recalculated from Munoz and Swenson, 1981). Brimhall and Crerar (1987) suggested that these differences were a function of the magma source; melting of F-rich biotite-bearing gneiss in the Precambrian craton of North American gives magmas associated with porphyry Mo mineralization, while melting of F-poor mafic-amphibolites yields magmas related to porphyry Cu mineralization. Therefore, the variation shown in the log (fH$_2$O)/(fHF) values among porphyry Cu deposits may be directly related to the composition of the exsolved

magmatic aqueous fluids, which may in turn depend on processes (assimilation/fractional crystallization) affecting magmas on their ascent through the crust.

Summary

The biotite from the alteration zones of Casino conform to the Fe-F and Mg-Cl avoidance principles, whereas the Fe-F and Mg-Cl trends of least-altered biotite from the Dawson Range batholith either represents a violation of the crystal-chemical principle or the presence of a fluid of a different F/Cl ratio. The biotite data from the Dawson Range batholith is consistent with available data on other, similar granitic rocks and indicates that the biotite chemical chompositions reflect variations in conditions of crystallization of a granitic body.

The oxide and halogen chemistry of biotite from the Casino porphyry Cu occurrence is distinctly different from that of biotite from the least-altered Dawson Range batholith. The notable elemental change between biotite from the least-altered and altered Dawson Range batholith is shown by the marked increase in the X_{Mg} value, and increase in F and Cl, and decrease in Mn content. The latter indicates that the elemental chemistry of biotite in the Dawson Range batholith, in alteration zones of the Casino deposit have been altered by hydrothermal fluids associated with alteration and mineralization of the porphyry system. The compositional changes in oxide (except TiO_2 and Al_2O_3) and halogen chemistry of biotite from alteration zones at Casino are consistent with those from other porphyry Cu deposits, although absolute concentrations vary considerably between deposits.

The fugacity ratios calculated for hydrothermal fluids associated with potassic alteration are similar for those determined for phyllic alteration, whereas higher log $(fH_2O)/(fHF)$ and less negative log $(fHF)/(fHCl)$ values are calculated for fluids associated with propylitic alteration. The log $(fH_2O)/(fHCl)$ and $(fHF)/(fHCl)$ ratios for

hydrothermal fluids for Casino and those established for porphyry Cu mineralization of Santa Rita, Hanover, Deboullie, Los Pelambres, Bakircay, Bingham, and Babine Lake are similar. In contrast, the log (fH_2O)/(fHF) values are variable between deposits and may be indicative of magmatic processes (assimilation/fractional crystallization) associated with the evolution of the melt, which may directly affect the composition of exsolved magmatic fluids that are related to porphyry mineralization.

References

Anderson, C. A., 1950. Alteration and metallization in the Bagdad porphyry copper deposit, Arizona. Economic Geology, 45: 609-628.

Banks, N. G., 1976. Halogen contents of the igneous minerals as indicators of magmatic evolution of rocks associated with the Ray porphyry copper deposits. Arizona Journal of Research. United States Geological Survey, 4: 91-117.

Batchelder, J., 1977. Light stable isotope and fluid inclusion study of the porphyry Cu deposit at Copper Canyon, Nevada. Economic Geology, 72: 60-70.

Beane, R.E., 1994. A graphic veiw of hydrothermal mineral stability relations. In: Lentz, D. R. (Ed.), Alteration and Alteration Processes Associated with Ore-Forming Systems. Geological Association of Canada, Short Course Notes, 11: 1-30.

Beane, R.E. and Bodnar, R.J., 1995. Hydrothermal fluids and hydrothermal alteration in porphyry copper deposits. In: Pierce, F. W., Bohm, J. G. (Eds.), Porphyry copper deposits of the American Cordillera. Arizona Geological Society Digest 20, Tucson, AZ: 83-93.

Bower, B., Payne, J., Delong, C., and Rebagliati, C. M., 1995. The oxide-gold supergene and hypogene zones at the Casino gold-copper-molybdenite deposit west-central Yukon. In: Schroeter, T. G. (Ed.), Porphyry Deposits of the Northwestern Cordillera of North America, Canadian Institute of Mining, Metallurgy and Petroleum, Special Volume 46: 352-366.

Bowman, J. R., Parry, W. T., Kropp, W. P., and Kruer, S. A., 1987. Chemical and isotopic evolution of hydrothermal solutions at Bingham, Utah. Economic Geology, 82: 395-428.

Brimhall, G. H., Jr., 1977. Early fracture-controlled disseminated mineralization at Butte, Montana. Economic Geology, 72: 37-59.

Brimhall, G. H., and Crerar, D. A., 1987. Ore fluids: Magmatic to supergene. In: Carmichael, I. S. E., Eugster, H. P. (Eds.), Thermodynamic modeling of geological materials: Minerals, fluids and melts. Reviews in Mineralogy, 17: 235-321.

Chakraborty, S., and Ganguly, J. 1990. Compositional zoning and cation diffusion in garnets. *In* Diffusion, atmoic ordering and mass transport: Selected topics in geochemistry. *Edited by* J. Ganguly. Advances in physical geochemistry **8:** 120-175.

Dodge, F. C. W., and Ross, D. C., 1971. Coexisting hornblendes and biotites from granitic rocks near the San Andreas Fault, California. Journal of Geology, 79: 158-172.

Dodge, F. C. W., Smith, V. C., and Mays, R. E., 1969. Biotites from granitic rocks of the central Sierra Nevada Batholith, California. Journal of Petrology, 10: 250-271.

Fortier, S. M., and Giletti, B. J., 1991. Volume self-diffusion of oxygen in biotite, muscovite, and phlogopite micas. Geochimica et Cosmochimica Acta, 55: 1319-1330.

Freer, R., and Dennis, P. F. 1982. Oxygen diffusion studies> I. A preliminary ion microprobe investigation of oxygen diffusion in some rock-forming minerals. Mineralogical Magazine, **45:** 179-192.

Godwin, C. I., 1976. Casino. In: Sutherland Brown, A. (Ed), Porphyry Deposits of the Canadian Cordillera. The Canadian Institute of Mining and Metallurgy Special Volume 15: 344-358.

Jacobs, D. C., and Parry, W. T., 1979. Geochemistry of biotite in the Santa Rita porphyry copper deposit, New Mexico. Economic Geology, 74: 860-887.

Jacobs, D. C., and Parry, W. T., 1976. A comparison of the geochemistry of biotite from some basin and range stocks. Economic Geology, 71: 1029-1035.

Kesler, S. E., Issigonis, M. J., Brownlow, A. H., Damon, P. E., Moore, W. J., Northcote, K. E., and Preto, V. A., 1975. Geochemistry of biotites from mineralized and barren intrusive systems. Economic Geology, 70: 559-567.

Lanier, G., Raab, W. J., Folsom, R. B., and Cone. S., 1978. Alteration of equigranular monzonite, Bingham Mining District, Utah. Economic Geology, 73: 1270-1286.

Loferski, P. J., and Ayuso, R. A., 1995. Petrography and mineral chemistry of the composite Deboullie pluton, northern Maine, U.S.A.: Implications for the genesis of Cu-Mo mineralization. Chemical Geology, 123: 89-105.

Mason, D. R., 1978. Compositional variations in ferromagnesian minerals from porphyry copper-generating and barren intrusions of the western Highlands, Papua New Guinea. Economic Geology, 73: 878-890.

Moore, W. J., and Czamanske, G. K., 1973. Compositions of biotites from unaltered and altered monzonitic rocks in the Bingham mining distinct, Utah. Economic Geology, 68: 269-280.

Munoz, J. L., 1984. F-OH and Cl-OH exchange in micas with applications to hydrothermal ore deposits. In: Bailey, S. W. (Ed.), Micas. Reviews in Mineralogy, 13: 469-494.

Munoz, J. L., 1990. F and Cl contents of hydrothermal biotites: A re-evaluation. Geological Society of America: Abstracts with Programs, 22: A135.

Munoz, J. L., 1992. Calculation of HF and HCl fugacities from biotite compositions: Revised equations. Geological Society of America, Abstracts with Programs, 24: A221.

Munoz, J. L., and Ludington, S. D., 1974. Fluoride-hydroxyl exchange in biotite. American Journal of Science, 274: 396-413.

Munoz, J. L., and Swenson, A., 1981. Chloride-hydroxyl exchange in biotite and estimation of relative HCl/HF activities in hydrothermal fluids. Economic Geology, 76: 2212-2221.

Nedachi, M., 1980. Chlorine and fluorine contents of rock-forming minerals of the Neogene granitic rocks in Kyushu, Japan. Mining Geology Special Issue 8: 39-48.

Parry, W. T., and Jacobs, D. C., 1975. Fluorine and chlorine in biotite from Basin and Range plutons. Economic Geology, 70: 554-558.

Parry, W. T., Ballantyne, G. H., and Wilson, J. C., 1978. Chemistry of biotite and apatite from a vesicular quartz latite porphyry plug at Bingham, Utah. Economic Geology, 73: 1308-1314.

Payne, J. G., Gonzalez, R. A., Akhurst, K., and Sisson, W. G., 1987. Geology of the Colorado Creek (115-J/9), and Prospector Mountain (115-I/5) map areas, western Dawson Range, west-central Yukon. Exploration and Geological Services Division, Yukon, Indian and Northern Affairs Canada, Open File 1987-3.

Roberts, S. A., 1973. Pervasive early alteration in the Butte District, Montana. Society of Economic Geology Guidebook, Butte Field Mtg: HH1-HH8.

Sheets, R. W., and Nesbitt, B. E. (submitted). Differentiation between highly mineralized and weakly mineralized porphyry Cu deposits using biotite chemistry. Economic Geology.

Stollery, G., Borcsik, M., and Holland, H. D., 1971. Chlorine in intrusives: a possible prospecting tool. Economic Geology, 66: 361-367.

Taylor, R. P., 1983. Comparison of biotite geochemistry of Bakircay, Turkey, and Los Pelambres, Chile, porphyry copper systems. Trans. Instn. Min. Metall. (Sect. B: Appl. Earth Sciences.), 92: B16-B22.

Volfinger, M., Robert, J. L., Vielzeuf, D., and Neiva, A. M. R., 1985. Structural control of the chlorine content of OH-bearing silicates (micas and amphiboles). Geochimica et Cosmochimica Acta, 49: 37-48.

Zhu, C., and Sverjensky, D. A., 1991. Partitioning of F-Cl-OH between minerals and hydrothermal fluids. Geochimica et Cosmochimica Acta, 55: 1837-1858.

Zhu, C., and Sverjensky, D. A., 1992. F-Cl-OH partitioning between biotite and apatite. Geochimica et Cosmochimica Acta, 56: 3435-3467.

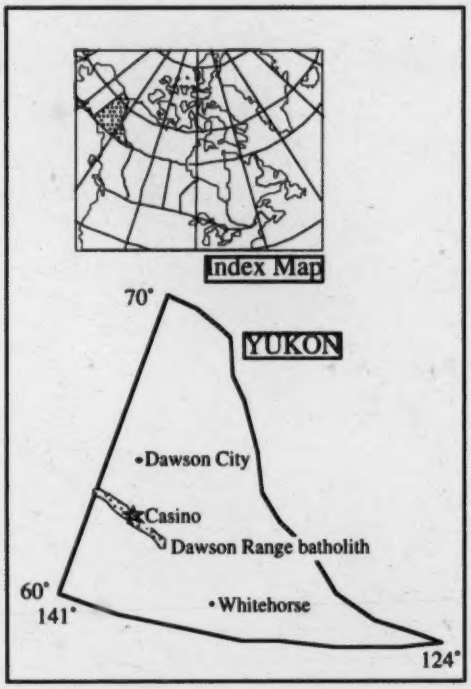

Fig. 4.1. Location map of the Casino porphyry Cu-Au-Mo occurrence, Dawson Range, west-central Yukon, Canada.

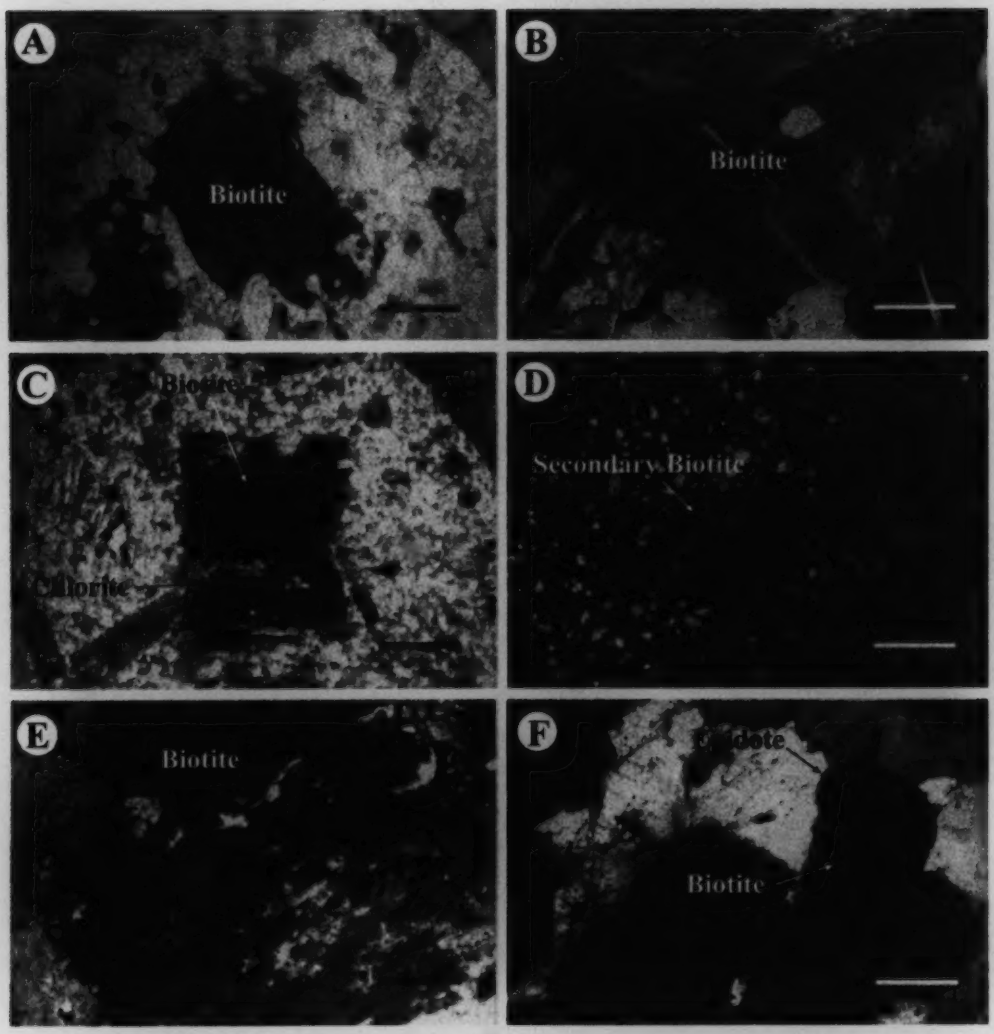

Fig. 4.2. Photomicrographs of biotite from the least-altered Dawson Range batholith and alteration zones of the Casino occurrence. A and B: Biotite from the least-altered Dawson Range batholith. C: Altered magmatic biotite from potassic altered Patton porphyry. D: Secondary biotite from potassic altered Dawson Range batholith. E: Altered magmatic from phyllic altered Dawson Range batholith. F: Altered magmatic from propylitic altered Dawson Range batholith. The scale bar on each photo represents 1 mm.

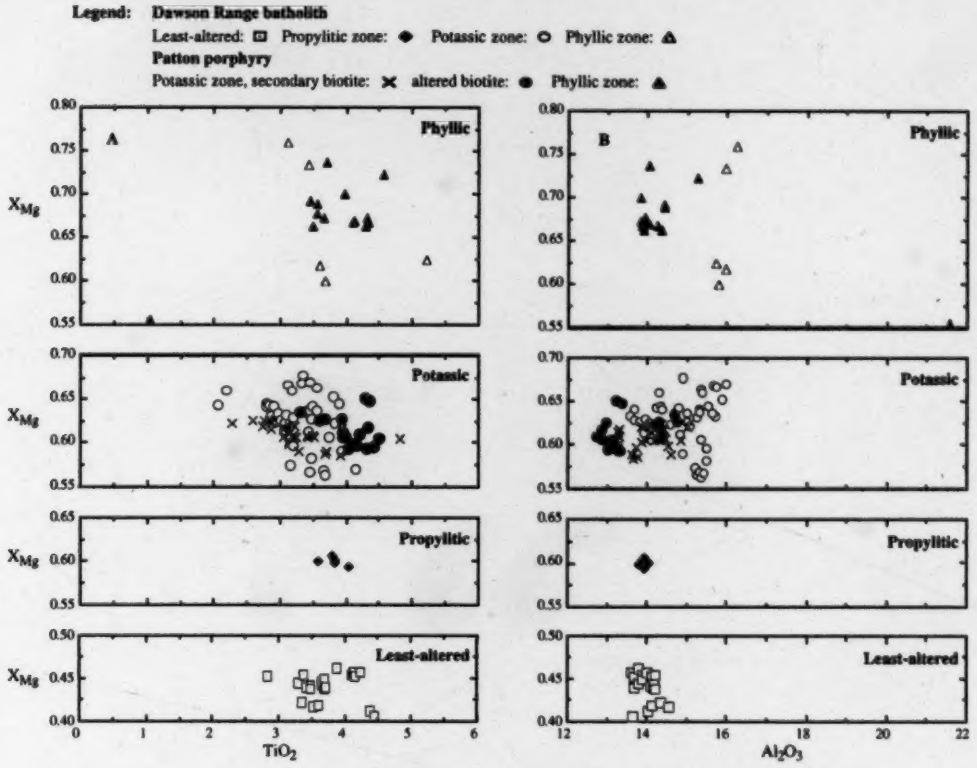

Fig. 4. 3. X_{Mg} vs. wt. % SiO_2, Al_2O_3, TiO_2, FeO, BaO, MnO, Na_2O, K_2O, F and Cl for least-altered biotite, plus altered and secondary biotite from propylitic, phyllic and potassic alteration zones. Each symbol represents an arithmetic mean of five microprobe spot analyses of a biotite.

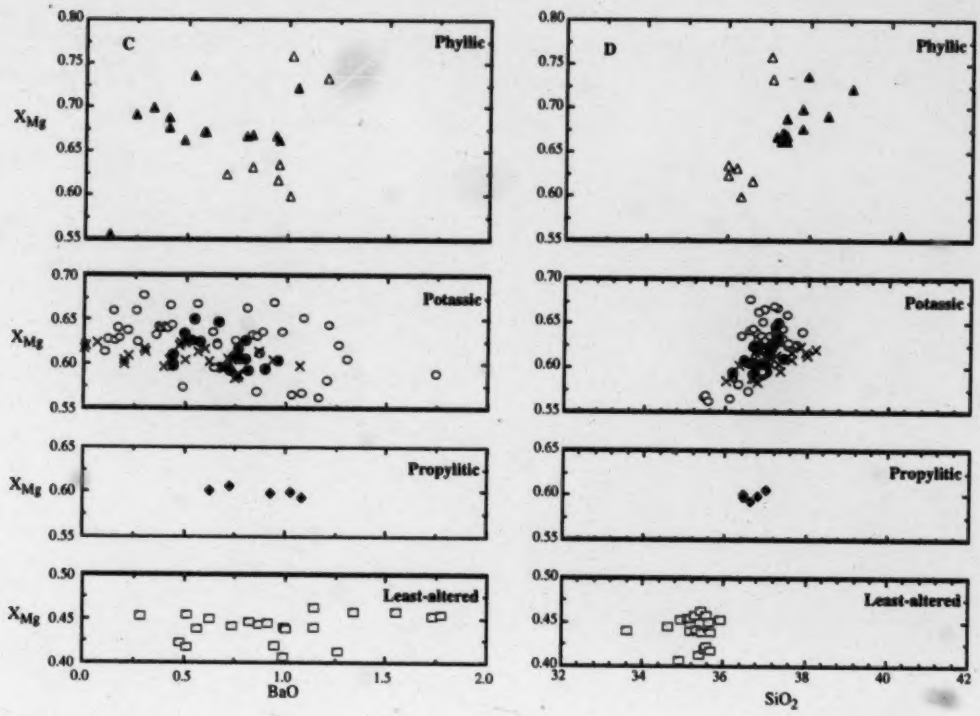

Fig. 4.3. Continued.

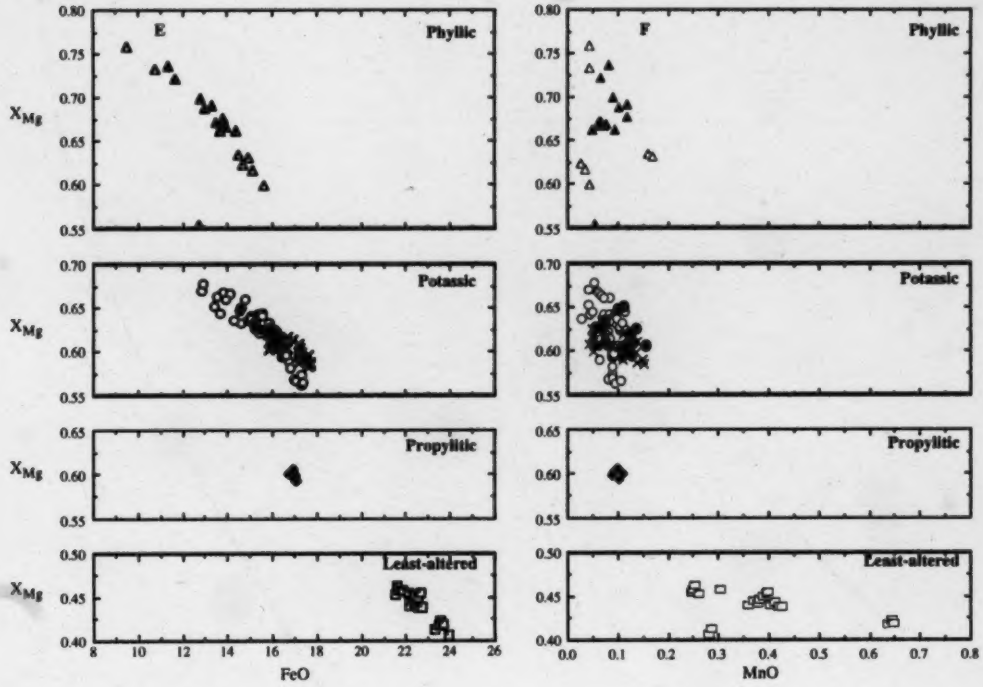

Fig. 4.3. Continued

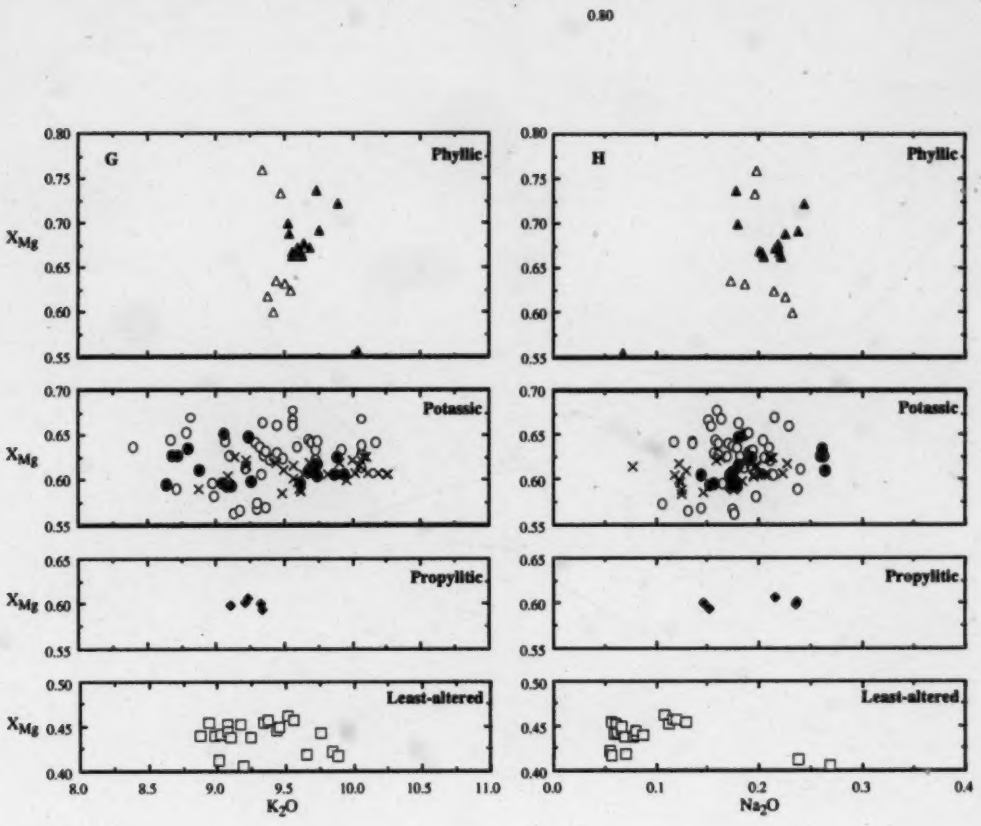

Fig. 4.3. Continued

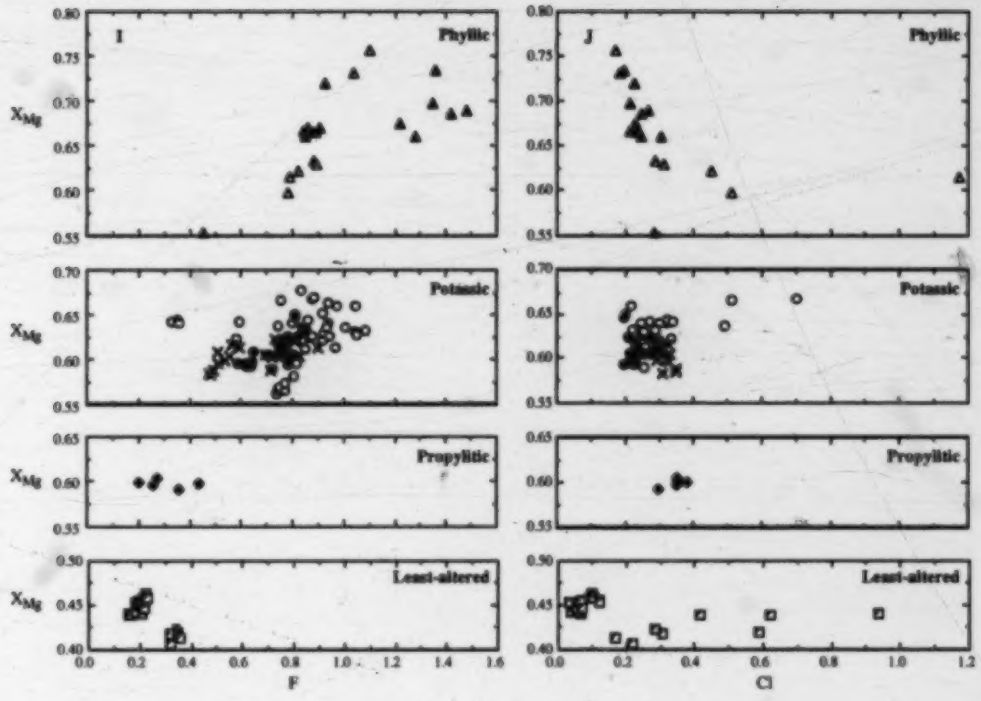

Fig. 4.3. Continued

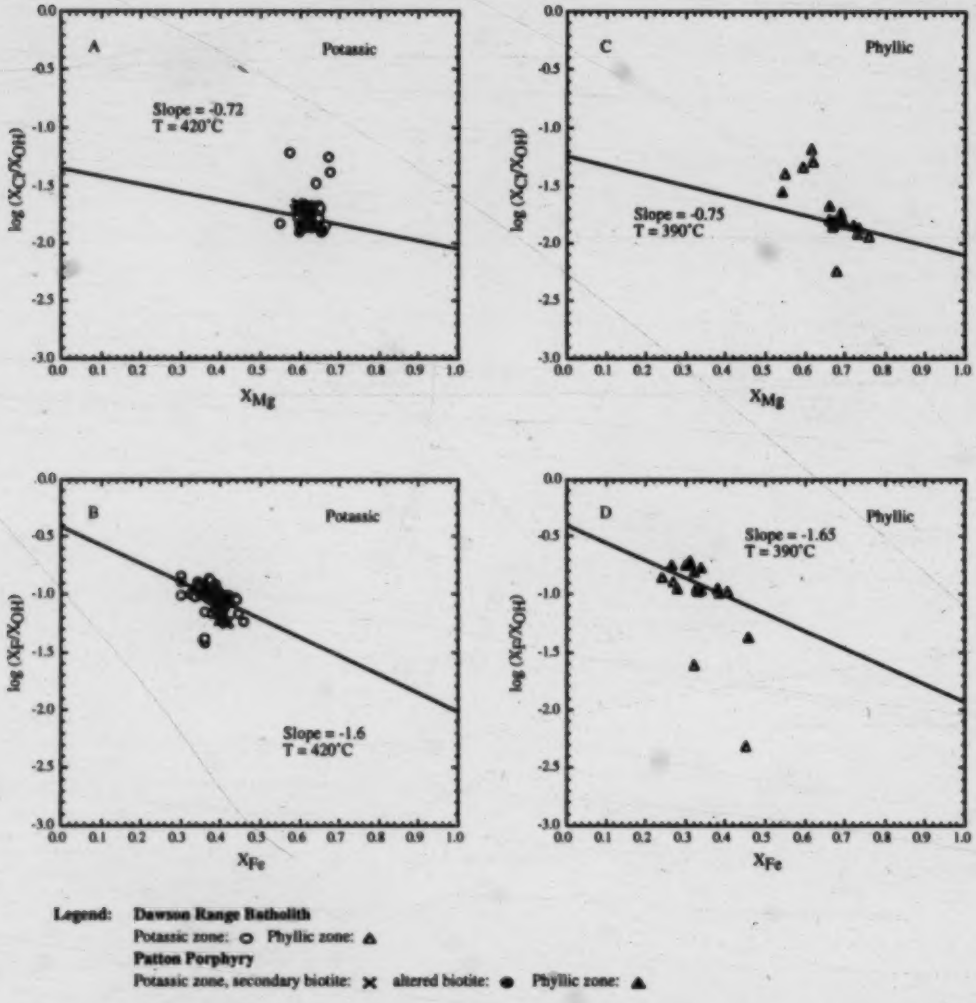

Fig. 4.4. Chemical data for biotites from the Casino occurrence. A and B plot secondary biotite of the Dawson Range batholith (open circles) and Patton Porphyry (crosses) and altered biotite of the Patton Porphyry (filled circles) from the potassic alteration zone. C and D plot hydrothermal biotite of the Dawson Range batholith (open triangles) and Patton Porphyry (filled triangles) from the phyllic alteration zone. Slopes on all plots are derived from the formulations of Zhu and Sverjensky (1991, 1992) and temperatures from fluid inclusion studies (Selby, unpub. data).

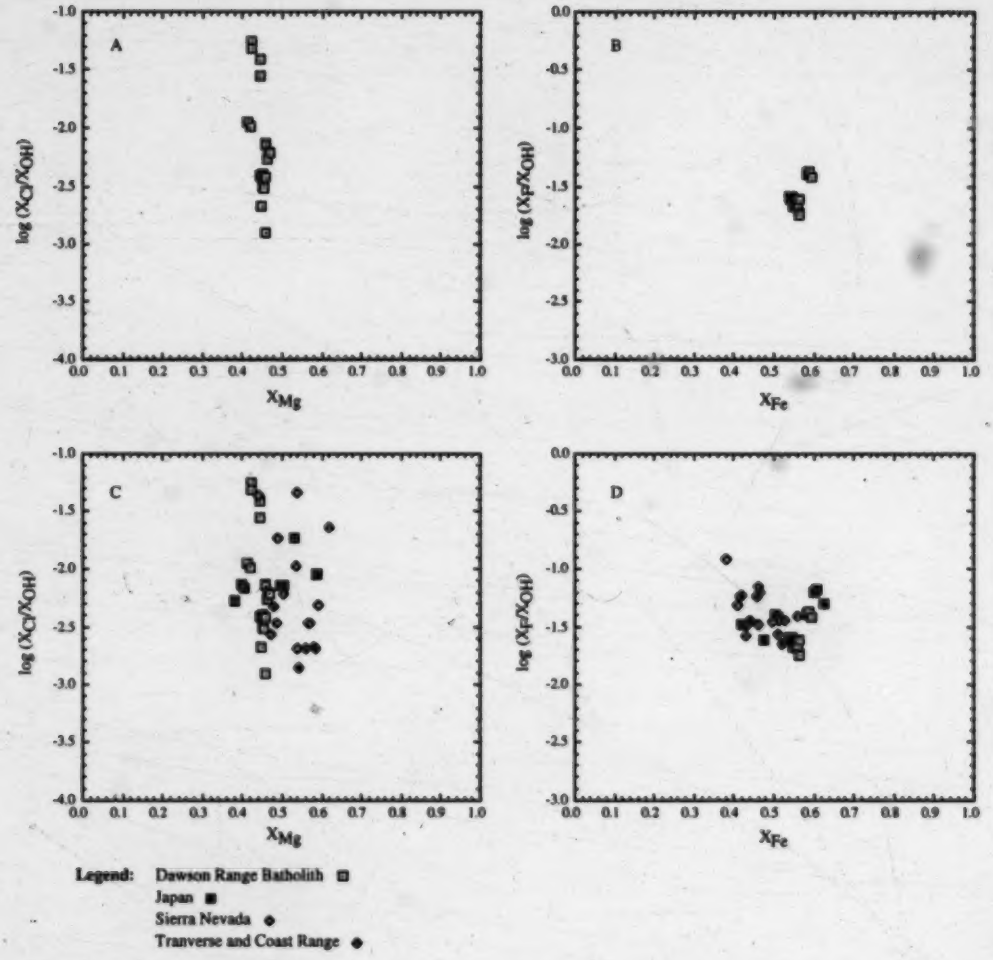

Fig. 4.5. Chemical data for least-altered biotite from the Dawson Range batholith. A and B: The scatter of the data showing the increase of log (X_{Cl}/X_{OH}) with similar X_{Mg} values, and the positive correlation between X_{Fe} and log (X_F/X_{OH}) illustrates either the violation of the Fe-F and Mg-Cl avoidance principles or biotite that coexisted with a F-rich/Cl-poor fluid. C and D: Data of the Dawson Range batholith (open square) and granitic bodies from Japan (filled square), Sierra Nevada (open diamond) and Tranverse and Coast Range (filled diamond), which are also not consistent with the Fe-F and Mg-Cl avoidance principles.

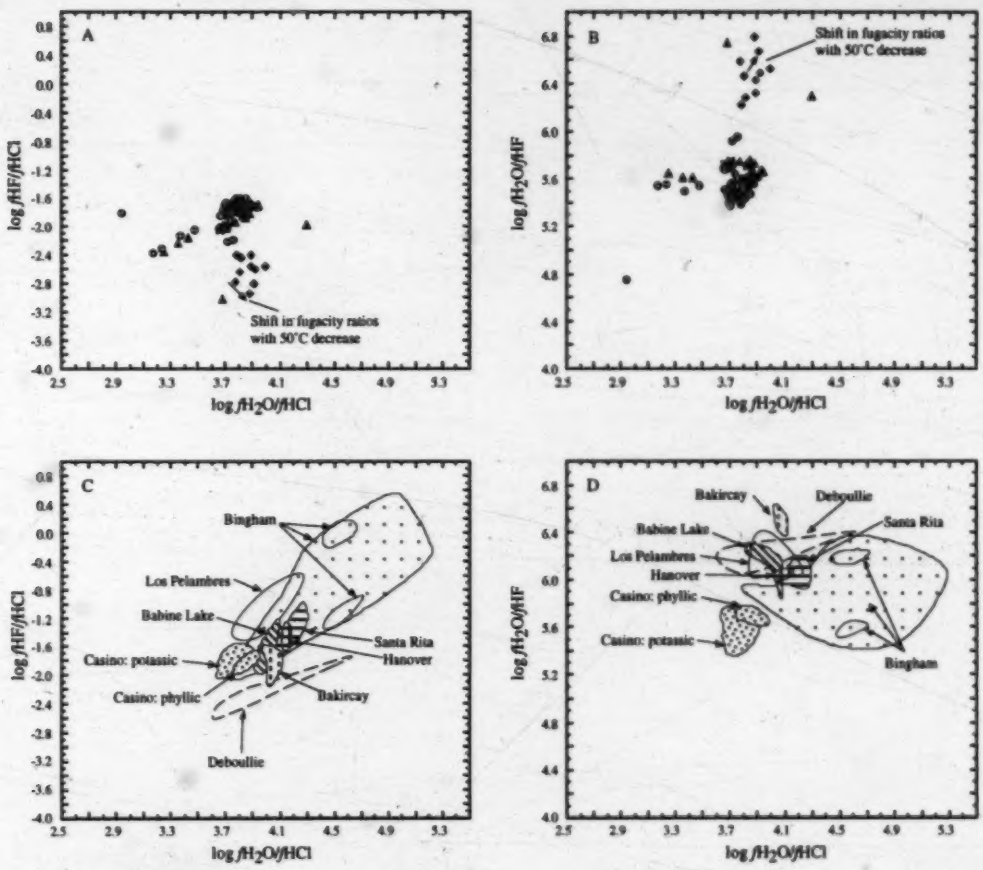

Legend for figures A and B

Dawson Range Batholith

Propylitic zone: ◆ Potassic zone: ● Phyllic zone: ▲

Patton Porphyry

Potassic zone secondary biotite: ✖ Altered biotite: ● Phyllic zone: ▲

Fig. 4.6. A and B: log (fH_2O)/($fHCl$), (fH_2O)/(fHF) and (fHF)/($fHCl$) ratios for the Casino occurrence. Fugacity ratios are calculated at 420, 390 and 350°C for potassic, phyllic and propylitic alteration, respectively. Also shown are fugacity ratios calculated at 300°C for propylitic alteration (open diamonds). C and D show fugacity ratios determined for Santa Rita, Los Pelambres, Bakircay, Hanover, Bingham, Babine Lake and Deboullie porphyry Cu deposits, plus the data from Casino.

Chapter V

Evidence for a non-magmatic component in potassic hydrothermal fluids of porphyry Cu-Au-Mo systems, Yukon, Canada*

*A version of this paper has been submitted for publication to Geochimica et Cosmochimica Acta, co-authored by Bruce E. Nesbitt, Robert A. Creaser, and Karlis Muehlenbachs of the Department of Earth and Atmospheric Sciences, University of Alberta, T6G 2E3, Canada, and Peter H. Reynolds of the Department of Earth Sciences, Dalhousie University, Halifax, Nova Scotia, Canada, B3H 3J5.

Introduction

Our current knowledge of the characteristics and origin(s) of the hydrothermal fluids of porphyry Cu deposits are derived mainly from stable isotope (oxygen and hydrogen) and fluid inclusion studies (e.g., Sheppard et al. 1969, 1971; Taylor 1974; Nash 1976; Sheppard and Gustafson 1976; Bodnar 1995; Hedenquist et al. 1998). These studies suggest that early, high-temperature potassic alteration is ultimately a product of a magmatic fluid (Sheppard et al. 1969, 1971; Sheppard and Taylor 1974; Sheppard and Gustafson 1976), and/or magmatic processes such as degassing (Taylor 1986, 1992; Hedenquist et al. 1998), or D/H fractionation between hypersaline liquid and vapor (Dobson et al. 1989; Horita et al. 1995). However, a few stable isotope and fluid inclusion studies have proposed that a non-magmatic fluid (basinal brine, seawater, meteoric water) play a role in this alteration process (Bowman et al. 1987; Dilles et al. 1992; Zaluski et al. 1994; Sheets et al. 1996).

This study presents and discusses fluid inclusion, stable (H) and radiogenic (Sr, Pb, Ar) isotopic compositions of minerals and inclusion fluids relating to potassic hydrothermal alteration at of the Casino, Cash, and Mt. Nansen Cu-Au-Mo porphyry

occurrences, Yukon, Canada. A reconnaissance fluid inclusion study is presented to show the mircothermometric characteristics of the hydrothermal fluids. Hydrogen isotopic compositions of the hydrothermal fluids are obtained from bulk fluid inclusion waters. To investigate further the characteristics and origin(s) of the potassic hydrothermal fluids, Sr, Pb, Ar isotope compositions of hydrothermal minerals (K-feldspar, pyrite, chalcopyrite and bornite) and quartz vein fluid inclusion waters were determined. Previous studies have analyzed Sr isotope compositions of whole rock samples from different alteration zones, with the results supporting the conclusions of the stable isotope and fluid inclusion studies that early fluids are magmatic in origin (Taylor and Fryer, 1983; Farmer and DePaolo, 1987). However, the isotope data determined herein are interpreted to indicate that potassic hydrothermal fluids may also contain a non-magmatic component, most likely a crustal fluid of meteoric origin. Oxygen isotope values of potassic-stage quartz veins from the Casino occurrence (Appendix IV) are similar to those for quartz veins of the Babine Lake porphyry Cu systems, British Columbia (Sheets and Nesbitt 1996). These data suggest that chemically evolved crustal fluids rather than pristine meteoric fluids were responsible for potassic alteration (Sheets et al. 1997), which is consistent with the interpretation of the Sr and Pb isotopic data of this study.

Mineralization and Hydrothermal Alteration

The Casino, Cash, and Mt. Nansen porphyry Cu-Au-Mo occurrences of the Dawson Range, Yukon-Tanana terrane, west-central Yukon, Canada (Fig. 5.1) are related to late Cretaceous porphyritic intrusions ($U\text{-}Pb_{zircon}$ = 72.4 ± 0.5 Ma for Casino, J. K. Mortensen pers. comm. 1997; $K\text{-}Ar_{biotite}$ = 70.5 ± 2.2 and 68.2 ± 1.6 for Mt. Nansen and Cash, respectively, Stevens et al. 1982). The porphyritic plutons intrude country rocks comprising the mid-Cretaceous Dawson Range batholith and Casino Plutonic Suite, and

the Devono-Mississippian Wolverine Creek Metamorphic Suite (Johnston 1995; Selby et al. 1999).

Previous studies described the mineralization and hydrothermal alteration characteristics of the Casino, Cash, and Mt. Nansen occurrences (Godwin 1976; Bower et al. 1996; Sawyer and Dickinson 1976; Sinclair et al. 1981; Hart and Langdon 1998). The following is a synopsis of these data, together with observations of this study. Casino is the largest porphyry occurrence in the Dawson Range with 675 million tonnes of 0.25 % Cu, 0.48 g/t Au and 0.024 % Mo. Mineralization and hydrothermal alteration of the porphyry occurrences are superimposed on the Cretaceous plutons and the neighboring country rocks. Hypogene mineralization is represented by chalcopyrite, pyrite, bornite, tetrahedrite, molybdenite, and gold. Chalcopyrite mineralization is disseminated and in veins, being typically concentrated inside the contact of the potassic and phyllic zones. Bornite and tetrahedrite are intergrown with chalcopyrite, though both are rare. The phyllic zone is characterized by disseminated and vein-hosted abundant pyrite and minor bornite. Gold occurs as inclusions and fracture fillings in pyrite and chalcopyrite grains.

Potassic, phyllic, propylitic, and argillic alteration types characterize the hypogene hydrothermal alteration zones. The potassic alteration is present in the core of the occurrences and consists of an assemblage of K-feldspar (orthoclase), biotite, magnetite and quartz. Potassic alteration is typically identified by K-feldspar bordering a quartz stockwork vein and as the matrix of hydrothermal breccias, occurring with or without biotite and magnetite. Quartz, pyrite, sericite and tourmaline (var. dravite) comprise the phyllic alteration assemblage. Fracture-controlled quartz veins and pervasive replacement of the pre-existing mineral phases characterize phyllic alteration. Tourmaline occurs as acicular radiating crystals intergrown with pyrite and quartz. Epidote, chlorite, calcite, sericite, quartz, and specular hematite characterize propylitic zones, which are poorly developed. Argillic alteration is locally recognized, associated

typically with late faults and sporadically developed in potassic and phyllic zones. The alteration assemblage consists of kaolinite, sericite, and montmorillonite.

Fluid Inclusions

A reconnaissance fluid inclusion study was conducted for the Casino occurrence, together with a petrographic examination for the Mt. Nansen occurrence. For Casino, the study investigated the fluid inclusion types, and their relative abundance, and the microthermometric characteristics in vein quartz associated with potassic and phyllic alteration assemblages (Appendix 5.A). These fluid inclusion types are present at Casino and Mt. Nansen: (1) multi-phase inclusions (liquid + vapor + daughter minerals); (2) vapor-rich inclusions (liquid + vapor ± daughter mineral); and (3) liquid-rich inclusions (liquid + vapor). At Casino, A Type quartz veins associated with potassic alteration assemblages contain 55 % Type 1 inclusions; 40 % Type 2 inclusions; and 5 % Type 3 inclusions, and D Type quartz veins with phyllic alteration assemblages contain 27 % Type 1 inclusions; 63 % Type 2 inclusions; and 10 % Type 3 inclusions. Quartz veins of potassic and phyllic stage alteration are dominated by Type 1 and 2 inclusions, with Type 2 inclusions being prevalent in phyllic stage quartz veins. Type 3 inclusions are a relatively minor component of the fluid inclusion assemblages.

Type 1 inclusions are primary, and range in size from 10 to 30 μm with negative crystal shapes. Mineral phases of halite, sylvite, chalcopyrite, and pyrite are present in Type 1 inclusions associated with potassic alteration. Type 1 inclusions in potassic veins homogenize by vapor bubble disappearance (ThL) and halite dissolution (ThH) with similar final homogenization temperatures, though possess a biomodal salinity composition. Type 1 inclusions in potassic veins homogenize by ThL at 427 ± 44°C and possess a salinity of 37 ± 2.6 wt. % NaCl eq. (n = 39), and by ThH at 417 ± 51°C with a salinity of 51 ± 5.3 wt. % NaCl eq [n = 22]. Type 1 fluid inclusions of phyllic alteration

assemblages also homogenize by ThH (376 ± 33°C with a salinity of 45 ± 3.3 wt. % NaCl eq. [n = 9]) and ThL (399 ± 61°C with a salinity of 35 ± 3.1 wt. % NaCl eq. [n = 12]). Final inclusion homogenization by ThH is dominant in veins of potassic alteration assemblages, with homogenization by ThL being typical of veins associated with phyllic alteration.

Type 2 inclusions are vapor-rich, characterized by a vapor bubble consisting of 60 to 90 % of the inclusion volume, with an unidentified opaque mineral phase (sulfide?) present in some inclusions. Distinct primary inclusions were observed in quartz growth zones (not coexisting with a Type 1 inclusion) and as isolated inclusions. Inclusions range from 5 to 15 μm (typically 10 μm) with negative crystal shapes. Eutectic (Te) temperatures of Type 2 inclusions in potassic quartz veins (–45 to –53°C [n = 4]), and of phyllic veins (–47 to -23°C [n = 4]) suggest the presence of components other than NaCl and KCl in the liquid phase. Final ice melting (Tfm) temperatures for Type 2 inclusions from potassic veins (–4.4 ± 1.5°C [n = 27]), and phyllic veins (–5 ± 3°C [n = 12]) yield salinities of 7 ± 2 wt. % and 8 ± 4 wt. % NaCl eq., respectively. Inclusions from phyllic veins with more negative Te and Tfm were observed in growth zones, whereas inclusions yielding less negative values are isolated. Type 2 inclusions from potassic quartz veins homogenize at 445 ± 44°C (n = 42), and inclusions from phyllic veins homogenize at 439 ± 43°C (n = 59).

Liquid-rich Type 3 inclusions are identified in quartz veins associated with potassic and phyllic alteration. Inclusions were typically observed as trails along healed microfractures suggesting a secondary origin. Inclusion size is typically ≈2 μm, and because of their size microthermometric analysis was not conducted.

Hydrogen Isotope Study

Plutonic quartz phenocrysts and quartz from veins associated with potassic and phyllic alteration assemblages were analyzed to determine the hydrogen isotope compositions of fluid inclusions (δD_{FI}) (Appendix 5.A; Table 5.1; Fig. 5.2). Quartz phenocrysts from the Mt. Nansen pluton yield δD_{FI} values of –91 and –113 ‰ (n = 2), which are depleted in deuterium relative to typical magmatic values (–40 to –80 ‰; Taylor, 1979; Fig. 5.2). However, quartz veins associated with potassic alteration from Mt. Nansen show even lower δD_{FI} values (–121 to –177 ‰; n = 4) relative to the plutonic quartz phenocrysts. Potassic alteration stage quartz veins from Casino and Cash also show similar δD_{FI} values (–140 to –181 ‰; n = 10; Fig. 5.2).

Hydrogen isotope composition of phyllic quartz veins from Casino, Cash, and Mt. Nansen range between –117 and –182 ‰. At Casino, δD_{FI} values of phyllic quartz veins possess higher hydrogen isotope compositions (–117 to –132 ‰; n = 10) than those of the potassic veins (–140 to –182 ‰; Fig. 5.2). At Mt. Nansen the only sample of phyllic-zone quartz analyzed possesses a higher δD_{FI} value than those the majority obtained for potassic veins (Table 5.1; Fig. 5.2). However, at Cash the δD_{FI} values of phyllic veins are very similar to those of potassic veins (Table 5.1; Fig. 5.2). The δD_{FI} compositions of phyllic veins, though typically higher than potassic veins, are still more depleted than the plutonic quartz phenocrysts.

Sr And Pb Isotope Study

Whole rock, magmatic apatite, hydrothermal K-feldspar and quartz vein fluid inclusion waters were analyzed for their Sr and Pb isotopic compositions (Appendix 5.A; Table 5.2). For the discussion below, Sr and Pb isotopic compositions are given as initial values for the time of the hydrothermal activity associated with porphyry mineralization and alteration (e.g., t = 70 Ma, given as $^{87}Sr/^{86}Sr_{t=70}$).

Magmatic Isotope Compositions

To determine the magmatic $^{87}Sr/^{86}Sr$ compositions of the plutons genetically associated to the porphyry hydrothermal system the least altered samples of plutons were analyzed. Magmatic apatite from the host plutons was also analyzed because the initial $^{87}Sr/^{86}Sr$ ratio of apatite is unlikely to be highly modified by hydrothermal activity (e.g., Creaser and Gray, 1992). The apatite and whole rock $^{87}Sr/^{86}Sr$ values from Casino are very similar (whole rock = 0.70541 to 0.70551; apatite = 0.70547), the difference being within analytical uncertainty (± 0.00002; Table 5.2). Apatite from the Cash and Mt. Nansen plutons possesses slightly more radiogenic $^{87}Sr/^{86}Sr$ compositions than whole-rock samples (Table 5.2), which may represent slight modifications to the Sr isotope system of either the whole rock or the apatite. The Pb isotopic compositions were determined only for the Patton porphyry. The analyzed samples show a very narrow range of $^{206}Pb/^{204}Pb_{70}$ (19.277 to 19.336), $^{207}Pb/^{204}Pb_{70}$ (15.638), and $^{208}Pb/^{204}Pb_{70}$ (38.829) ratios (Table 5.3).

Potassic Alteration Stage Isotope Compositions

Hydrothermal K-feldspar and fluid inclusion waters from vein quartz were analyzed to determine the Sr isotope composition of the hydrothermal fluids associated with potassic alteration (Appendix 5.A; Table 5.2). Unleached K-feldspar samples (Appendix 5.A) possess $^{87}Sr/^{86}Sr_{t=70}$ values from 0.70561 to 0.70852 (Table 5.2). The $^{87}Sr/^{86}Sr_{t=70}$ values range from magmatic values determined from whole-rock and apatite analyses to increasingly radiogenic compositions (Table 5.2, Fig. 5.3A). If potassic hydrothermal fluids are entirely magmatic in origin then a preliminary interpretation of this data might be that post-potassic hydrothermal fluids modified the Sr isotope system of the hydrothermal K-feldspar. To evaluate this possibility, selected K-feldspar samples

were treated with various leach and cleaning protocols which progressively etch K-feldspar along mineral surfaces, edges and cleavage planes, removing possible contaminants such as sericite, calcite and gypsum, as well as exchangeable Sr and Pb cations (Appendix 5.A). Three of the five leached K-feldspars possess less radiogenic $^{87}Sr/^{86}Sr_{t=70}$ compositions, and two show an increase in the $^{87}Sr/^{86}Sr_{t=70}$ compositions in comparison to the unleached K-feldspar (Fig. 5.3B; Table 5.2). Importantly, four of the five leached K-feldspar samples have more radiogenic Sr isotope composition than inferred magmatic values.

The fact that two leached K-feldspar samples possess more radiogenic compositions than the unleached counterpart (DS140, 147) suggests that any modification to the Sr systematics of K-feldspar is either from carbonate, gypsum, and/or cation exchange on lattice sites between K-feldspar and a less radiogenic hydrothermal fluid. Using a electrochemical cleaning technique to remove carbonate, sulfate and surface ion particles (Appendix 5.A) we obtained virtually the same values for DS106 as for the leached counterpart, whereas K-feldspar sample DS162 gave intermediate values between the bulk and leached analyses (Table 5.2, Fig. 5.3B). The latter suggests that minerals contaminating K-feldspar vary between carbonates, sulfates and silicates. However, XRD analysis of the K-feldspar samples did not identify any impurities.

The Pb isotopic compositions were also determined for selected hydrothermal K-feldspars from the Casino occurrence. The analyzed leached K-feldspar samples show a wide range of $^{206}Pb/^{204}Pb$ (19.217 to 19.276), $^{207}Pb/^{204}Pb$ (15.576 to 15.647), and $^{208}Pb/^{204}Pb$ (38.697 to 38.919) ratios (Table 5.3). The Pb isotopic ratios of the K-feldspars are both higher and lower than the initial Pb isotopic ratios for whole rock analyses of the Casino pluton (Table 5.3; Fig. 5.4). The more radiogenic Pb initial isotopic compositions of the Casino pluton in comparison to four of the six hydrothermal leached K-feldspar samples (Table 5.3; Fig. 5.4) may be the result of radiogenic Pb, present as sulphides,

being introduced to the Casino pluton by the hydrothermal system. The latter is evident from the Pb isotopic composition of sulphides from the phyllic zone, which typically have more radiogenic composition than K-feldspar (below, Table 5.3). Therefore, we suggest that the least radiogenic Pb isotopic ratios of the K-feldspar (DS65A, 73) probably represent the upper limit of magmatic Pb isotopic composition (Table 5.3; Fig. 5.4). Furthermore, the spread in $^{207}Pb/^{204}Pb$ of leached K-feldspar is mirrored by $^{87}Sr/^{86}Sr_{t=70}$ for the same samples (Fig. 4B), which is broadly shown for $^{208}Pb/^{204}Pb$ vs. $^{87}Sr/^{86}Sr_{t=70}$ (Figs. 4C). A sample of chalcopyrite from a potassic alteration assemblage possesses similar Pb isotopic values to the K-feldspar samples (Table 5.3).

Fluid inclusion waters in quartz veins bordered by a potassic alteration assemblage were analyzed for their Sr and Pb isotopic compositions. Bulk, leachate, and residue Sr isotope compositions of quartz veins are similar to the $^{87}Sr/^{86}Sr_{t=70}$ compositions to the K-feldspar samples (Table 5.2). The Rb-Sr data of quartz-K-feldspar sample pairs (DS106, 140, 147, 162) are plotted in coordinates of $^{87}Sr/^{86}Sr$ and $^{87}Rb/^{86}Sr$ (Fig. 5.5), together with the whole rock and magmatic apatite data of the Casino pluton, and a 72.4 Ma reference isochron ($U\text{-}Pb_{zircon}$ age of the Casino porphyry). The array of Rb-Sr data of quartz and K-feldspar approximately fit a 72.4 Ma isochron (Fig. 5.5). The 72.4 Ma reference isochron extrapolated through the quartz and K-feldspar data shows that the initial $^{87}Sr/^{86}Sr$ compositions range from 0.7078 to 0.7079, which are significantly different from the initial composition of the Casino pluton (~ 0.7053) (Fig. 5.5). In turn, these data show that the initial $^{87}Sr/^{86}Sr$ compositions of hydrothermal fluids associated with potassic alteration is significantly different from that of purely magmatic fluids that would have been generated by the Casino pluton.

Phyllic Alteration Isotope Compositions

To determine the Sr isotope composition of hydrothermal fluids associated with phyllic alteration the Sr isotope composition of fluid inclusions in quartz veins were analyzed. The $^{87}Sr/^{86}Sr_{t=70}$ values of leachates from quartz veins are between 0.70658 and 0.70724 (Table 5.2). The $^{87}Sr/^{86}Sr_{t=70}$ values for phyllic hydrothermal fluids are within the mid-range of those determined for potassic alteration and are greater than those established for magmatic values (Table 5.2).

Pb isotopic compositions for phyllic hydrothermal fluids were determined from pyrite and bornite. The sulfides possess Pb isotopic ratios similar to or greater than most radiogenic compositions of K-feldspar (Table 5.3). However, pyrite sample DS43 possesses a less radiogenic composition than all the K-feldspar samples (Table 5.3).

Argon Isotope Study

An argon isotope study was undertaken on selected hydrothermal K-feldspar samples to determine their age and isotopic composition of non-radiogenic argon (Appendix 5.A). The data are presented in conventional $^{40}Ar/^{39}Ar$ age spectrum diagrams (Fig. 5.6). Seven of the nine samples yielded uniform apparent ages over almost the entire gas release spectrum; the remaining two (DS106, DS162) produced spectra with slight age gradients. There is no evidence of significant resetting of ages in any spectra (e.g., by post-potassic alteration). Apparent $^{37}Ar/^{39}Ar$ ratios are effectively zero for all samples over the latter part of the gas release (Fig. 5.6). Initial non-zero values, comprising up to 30 % of the ^{39}Ar release, are attributed to the outgassing of a minor Ca-rich phase, perhaps plagioclase and/or gypsum. The isotopic data characterized by zero $^{37}Ar/^{39}Ar$ values are assumed to be K-feldspar derived; these are shown (following blank correction, Appendix 5.A) on isotope correlation diagrams (Fig. 5.7). Eight of the nine samples yielded straight-line plots with no scatter in the data beyond what is expected

from experimental uncertainties. The isochron ages of these samples range between 68.2 ± 0.7 and 72.6 ± 0.6 Ma. The remaining sample, DS106, yielded a spectrum with an age gradient and a correlation plot with more scatter; the age from the latter is somewhat higher and less certain (73.4 ± 0.8 Ma). Apparent $^{40}Ar/^{36}Ar$ initial ratios for seven of the nine samples range from 286 ± 2 to 292 ± 2 (mean 290 ± 3); two samples (DS97-87 and DS97-38) have ratios somewhat higher, but these also have higher uncertainties.

Apparent ages obtained in this study are in close agreement with previously published data for plutons genetically associated with porphyry mineralization and alteration. For example, the $^{40}Ar/^{39}Ar$ ages from Casino yield ages between 71.9 ± 0.7 and 73.4 ± 0.8 Ma respectively, closely bracketing the U-Pb zircon age of the Patton Porphyry (72.4 ± 0.5 Ma; J. K. Mortensen, pers. comm.). Furthermore, samples from Mt. Nansen yield ages (68.2 ± 0.7 to 69.5 ± 0.6 Ma) very similar to the age of the Mt. Nansen pluton (K-Ar biotite age = 70.5 ± 2.2 Ma; Stevens et al., 1982), and a sample from Cash yielded an age (68.3 ± 0.8 Ma) very similar to the Cash pluton (K-Ar biotite age = 68.2 ± 0.5 Ma; Stevens et al., 1982). The apparent $^{40}Ar/^{36}Ar$ initial ratios determined for the K-feldspar samples are for the most part within the range determined for the atmosphere during Cretaceous time (295 ± 5; Landis and Snee, 1990), but is also indistinguishable from the present day ratio (Faure, 1986). The location of the non-radiogenic gas in the samples is problematic. The non-radiogenic ^{36}Ar persists throughout the heating schedule for all samples, typically being between 1.0 to 4.8 mV, which are values well above the blank values (0.3 mV) (Appendix 5.A), so the non-radiogenic argon must be in a retentive phase. The separates used in these analyses were carefully prepared and checked by XRD analysis, and no impurities or fluid inclusions were observed. However, this does not preclude the presence of very small impurities that could serve as hosts for the non-radiogenic gas. Otherwise, this gas must be contained within the feldspar lattice itself. The presence of retentive non-radiogenic argon with a

atmospheric-like composition within the K-feldspar lattice suggests that atmospheric-like argon was present in the hydrothermal fluids associated with potassic alteration.

Discussion

Potassic Hydrothermal Fluids

The Sr and Pb isotopic data of K-feldspar and quartz that precipitated from potassic alteration show isotopic compositions mostly more radiogenic than determined magmatic values. Hitherto, hydrothermal fluids of porphyry systems associated with potassic alteration have been suggested to be entirely magmatic in origin (e.g., Sheppard and Taylor 1974; Burnham 1979; Cline and Bodnar 1991; Hedenquist et al. 1998 and references therein). If hydrothermal fluids associated with potassic alteration are wholly derived from magmatic processes (e.g., second boiling, Burnham 1979) the Sr and Pb isotope compositions of K-feldspar and quartz veins should be identical to the magmatic values; however, this is not the case for the porphyry occurrences studied here. Furthermore, δD_{FI} values of quartz veins dominated by saline and vapor-rich inclusion types are depleted relative to waters from plutonic quartz phenocrysts (–91 to –113 ‰; this study) and those traditionally regarded as magmatic (–40 to –80 ‰; Taylor 1979). Also, hydrothermal K-feldspars contain a component of atmospheric Ar. The resultant isotope compositions of K-feldspar and quartz determined in this study may be the product of:

1) Inheritance of pre-existing isotope compositions from host rocks

2) Post-potassic alteration isotope exchange

3) Replenishment of the magma chamber with a magma of different isotopic composition

4) Component(s) of the hydrothermal fluids of non-magmatic origin

Inheritance of preexisting isotope compositions from host rocks

The potassic alteration zone of the porphyry systems studied is superimposed upon the related plutons and the country rocks. The country rocks consist dominantly of the Dawson Range batholith and metamorphic rocks of the Yukon-Tanana terrane, which possess more radiogenic isotope compositions (e.g., $^{87}Sr/^{86}Sr_{t=70}$ = 0.707 to 0.722, and $^{206}Pb/^{204}Pb_{t=70}$ 19.191 to 19.629, $^{207}Pb/^{204}Pb_{t=70}$ 15.677 to 15.793, $^{208}Pb/^{204}Pb_{t=70}$ 38.922 to 39.386; cf. Selby et al., 1999) than the mineralized late Cretaceous plutons ($^{87}Sr/^{86}Sr_{t=70}$ = 0.7055, and $^{206}Pb/^{204}Pb_{t=70}$ 19.217, $^{207}Pb/^{204}Pb_{t=70}$ 15.615, $^{208}Pb/^{204}Pb_{t=70}$ 38.782). The more radiogenic isotope compositions of the hydrothermal minerals may be a result of inheriting the isotopic compositions from the host rocks on to which the potassic alteration assemblage was superimposed. However, no correlation between associated country rock type and Sr and Pb isotopic compositions of the hydrothermal K-feldspar is observed. For example, K-feldspar sample DS65 is from potassic altered Dawson Range batholith, but, possesses a Sr and Pb isotopic composition most like the magmatic value of the Casino pluton (Table 5.2). Furthermore, K-feldspar samples DS97-87 and 89 from the Mt. Nansen pluton possess Sr isotope compositions similar to the Dawson Range batholith (Table 5.2). In addition, the Sr isotope compositions of quartz veins record those directly related to the hydrothermal fluids, which are similar to the K-feldspar compositions. The latter also suggests that the $^{87}Sr/^{86}Sr_{t=70}$ values directly reflect those of the hydrothermal fluids associated with potassic alteration and not the inheritance of isotopic compositions from the wallrock.

Modification of isotopic compositions

Petrographic examination of K-feldspar samples for Sr isotopic analysis noted sericite alteration. However, sericite was not identified by XRD analysis of the same samples, suggesting abundance < 5 %. We envision any modification of the K-feldspar

Sr and Pb isotopic compositions to be a product of ion exchange between a hydrothermal fluid and mineral lattice and diffusive element exchange. Ions in the hydrothermal fluid can replace exchangeable ions in K-feldspar surfaces, edges, and defects (Blum and Stillings, 1995). Ion exchange in K-feldspar is shown to be to a depth of several unit cells (~ 37Å) (Petrovic et al., 1976; Schweda, 1989). Schweda (1990) demonstrated that in the presence of saline solutions similar to the hydrothermal fluid at Casino, ion exchange is inhibited, and further suggested that ion exchange beneath the K-feldspar surface inhibits ion exchange in the surface. The minor depth of ion exchange suggests that Sr and Pb isotopic compositions were not significantly affected by ion exchange via hydrothermal fluids. Furthermore, the minor abundance of sericite, is unlikely to be a factor in generating the initial Sr isotopic compositions of K-feldspar observed here. The removal of any surface of the K-feldspar subjected to ion exchange and sericite alteration were removed through applied acid cleaning protocols – leached K-feldspar samples (Appendix 5.A).

To test if the Sr and Pb isotope compositions were modified by the interaction of post-potassic hydrothermal fluids the closure temperature of Sr and Pb diffusion in feldspar are determined using the parameters of Giletti (1991), Cherniak and Watson (1992), and Cherniak (1995) and the formulation of Dobson (1973) (Appendix 5.B). The diffusion parameters of Cherniak and Watson (1992) and Cherniak (1995) are based on the chemical diffusion under anhydrous conditions of Sr and Pb, which is rate-limited by the charge compensating ions Al and Si, with the diffusion parameters of Giletti (1991) determined for self-diffusion (direct element-element exchange) under hydrous conditions. The diffusion parameters of Cherniak and Watson (1992) and Cherniak (1995) are applicable to a hydrothermal environment, the data of Giletti (1991) and Giletti and Classerly (1992) suggesting that the presence of a hydrous medium has little effect on the Sr diffusion in feldspars. Furthermore, the minimal influence of a hydrous

medium on Pb diffusion in zircons suggests that water medium has little effect on the diffusion of cations in silicate minerals (Cherniak and Watson 1998).

The closure temperature is a function of the effective radius of diffusion of mineral and cooling rate (Dobson 1973). Recent developments in evaluating the longevity of porphyry hydrothermal systems cooling from 900 to 200°C using numerical modeling and $^{40}Ar/^{39}Ar$ geochronology, suggest a duration of 33,000 to 230,000 years (Marsh et al. 1997). These duration times yield cooling rates of $7.41*10^{-10}$ to $9.67*10^{-11}$°Cs^{-1}. The grain size of hydrothermal K-feldspar is typically 2 mm, which yields diffusion radii of 1 mm. Using the Sr data of Cherniak and Watson (1992) and the life span of the hydrothermal system (Marsh et al., 1997), closure temperatures (Tc) of 860 to 940°C are determined; the Sr data of Giletti (1991) yield Tc values of 675 to 770°C. The Pb data of Cherniak (1995) yield Tc values of 1225 to 1350°C.

Twinned K-feldspar results in smaller more effective diffusion domains (≈10 μm) (Cherniak and Watson 1992). The diffusion radii of 5 μm and Sr data of Cherniak and Watson (1992) yield Tc values of 580 to 710°C, and using the Sr data of Giletti (1991) Tc values of 375 to 420°C are calculated. Recalculating the Tc for Pb using a 5 μm diffusion radii yields Tc values of 800 and 860°C. The calculated Tc are equal to and typically higher than homogenization temperatures determined from fluid inclusion studies, suggesting that Sr and Pb isotope exchange did not occur with the late stage hydrothermal fluids. However, the Sr data of Giletti (1991) suggest that only at the slowest cooling rates and the smallest diffusion radii will the Sr isotope composition be modified by the late stage hydrothermal fluids.

To evaluate if the 10 μm diffusion domains were effective diffusion channels to yield the $^{87}Sr/^{86}Sr_{t=70}$ values of K-feldspar of this study the distance of Sr diffusion was calculated. The diffusion of Sr is a function of temperature and time (Appendix C1). The lowest calculated Sr Tc was 375°C, determined for the slowest cooling rate ($9.67*10^{-11}$

^{11}°Cs^{-1}, for a system with a 230,000 year duration). For a hydrothermal system with a longevity of 230,000 years the time necessary to cool to the Tc of 375°C is 173,000 years; using the latter age and the diffusion coefficient determined from the parameters of Giletti (1991) a diffusion distance of 3 μm is calculated. The diffusion distance of 3 μm is 1/666th of the K-feldspar thickness; therefore, it is most unlikely that the Sr isotopic ratio of the crystal core will be modified. In addition, the Tc (375°C) is reached in 173,000 years, and therefore, to significantly modify the core Sr isotope composition of the K-feldspar, temperatures > 775°C would be necessary (Cherniak and Watson 1992). The latter is unlikely, because all homogenization temperatures determined from fluid inclusion were < 500°C.

The closure temperatures determined for Sr and Pb diffusion in K-feldspar suggest that the initial Sr and Pb isotopic compositions will not significantly be modified during cooling of a porphyry hydrothermal system. However, slight modifications of the initial Sr isotope composition are suggested from the data of Giletti (1991), which are shown from the isotopic values of the leached and unleached K-feldspar samples (Table 2; Fig. 3). The above discussion suggests that K-feldspar records the initial Sr and Pb isotopic compositions of hydrothermal fluids associated with potassic alteration and were not significantly altered by subsequent fluids related to late stage alteration assemblages.

Furthermore, sericite, though not identified from XRD analysis of the K-feldspars, most likely is not a factor in generating the $^{87}Sr/^{86}Sr_{t=70}$ ratios of K-feldspar, because sericite is a Rb-rich mineral and would generate high $^{87}Sr/^{86}Sr$ ratios through ^{87}Rb decay. However, the product of any radiogenic ^{87}Sr generated by ^{87}Rb decay in sericite is removed by calculating the initial $^{87}Sr/^{86}Sr$ ratios of the K-feldspars.

Replenishment of the magma chamber

The porphyry occurrences of this study are much like other porphyries in that they are represented by more than one pluton body. Typically, two cylindrical pluton bodies

are present at the occurrences. At Casino and Cash these bodies were sampled and analyzed for their Sr isotope composition (Table 2). The $^{87}Sr/^{86}Sr_{t=70}$ compositions of each body for each occurrence are very similar, with the εNd values, and rare earth element chemistry for the bodies of the Casino occurrence being virtually identical (Selby et al. 1999). The latter suggests that the material replenishing the magma chamber during the emplacement of the plutons is of a very similar composition, and that replenishment of the magma chamber with a magma of different isotopic composition in this case is not likely to be the cause of the observed isotope compositions of K-feldspar and quartz vein fluid inclusion waters.

Component(s) of the hydrothermal fluids of non-magmatic origin

The above discussion suggests that Sr and Pb isotopic compositions of K-feldspar most likely represent values of the hydrothermal fluids associated with potassic alteration and not later stage fluid overprint or the replenishment of the magma chamber. K-feldspar and quartz veins possess Sr, Pb, H, and Ar isotopic compositions differing from those of the plutons. If potassic hydrothermal fluids are entirely magmatic in origin (e.g., Burnham 1979; Hedenquist and Lowenstern 1994) then the isotope compositions of the hydrothermal minerals would be identical to those of the pluton from which the hydrothermal fluids are derived. Therefore, the isotopic data of this study suggest a non-magmatic component mixing with the pluton-derived potassic hydrothermal fluids.

The Sr and Pb isotopic compositions of the fluid could have been inherited from the neighboring country rocks transferred via regional crustal fluids. The neighboring country rocks consist dominantly of the Dawson Range batholith and metamorphic rocks of the Yukon-Tanana terrane. In crystalline terrains Sr and Pb isotopic compositions of groundwaters are similar to whole rock compositions (Erel et al. 1994; Blum et al. 1994; Clow et al. 1997). The following discussion considers mixing Sr derived from the

country rocks and the plutons to establish the K-feldspar Sr isotope compositions. The average $^{87}Sr/^{86}Sr_{t=70}$ composition of the country rocks in the study area is 0.70972 (Selby et al. 1999). Using the $^{87}Sr/^{86}Sr_{t=70}$ values of the country rocks and the plutons to represent the composition of crustal and magmatic water, respectively, calculations using a two component mixing equation (Faure 1986, p.142) indicate that 13 to 81 % crustal fluids are necessary to produce the observed K-feldspar Sr isotope compositions (Appendix D).

The low δD compositions of potassic hydrothermal fluids of this study also support the proposal that a component of the fluid is exotic to the pluton. Previous studies have interpreted low δD values for early stage hydrothermal fluids to be of a non-magmatic origin e.g., seawater or meteoric (Dilles et al. 1992; Zaluski et al. 1994; Sheets et al. 1996). However, low δD values suggesting the presence of a non-magmatic water component have recently been reinterpreted to be the result of magma degassing (Hedenquist et al. 1998). Previous arguments against the process of degassing generating low δD values were based on the correlation with the δD of paleo-meteoric waters (Sheets and Nesbitt 1996). Moreover, degassing depletes deuterium in the magmatic fluid, which is directly correlated to the decrease in the weight percentage of water (Taylor 1983; Dobson et al. 1989). The plutonic quartz phenocrysts of this study possess δD values between –91 and –113 ‰. These values are similar to δD values from plutonic systems that are associated with 0.25 to 0.5 wt. % H_2O in the magmatic system (Taylor 1988), suggesting that a similar weight percent H_2O existed in the magmatic systems of the Casino, Cash, and Mt. Nansen. These low H_2O contents («0.5 wt. %) will be insufficient to produce the necessary mechanical energy to generate the extensive fracturing of breccias and stockworks (Burnham and Ohmoto 1980), which characterize the potassic hydrothermal stage of porphyry systems studied here. Furthermore, the δD composition of the bulk exsolved fluid, which is similar to that of vapor, will have a δD

value ≈20 ‰ heavier than the hypersaline fluid (Horita et al. 1995), and therefore the exsolved magmatic fluid for the occurrences of this study yield a δD of –120 to –160 ‰. The estimation of the δD of the exsolved fluid is still depleted relative to the plutonic quartz phenocrysts (–91 to –113 ‰). It is probable that the δD of the plutonic quartz phenocrysts of this study represent degassing of the magma chamber. However, based on the above discussion degassing of the magmatic system cannot alone produce the observed low δD of the potassic hydrothermal fluids (–140 to –180 ‰), suggesting magmatic fluids mixed with a non-magmatic low δD fluid.

The combined isotopic data suggest that components of Sr, Pb, H, and Ar of the hydrothermal fluids are not wholly derived from the magmatic system associated with the porphyry occurrences of Casino, Cash, and Mt. Nansen. Crustal fluids of similar isotopic composition to the country rocks interacting with the magmatic fluids of the plutons may explain the Sr and Pb isotopic compositions of potassic hydrothermal fluids. Hydrogen isotope compositions may represent degassing of the pluton to initially lower the magmatic δD_{FI} value (plutonic quartz phenocrysts) and the mixing of low δD fluids (potassic-stage quartz vein compositions). In regard to the latter, the extremely depleted δD_{FI} values coincide with the paleo-meteoric water values of the Yukon (McInnes et al. 1987) the atmospheric argon composition suggesting that a component of the hydrothermal fluids of potassic alteration was of meteoric origin.

Phyllic Fluids

The discussion thus far has concentrated on the characteristics of hydrothermal fluids associated with potassic alteration. The geochemical characteristics of potassic fluids are consistent for the Casino, Cash, and Mt. Nansen occurrences; however, this is not the case for phyllic fluids. At Casino, phyllic veins possess higher δD_{FI} compositions by ≈20 ‰ compared to potassic quartz veins (Fig. 2). The phyllic veins at Cash possess

similar δD_{FI} values to potassic veins, and at Mt. Nansen the one phyllic vein analyzed has a heavier δD_{FI} value than three of four potassic veins (Fig. 5.2). Sr isotope compositions of phyllic quartz veins (0.70658 to 0.70724) from Casino fall in the middle of the range of the potassic alteration (0.70561 to 0.70852), and Pb isotopic compositions are typically more radiogenic than the K-feldspar and chalcopyrite values (Table 5.3).

The dominance of vapor-rich inclusions in phyllic quartz veins of Casino and Mt. Nansen may explain the 20 ‰ higher δD compositions of the fluids by the D/H fractionation between hypersaline fluid and vapor (Horita et al. 1995). The δD_{FI} values are still depleted relative to the values of the plutonic quartz phenocrysts of this study, and those traditionally accepted as magmatic (Taylor 1979). The δD isotopic composition of the vapor is similar to that of the exsolved fluid from the magma (Dobson et al. 1989). Again, the δD_{FI} of phyllic veins, if derived through degassing, would equate to water concentrations «0.5 wt. %, insufficient to develop the mechanical energy for fracturing to produce the quartz veining of the phyllic stage (Burnham and Ohmoto 1980). Furthermore, Sr and Pb isotopic compositions are more radiogenic than the magmatic values, suggesting that components of Sr and Pb are non-magmatic as proposed for the potassic fluids. The Sr isotope compositions are calculated to represent a 63 to 73 % crustal fluid component of phyllic-stage hydrothermal fluids.

Implications

Previous studies of potassic alteration of porphyry systems consider the ultimate origin of the fluids to be magmatic (cf. Burnham 1979; Cline and Bodnar 1991; Hedenquist and Lowenstern 1994; Hedenquist et al. 1998 and references therein). However, a non-magmatic fluid component of the Yukon occurrences and other deposits (Bowman et al. 1987; Dilles et al. 1992; Sheets and Nesbitt 1996) raises the question of how and where external fluids interact with the magmatic fluids. Sheets and Nesbitt

(1996) considered that the external fluids diffused into the undersaturated portion of the melt, invoking the model proposed by Shinohara et al. (1995). Difficulties are encountered, however, explaining the Sr and Pb isotopic compositions by diffusion. Sr diffusion between melts of different isotopic compositions show that the $^{87}Sr/^{86}Sr$ value is only affected over small distances (≈25 m) across the boundary of the melts (Baker 1989). Pb has similar diffusion rates to Sr (Lesher 1994), which suggests that the Pb isotopic compositions are also only likely to be affected over small distances. Moreover, Sr and Pb diffusion is a rate-limited and therefore diffusion alone would not explain the range of more radiogenic Sr and Pb isotopic compositions observed in this study.

We propose that crustal fluids are a component of the potassic hydrothermal fluids. The permeabilities of crystalline rocks suggest crustal fluids freely convect to ≈ 400°C (Brace 1980; 1984). At temperatures ≥ 400°C the rock permeability decreases as the brittle/ductile transition is approached (Brace 1980). Temperatures ≥ 400°C are reached approximately at 6 km or less in active volcanic regions (Lachenbruch and Sass 1980), which suggest that the plutons associated with porphyry mineralization behave in a more ductile manner, especially near the magma chamber. A rock rheology near the brittle/ductile transition will fracture at high strain rates (Fournier 1991) like those generated by the exsolving fluid during the crystallization of the magma chamber (Burnham and Ohmoto 1980). During fracturing, i.e. the formation of hydrothermal breccias and stockworks, it is suggested that the crustal and magmatic fluids mix.

A problem encountered in mixing crustal and magmatic fluids externally from the magma chamber is the dilution of the salinity of the hydrothermal fluids, and the mixing of fluids of contrasting density. Crustal fluids of the Canadian Cordillera possess a salinity (2 to 14 wt. % NaCl eq.; Nesbitt and Muehlenbachs, 1995) similar to the bulk exsolved magmatic fluid (2 to 10 wt. % NaCl eq.; Burnham 1979; Bodnar 1995; Hedenquist et al. 1998). Magmatic fluids of low salinity are released from the magma

chamber and rise through the intrusion (Shinohara et al. 1995; Shinohara and Hedenquist 1997) to a depth where fluid immiscibility occurs (Fournier 1987). Crustal and magmatic fluids of similar salinity can mix to form a homogeneous fluid composition below the depth of fluid immiscibility, which then rise in the same manner as magmatic fluids forming a hypersaline brine.

At Casino, Type 1 inclusions that homogenize by halite dissolution suggest a hypersaline brine (≈50 wt. NaCl eq.) was formed during the crystallizing of the melt. However, coexisting hypersaline and vapor-rich inclusions suggest that a low salinity (2 to 10 wt. % NaCl eq.) hydrothermal fluid ascended to a depth where fluid immiscibility occurred. The density difference of the hypersaline and low salinity fluids cause the magmatic fluids not to be mixed, though the low salinity crustal and magmatic fluids mix freely. The Sr and Pb isotopic compositions most like the magmatic compositions may represent the earliest potassic hydrothermal fluids, being similar to the inferred magmatic composition. Nonetheless, the Sr, Pb and H isotopic data indicate a non-magmatic component in these fluids. During the evolution of the potassic hydrothermal stage the fracture density increases, which allowed a greater influx of crustal fluids into the hydrothermal system. The latter is supported by the more radiogenic Sr and Pb isotopic compositions.

Sheets et al. (1996) posed the question of how common are low δD values for early fluids of porphyry systems? The data of this study suggest that low δD values are present in the Casino, Cash, and Mt. Nansen porphyry systems of the Yukon and are likely where δD values of meteoric waters are distinct from magmatic fluids. A question arising from the data discussed in the paper is how common are external fluids in the potassic stage hydrothermal fluids in porphyry systems worldwide? External fluids being a component of potassic hydrothermal fluids have been invoked for a few deposits of North America (Bowman et al. 1987; Dilles et al.,1992; Zaluski et al. 1994; Sheets and

Nesbitt 1996), although the majority of porphyry systems of North America and South America and South Pacific are regarded to have early fluids of purely a magmatic origin (e.g., Sheppard and Gustafson 1976; Kusakabe et al. 1990; Hedenquist et al. 1998 and references therein). The results of this study indicate that the origin of hydrothermal fluids responsible for potassic-stage alteration may differ globally and therefore challenge the hypothesis of these fluids being wholly magmatic in origin. Applying the detailed approach used in this study may aid in determining the characteristics of fluids in potassic-stage alteration, which will assist in developing a more comprehensive understanding of the origin(s) of fluids in these systems, not only for specific regions, but also globally.

References

Baker, D. R. 1989. Tracer versus trace element diffusion: Diffusional decoupling of Sr concentration from Sr isotope composition. Geochimica et Cosmochimica Acta, **53:** 3015-3023.

Blum, J. D., Erel, Y., and Brown, K. 1994. 87Sr/86Sr ratios of Sierra Nevada stream waters: Implications for relative mineral weathering rates. Geochimica et Cosmochimica Acta, **58:** 5019-5025.

Bodnar, R. J., Burnham, C. W., and Sterner, S. M. 1985. Synthetic fluid inclusions in natural quartz. III. Determinations of phase equilibrium properties in the system H_2O-NaCl to 1000°C and 1500bars. Geochimica et Cosmochimica Acta, **49:** 1861-1873.

Bodnar, R. J., and Vityk, M. O. 1995. Intrepretation of microthermometric data for H_2O-NaCl fluid inclusions. *In* Fluid inclusions in minerals: methods and applications. *Edited by* Benedetto De Vivo and M. L. Frezzotti. 117-131

Bower, B., Payne, J., Delong, C., and Rebagliati, C. M. 1995. The oxide-gold supergene and hypogene zones at the Casino gold-copper-molybdenite deposit west-central Yukon. *In* Porphyry Deposits of the Northwestern Cordillera of North America. *Edited by* T. G. Schroeter. Canadian Institute of Mining, Metallurgy and Petroleum, Special Volume 46 352-366.

Bowman, J. R., Parry, W. T., Kropp, W. P., and Kruer, S. A. 1987. Chemical and isotopic evolution of hydrothermal solutions at Bingham, Utah. Economic Geology, **82:** 395-428.

Brace, W. F. 1980. Permeability of crystalline and argillaceous rocks. International Journal of Rock Mechanics, Mineral Science and Geomechanics Abstracts, **17:** 241-251.

Brace, W. F. 1984. Permeability of vrystalline rocks: New in situ measurements. Journal of Geophysical Research, **89:** 4327-4330.

Burnham, C. W., 1979, Magmas and hydrothermal fluids. *In* Geochemistry of Hydrothermal Ore Deposits. *Edited by* H. L. Barnes. 77-136 p.

Burnham, C. W., and Ohmoto, H. 1980. Late-stage processes of felsic magmatism. Mining Geology Special Issue, **8:** 1-11.

Cherniak, D. J. 1995. Diffusion of lead in plagioclase and K-feldspar: an investigation using rutherford backscattering and resonant nuclear reaction analysis. Contributions to Mineralogy and Petrology, **120:** 358-371.

Cherniak, D. J., and Watson, E. B. 1992. A study of strontium diffusion in K-feldspar, Na-K feldspar and anorthite using rutherford backscattering spectroscopy. Earth and Planetary Science Letters, **113:** 411-425.

Cherniak, D. J., and Watson, E. B. 1998. Pb Diffusion in Zircon. Geological Society of American Abstracts with Programs, **30:** A-213.

Cline, J. C., and Bodnar, R. J. 1991. Can economic porphyry copper mineralization be generated by a typical calc-alkaline melt? Journal of Geophysical Research, **96:** 8113-8126.

Clow, D. W., Mast, M. A., Bullen, T. D., and Turk, J. T. 1997. Strontium 87/strontium 86 as a tracer of mineral weathering reactions and calcium sources in an alpine/subapline watershed, Loch Vale, Colorado. Water Resources Research, **33:** 1335-1351.

Coleman, M. l., Sheppard, T. J., Durham, J. J., Rouse, J. E., and Moore, G. R. 1982. Reduction of water with zinc for hydrogen isotope anaylsis. Analytical Chemistry, **54:** 993-995.

Craig, H. 1961a. Standards for reporting concentration of deuterium and oxygen- 18 in natural waters. Science, **133:** 1833-1834.

Creaser, R. A., and Gray, C. M. 1992. Preserved initial $^{87}Sr/^{86}Sr$ in apatite from altered felsic igneous rocks: A case study from the middle Proterozoic of south Australia. Geochimica et Cosmochimica Acta, **56:** 2789-2795.

Dilles, J. H., Solomon, C. G., Taylor, H. P., Jr., and Einaudi, M. T. 1992. Oxygen and hydrogen isotope characteristics of hydrothermal alteration at the Ann-Mason porphyry copper deposit, Yerington, Nevada. Economic Geology, **87:** 44-63.

Cumming, G. L., and Krstic, D. 1987. Geochronology at the Namew Lake Ni-Cu deposit, Flin Flon area, Manitoba, Canada: a Pb-Pb study of whole rocks and ore minerals. Canadian Journal of Earth Sciences, **28:** 1328-1339.

Dobson, M. H. 1973. Closure temperatures in cooling geochronolgical and petrological systems. Contributions to mineralogy and petrology, **40:** 259-274.

Dobson, P. F., Epstein, S., and Stolper, E. M. 1989. Hydrogen isotope fractionation between coexisting vapor and silicate glasses and melts at low pressure. Geochimica et Cosmochimica Acta, **53:** 2723-2730.

Erel, Y., Harlavan, Y., and Blum, J. D. 1994. Lead isotope systematics of granitoid weathering. Geochimica et Cosmochimica Acta, **58:** 5299-5306.

Farmer, G. L., and DePaolo, D. J. 1987. Nd and Sr isotope study of hydrothermally altered granite at San Manuel, Arizona: Implications for element migration paths during the formation of porphyry copper ore deposits. Economic Geology, **82:** 1142-1151.

Faure, G., 1986, Principles of Isotope Geology, John Wiley & Sons, 589 p.

Fournier, R. O. 1987. Conceptual models of brine evolution of magmatic-hydrothermal systems. *In* Volcanism in Hawaii. *Edited by* R. W. Decker, T. L. Wright, and . H. Stauffer. U. S. Geological Survey Professional Paper 1487-1506.

Fournier, R. O. 1991. The transition from hydrostatic to greater than hydrostatic fluid pressure in presently active continental hydrothermal systems in crystalline rock. Geophysical Research Letters, **18:** 955-958.

Giletti, B. J. 1991. Rb and Sr diffusion in alkali feldspars, with implications for cooling histories of rocks. Geochimica et Cosmochimica Acta, **66:** 1331-1343.

Giletti, B. J., and Classerly, J. E. D. 1992. Diffusion kinetics of Sr in plagioclase feldspars (abstr.). EOS, **73:** 373.

Godwin, C. I. 1976. Casino. *In* Porphyry Deposits of the Canadian Cordillera. *Edited by* A. Sutherland Brown. Canadian Institute of Mining and Metallurgy, special volume 15 344-354.

Hart, C. J. R., and Langdon, M. 1998. Geology and mineral deposits of the Mount Nansen camp, Yukon. In: Yukon Exploration and Geology 1997, Exploration and Geological Services Division, Yukon, Indian and Northern Affairs Canada 129-138.

Hedenquist, J. W., Arribas, A., Jr., and Reynolds, T. J. 1998. Evolution of an intrusion-centered hydrothermal system: Far Southeast-Lepanto porphyry and epithermal Cu-Au deposits, Philippines. Economic Geology, **93:** 373-404.

Hedenquist, J. W., and Lowenstern, J. B. 1994. The role of magmas in the formation of hydrothermal ore deposits. Nature, **370:** 519-527.

Horita, J., Cole, D. R., and Wesolowski, D. J. 1995. The activity-composition relationship of oxygen and hydrogen isotopes in aqueous salt solutions: III. Vapor-liquid water equilibration of NaCl solutions to 350°C. Geochimica et Cosmochimica Acta, **59:** 1139-1151.

Housh, T., and Bowring, S. A. 1991. Lead isotopic heterogeneities within alkali feldspars: Implications for the determination of initial lead isotopic compositions. Geochimica et Cosmochimica Acta, **55:** 2309-2316.

Johnston, S. T. 1995. Geological compilation with interpretation from geophysical surveys of the northern Dawson Range, central Yukon (115-J/9 and 115-J/10, 115-I/12, 1:100 000 scale map). Exploration and Geological Services Division, Yukon, Indian and Northern Affairs Canada, Open File 1995-2(G).

Kusakabe, M., Hori, M., and Matsuhisa, Y. 1990. Primary mineralization-alteration of the El Teniente and Rio Blanco porphyry copper deposits, Chile. Stable isotopes, fluid inclusions and Mg2+/Fe2+/Fe3+ ratios of hydrothermal biotite. Perth, University of Western Australia, Geology Department Publication 30 244-259.

Lachenbruch, A. H., and Sass, J. H. 1980. Heat flow and energetics of the San Andreas fault zone. Journal of Geophysical Research, **85:** 6185-6222.

Landis, G. P., and Snee, L. W. 1990. $^{40}Ar/^{39}Ar$ systematics in amber and preservation of earth paleoatmospheres in primary gas bubbles in amber. Geological Society of America Abstracts with Programs, **22:** A173.

Langmuir, C. H. R. D., Vocke, J., Hanson, G. N., and Hart, S. R. 1978. A general mixing equation with applications to icelandic basalts. Earth Planetary Science Letters, **37:** 380-392.

Lesher, C. E. 1994. Kinetics of Sr and Nd exchange in silicate liquids: Theory, experiments, and applications to uphill diffusion, isotopic equilibration, and irreversible mixing magmas. Journal of Geophysical Research, **99:** 9585-9604.

Marsh, T. M., Einaudi, M. T., and McWilliams, M. 1997. $^{40}Ar/^{39}Ar$ geochronolgy of Cu-Au and Au-Ag mineralization in the Potrerillos district, Chile. Economic Geology, **92:** 784-806.

McInnes, B. I. A., Crocket, J. H., and Goodfellow, W. D. 1990. The laforma deposit, an atypical epithermal-Au system at Freeold Mountain, Yukon Territory, Canada. Journal of Geochemical Exploration, **36:** 73-102.

Nesbitt, B. E., and Muehlenbachs, K. 1995. Geochemical studies of the origins and effects of synorogenic crustal fluids in the southern Omineca Belt of British Columbia, Canada. Geological Society of America Bulletin, **107:** 1033-1050.

Petrovic R., Berner R. A., and Goldhaber M. B. 1976 Rate control in dissolution of alkali feldspars — I. Study of residual feldspar grains by X-ray photoelectron spectroscopy. Geochimica et Cosmochimica Acta **40:** 537-548.

Samson, S. D., and Alexander, E. C. 1987. Calibration of the interlaboratory $^{40}Ar/^{39}Ar$ dating standard MMhb-1. Chemical Geology, **66:** 27-34.

Sawyer, J. P. B., and Dickinson, R. A. 1976. Mount Nansen. Porphyry Deposits of the Canadian Cordillera. Canadian Institute of Mining and Metallurgy, special volume 15 336-343.

Schweda P. 1989 Kinetics of alkali feldspar dissolution at low temperature. *In* Proceedings of the 6th International Symposium on Water-Rock interaction, *Edited by* D. L. Miles, 609-612.

Schweda P. (1990) Kinetics and mechanism of alkali feldspar dissolution at low temperatures. *PhD dissertation, Stockholm University.*

Selby, D., Creaser, R. A., and Nesbit, B. E. In press. Major and trace element compositions and Sr-Nd-Pb systematics of crystalline rocks from the Dawson Range, Yukon, Canada. Canadian Journal of Earth Sciences.

Sheets, R. W., Nesbitt, B. E., and Muehlenbachs, K. 1996. A meteoric water component in magmatic fluids from porphyry copper mineralization, Babine lake area, British Columbia. Geology, **24:** 1091-1094.

Sheets, R. W., Nesbitt, B. E., Muehlenbachs, K., Zaluski, G., and Tebar, H. 1997. Meteoric water interaction in porphyry copper mineralization of central British Columbia. *In* Geofluids II 1997 Contributions to the Second International Conference on Fluid Evolution, Migration and Interaction in Sedimentary Basins and Orogenic Belts. *Edited by* J. P. Hendry, P. F. Carey, J. Parnell, A. H. Ruffell and R. H. Worden, 205-208.

Sheppard, S. M. F., and Gustafson, L. B. 1976. Oxygen and hydrogen isotopes in the porphyry copper deposit at El Salvador, Chile. Economic Geology, **71:** 1549-1559.

Sheppard, S. M. F., Nielsen, R. L., and Taylor, H. P., Jr. 1969. Oxygen and hydrogen sotope ratios of clay minerals from porphyry copper deposits. Journal of Economic Geology, **64:** 755-777.

Sheppard, S. M. F., Nielsen, R. L., and Taylor, H. P., Jr. 1971. Hydrogen and oxygen isotope ratios in minerals from porphyry copper deposits. Journal of Economic Geology, **66:** 515-542.

Sheppard, S. M. F., and Taylor, H. P., Jr. 1974. Hydrogen and oxygen isotope evidence for the origins of water in the Boulder batholith and the Butte ore deposits. Economic Geology, **69:** 926-946.

Shinohara, H., and Hedenquist, J. W. 1997. Constraints on magma degassing beneath the Far Southeast Porphyry Cu-Au deposit, Philippines. Journal of Petrology, **38:** 1741-1752.

Shinohara, H., Kazahaya, K., and Lowenstern, J. B. 1995. Volatile transport in a converting magma column: Implications for porphyry Mo mineralization. Geology, **23:** 1091-1094.

Sinclair, W. D., Cathro, R. J., and Jensen, E. M. 1981. The Cash porphyry copper-molybdenum deposit, Dawson Range, Yukon Territory. Canadian Institute of Mining and Metallurgy Bulletin, **74:** 67-75.

Stevens, R. D., Delabio, R. N., and Lachance, G. R. 1982. Age determinations and geological studies; K-Ar isotopic ages, Report 16. Geological Survey of Canada, Paper 82-2 52.

Taylor, B. E., 1988, Degassing of rhyolitic magmas: hydrogen isotope evidence and implications for magmatic-hydrothermal ore deposits, Canadian Institute of Mining and Metallurgy, 33-49 p.

Taylor, B. E. 1992. Degassing of H_2O from rhyolite magma during eruption and shallow intrusion, and the isotopic composition of magmatic water in hydrothermal systems. Geological Survey of Japan Report 279 190-194.

Taylor, B. E., Eichelberger, J. C., and Westrich, H. R. 1983. Hydrogen isotopic evidence of rhyolitic magma degassing during shallow intrusion and eruption. Nature, **306:** 541-545.

Taylor, H., Jr. 1979. Oxygen and hydrogen isotope relationships in hydrothermal mineral deposits. *In* Geochemistry of hydrothermal ore deposits. *Edited by* H. L. Barnes. 236-272.

Taylor, H. P., Jr., and Sheppard, S. 1986. Igneous rocks: I. Processes of isotopic fractionation and isotope systematics. Reviews in Mineralogy, **16:** 227-271.

Taylor, R. P., and Fryer, B. J. 1983. Strontium isotope geochemistry of the Santa Rita porphyry copper deposit, New Mexico. Economic Geology, **78:** 170-174.

Todt, W., Cliff, R. A., Hanser, A., and Hofmann, A. W. 1996. Evaluation of ^{202}Pb-^{205}Pb double spike for high-precision lead isotope analysis. *In* Earth process: Reading the isotopic code. *Edited by* A. I. Basu and S. R. Hart. Geophysical Monograph 95. 429-437.

Zaluski, G., Nesbitt, B. E., and Muchlenbachs, K. 1994. Hydrothermal alteration and stable isotope systematics of the Babine Porphyry Cu deposits, British Columbia: Implications for fluid evolution of porphyry systems. Economic Geology, **89:** 1518-1541.

Appendices

Appendix 5.A

Analytical Procedures

Samples of porphyritic rocks related to porphyry Cu-Mo±Au mineralization from the Casino, Cash, and Mt. Nansen occurrences, and mineral separates of hydrothermal alteration assemblages were analyzed for their Sr and Pb isotopic compositions, and Rb and Sr contents by

isotope dilution mass spectrometry. K-feldspar, apatite, quartz and sulfide minerals were isolated by conventional crushing and separation techniques. Sr and Pb isotopic analyses were performed at the University of Alberta in the Earth and Atmospheric Sciences Radiogenic Isotope Facility.

Whole rock powdered, and K-feldspar, apatite, and quartz samples for Sr isotope analysis were weighed and totally spiked with tracer solutions of ^{84}Sr plus ^{87}Rb. Spiked whole rock, and K-feldspar, and quartz, samples were dissolved in a 5:2/5:1 mix of vapor-distilled concentrated HF and HNO_3 in sealed PFA Teflon vials at 160°C for ≈ 120/24 hours, respectively. Apatite samples were dissolved in 5 ml of 1.5N HCl. Selected K-feldspar samples for Sr isotope analysis were treated to a five-stage leach process to remove any radiogenic Sr incorporated subsequent to the initial crystallization of the crystal, prior to being dissolved. The leaching procedure is: leach 1, 2N HCl; leach 2, 6N HCl; leach 3, 16N HNO_3; leach 4, 16N HNO_3 + 1 drop of 24N HF, at 160°C for ≈ 24 hours per leach (Cumming and Krstic 1987), leach 5, 8:1 mix of 24N HF and 8N HNO_3 at 160°C for ≈ 20 minutes and repeated three times (Housh and Bowring 1991). The residual material was then spiked and dissolved as described above for unleached K-feldspar samples.

For Sr isotope analysis of fluid inclusion waters of vein quartz, clean quartz grains were picked with the aid of a microscope. The hand-picked material were then cleaned to remove trace amounts of carbonate and sulfate material using 50:50 acetone-ethanol mix, 6.2N HCl at ≈ 80°C for 1 hour and millipore water at ≈ 80°C for 1 hour. Further, to remove surface ions from the quartz grains the material was placed into an electrolytic cell (consisting of a PFA Teflon U-shaped tube, millipore water and platinum electrodes), with a 90 V DC applied. The conductivity of the millipore water from the cell was measured every 24 hours until the conductivity equalled that of millipore water (0.10 μS). Cleaned quartz samples were treated as bulk and crush leach samples. Crush leach samples were crushed in millipore water using a sapphire crucible and then centrifuged. The leachate was decanted and treated as one sample, and the remaining quartz was treated as a second sample (residue). All quartz samples were dissolved in a 5:2 mix of vapor-distilled concentrated HF and HNO_3 in sealed PFA Teflon vials at 160°C for ≈ 72 hours.

The resultant fluoride solutions of all samples were evaporated to dryness, then converted to chloride solutes by the addition of 6N HCl to the residue and heated at 160°C for ≈ 24 hours. The resultant chloride solutes were evaporated to dryness, then 0.75N HCl was added to the residue of the whole rock and apatite samples, and an Oxalic-HCl mix added to the K-feldspar and quartz samples, and was then heated for ≈ 2 hours at 160°C. Rb and Sr were separated from the chloride solutions using BioRad AG50-X8 200-400 mesh cation resin in PFA Teflon columns. Chemical processing blanks are < 400 pg for Sr and < 100 pg for Rb.

Powdered whole-rock samples for Pb analysis were weighed and dissolved in a 5:2 mix of vapor-distilled concentrated HF and HNO_3 in sealed PFA Teflon vials at 160°C for ≈ 72 hours. Samples of pyrite, chalcopyrite, and bornite were dissolved in a 1:1 mix of 12N HCl and 16N HNO_3 (aqua regia) at 160°C for ≈ 24 hours. K-feldspar samples were treated with a five-stage leach process as described for leached K-feldspars for Sr isotope analysis, in order to remove any radiogenic Pb that was incorporated after the genesis of the mineral phase. The samples were then dissolved in concentrated HF. The fluoride solutions of whole rock powders and K-feldspars, and chloride solutions of sulfide samples were evaporated to dryness and converted to chloride solutions with addition of 6N HCl, and then to bromide solutions with the addition of 0.5N HBr. Pb was separated from the cooled solutions using HBr-HNO_3-based chromatography with BioRad AG1-X8 200-400 mesh anion resin in heatshrink FEP Teflon columns (procedure modified from Lugmair and Galer 1992). Pb processing blanks are ≈150 pg.

The isotopic composition of the purified Pb and Rb fractions were analyzed using a MM30 mass spectrometer, with Sr fractions analyzed using a VG354 5-collector mass spectrometer. The measured Sr isotope ratios were corrected for mass fractionation and discrimination by normalizing to $^{86}Sr/^{88}Sr = 0.1194$. The isotopic reference standard measured at the time of the isotopic measurements are as follows: $^{87}Sr/^{86}Sr = 0.710238 \pm 0.000012$, 0.710215 ± 0.000035 and 0.710230 ± 0.00002 (SRM 987 standard); $^{206}Pb/^{204}Pb = 0.13\%.\ a.m.u.^{-1}$; $^{207}Pb/^{204}Pb = 0.14\%.\ a.m.u.^{-1}$; and $^{208}Pb/^{204}Pb = 0.11\%.\ a.m.u.^{-1}$, which were established by repeated measurement of the standard NBS 981 using the reference isotopic values of Todt et al. (1996).

Hydrogen isotope analyses were performed at the University of Alberta in the Earth and Atmospheric Sciences Stable Isotope Facility. Hydrogen isotope analyses of waters from fluid inclusions in quartz were conducted by thermal decrepitation, with hydrogen generated from the extracted water using the zinc reduction method of Coleman et al. (1982). Hydrogen isotope data are reported relative to SMOW (Craig, 1961), in δ notation for values in per mil (‰), with an analytical uncertainty (1σ) of $\pm$ 0.5 ‰.

Fluid inclusion microthermometry data were determined using a modified USGS gas-flow heating-freezing stage at the University of Alberta in the Earth and Atmospheric Sciences Fluid Inclusion Laboratory. Calibration of the stage was determined using pure H_2O and CO_2 inclusions for freezing temperatures and the critical point of pure H_2O for heating temperatures, with uncertainty of measurements of $\pm$ 0.2°C for freezing and $\pm$ 2°C for heating to 300°C. Salinities were calculated from final ice-melting and halite dissolution temperatures using the expressions of Bodnar and Vityk (1995) and Bodnar et al. (1985) for the H_2O-NaCl system.

Selected samples of K-feldspar analyzed for the Sr and Pb isotope compositions were also used in the Ar isotope/age study, which was performed at the Department of Earth Sciences at Dalhousie University. In preparation for analysis, the samples were wrapped in Al foil and arranged in an irradiation canister with aliquots of the hornblende standard, MMhb1 (which has an assumed age of 520 $\pm$ 2 Ma; Samson and Alexander, 1987). The canister was shielded with Cd and irradiated in the McMaster University nuclear reactor. In the argon laboratory, step-heating analyses were carried out using an internal tantalum resistance furnace of the double-vacuum type. A Nd-YAG laser system used in continuous mode with a wavelength of 1064 nm was used to conduct the laserprobe analyses. A VG 3600 mass spectrometer, using Faraday and electron multiplier collectors, was used to determine the argon isotope compositions. Errors are quoted at the 2σ level, but do not allow for the error in the age of the standard.

Appendix 5.B

Closure Temperatures

The interative equation of Dobson (1973) is used to determine the closure temperature (Tc):

$$Tc = \frac{Q/R}{\ln[(-AR T_c^2 (Do/ a^2))/(Q(dT/dt))]}$$

where: Q = activation energy; Do = pre-exponential factor; a = diffusional radii; A = diffusional anisotropy factor set to 55 for spherical geometry; R = gas constant; dT/dt = cooling rate. Q and Do are obtained from the data of Giletti (1991), Cherniak and Watson (1992) and Cherniak (1995). Cooling rates are based on the longevity of a porphyry hydrothermal system of 33,000, and 230,000 years cooling from 900 to 200°C.

Appendix 5.C

Sr Diffusion Distance

The distance of strontium diffusion is determined by the following formula:

$$x = (Dt)^{1/2}$$

where: D = diffusion coefficient at a given temperature (Do.exp (-Q/RT), Do = pre-exponential factor; Q = activation energy; R = gas constant; T = temperature (K).

Appendix 5.D

The two component mixing equation of Faure (1986, p. 142, eqn. 9.10) was used to calculate the percentage of crustal fluid in the hydrothermal fluid at Casino. This equation yields the $^{87}Sr/^{86}Sr_{t=70}$ composition of K-feldspar (potassic-stage alteration) or fluid inclusion water composition (phyllic-stage alteration).

$$\left(\frac{^{87}Sr}{^{86}Sr}\right)_M = \frac{Sr_A Sr_B\left[\left(\frac{^{87}Sr}{^{86}Sr}\right)_B - \left(\frac{^{87}Sr}{^{86}Sr}\right)_A\right]}{Sr_M\left(Sr_A - Sr_B\right)} + \frac{Sr_A\left(\frac{^{87}Sr}{^{86}Sr}\right)_A - Sr_B\left(\frac{^{87}Sr}{^{86}Sr}\right)_B}{Sr_A - Sr_B}$$

Where: $^{87}Sr/^{86}Sr$ is the isotopic composition of the mixed component – the hydrothermal fluid (M), country rocks (A), and host pluton (B); SrM, A, and B is the concentration of Sr in the mixed component, country rocks and the host pluton, respectively.

For this study the $^{87}Sr/^{86}Sr$ composition of country rocks is an average of compositions calculated at 70 Ma (A = 0.7097, cf. Selby et al., 1999), and host pluton is the isotopic composition of the Casino pluton (B = 0.70541). In crystalline terrains crustal fluids derive approximately 1.11 % of their Sr from the country rock (Blum et al., 1994). This yields a Sr content for the crustal fluid (SrA) ~ 4.1 ppm based on average Sr content of the country rocks (370 ppm), cf. Selby et al., 1999). Magmatic hypersaline brines have been shown to contain ~ 30 ppm Sr (Heinrich et al., 1992). This value is used as an approximation for the Sr content of the magmatic hydrothermal fluid (SrB).

The equation is solved interatively with respect to Sr contents of the component mixture – the hydrothermal fluid (SrM). The SrM value for each K-feldspar/fluid inclusion water isotopic composition is converted to yield a percentage of crustal fluid present in the hydrothermal fluid by dividing through by the Sr content of the Casino pluton.

Table 5.1. δD compositions of quartz phenocrysts and veins from potassic and phyllic alteration assemblages of the Casino, Cash and Mt. Nansen porphyry occurrences.

Sample #	Mineral Type	δD (per mil) SMOW
Casino		
	Potassic	
DS106	QTZ	-140
DS128	QTZ	-159
DS140	QTZ	-174
DS147	QTZ	-181
DS162	QTZ	-148
	Phyllic	
DS30	QTZ	-127
DS32	QTZ	-144
DS56	QTZ	-121
DS80	QTZ	-118
DS102	QTZ	-117
DS118	QTZ	-123
DS132	QTZ	-130
DS146	QTZ	-132
Cash		
	Potassic	
DS97-9	QTZ	-160
DS97-28	QTZ	-148
DS97-37	QTZ	-167
	Phyllic	
DS97-7	QTZ	-182
DS97-12	QTZ	-178
DS97-32	QTZ	-161
DS97-33	QTZ	-164
Mt.Nansen		
	Phenocrysts	
DS97-82	QTZ	-113
DS97-86	QTZ	-91
	Potassic	
DS97-87	QTZ	-164
DS97-88	QTZ	-177
DS97-96	QTZ	-121
DS97-97	QTZ	-152
	Phyllic	
DS97-93	QTZ	-145

Table 5.2. Rb and Sr concentrations and isotope compositions of the late Cretaceous plutons, apatite, K-feldspar, and quartz from the Casino, Cash, and Mt. Nansen porphyry occurrences.

Sample #	Rock/ Mineral Type	Rb (ppm)	Sr (ppm)	$^{87}Rb/^{86}Sr$	$^{87}Sr/^{86}Sr$ t=70	$^{87}Sr/^{86}Sr$ t=0
Casino						
Least-altered						
DS64	CP	102.37	767.92	0.378	0.70551	0.70588
DS64	AP	3.44	315.87	0.031	0.70547	0.70550
DS113	CP	66.40	956.47	0.197	0.70541	0.70561
Potassic						
DS65	KSP	156.50	332.06	1.337	0.70566	0.70699
DS65A	KSP	146.49	325.83	1.276	0.70561	0.70688
DS65A	KSP(L)	6.77	3.84	1.606	0.70551	0.70711
DS73	KSP	240.43	206.70	3.301	0.70613	0.70941
DS81	KSP	211.17	478.13	1.253	0.70572	0.70696
DS106	KSP	247.41	381.57	1.840	0.70700	0.70883
DS106	KSP(L)	80.78	90.46	2.534	0.70653	0.70905
DS106	KSP(U)	274.89	315.75	2.470	0.70659	0.70905
DS106	QTZ(B)	11.23	87.87	0.363	0.70719	0.70755
DS106	QTZ(R)	7.65	11.27	1.926	0.70686	0.70877
DS106	QTZ(L)	0.41	2.97	0.389	0.70684	0.70723
DS140	KSP	285.15	597.44	1.354	0.70764	0.70899
DS140	KSP(L)	25.65	61.78	1.178	0.70789	0.70906
DS140	QTZ(B)	110.95	229.02	1.375	0.70775	0.70892
DS140	QTZ(R)	34.54	74.00	1.325	0.70746	0.70878
DS140	QTZ(L)	0.30	2.06	0.412	0.70739	0.70780
DS147	KSP	110.34	98.73	3.171	0.70582	0.70897
DS147	KSP(L)	0.83	2.41	0.979	0.70752	0.70850
DS147	QTZ(B)	2.87	53.13	0.154	0.70679	0.70695
DS147	QTZ(R)	1.61	8.41	0.544	0.70696	0.70750
DS147	QTZ(L)	0.46	2.37	0.554	0.70684	0.70739
DS162	KSP	318.98	261.03	3.468	0.70852	0.71197
DS162	KSP(L)	230.04	178.29	3.661	0.70834	0.71198
DS162	KSP(U)	317.55	247.18	3.646	0.70843	0.71206
DS162	QTZ(B)	10.88	14.45	2.138	0.70841	0.71053
Phyllic						
DS30	QTZ(L)	0.23	0.40	1.644	0.70658	0.70821
DS32	QTZ(L)	0.21	0.12	4.834	0.70724	0.71205
DS132	QTZ(L)	0.22	0.41	1.487	0.70722	0.70870
Cash						
DS97-7	CP	89.00	494.11	0.511	0.70553	0.70604
DS97-12	CP	104.16	488.28	0.605	0.70552	0.70613
DS97-12	AP	2.971	397.49	0.021	0.70610	0.70613
DS97-38	KSP	167.14	318.26	1.490	0.70581	0.70729

Table 5.2 continued

Sample #	Rock/ Mineral Type	Rb (ppm)	Sr (ppm)	$^{87}Rb/^{86}Sr$	$^{87}Sr/^{86}Sr$ t=70	$^{87}Sr/^{86}Sr$ t=0
Mt. Nansen						
DS97-86	MNP	119.93	716.90	0.475	0.70487	0.70534
DS97-86	AP	0.92	252.76	0.010	0.70533	0.70534
DS97-87	KSP	165.95	183.82	2.515	0.70702	0.70952
DS97-89	KSP	405.52	264.08	4.357	0.70631	0.71065
DS97-90	KSP	308.69	351.05	2.495	0.70666	0.70914
DS97-97	KSP	260.10	314.11	2.350	0.70648	0.70882

Abbreviations: CP = Casino porphyry; CP = Cash porphyry; MNP = Mt. Nansen Porphyry, Ap = Apatite, KSP = K-feldspar where L = leached, U = U-cell cleaning, QTZ = Quartz with B = bulk sample, L = leachate, R = residue.

Table 5.3. Pb isotopic compositions of the Casino pluton, K-feldspar, pyrite, chalcopyrite, and bornite of the potassic and phyllic alteration assemblages of the Casino occurrence.

Sample	Rock/ Mineral Type	U (ppm)[1]	Th (ppm)[1]	Pb (ppm)[1]	$^{206}Pb/^{204}Pb$ t = 0	$^{207}Pb/^{204}Pb$ t = 0	$^{208}Pb/^{204}Pb$ t = 0
CP							
DS64	CP	2.72	6.7	9	19.550	15.639	39.003
DS113	CP	4.38	7.12	9.78	19.595	15.639	39.011
Potassic							
DS65	KSP				19.273	15.614	38.822
DS65A	KSP				19.254	15.605	38.769
DS65AL4	KSP				19.259	15.576	38.697
DS73	KSP				19.217	15.615	38.782
DS81	KSP				19.239	15.617	38.806
DS106	KSP				19.269	15.647	38.919
DS162	KSP				19.276	15.641	38.870
DS162	CPY				19.228	15.610	38.831
Phyllic							
DS16	PY				19.384	15.625	38.801
DS43	PY				19.188	15.589	38.734
DS82	PY				19.467	15.649	39.173
DS102	PY				19.241	15.641	38.879
DS134	BN				19.538	15.637	39.129

Table 5.3 continued.

Sample	Rock/ Mineral Type	$^{206}Pb/^{204}Pb$ t = 70	$^{207}Pb/^{204}Pb$ t = 70	$^{208}Pb/^{204}Pb$ t = 70
CP				
DS64	CP	19.336	15.638	38.829
DS113	CP	19.277	15.638	38.829
Potassic				
DS65	KSP	19.273	15.614	38.822
DS65A	KSP	19.254	15.605	38.769
DS65AL4	KSP	19.259	15.576	38.697
DS73	KSP	19.217	15.615	38.782
DS81	KSP	19.239	15.617	38.806
DS106	KSP	19.269	15.647	38.919
DS162	KSP	19.276	15.641	38.870
DS162	CPY	19.228	15.610	38.831
Phyllic				
DS16	PY	19.384	15.625	38.801
DS43	PY	19.188	15.589	38.734
DS82	PY	19.467	15.649	39.173
DS102	PY	19.241	15.641	38.879
DS134	BN	19.538	15.637	39.129

Abbreviations: CP = Casino porphyry; KSP = K-feldspar; PY = pyrite; CPY = chalcopyrite. [1]Data from Selby et al., 1999.

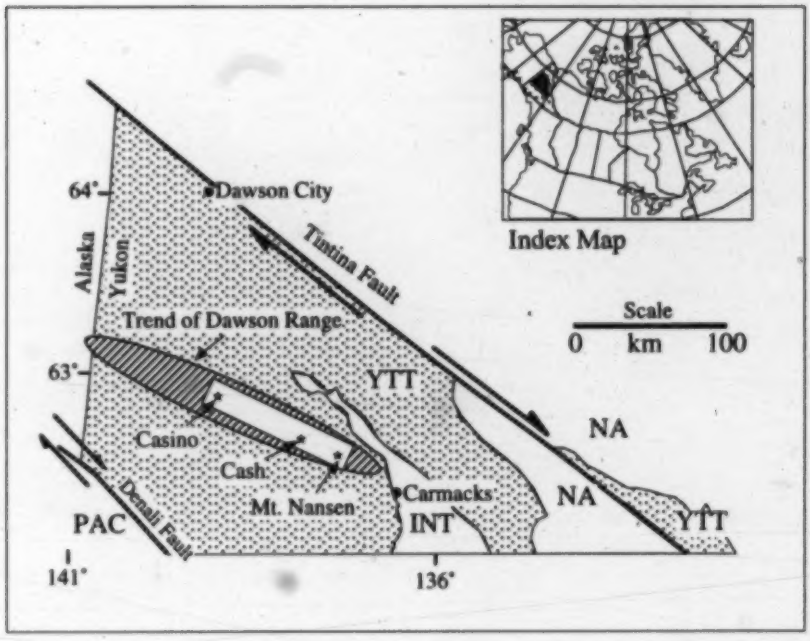

Fig. 5.1. Location of the Casino, Cash, and Mt. Nansen, porphyry Cu-Au-Mo occurrences of west-central, Yukon, Canada. Terrane map of the Yukon is modified after Wheeler and Mcfreely 1991. The abbreviations: NA, North America; YTT, Yukon-Tanana terrane; INT, Intermontane Belt; PAC, Phanerozoic accreted terranes.

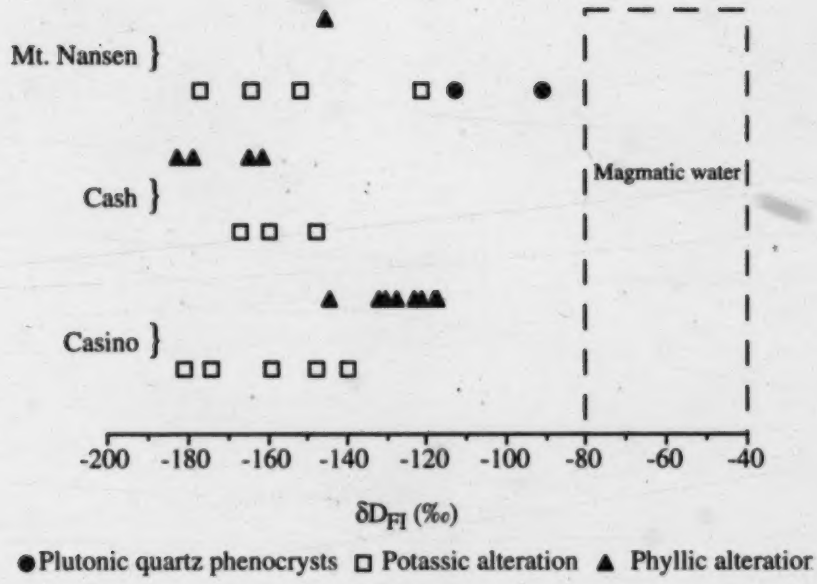

Fig. 5.2. δD_{FI} values for fluid inclusion fluids for the Casino, Cash, and Mt. Nansen Cu-Au-Mo occurrences. The magmatic water composition is from Taylor (1979).

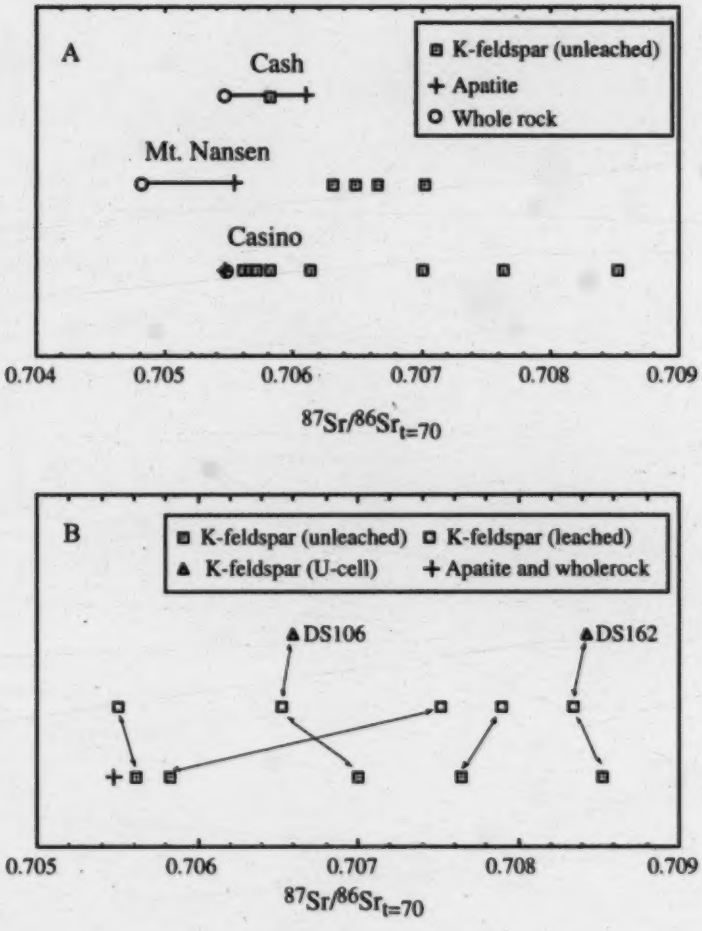

Fig. 5.3. A: Plot of the $^{87}Sr/^{86}Sr_{t=70}$ compositions of whole rock samples of the late Cretaceous plutons, magmatic apatite, and unleached hydrothermal K-feldspar of the Casino, Cash, and Mt. Nansen Cu-Au-Mo occurrences. K-feldspar samples possess $^{87}Sr/^{86}Sr_{t=70}$ similar to and of more radiogenic composition relative to the magmatic $^{87}Sr/^{86}Sr_{t=70}$ values. B: Plot of the $^{87}Sr/^{86}Sr_{t=70}$ values of unleached, leached, and U-cell cleaned K-feldspars and magmatic compositions for the Casino occurrence. Leached K-feldspar samples still show $^{87}Sr/^{86}Sr_{t=70}$ compositions greater than those determined for the magmatic values.

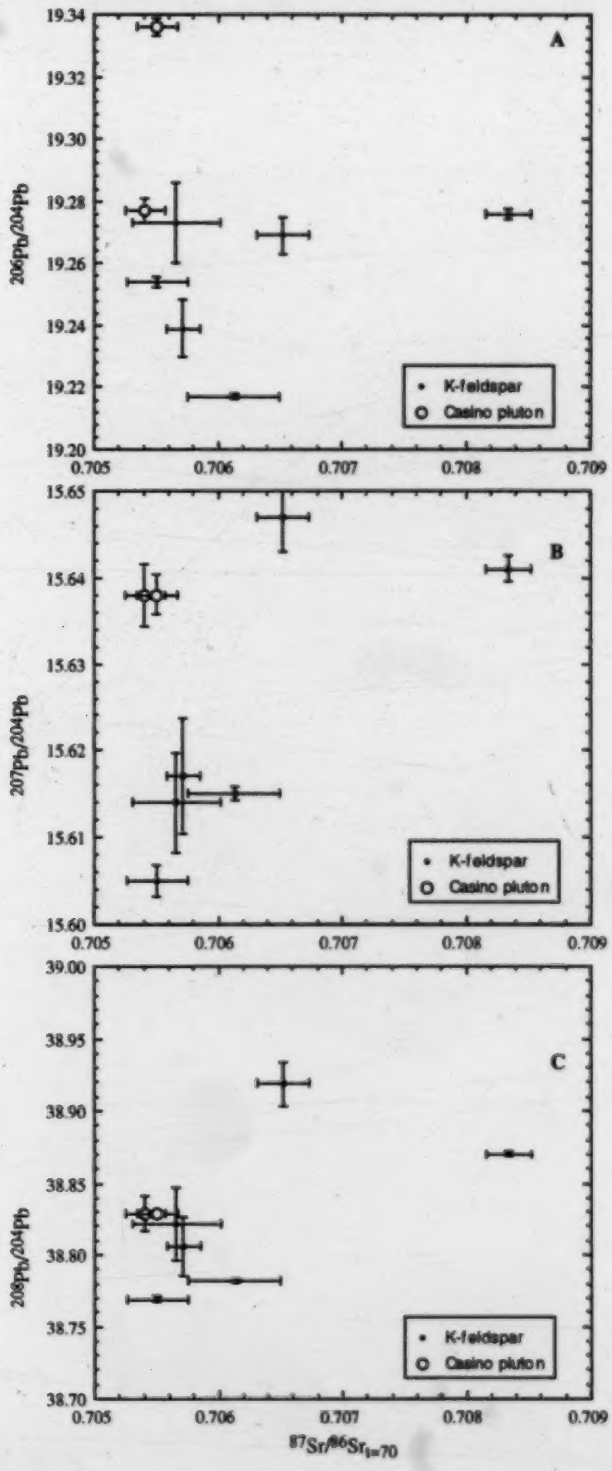

Figure caption overleaf.

Fig. 5.4. Plot of Pb isotopic ratios versus $^{87}Sr/^{86}Sr_{t=70}$ compositions of leached K-feldspar samples of the Casino occurrence. The more radiogenic compositions shown for $^{87}Sr/^{86}Sr_{t=70}$ is mirrored for identical samples for common Pb. Errors are shown at 2σ.

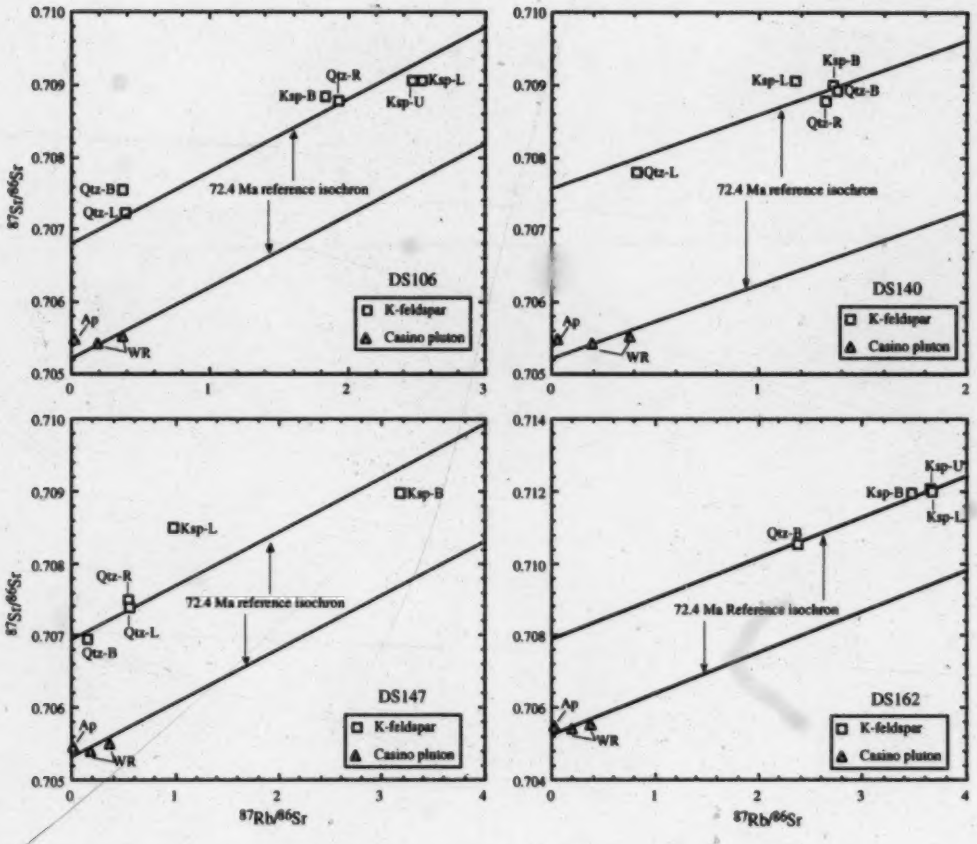

Fig. 5.5. $^{87}Rb/^{86}Sr$ vs. $^{87}Sr/^{86}Sr$ plot for fluid inclusion waters in vein quartz and K-feldspar samples. Also plotted are the whole rock and apatite isotopic data and a 72.4 Ma reference isochron. See text for discussion. Abbreviations: Ksp = K-feldspar where B = bulk, L = leached, U = U-cell cleaning; Qtz = vein quartz where B = bulk sample, L = leachate, R = residue.

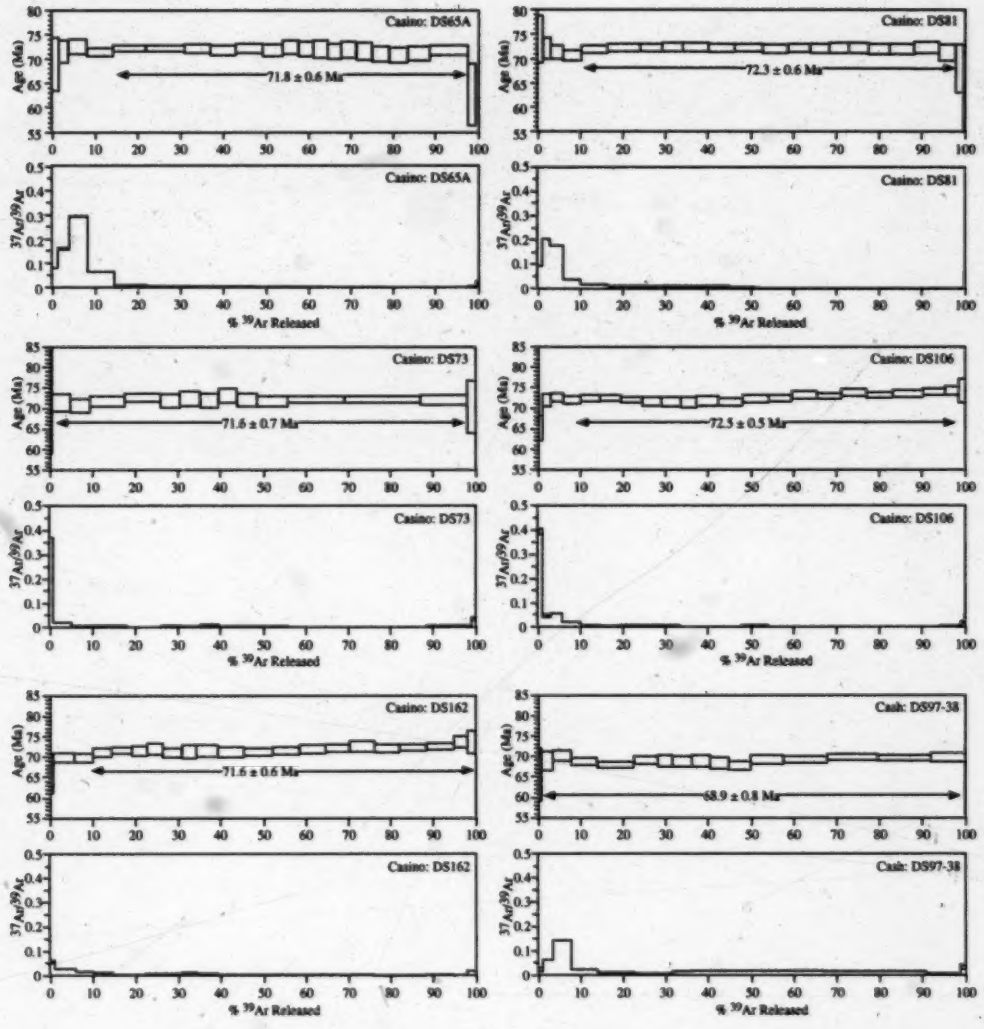

Fig. 5.6. $^{40}Ar/^{39}Ar$ age spectrum and $^{37}Ar/^{39}Ar$ plots of the hydrothermal K-feldspar samples from the Casino (DS65A, 73, 81, 106 and 162, this page), Cash (DS97-38, this page) and Mt. Nansen (DS97-87, 89 and 90 overleaf) occurrences. See text for discussion.

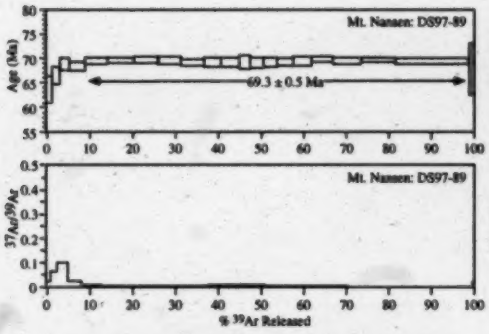
Mt. Nansen: DS97-89
Age (Ma)
69.3 ± 0.5 Ma
Mt. Nansen: DS97-89
37Ar/39Ar
% 39Ar Released

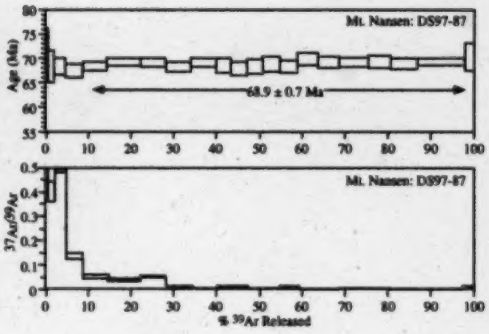
Mt. Nansen: DS97-87
Age (Ma)
68.9 ± 0.7 Ma
Mt. Nansen: DS97-87
37Ar/39Ar
% 39Ar Released

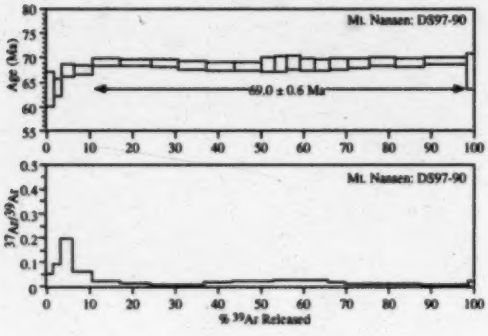
Mt. Nansen: DS97-90
Age (Ma)
69.0 ± 0.6 Ma
Mt. Nansen: DS97-90
37Ar/39Ar
% 39Ar Released

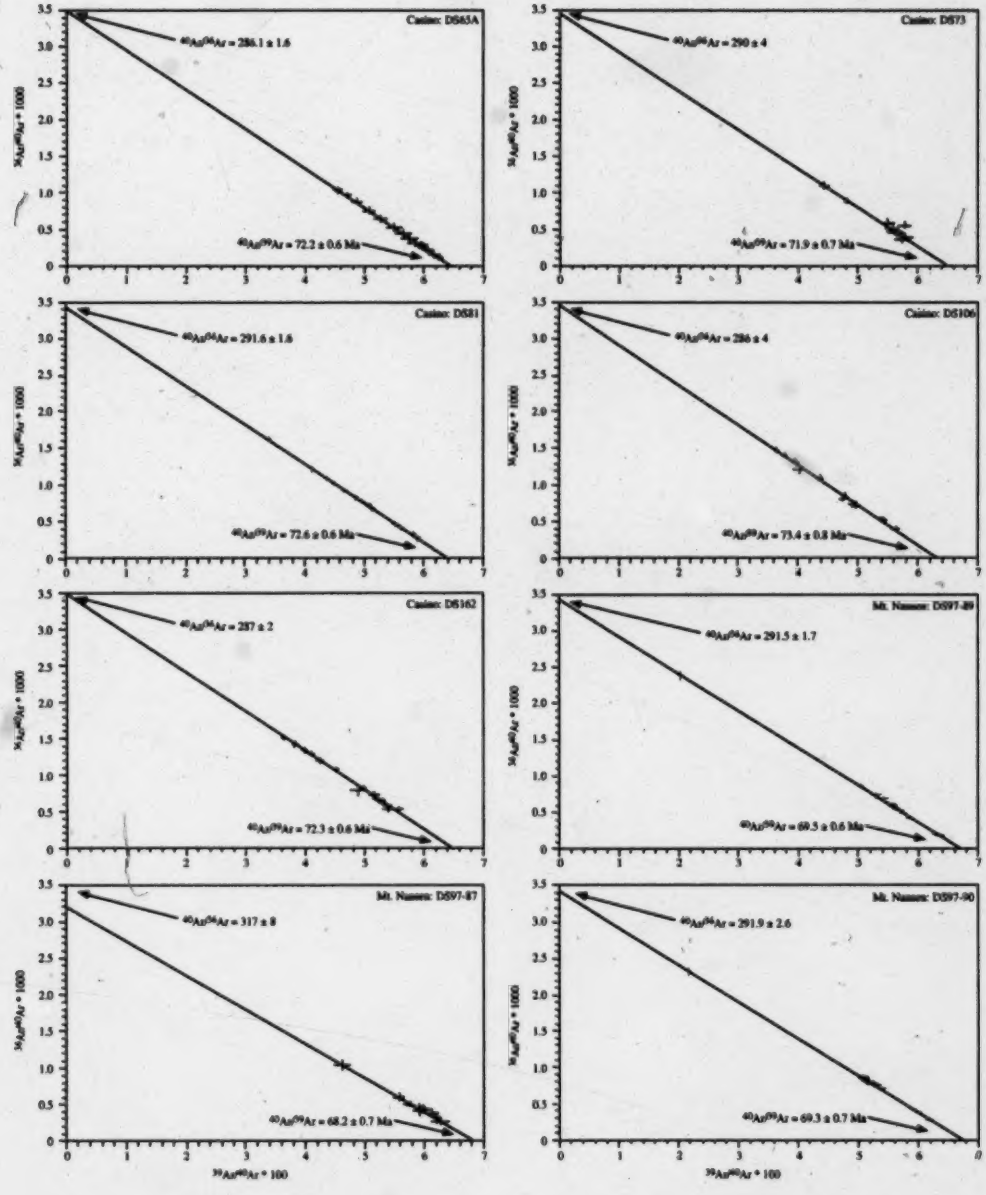

Fig. 5.7. $^{39}Ar/^{40}Ar$ versus $^{36}Ar/^{40}Ar$ isotope correlation plots of the hydrothermal K-feldspar samples from the Casino (DS65A, 73, 81, 106, and 162, this page), Mt. Nansen (DS97-87, 89, and 90, this page) and Cash (DS97-38, overleaf). See text for discussion.

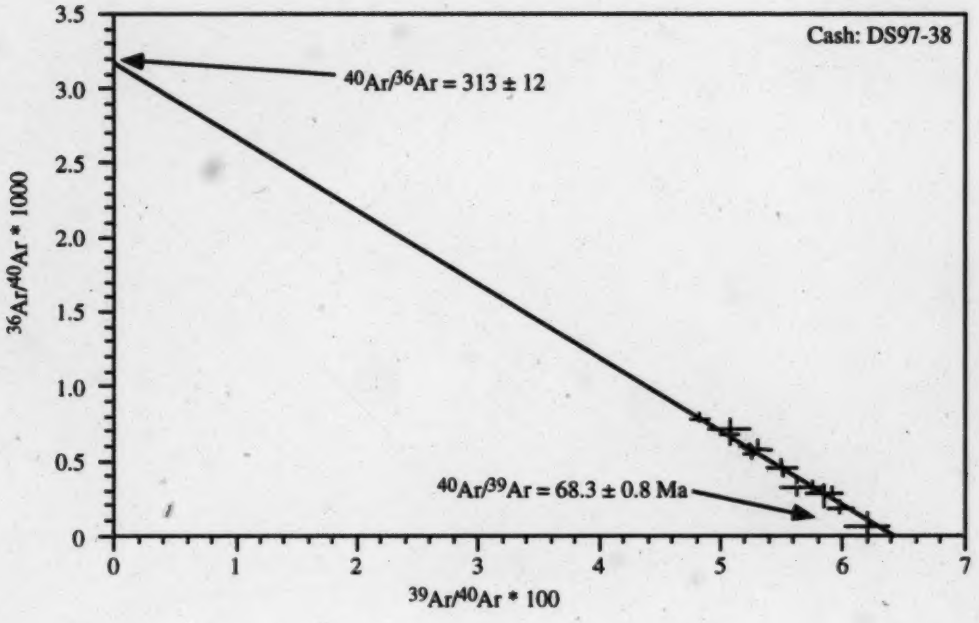
Cash: DS97-38
$^{40}Ar/^{36}Ar = 313 \pm 12$
$^{40}Ar/^{39}Ar = 68.3 \pm 0.8$ Ma
$^{36}Ar/^{40}Ar * 1000$
$^{39}Ar/^{40}Ar * 100$
3.5
3.0
2.5
2.0
1.5
1.0
0.5
0
0
1
2
3
4
5
6
7

Chapter VI

Summary

In this dissertation, major-, trace- and rare-earth-element, stable and radiogenic isotope data, biotite chemistry and fluid inclusion characteristics of igneous and metamorphic rocks, and minerals have provided new information on the origin of hydrothermal fluids associated with porphyry Cu and Mo systems of British Columbia and Yukon. These techniques were also used to evaluate the provenance of crystalline rocks of the Dawson Range of west-central Yukon. The data were examined in detail to contribute toward a more comprehensive understanding of porphyry Cu and Mo systems, specifically the origin of the hydothermal fluids.

In Chapter 2, I discuss the evolution of the hydrothermal fluids of the Endako porphyry Mo deposit, central British Columbia. The Endako deposit comprises K-feldspar, sericite, and kaolinite alteration assemblages. Molybdenum mineralization is associated with both stockwork and structurally controlled ribbon-textured veins. Quartz-biotite and quartz-K-feldspar pairs representing oxygen isotope equilibrium yield temperatures in good agreement with estimated primary fluid inclusion trapping temperatures (~440°C). However, oxygen isotope results of quartz-biotite and quartz-K-feldspar pairs from K-feldspar alteration assemblages also show that these phases represent non-equilibrium conditions. The hydrogen and oxygen isotope compositions of fluid inclusion waters from quartz veins range from –105 to –173 ‰ and 3.3 to 5.4‰, respectively, which depart from values reported for other porphyry molybdenum deposits. The fluid inclusion characteristics (salinity, homogenization temperature) are similar to most other porphyry molybdenum deposits. However, at Endako vapor-rich fluid inclusions are absent, suggesting that saline fluids were not generated through

immiscibility of hydrothermal fluids at any time during evolution of the hydrothermal system. Solute chemistry studies of fluid inclusion waters indicate that ore-forming fluids from Endako have low Br/Cl, Br/Na and High I/Cl, I/Br ratios in comparison to Porgera (epithermal), Babine lake (porphyry Cu) and St. Austell, Capitan Pluton (vein) deposits associated with magmatic processes. Results from fluid inclusion and solute chemistry studies indicate that hydrothermal fluids, exsolved from a crystallizing melt, were involved in the formation of the Endako molybdenum deposit. However, oxygen and hydrogen isotope compositions deviate from the generally accepted magmatic compositions, which suggest the early involvement of meteoric water in the ore-forming fluids.

In Chapter 3, I discuss the Devono-Mississippian Wolverine Creek Metamorphic Suite; mid-Cretaceous Dawson Range batholith; mid-Cretaceous Casino Plutonic Suite; and late Cretaceous plutons. The major significance of this chapter with respect to main theme of this dissertation was establishing the origin of the magmas generating plutons associated with porphyry Cu mineralization and hydrothermal alteration. The objective of the latter was to determine if anomalous hydrogen isotope compositions for fluids associated with potassic-stage alteration are a product of meteoric water or crustal assimilation of material depleted in deuterium. Geochemical and isotopic data established that the magmas were derived from a mantle source related to active subduction with minor crustal inheritance. Therefore, the light hydrogen isotope compositions for fluids responsible for potassic alteration were not a product of crustal assimilation of material depleted in deuterium. The latter is discussed further in Chapter 5.

Further in Chapter 3, I discuss the isotopic and other geochemical data for the Wolverine Creek Metamorphic Suite metasedimentary rocks, which indicate that the

detrital components were derived from two distinct source rocks: (1) the North America craton, which contributed evolved felsic, upper crustal material and (2) a calc-alkaline arc, which shed juvenile mafic-intermediate material. The geochemical affinity of the metaigneous rocks indicate that the Yukon-Tanana terrane represented a continental arc during Devonian-Mississippian times, with magmas derived from geochemically primitive sources and partial melting of the Yukon-Tanana terrane supracrustal rocks. The Dawson Range batholith likely represents crustally-derived magmas from the Yukon-Tanana terrane during the mid-Cretaceous, with the contemporaneous Casino Plutonic Suite representing a late-stage fractionate of these magmas.

In Chapter 4, the chemical compositions of biotites determined from the Dawson Range batholith and the alteration zones of the Casino Cu-Au-Mo occurrence, Yukon Territory, Canada show chemical trends from least-altered to propylitic to phyllic to potassic alteration. Biotites from the propylitic, phyllic and potassic alteration zones of the Casino occurrence possess higher X_{Mg}, Al_2O_3, SiO_2, F, Cl, lower MnO, and typically lower TiO_2, and BaO contents than biotites outside of these alteration zones. These trends are similar to those observed from other porphyry Cu deposits; however, the concentration of the oxides and halogens components vary between deposits. Hydrothermal fluids associated with potassic and phyllic alteration possessed similar log $(fH_2O)/(fHCl)$, $(fH_2O)/(fHF)$ and $(fHCl)/(fHF)$ ratios, with phyllic fluids having higher log $(fH_2O)/(fHCl)$ and $(fH_2O)/(fHF)$ values. Fluids associated with propylitic alteration had distinct log $(fHF)/(fHCl)$ and $(fH_2O)/(fHF)$ values. The $fH_2O/fHCl$ and $fHCl/fHF$ ratios established for Casino are similar to values from other porphyry deposits; however, fH_2O/fHF values are shown to be highly variable between porphyry deposits. The differences in log $(fH_2O)/(fHF)$ values between deposits may reflect the magmatic processes (assimilation/fractional crystallization) associated with the evolution of the

melt, which may directly affect the composition of exsolved magmatic fluids associated with porphyry mineralization

Chapter 5 presents a discussion on the isotopic compositions of the hydrothermal fluids of late Cretaceous porphyry Cu-Au-Mo systems of the Dawson Range, west-central Yukon. The isotopic (H, Sr, Pb, Ar) and fluid inclusion data for hydrothermal fluids associated with potassic alteration of the late Cretaceous porphyry occurrences, west central Yukon, provide new a insight for the origins of the hydrothermal fluids in these systems. Potassic quartz veins contain a dominant assemblage of saline (35 to 55 wt. % NaCl eq.) and vapor-rich fluid inclusions, which possess δD values between –120 and –180 ‰. Phyllic quartz veins are dominated by vapor-rich fluid inclusions with δD values similar to or higher than those associated with potassic fluids (–117 to –132 ‰). These δD values deviate significantly from values of plutonic quartz phenocrysts (–91 to –113 ‰), and values typically reported for primary fluids of porphyry-style mineralization (–40 to –100 ‰). However, the low δD values observed are similar to those established for the Babine Lake porphyry deposits. In Chapter 3 it was shown that the magmas generating the plutons associated with porphyry mineralization and alteration had a minor crustal component. Therefore, this process did not lead to the generation of the low δD values for fluids associated with potassic alteration.

The $^{87}Sr/^{86}Sr_{t=70}$ values of the late Cretaceous plutons are 0.7055 (Casino), 0.7048 (Mt. Nansen), and 0.7055 (Cash). Hydrothermal K-feldspar $^{87}Sr/^{86}Sr_{t=70}$ compositions range from values similar to those of the late Cretaceous plutons, to increasingly radiogenic values (Casino: 0.70551 to 0.70834, n = 8; Mt. Nansen: 0.7063 to 0.7070, n = 4; Cash: 0.7058, n = 1). The inclusion fluids of potassic quartz veins possess $^{87}Sr/^{86}Sr_{t=70}$ values that are virtually identical to coexisting K-feldspar Sr isotopic compositions. The Pb isotopic compositions of hydrothermal K-feldspar samples show an increasingly

radiogenic trend broadly correlated with increasing $^{87}Sr/^{86}Sr$. Fluid inclusion waters of phyllic quartz veins possess $^{87}Sr/^{86}Sr_{t=70}$ more radiogenic than the late Cretaceous plutons, but intermediate compositions relative potassic alteration quartz veins. Pyrite and bornite Pb isotopic compositions are similar to, or more radiogenic than, K-feldspar Pb isotopic values.

Hydrothermal K-feldspar samples yield $^{40}Ar/^{39}Ar$ ages (Casino = 71.8 ± 0.6 and 72.3 ± 0.6 Ma; Mt. Nansen = 69.3 ± 0.5 and 69.0 ± 0.6 Ma; Cash = 68.3 ± 0.8 Ma) similar to those obtained for late Cretaceous plutons. The $^{40}Ar/^{36}Ar$ values (285 to 292) of the K-feldspar samples are similar to the atmospheric compositions (295 ± 5) during the late Cretaceous time.

The evaluation of the isotopic data suggests that inheritance of pre-existing isotope compositions from the host rocks, post-potassic alteration isotope exchange, or the replenishment of the magma chamber with magma of different isotopic composition cannot explain the isotope data. However, H, Sr, Pb, and Ar isotopic results are compatible with the presence of a low δD, radiogenic Sr and Pb, and atmospheric Ar component in the potassic ore-fluids, and thus, these data suggest that the potassic ore-fluids are not purely magmatic. On the basis of H, Sr, Pb, and Ar isotope compositions observed here, I propose that crustal fluids must be a component in the potassic hydrothermal fluids in porphyry mineralization of the Yukon.

The research presented in this dissertation has increased the knowledge of the geochemical characteristics and origin(s) of hydrothermal fluids associated with porphyry copper and molybdenum mineralization. Specifically, I have shown that low δD values of fluids responsible for potassic alteration are not restricted to the Babine Lake deposits, but are more common to porphyry deposits of the Canadian Cordillera. A possible mechanism for generating these low δD values was assimilation of crustal material

depleted in deuterium. I have demonstrated that crustal assimilation was not a major factor in generating the magma associated with the plutons related to porphyry alteration and mineralization, and moreover was not the process producing the low δD values. Further, radiogenic isotopes established that hydrothermal fluids associated with potassic alteration possess a more radiogenic composition than that of the host pluton, and indicate a significant crustal contribution via crustal fluids to the porphyry system.

The isotopic signatures of hydrothermal fluids shown in this dissertation may have not been previously recognized in many areas worldwide, because: (1) at the time of porphyry mineralization the meteoric water signature may have not been significantly different to magmatic values, (2) in juvenile arc environments where porphyry deposits may occur a crustal contribution to the hydrothermal fluids is less likely to be observed as the neigboring country rocks would have similar radiogenic compositions to the plutons associated with the porphyry system, and (3) previous studies have not investigated fluids responsible for potassic alteration in such detail. Nonetheless, I have shown that in porphyry systems in the Canadian Cordillera potassic-stage hydrothermal fluids have a crustal (non-magmatic) component. This thesis raises several crucial questions regarding porphyry Cu-Mo deposits. How common are non-magmatic fluids in potassic-stage alteration in porphyry systems worldwide? Do processes associated with porphyry systems differ globally? What is the role of non-magmatic fluids in the generation of an economic porphyry deposit? How do non-magmatic fluids interact with magmatic fluids? The contribution of this thesis has been to identify a non-magmatic component in fluids associated with potassic alteration, but one can only speculate on the implications of non-magmatic fluid involvement in porphyry systems. The presence of non-magmatic fluids may be an essential component in the formation of a porphyry deposit by increasing the amount of water, which may extend the longevity of the hydrothermal

system and/or the amount of water available for transporting metals. This maybe evident from hydrogen isotope compositions from the Babine Lake porphyry systems, where plutons bereft of mineralization are characterized typically by higher δD values than plutons bearing economic mineralization. Alternatively, it may be suggested that non-magmatic fluids reduce the economic potential of a porphyry system by dilution and cooling of the ore-bearing magmatic fluids, which may decrease the longevity of the hydrothermal system. Further detailed research on porphyry deposits and occurrences of the Canadian Cordillera, and worldwide will inevitably provide the necessary knowledge for a more comprehensive understanding of fluid origin and processes associated with porphyry systems.

Appendix I

Oxygen, carbon and hydrogen isotope data from the Endako molybdenite deposit.

Sample #	Mineral/ Rock type	Description	$\delta^{18}O$ (‰)	δD (‰)	$\delta^{13}C$ (‰)
		Pre-Mineral Dikes			
3267.A2	PG	Qtz-Ksp-bio-plag-mag-py-Mo	6.9		
3102.3	QFP	Qtz-Ksp-plag-mag	6.2		
3058.W2	QFP	Qtz-Ksp-bio-plag-mag-py-Mo	6.7		
2794.1	QFP	Qtz-Ksp-plag-mag-py-Mo	6.9		
West Denak	PG	Qtz-Ksp-bio-plag-chl-ser-mag-py-Mo	2.7		
		K-feldspar Alteration			
3267.4	EQM	Qtz-Ksp-plag-bio-mag+minor alt kao-ser-chl	7.2		
3146.1	EQM	"	7.5		
2794.1	EQM	"	7.1	-159	
2706.1	EQM	"	6.7		
2706.6	EQM	"			
2706.9	EQM	"	6.7		
RB856	EQM	"	6.5	-167	
RB857	EQM	"	6.3	-134	
3267.8	Ksp	Hydrothermal Ksp from weakly altered EQM	6.2	-146	
3146.1B	Ksp	Hydrothermal Ksp from intensely altered EQM	2.5	-162	
3102.11	Ksp	Hydrothermal Ksp from weakly altered EQM	5.5		
2794.1	Ksp	Hydrothermal Ksp from weakly altered EQM	6.5		
RB856	Ksp	Hydrothermal Ksp from weakly altered EQM	6.1		
2706.6	Ksp	Hydrothermal Ksp from moderately altered EQM	6.6		
2706.7	Ksp	Hydrothermal Ksp from intensely altered EQM	5.3		
S803.130	Ksp	Hydrothermal Ksp from moderately altered EQM	4.2		
3146.1B	Biotite	Hydrothermal biotite from weakly altered EQM	3.9		
RB856	Biotite	Hydrothermal biotite from weakly altered EQM	4.2		
2794.1	Biotite	Hydrothermal biotite from weakly altered EQM	4.5		
2706.6	Biotite	Hydrothermal biotite from moderately altered EQM	3.1		
2706.7	Biotite	Hydrothermal biotite from intensely altered EQM	4.2		
2706.7	Biotite	Hydrothermal biotite from intensely alt EQM	2.0		
S820.207.8	Biotite	Hydrothermal biotite from weakly altered EQM	3.0		
3267.8	St.wk qtz	Vein quartz-Mo with Ksp selvage	8.0	-135	
3267.A2	St.wk qtz	Vein quartz-Mo with Ksp-bio selvage	8.5	-125	
3146.1	St.wk qtz	Vein quartz-Mo with Ksp selvage	8.3	-145	
3146.1B	St.wk qtz	Vein quartz-Mo with Ksp selvage	8.8	-150	
3146.2	St.wk qtz	Vein quartz-Mo-py with Ksp-bio selvage	8.4		
3102.11	St.wk qtz	Vein quartz with Ksp selvage + minor Mo	8.2	-128	
2794.1	St.wk qtz	Vein quartz with Ksp selvage + minor Mo	8.2	-143	
RB857	St.wk qtz	Vein quartz-Mo with Ksp selvage	8.4		
S820.207.8	St.wk qtz	Vein quartz-Mo-mag with Ksp-bio selvage	8.6		
		Sericite Alteration			
3267.M	Qtz py vn	Qtz-py-mag with musc-ser selvages	8.2		
3267.S	Rib qtz	Qtz-py-mag with musc-ser selvages op by kao	8.2	-140	
3102.2	Rib qtz	Qtz-py-mag with musc-ser selvages op by kao	8.7	-130	
2706.SWB	Rib qtz	Qtz-py-mag with musc-ser selvages op by kao	8.8	-117	
2706.7	Br Rib qtz	Weakly Br qtz with kao-Cc	8.8	-105	

Appendix I continued

Sample #	Mineral/ Rock type	Description	$\delta^{18}O$ (‰)	δD (‰)	$\delta^{13}C$ (‰)
3058.WO	Br Rib qtz	Weakly Br qtz with kao-Cc	8.1	-173	
3058.1	Rib qtz	Qtz-py-mag with musc-ser selvages op by kao	9.0	-152	
3058W1	Rib qtz	Qtz-py-mag with musc-ser selvages op by kao	9.5	-170	
3058.W3	Br Rib qtz	Weakly Br qtz with kao-Cc	8.4		
West Denak	Rib qtz	Qtz-py-mag with musc-ser selvages op by kao	8.2		
S822.692	Rib qtz	Qtz-py-mag with musc-ser selvages op by kao	8.0		
S822.636	Br Rib qtz	Weakly Br qtz with kao-Cc	8.5		
RB862C	Br Rib qtz	Intensely Br qtz with kao-Cc	6.7	-164	
RB862	Rib qtz	Qtz-py-mag with musc-ser selvages op by kao	8.8	-157	
S822.190	Sericite	Qtz-py-sericite envelope	5.6		
		Kaolinite Alteration			
2706.3	EQM	Qtz-plag-Ksp-Bio+chl-ser-kao	6.6		
3058.W1	EQM	Qtz-plag-Ksp-Bio+chl-ser-kao	5.5		
3058.1A	EQM	Qtz-plag-Ksp-Bio+chl-ser-kao	5.5		
3146.1	EQM	Qtz-plag-Ksp-Bio+chl-ser-kao	5.6		
3102.11	EQM	Qtz-plag-Ksp-Bio+chl-ser-kao	5.5		
3102.11B	EQM	Qtz-plag-Ksp-Bio+chl-ser-kao	5.2		
2706.2	EQM	Qtz-plag-Ksp-Bio+chl-ser-kao	7.3		
2706.7	EQM	Qtz-plag-Ksp-Bio+chl-ser-kao	7.5		
S803.130	Clinochore	Intensely altered EQM	-2.1		
RB858	Kaolinite	Kao from alteration selvages	6.8	-156	
2706.6	Kaolinite	"	6.7		
2706.7	Kaolinite	"	6.6		
		Post Mineralization			
3267.S1	Cc vn+wr	Cc cross cut stwk vein	6.2		-2.5
3267.S2	Cc vn+wr	Cc cross cut stwk vein	10.5		-2.8
3267.ST	Cc vn+wr	Cc cross cut stwk vein	9.6		-4.9
3146.12	Calcite vn	Within fault Br dipping south Mo vn	-3.8	-105	-4.4
3146.2A	Cc vn+wr	Cc vn in rib vn	10		-3.5
3146.2B	Cc vn+wr	Cc vn in rib vn	9.6		-3.9
3102.E1	Calcite vn	Cc vn in south basalt fault	3.9	-192	-2.0
3102.4	Calcite vn	Cc vn in EQM	2.6		-2.2
3058.1B	Cc vn+wr	Cc in Br rib vn	5.5		-4.1
2794.1	Cc vn+wr	Cc vn in EQM	4.7		-3.9
2794.PB	Calcite vn	Cc ass with porp post-mineral dyke	4.3		-3.0
2706.B1	Calcite vn	Cc ass with andesitic dyke	4.6		-3.9
2706.B2	Calcite vn	Cc amygdules in post-mineral dike	7.9		-4.9
2706.7	Calcite vn	Cc vn in Br rib vn	12.7		-4.4
2707.8A	Calcite vn	Cc vn ass with post-mineral dike	9.9		-5.4
2706.8B	Calcite vn	Cc vn ass with post-mineral dike	4.6	-147	-4.6
S803.92	Calcite vn	Cc vn in EQM	3.2		-6.2
S822.450	Calcite vn	Cc vn ass with post-mineral dike	4.5		-4.5
S822.692	Cc vn+wr	Cc vn croos cut stwk vein	8.9		-4.2
S822.655	Calcite vn	Cc vn in EQM	8.6		-3.7
RB862C	Cc vn+wr	Cc veins in brecciated rib vn	11.1		-3.5
RB862	Cc vn+wr	Cc veins in brecciated rib vn	11.1		-4.8
EQM 1	Calcite vn	Cc vn with basalt dike SW of mine (679)(864)	4.5	-105	-7.8

Appendix I continued

Sample #	Mineral/ Rock type	Description	$\delta^{18}O$ (‰)	δD (‰)	$\delta^{13}C$ (‰)
EQM 3	Calcite vn	Cc vn with EQM east of mine (676)(907)	1.8	-112	-5.2
3102.11	Chalcedony	Post-mineral veins	7.3		
2706.9	Chalcedony	Post-mineral veins	8.7		
3102.WB	Basalt	Hydrothermally alt-plag-ser-Cc-bio	-2.4		
3102.PB	Porp Basalt	Plag, ol-alt fine gr matrix	1.4		
3058.E	Basalt	Plag-Cc-alt fine gr matrix Cc amyldales	1.8		
3058.W	Basalt	"	1.1		
2706.SW	Basalt	"	4.5		
2706.B	Basalt	"	1.6		
3102.WB	Biotite	Magmatic biotite	3.6		
3102.3	Mont+ill	Clay mixture from south basalt fault	5.7		
3058E	Mix clays	"	2.1		
3102.11	Br wr	Plag-Ksp-Qtz-chl-kao-ser-Cc-py-Mo	6.9		
3058.1	Br wr	"	7.9		
3058.1B	Br wr	"	8.2		

First part of sample number before period denotes the bench number. RB denotes samples collected by Bruce E. Nesbitt. Sample numbers beginning with S denote samples taken from diamond drill core.
Abbrevations: St.work = stockwork veins, Wr = whole-rock, Qtz = quartz, K-fsp = K-feldspar, QFP = Quartz feldspar porphyry, PG = Porphyryitic granite, EQM = Endako quartz monzonite, Cc = Calcite, Br = Brecciated, Mo = molybdenite, Py = pyite, Mag = magnetite, Porp = porphyritic, Mont = Montmorillonite, Ol = Olivine, Plag = plagioclase, Chl = chlorite, Bio = Biotite, Ser= Sericite, Ka = Kaolinite, Alt = altered, Vn = vein
Oxygen and hydrogen isotope data are reported relative to SMOW and carbon isotope data relative to PDB.
Grid references from Map sheet 93K/3

Appendix II

Oxygen isotope data from the neighboring country rocks of the Casino occurrence.

Sample#	Rock Type	$\delta^{18}O$ (per mil, SMOW)
Casino Plutonic Suite		
DS185	Fine grained quartz monzonite	8.3
DS210	Fine grained quartz monzonite	8.0
DS221	Medium grained quartz monzonite	8.3
Dawson Range Batholith		
DS209	Hornblende>biotite quartz diorite	7.2
Wolervine Creek Metamorphic Suite		
Metasedimentary		
DS192	Graphitic-micaeous quartzite	13.1
DS232	Micaeous quartzite	18.4
Meta-igneous		
DS193	Qtz-bio-plag-mirocline-gneiss	9.5
DS194	K-feldspar-qtz-bio gneiss	10.3

Appendix III

Chemical composition of biotites from the Casino porphyry Cu-Au-Mo occurrence

Sample #	Rock/Type	SiO_2	TiO_2	Al_2O_3	FeO	MnO	MgO	BaO	CaO	Na_2O	K_2O	F	Cl	Total
DS190	DRB-M LA	35.32	4.49	14.11	23.25	0.28	9.13	1.46	0.08	0.13	9.04	0.33	0.15	97.58
DS190	DRB-M LA	36.28	4.20	13.89	22.96	0.29	9.71	0.47	0.07	0.12	9.49	0.38	0.14	97.80
DS190	DRB-M LA	35.51	4.37	14.02	23.30	0.30	9.24	1.26	0.08	0.13	9.14	0.35	0.15	97.65
DS190	DRB-M LA	34.70	4.73	13.80	23.36	0.27	8.69	1.91	0.18	0.10	8.53	0.33	0.15	96.57
DS190	DRB-M LA	34.95	4.09	14.23	23.23	0.27	9.40	1.21	0.20	0.71	8.87	0.37	0.22	97.54
DS190	DRB-M LA	33.24	4.70	12.88	28.03	0.30	9.13	0.85	0.10	0.11	8.62	0.34	0.11	98.24
DS190	DRB-M LA	35.67	4.46	13.94	23.33	0.26	9.37	0.96	0.12	0.10	9.26	0.29	0.13	97.73
DS190	DRB-M LA	35.84	4.42	13.91	22.96	0.25	9.35	0.96	0.07	0.10	9.38	0.32	0.14	97.55
DS190	DRB-M LA	33.57	4.57	13.42	21.73	0.26	8.46	1.49	0.25	0.93	9.11	0.32	0.53	94.38
DS190	DRB-M LA	36.00	3.97	13.83	23.26	0.30	9.60	0.66	0.09	0.10	9.55	0.30	0.16	97.66
DS209	DRB-M LA	45.12	1.20	7.67	18.52	0.50	11.15	0.08	11.22	1.20	0.88	0.07	0.07	97.64
DS209	DRB-M LA	45.42	1.16	7.28	18.68	0.49	11.30	0.09	11.22	1.12	0.75	0.08	0.09	97.61
DS209	DRB-M LA	45.87	1.13	7.27	18.39	0.51	11.29	0.12	11.10	1.22	0.86	0.08	0.08	97.85
DS209	DRB-M LA	45.92	0.88	7.04	18.60	0.50	11.48	0.11	11.47	0.99	0.74	0.08	0.04	97.80
DS209	DRB-M LA	44.86	0.95	7.91	18.90	0.48	10.93	0.06	11.37	1.15	0.96	0.09	0.07	97.66
DS209	DRB-M LA	45.22	0.92	7.45	18.86	0.45	11.08	0.07	11.19	1.14	0.89	0.11	0.09	97.38
DS209	DRB-M LA	44.98	1.69	7.57	18.14	0.50	11.24	0.08	11.14	1.34	0.94	0.11	0.11	97.76
DS209	DRB-M LA	45.18	1.47	7.24	18.24	0.48	11.38	0.13	11.34	1.08	0.88	0.08	0.06	97.52
DS209	DRB-M LA	45.51	1.39	7.32	18.11	0.46	11.57	0.14	11.70	1.01	0.84	0.09	0.05	98.12
DS209	DRB-M LA	44.78	0.96	7.66	18.97	0.50	10.87	0.08	11.58	1.09	0.93	0.07	0.06	97.50
DS209	DRB-M LA	35.23	4.68	13.89	21.82	0.31	10.33	1.79	0.01	0.13	9.23	0.23	0.10	97.63
DS209	DRB-M LA	35.67	4.27	13.85	21.58	0.33	10.43	0.79	0.05	0.12	9.94	0.22	0.05	97.20
DS209	DRB-M LA	35.47	4.45	13.98	21.96	0.29	10.37	1.90	0.05	0.12	9.10	0.18	0.12	97.89
DS209	DRB-M LA	36.01	3.48	13.79	21.62	0.27	10.86	0.29	0.02	0.08	10.24	0.24	0.07	96.85
DS209	DRB-M LA	35.12	4.57	14.22	21.95	0.31	9.97	1.98	0.01	0.14	9.20	0.21	0.11	97.66
DS209	DRB-M LA	35.60	3.87	14.00	21.86	0.29	10.49	1.28	0.02	0.11	9.60	0.26	0.08	97.32
DS209	DRB-M LA	35.19	4.24	13.96	22.07	0.29	10.08	2.01	0.01	0.14	9.03	0.24	0.15	97.26
DS209	DRB-M LA	35.40	3.96	13.73	21.77	0.31	10.32	1.73	0.00	0.11	9.22	0.20	0.09	96.73
DS209	DRB-M LA	34.53	4.40	13.88	21.70	0.24	10.06	2.59	0.00	0.13	8.82	0.18	0.10	96.53
DS209	DRB-M LA	35.78	3.42	13.55	21.13	0.23	10.96	0.19	0.02	0.10	9.92	0.25	0.09	95.51
DS209	DRB-M LA	35.82	3.35	13.50	21.34	0.21	11.07	0.11	0.00	0.08	10.03	0.21	0.09	95.71
DS209	DRB-M LA	35.72	3.74	13.83	21.15	0.22	10.45	0.22	0.00	0.07	10.05	0.23	0.08	95.64
DS209	DRB-M LA	34.82	4.43	13.49	21.75	0.26	10.00	2.66	0.01	0.13	8.85	0.21	0.14	96.64
DS209	DRB-M LA	34.47	4.58	13.64	21.94	0.26	9.92	2.99	0.00	0.12	8.86	0.25	0.13	97.02
DS209	DRB-M LA	34.71	4.54	13.72	22.11	0.27	9.91	2.79	0.01	0.12	8.86	0.21	0.10	97.24
DS209	DRB-M LA	36.10	3.51	13.58	22.10	0.25	10.82	0.18	0.04	0.08	9.79	0.22	0.08	96.64
DS209	DRB-M LA	35.96	3.85	13.44	21.23	0.24	10.61	0.25	0.02	0.13	10.05	0.18	0.08	95.96
DS209	DRB-M LA	35.39	3.76	13.52	20.84	0.19	10.94	0.39	0.00	0.10	9.79	0.18	0.09	95.10
DS209	DRB-M LA	34.84	4.24	13.89	22.34	0.25	10.05	2.47	0.00	0.12	9.08	0.21	0.13	97.49
DS209	DRB-M LA	34.72	4.40	13.93	22.26	0.27	10.17	2.21	0.03	0.12	9.18	0.20	0.14	97.51
DS209	DRB-M LA	34.94	4.13	13.86	22.15	0.27	10.40	1.89	0.03	0.15	9.15	0.17	0.12	97.15
DS209	DRB-M LA	35.61	3.86	13.88	21.77	0.22	10.52	1.19	0.01	0.13	9.62	0.19	0.11	96.99
DS209	DRB-M LA	35.36	3.91	13.76	21.84	0.24	10.65	1.14	0.02	0.11	9.66	0.19	0.08	96.87
DS209	DRB-M LA	35.00	4.04	13.71	21.88	0.22	10.32	1.73	0.03	0.13	9.29	0.17	0.12	96.54
DS209	DRB-M LA	34.83	4.90	13.70	22.08	0.25	9.70	3.02	0.00	0.08	8.94	0.18	0.12	97.69
DS209	DRB-M LA	34.13	4.45	13.47	21.56	0.25	9.50	2.52	0.03	0.13	8.66	0.14	0.11	94.87
DS209	DRB-M LA	34.61	4.69	13.59	21.86	0.28	9.82	2.69	0.04	0.14	8.77	0.17	0.15	96.70

Sample #	Rock/Type	SiO_2	TiO_2	Al_2O_3	FeO	MnO	MgO	BaO	CaO	Na_2O	K_2O	F	Cl	Total
DS209	DRB-M LA	35.83	3.47	13.83	21.51	0.24	10.55	0.41	0.08	0.09	9.88	0.16	0.10	96.07
DS209	DRB-M LA	35.45	3.12	13.78	20.72	0.29	10.66	0.27	0.14	0.07	9.25	0.18	0.11	93.93
DS209	DRB-M LA	34.56	4.16	13.57	21.17	0.23	10.12	1.48	0.06	0.15	8.89	0.24	0.13	94.64
DS209	DRB-M LA	45.67	1.09	7.25	18.20	0.50	11.07	0.07	11.23	1.11	0.76	0.13	0.10	97.09
DS209	DRB-M LA	45.43	1.14	7.13	18.20	0.49	11.24	0.05	11.38	1.17	0.77	0.16	0.10	97.16
DS209	DRB-M LA	46.54	0.88	6.81	17.85	0.43	11.75	0.04	11.64	0.88	0.62	0.12	0.05	97.56
DS209	DRB-M LA	45.31	1.04	7.55	18.40	0.46	10.98	0.09	11.36	1.16	0.88	0.10	0.10	97.37
DS209	DRB-M LA	45.44	0.93	7.65	17.85	0.44	10.98	0.04	11.61	1.02	0.84	0.13	0.06	96.92
DS209	DRB-M LA	45.55	0.86	7.14	18.00	0.46	11.05	0.00	11.51	1.06	0.75	0.09	0.06	96.46
DS189	DRB-M LA	34.83	3.29	13.97	22.42	0.37	10.11	1.31	0.00	0.10	9.17	0.21	0.05	95.73
DS189	DRB-M LA	34.00	3.32	13.83	22.63	0.38	10.22	1.23	0.03	0.08	8.51	0.22	0.05	94.37
DS189	DRB-M LA	34.29	3.29	13.52	22.08	0.40	9.82	0.65	0.13	0.09	8.72	0.17	0.06	93.13
DS189	DRB-M LA	34.85	3.25	13.75	22.21	0.34	10.26	0.75	0.02	0.08	9.44	0.20	0.05	95.11
DS189	DRB-M LA	33.25	3.46	13.50	22.53	0.39	9.84	1.48	0.00	0.09	9.01	0.21	0.07	93.71
DS189	DRB-M LA	33.23	3.46	13.61	22.53	0.36	10.15	1.08	0.04	0.09	8.98	0.22	0.08	93.71
DS189	DRB-M LA	34.07	3.30	13.55	22.37	0.35	9.91	1.11	0.06	0.07	8.94	0.20	0.07	93.91
DS189	DRB-M LA	34.34	3.47	13.92	22.23	0.34	9.79	1.06	0.05	0.07	9.02	0.21	0.05	94.45
DS189	DRB-M LA	44.35	1.27	7.11	18.84	0.60	10.98	0.08	11.11	1.33	0.62	0.07	0.07	96.40
DS189	DRB-M LA	43.89	1.13	7.82	19.76	0.58	10.17	0.00	11.13	1.37	0.70	0.08	0.08	96.67
DS189	DRB-M LA	45.38	1.20	6.91	19.13	0.61	11.05	0.02	11.12	1.28	0.61	0.07	0.05	97.38
DS189	DRB-M LA	43.64	0.94	7.92	19.90	0.59	10.25	0.06	11.37	1.34	0.92	0.11	0.09	97.06
DS189	DRB-M LA	43.69	0.91	8.06	19.90	0.63	10.02	0.07	11.32	1.29	0.94	0.07	0.07	96.93
DS189	DRB-M LA	44.11	1.00	7.72	19.40	0.60	10.39	0.02	11.33	1.19	0.83	0.05	0.06	96.66
DS189	DRB-M LA	34.26	3.36	13.98	22.81	0.39	10.18	1.28	0.05	0.07	8.62	0.22	0.06	95.17
DS189	DRB-M LA	34.95	3.59	13.87	22.46	0.37	10.09	1.09	0.04	0.06	9.15	0.19	0.08	95.85
DS189	DRB-M LA	35.42	3.81	13.76	22.58	0.38	10.02	0.97	0.00	0.07	9.54	0.18	0.09	96.72
DS189	DRB-M LA	35.32	4.12	14.45	22.04	0.41	9.53	1.05	0.02	0.06	9.59	0.23	0.07	96.77
DS189	DRB-M LA	35.37	3.64	13.92	21.23	0.37	10.58	0.26	0.07	0.06	9.70	0.21	0.07	95.37
DS189	DRB-M LA	35.51	3.70	13.93	22.14	0.37	10.23	0.68	0.00	0.06	9.91	0.22	0.05	96.68
DS189	DRB-M LA	35.57	3.65	13.97	22.11	0.39	10.45	0.73	0.03	0.09	9.71	0.22	0.07	96.87
DS189	DRB-M LA	35.74	3.53	13.97	22.47	0.39	10.40	0.64	0.04	0.07	9.74	0.20	0.07	97.16
DS189	DRB-M LA	36.28	3.55	14.10	21.67	0.38	10.70	0.30	0.03	0.04	9.90	0.23	0.05	97.11
DS189	DRB-M LA	35.22	3.59	13.99	22.16	0.40	10.47	0.56	0.08	0.05	8.87	0.24	0.11	95.61
DS189	DRB-M LA	35.73	3.57	14.27	22.69	0.44	10.38	1.05	0.00	0.05	9.99	0.21	0.05	98.34
DS189	DRB-M LA	35.69	3.52	14.17	22.36	0.41	10.23	1.04	0.00	0.05	9.82	0.21	0.06	97.45
DS189	DRB-M LA	35.42	3.55	14.11	22.54	0.44	10.16	1.21	0.00	0.07	9.52	0.21	0.08	97.21
DS189	DRB-M LA	35.37	4.04	14.61	21.93	0.41	9.11	0.50	0.05	0.04	9.75	0.16	0.08	95.96
DS189	DRB-M LA	35.38	3.74	13.80	22.43	0.39	10.00	1.21	0.02	0.08	9.63	0.23	0.08	96.86
DS189	DRB-M LA	35.54	3.59	13.99	22.73	0.41	10.29	0.75	0.07	0.07	9.53	0.21	0.06	97.13
DS189	DRB-M LA	36.08	3.63	13.75	22.62	0.37	10.65	0.47	0.04	0.07	9.57	0.19	0.06	97.40
DS189	DRB-M LA	35.18	3.75	13.48	22.37	0.39	10.25	0.54	0.05	0.09	9.44	0.17	0.06	95.67
DS189	DRB-M LA	35.54	4.00	14.11	22.17	0.43	9.94	0.67	0.02	0.05	9.76	0.20	0.06	96.83
DS189	DRB-M LA	35.17	2.78	14.15	22.71	0.35	10.46	0.12	0.09	0.05	8.53	0.20	0.03	94.55
DS189	DRB-M LA	46.45	1.16	6.73	17.83	0.68	11.85	0.03	10.84	1.16	0.57	0.02	0.02	97.31
DS189	DRB-M LA	45.53	1.40	7.36	18.19	0.61	11.38	0.05	11.10	1.28	0.62	0.05	0.03	97.56
DS189	DRB-M LA	44.51	1.00	8.11	19.66	0.61	10.24	0.04	11.37	1.19	0.87	0.08	0.06	97.70
DS189	DRB-M LA	44.82	1.14	8.12	19.62	0.65	10.41	0.00	11.41	1.25	0.85	0.05	0.06	98.33
DS189	DRB-M LA	45.63	1.32	7.33	17.88	0.68	11.33	0.03	11.02	1.35	0.62	0.05	0.07	97.27
DS189	DRB-M LA	44.95	0.94	7.80	19.63	0.66	10.22	0.07	11.53	1.19	0.82	0.07	0.05	97.87
DS189	DRB-M LA	35.12	3.90	14.03	22.57	0.43	9.86	1.74	0.00	0.12	9.39	0.17	0.10	97.33
DS189	DRB-M LA	35.44	3.80	13.91	22.52	0.37	10.16	1.16	0.00	0.08	9.62	0.18	0.12	97.25

Sample #	Rock/Type		SiO_2	TiO_2	Al_2O_3	FeO	MnO	MgO	BaO	CaO	Na_2O	K_2O	F	Cl	Total
DS189	DRB-M	LA	35.66	3.62	13.93	22.72	0.35	10.22	1.03	0.00	0.07	9.76	0.20	0.07	97.53
DS187	DRB-M	LA	35.14	3.96	14.32	22.39	0.40	9.62	1.43	0.00	0.10	8.94	0.19	0.09	96.46
DS187	DRB-M	LA	35.93	3.13	14.07	22.50	0.47	10.12	0.15	0.04	0.06	9.35	0.15	0.28	96.12
DS187	DRB-M	LA	35.35	3.52	14.05	22.87	0.44	9.94	0.72	0.00	0.08	9.17	0.11	0.09	96.27
DS187	DRB-M	LA	35.02	3.71	13.97	22.81	0.40	9.81	1.11	0.00	0.08	9.04	0.15	0.65	96.53
DS187	DRB-M	LA	35.78	3.50	13.99	22.70	0.39	10.34	0.51	0.00	0.08	9.13	0.18	0.09	96.58
DS233	DRB-M	LA	35.61	3.66	14.53	23.39	0.64	9.53	1.12	0.00	0.06	9.67	0.33	0.38	98.68
DS233	DRB-M	LA	35.48	3.37	14.16	23.33	0.62	9.85	0.81	0.01	0.06	9.66	0.37	0.94	98.28
DS233	DRB-M	LA	35.73	3.70	14.69	22.84	0.59	9.70	0.65	0.10	0.06	9.86	0.36	0.66	98.64
DS233	DRB-M	LA	35.28	3.41	14.29	23.92	0.66	9.35	0.65	0.09	0.06	9.66	0.30	0.85	98.20
DS95	DRB-M	PR	36.97	3.96	14.10	17.10	0.14	14.23	1.12	0.00	0.14	9.19	0.35	0.31	97.39
DS95	DRB-M	PR	36.57	4.05	13.87	16.87	0.11	13.95	1.20	0.00	0.16	9.29	0.43	0.36	96.59
DS95	DRB-M	PR	36.56	3.81	14.01	17.23	0.11	14.26	1.03	0.00	0.16	9.39	0.40	0.35	97.07
DS95	DRB-M	PR	36.85	3.60	14.11	17.12	0.12	14.16	0.95	0.00	0.10	9.76	0.45	0.36	97.31
DS95	DRB-M	PR	36.88	3.30	13.99	16.82	0.11	14.38	0.56	0.00	0.12	9.38	0.47	0.35	96.08
DS95	DRB-M	PR	36.80	3.67	14.15	16.98	0.10	14.33	1.30	0.00	0.21	9.32	0.47	0.37	97.40
DS95	DRB-M	PR	36.89	3.55	14.14	17.11	0.11	14.33	1.39	0.00	0.16	9.14	0.41	0.35	97.33
DS95	DRB-M	PR	36.71	3.04	14.18	17.14	0.10	14.90	0.70	0.02	0.13	9.23	0.48	0.37	96.73
DS95	DRB-M	PR	36.84	4.03	14.06	17.18	0.10	13.77	1.16	0.00	0.15	9.24	0.32	0.34	96.97
DS95	DRB-M	PR	36.29	4.29	13.86	17.09	0.10	13.81	1.38	0.00	0.18	9.20	0.30	0.24	96.57
DS95	DRB-M	PR	36.63	4.22	13.92	17.07	0.10	13.98	1.21	0.00	0.14	9.34	0.32	0.22	96.96
DS95	DRB-M	PR	36.66	4.14	14.01	17.30	0.11	13.98	1.15	0.00	0.15	9.36	0.38	0.37	97.37
DS95	DRB-M	PR	36.77	3.62	13.91	16.67	0.09	14.00	0.51	0.00	0.13	9.59	0.46	0.34	95.82
DS104	DRB-M	PR	36.22	3.70	13.85	16.84	0.09	14.11	0.69	0.00	0.23	9.09	0.23	0.38	95.25
DS104	DRB-M	PR	36.36	3.82	13.97	16.94	0.09	14.18	0.67	0.02	0.24	9.25	0.20	0.38	95.94
DS104	DRB-M	PR	37.09	3.74	14.09	16.46	0.09	14.51	0.50	0.00	0.25	9.35	0.24	0.39	96.50
DS104	DRB-M	PR	36.50	3.84	13.70	16.75	0.09	14.21	0.59	0.00	0.23	9.26	0.19	0.40	95.59
DS104	DRB-M	PR	36.24	4.12	13.86	16.75	0.10	13.91	0.69	0.00	0.23	9.16	0.16	0.35	95.43
DS104	DRB-M	PR	36.98	3.86	13.90	17.20	0.10	14.57	0.88	0.03	0.19	9.17	0.25	0.36	97.30
DS104	DRB-M	PR	36.91	3.99	14.00	17.15	0.11	14.31	0.81	0.01	0.24	9.28	0.26	0.34	97.22
DS104	DRB-M	PR	36.69	3.91	13.91	17.01	0.10	14.28	0.98	0.04	0.24	9.14	0.24	0.39	96.73
DS104	DRB-M	PR	37.02	3.91	14.01	17.02	0.12	14.57	0.76	0.03	0.21	9.19	0.24	0.31	97.21
DS104	DRB-M	PR	37.51	3.33	13.96	16.23	0.08	15.33	0.23	0.04	0.20	9.42	0.37	0.36	96.83
DS104	DRB-M	PR	36.37	3.76	13.74	17.15	0.10	13.85	0.90	0.01	0.25	9.07	0.27	0.33	95.61
DS104	DRB-M	PR	36.30	3.95	14.02	17.19	0.09	14.14	1.14	0.03	0.25	8.92	0.26	0.35	96.45
DS104	DRB-M	PR	36.83	4.02	13.83	17.06	0.09	14.29	0.88	0.02	0.26	9.13	0.23	0.34	96.80
DS104	DRB-M	PR	36.70	3.81	13.72	16.67	0.08	14.58	0.79	0.02	0.21	9.35	0.28	0.36	96.36
DS104	DRB-M	PR	36.17	3.62	13.77	16.91	0.09	14.11	0.93	0.02	0.20	9.09	0.26	0.39	95.36
DS44	PP-M	PH	37.95	4.00	14.04	11.52	0.10	17.56	0.56	0.01	0.18	9.75	1.40	0.21	96.63
DS44	PP-M	PH	37.93	3.60	14.24	11.29	0.09	17.55	0.54	0.00	0.18	9.80	1.30	0.20	96.12
DS44	PP-M	PH	38.00	3.62	13.88	11.28	0.05	17.71	0.50	0.00	0.20	9.66	1.37	0.20	95.86
DS44	PP-M	PH	37.89	3.61	14.07	11.53	0.10	17.62	0.54	0.00	0.17	9.81	1.32	0.21	96.25
DS44	PP-M	PH	38.19	3.70	14.17	11.19	0.07	17.91	0.55	0.00	0.16	9.72	1.41	0.17	96.61
DS44	PP-M	PH	37.10	3.55	13.76	14.72	0.10	15.53	0.51	0.00	0.20	9.69	1.15	0.32	96.06
DS44	PP-M	PH	37.55	3.58	13.94	14.61	0.11	15.75	0.74	0.00	0.20	9.55	1.25	0.32	96.99
DS44	PP-M	PH	37.12	3.55	13.91	14.66	0.09	15.67	0.53	0.02	0.18	9.66	1.28	0.33	96.38
DS44	PP-M	PH	37.26	3.48	13.87	14.08	0.08	15.70	0.38	0.00	0.23	9.63	1.43	0.28	95.75
DS44	PP-M	PH	38.18	3.35	14.16	13.82	0.10	16.36	0.28	0.00	0.22	9.65	1.30	0.27	97.07
DS44	PP-M	PH	38.39	3.59	13.91	12.99	0.09	16.95	0.20	0.03	0.20	9.85	1.31	0.21	97.11
DS44	PP-M	PH	38.11	3.84	13.92	12.59	0.10	16.64	0.36	0.16	0.13	9.45	1.25	0.22	96.19
DS44	PP-M	PH	37.12	5.69	13.81	12.79	0.08	16.20	0.51	0.03	0.20	9.50	1.44	0.22	96.91

Sample #	Rock/Type		SiO_2	TiO_2	Al_2O_3	FeO	MnO	MgO	BaO	CaO	Na_2O	K_2O	F	Cl	Total
DS44	PP-M	PH	37.76	3.16	13.73	12.79	0.08	16.95	0.50	0.05	0.21	9.29	1.47	0.24	95.56
DS44	PP-M	PH	37.81	3.65	13.88	12.82	0.11	16.64	0.13	0.04	0.17	9.57	1.27	0.19	95.69
DS44	PP-M	PH	37.47	3.79	14.45	13.55	0.11	15.54	0.51	0.03	0.25	9.35	1.34	0.30	96.06
DS44	PP-M	PH	37.71	3.64	14.65	12.25	0.10	16.31	0.40	0.10	0.19	9.68	1.55	0.18	96.05
DS44	PP-M	PH	37.60	3.60	14.45	13.76	0.12	15.74	0.30	0.05	0.22	9.59	1.27	0.27	96.35
DS44	PP-M	PH	37.71	3.50	14.67	13.45	0.10	16.27	0.73	0.01	0.25	9.77	1.45	0.28	97.52
DS44	PP-M	PH	36.85	3.25	14.09	11.71	0.08	16.07	0.13	0.05	0.22	9.33	1.50	0.22	92.83
DS44	PP-M	PH	38.37	3.46	14.31	13.73	0.12	16.27	0.20	0.04	0.24	9.75	1.42	0.28	97.52
DS44	PP-M	PH	38.45	3.53	14.17	13.67	0.13	16.55	0.19	0.01	0.25	9.71	1.38	0.27	97.67
DS44	PP-M	PH	38.69	3.39	14.46	12.70	0.11	16.84	0.14	0.01	0.23	9.81	1.58	0.22	97.46
DS44	PP-M	PH	38.07	3.39	14.50	13.13	0.11	16.52	0.58	0.01	0.21	9.66	1.59	0.30	97.33
DS44	PP-M	PH	38.72	3.50	14.73	13.16	0.12	16.61	0.17	0.01	0.27	9.89	1.44	0.27	98.23
DS44	PP-M	PH	37.51	3.61	14.06	13.87	0.15	16.32	0.77	0.00	0.20	9.75	1.14	0.23	97.08
DS44	PP-M	PH	37.79	3.98	14.10	13.58	0.11	16.44	0.61	0.01	0.22	9.71	1.03	0.22	97.31
DS44	PP-M	PH	37.90	3.53	13.83	14.63	0.12	16.13	0.26	0.01	0.21	9.71	1.20	0.25	97.22
DS44	PP-M	PH	38.06	3.17	13.56	13.01	0.10	16.31	0.21	0.07	0.21	9.44	1.33	0.21	95.06
DS44	PP-M	PH	38.01	3.53	14.20	13.92	0.13	15.94	0.24	0.01	0.26	9.61	1.40	0.24	96.84
DS111	PP-M	PH	37.25	3.50	13.57	14.31	0.05	15.95	0.55	0.00	0.20	9.54	0.92	0.21	95.61
DS111	PP-M	PH	37.25	3.47	13.64	14.80	0.08	15.85	0.36	0.01	0.20	9.77	0.93	0.23	96.15
DS111	PP-M	PH	36.90	3.73	13.34	14.94	0.08	15.26	0.88	0.00	0.23	9.45	0.89	0.24	95.50
DS111	PP-M	PH	37.49	4.01	14.31	12.97	0.08	15.75	0.96	0.00	0.24	9.36	0.95	0.22	95.89
DS111	PP-M	PH	37.98	3.65	14.35	11.82	0.04	15.97	0.20	0.00	0.21	9.93	0.86	0.23	94.83
DS111	PP-M	PH	37.22	4.37	13.51	14.55	0.08	15.59	0.60	0.00	0.22	9.77	0.94	0.25	96.65
DS111	PP-M	PH	37.44	4.11	14.31	13.05	0.07	15.78	0.86	0.00	0.22	9.56	0.90	0.23	96.09
DS111	PP-M	PH	37.29	4.45	14.17	13.60	0.09	15.17	0.96	0.00	0.23	9.61	0.85	0.24	96.24
DS111	PP-M	PH	37.15	4.37	13.46	14.89	0.08	15.31	0.57	0.00	0.21	9.62	0.86	0.25	96.33
DS111	PP-M	PH	37.40	4.39	13.92	13.44	0.07	15.82	1.02	0.00	0.23	9.56	0.89	0.21	96.51
DS111	PP-M	PH	37.56	4.48	13.97	12.37	0.07	16.41	1.12	0.00	0.26	9.45	0.94	0.24	96.42
DS111	PP-M	PH	37.56	4.50	14.80	10.58	0.06	16.22	1.15	0.00	0.23	9.54	0.86	0.21	95.29
DS111	PP-M	PH	37.59	4.34	14.76	11.12	0.07	16.09	0.84	0.00	0.21	9.62	0.87	0.21	95.31
DS111	PP-M	PH	45.22	5.05	18.33	12.83	0.06	19.42	1.07	0.05	0.26	11.31	1.13	0.24	114.44
DS111	PP-M	PH	37.46	4.51	14.60	11.21	0.06	16.05	1.08	0.01	0.26	9.58	0.84	0.22	95.48
DS111	PP-M	PH	37.22	4.16	13.57	14.94	0.08	15.01	0.62	0.00	0.22	9.62	0.78	0.21	96.06
DS111	PP-M	PH	37.58	4.02	13.69	13.50	0.07	15.86	0.48	0.00	0.20	9.68	0.92	0.16	95.73
DS111	PP-M	PH	37.07	4.16	13.45	15.32	0.08	15.17	0.88	0.01	0.20	9.57	0.80	0.22	96.54
DS111	PP-M	PH	37.63	4.52	14.82	12.17	0.08	15.52	1.18	0.00	0.20	9.45	0.87	0.22	96.24
DS111	PP-M	PH	37.77	3.82	14.80	12.60	0.09	15.46	0.97	0.01	0.19	9.63	0.88	0.26	96.04
DS111	PP-M	PH	37.53	4.26	13.57	14.31	0.05	15.32	0.31	0.00	0.25	9.77	0.85	0.23	96.02
DS111	PP-M	PH	37.42	4.33	14.37	13.34	0.07	15.14	0.61	0.00	0.23	9.72	0.85	0.23	95.91
DS111	PP-M	PH	37.19	4.31	14.04	13.76	0.08	15.28	0.37	0.00	0.22	9.73	0.84	0.24	95.64
DS111	PP-M	PH	37.20	4.34	14.06	13.44	0.07	15.27	1.03	0.00	0.21	9.50	0.86	0.25	95.80
DS111	PP-M	PH	37.46	4.34	13.78	12.51	0.05	16.15	0.65	0.00	0.19	9.71	0.92	0.22	95.55
DS111	PP-M	PH	37.36	4.10	14.36	13.75	0.05	15.31	0.93	0.00	0.21	9.60	0.85	0.24	96.34
DS111	PP-M	PH	37.06	4.27	13.97	14.07	0.06	15.30	1.01	0.00	0.21	9.50	0.89	0.24	96.15
DS111	PP-M	PH	37.28	4.12	13.75	14.66	0.08	15.19	0.69	0.04	0.19	9.71	0.86	0.23	96.39
DS111	PP-M	PH	37.40	3.64	15.51	11.11	0.05	16.12	1.22	0.00	0.22	9.56	0.99	0.23	95.58
DS111	PP-M	PH	36.99	4.45	13.75	14.98	0.06	15.02	0.86	0.03	0.20	9.47	0.79	0.25	96.45
DS111	PP-M	PH	36.83	4.39	14.16	14.40	0.07	14.65	0.87	0.00	0.26	9.65	0.84	0.22	95.93
DS111	PP-M	PH	37.17	4.33	13.92	14.91	0.06	14.62	0.86	0.00	0.21	9.59	0.82	0.22	96.30
DS111	PP-M	PH	37.29	4.46	13.82	14.86	0.03	14.66	1.07	0.03	0.22	9.40	0.82	0.26	96.50
DS111	PP-M	PH	37.62	4.05	14.84	13.01	0.03	15.34	0.85	0.02	0.22	9.68	0.92	0.26	96.38

Sample #	Rock/Type		SiO_2	TiO_2	Al_2O_3	FeO	MnO	MgO	BaO	CaO	Na_2O	K_2O	F	Cl	Total
DS111	PP-M	PH	37.64	4.31	15.25	11.04	0.06	15.35	1.14	0.02	0.21	9.51	0.86	0.27	95.23
DS20	DRB-M	PH	37.17	3.56	16.00	11.21	0.03	16.11	1.27	0.00	0.21	9.42	0.98	0.19	95.70
DS20	DRB-M	PH	37.07	3.77	15.72	11.84	0.05	15.73	1.20	0.00	0.21	9.54	0.87	0.17	95.76
DS20	DRB-M	PH	37.01	3.84	16.07	11.22	0.05	16.05	1.64	0.00	0.18	9.26	0.94	0.21	96.02
DS20	DRB-M	PH	37.17	3.23	15.94	10.21	0.05	17.18	1.02	0.00	0.23	9.69	1.19	0.16	95.54
DS20	DRB-M	PH	37.24	3.03	16.05	9.19	0.05	17.83	0.94	0.00	0.17	9.63	1.24	0.17	94.97
DS20	DRB-M	PH	36.99	3.25	16.19	10.85	0.05	16.19	1.11	0.00	0.18	9.38	1.02	0.19	94.94
DS20	DRB-M	PH	36.41	3.07	15.98	10.08	0.03	16.20	1.13	0.10	0.20	8.87	1.06	0.20	92.83
DS20	DRB-M	PH	36.97	3.09	16.41	9.66	0.03	16.50	0.97	0.05	0.19	9.38	1.06	0.17	94.01
DS20	DRB-M	PH	37.22	3.11	16.45	9.76	0.06	16.61	1.06	0.05	0.21	9.49	1.09	0.16	94.75
DS20	DRB-M	PH	37.27	3.17	16.54	9.21	0.06	16.96	1.06	0.04	0.20	9.38	1.07	0.17	94.63
DS20	DRB-M	PH	37.40	3.06	16.32	9.31	0.06	17.13	1.09	0.10	0.21	9.39	1.16	0.18	94.88
DS20	DRB-M	PH	37.26	3.23	15.99	9.07	0.05	17.54	0.79	0.00	0.19	9.52	1.20	0.16	94.45
DS36	DRB-M	PH	63.11	0.00	17.75	0.37	0.00	0.17	0.33	0.00	0.51	15.59	0.00	0.10	97.90
DS36	DRB-M	PH	55.66	0.21	23.85	2.37	0.00	1.64	0.00	0.35	4.06	5.60	0.00	0.00	93.74
DS36	DRB-M	PH	30.62	0.14	20.75	16.34	0.11	20.50	0.00	0.00	0.01	1.75	0.29	0.10	90.46
DS36	DRB-M	PH	62.43	0.00	18.92	0.18	0.00	0.29	0.21	0.46	4.56	8.58	0.00	0.00	95.64
DS36	DRB-M	PH	34.36	0.12	21.84	14.16	0.06	16.06	0.00	0.00	0.00	2.74	0.16	0.10	89.50
DS36	DRB-M	PH	61.81	0.02	18.55	0.26	0.00	0.06	0.70	0.11	0.66	15.76	0.00	0.00	97.93
DS36	DRB-M	PH	62.96	0.00	18.18	0.10	0.00	0.00	0.42	0.00	0.69	16.08	0.00	0.00	98.42
DS36	DRB-M	PH	62.91	0.00	18.65	0.09	0.00	0.00	1.17	0.20	0.78	15.73	0.00	0.38	99.82
DS36	DRB-M	PH	59.07	0.01	21.54	1.07	0.00	0.54	0.35	0.05	1.54	13.26	0.00	1.35	98.46
DS36	DRB-M	PH	57.17	0.18	21.58	1.65	0.00	1.15	0.36	0.17	0.89	12.49	0.04	0.48	96.02
DS36	DRB-M	PH	56.74	0.15	22.48	1.99	0.00	1.33	0.25	0.22	0.93	11.32	0.05	1.16	96.34
DS23	DRB-M	PH	36.56	3.88	15.34	15.38	0.05	13.64	0.94	0.00	0.23	9.44	0.70	0.00	95.86
DS23	DRB-M	PH	36.27	3.33	16.22	15.92	0.05	12.63	0.86	0.00	0.24	9.53	0.76	1.70	96.80
DS23	DRB-M	PH	36.12	3.78	15.82	15.46	0.04	13.08	0.95	0.00	0.22	9.37	0.78	0.00	95.29
DS23	DRB-M	PH	36.44	3.75	15.64	15.84	0.03	13.09	0.92	0.14	0.23	9.47	0.86	0.38	96.35
DS23	DRB-M	PH	36.27	3.74	16.04	15.55	0.06	13.02	1.42	0.02	0.25	9.33	0.82	0.47	96.52
DS23	DRB-M	PH	36.98	3.69	15.85	14.78	0.05	13.99	0.89	0.00	0.27	9.44	0.81	0.95	97.15
DS23	DRB-M	PH	36.72	3.67	16.11	14.74	0.02	13.91	1.03	0.00	0.21	9.40	0.78	0.29	96.47
DS23	DRB-M	PH	36.37	3.82	15.82	15.02	0.04	13.63	1.02	0.00	0.23	9.46	0.79	1.14	96.75
DS23	DRB-M	PH	36.47	3.61	15.81	15.37	0.04	13.63	0.93	0.01	0.22	9.40	0.70	2.36	97.71
DS23	DRB-M	PH	36.59	3.22	16.31	15.57	0.03	13.02	0.87	0.00	0.20	9.22	0.87	1.14	96.41
DS23	DRB-M	PH	32.87	12.63	14.68	13.92	0.01	12.93	0.66	0.00	0.11	8.97	0.76	0.00	97.21
DS23	DRB-M	PH	37.37	3.56	15.58	14.58	0.02	13.97	0.16	0.00	0.26	9.78	0.78	0.00	95.73
DS23	DRB-M	PH	36.84	3.05	16.41	15.10	0.05	13.88	0.63	0.01	0.21	9.68	0.90	0.00	96.38
DS23	DRB-M	PH	36.61	3.21	16.20	14.70	0.05	13.82	0.83	0.00	0.26	9.77	0.83	0.29	96.14
DS23	DRB-M	PH	36.47	3.73	15.89	15.10	0.02	13.50	1.22	0.00	0.24	9.54	0.86	1.99	97.73
DS169	PP-M	PH	35.67	0.76	20.57	15.88	0.12	11.45	0.17	0.16	0.06	10.34	0.47	0.48	95.80
DS169	PP-M	PH	42.73	1.42	23.61	9.36	0.06	6.03	0.08	0.04	0.07	10.13	0.29	0.57	94.13
DS169	PP-M	PH	38.09	1.16	19.22	15.73	0.05	11.11	0.10	0.09	0.07	10.34	0.58	0.00	96.29
DS169	PP-M	PH	43.28	0.69	23.10	10.67	0.03	6.85	0.18	0.08	0.06	8.99	0.38	0.38	94.45
DS169	PP-M	PH	41.70	1.16	21.45	11.99	0.03	8.58	0.10	0.00	0.08	10.45	0.55	0.00	95.86
DS169	PP-M	PH	46.18	0.83	23.55	8.70	0.00	5.57	0.08	0.05	0.08	9.78	0.38	0.00	95.02
DS169	PP-M	PH	39.12	1.28	19.08	15.36	0.05	10.18	0.06	0.08	0.06	9.92	0.63	0.00	95.56
DS169	PP-M	PH	44.67	0.90	23.94	8.88	0.00	5.75	0.11	0.22	0.12	9.57	0.33	0.00	94.35
DS169	PP-M	PH	48.03	0.74	25.67	6.60	0.00	4.25	0.11	0.08	0.06	9.55	0.28	0.00	95.25
DS169	PP-M	PH	0.00	0.01	0.22	10.84	0.17	14.23	0.02	27.24	0.03	0.17	0.00	0.00	52.93
DS64	PP-M	POT	36.76	4.72	12.98	16.52	0.14	13.94	0.82	0.03	0.17	8.85	0.63	0.25	95.48
DS64	PP-M	POT	36.29	4.55	12.94	16.63	0.14	13.59	0.99	0.06	0.16	8.59	0.71	0.20	94.51

Sample #	Rock/Type		SiO_2	TiO_2	Al_2O_3	FeO	MnO	MgO	BaO	CaO	Na_2O	K_2O	F	Cl	Total
DS64	PP-M	POT	36.83	4.68	12.96	16.55	0.14	13.57	0.98	0.02	0.12	8.76	0.72	0.25	95.21
DS64	PP-M	POT	34.76	4.44	12.67	16.28	0.09	12.98	0.87	0.07	0.17	8.23	0.91	0.21	91.26
DS64	PP-M	POT	35.88	3.56	13.35	15.78	0.13	13.53	0.70	0.07	0.15	8.55	0.97	0.20	92.42
DS64	PP-M	POT	36.23	4.54	12.92	16.52	0.12	13.58	0.96	0.03	0.13	8.80	0.72	0.21	94.41
DS64	PP-M	POT	36.98	4.51	13.00	15.90	0.10	14.13	1.00	0.00	0.16	9.71	0.76	0.24	96.12
DS64	PP-M	POT	36.44	4.46	12.75	16.13	0.11	13.94	0.87	0.02	0.16	9.79	0.80	0.21	95.30
DS64	PP-M	POT	36.79	4.40	12.77	15.82	0.11	14.27	0.83	0.01	0.16	9.75	0.63	0.25	95.46
DS64	PP-M	POT	36.81	4.63	13.14	16.44	0.11	13.41	1.06	0.09	0.18	9.73	0.82	0.22	96.26
DS64	PP-M	POT	36.69	4.60	12.77	16.13	0.11	13.98	1.02	0.02	0.17	9.69	0.81	0.25	95.84
DS64	PP-M	POT	36.90	4.39	13.17	16.22	0.11	13.78	0.93	0.06	0.19	9.72	1.02	0.22	96.23
DS64	PP-M	POT	36.74	4.01	12.40	15.37	0.13	14.58	0.45	0.00	0.20	9.83	0.60	0.21	94.20
DS64	PP-M	POT	36.72	4.03	12.67	15.21	0.12	14.60	0.65	0.01	0.16	9.96	0.61	0.23	94.65
DS64	PP-M	POT	36.66	4.36	12.72	15.88	0.13	14.15	0.64	0.00	0.18	9.79	0.60	0.23	95.04
DS64	PP-M	POT	36.17	4.23	12.85	16.29	0.16	13.57	0.98	0.01	0.16	9.45	0.72	0.26	94.48
DS64	PP-M	POT	36.16	4.30	12.68	15.99	0.13	13.71	0.97	0.01	0.15	9.50	0.60	0.26	94.14
DS64	PP-M	POT	36.08	4.25	12.86	16.30	0.12	13.23	0.70	0.00	0.19	9.50	0.74	0.26	93.85
DS64	PP-M	POT	37.38	4.15	12.75	15.40	0.14	15.00	0.60	0.00	0.17	9.86	0.65	0.23	96.02
DS64	PP-M	POT	36.66	4.27	12.72	15.73	0.14	14.38	0.87	0.02	0.17	9.75	0.72	0.22	95.29
DS64	PP-M	POT	37.14	4.22	12.59	15.39	0.14	15.02	0.45	0.00	0.17	9.95	0.63	0.25	95.65
DS64	PP-M	POT	36.80	4.38	12.93	16.17	0.11	13.90	0.97	0.00	0.18	9.57	0.93	0.21	95.71
DS64	PP-M	POT	37.08	4.43	12.84	15.97	0.11	14.27	0.85	0.02	0.20	9.62	0.81	0.24	96.03
DS64	PP-M	POT	37.14	4.46	13.11	16.00	0.10	13.88	0.79	0.00	0.19	9.64	0.86	0.20	95.96
DS64	PP-M	POT	37.30	4.10	12.84	15.75	0.13	14.96	0.61	0.02	0.16	9.81	0.56	0.21	96.17
DS64	PP-M	POT	37.02	4.21	12.60	15.70	0.16	14.83	0.42	0.01	0.17	9.98	0.57	0.20	95.57
DS64	PP-M	POT	37.10	3.74	12.96	16.22	0.22	15.08	0.78	0.02	0.18	10.08	0.53	0.22	96.84
DS64	PP-M	POT	37.08	3.90	13.59	17.45	0.12	13.18	1.03	0.05	0.19	9.93	0.99	0.21	97.24
DS64	PP-M	POT	36.52	3.98	13.41	16.51	0.16	14.12	0.79	0.03	0.16	10.08	0.85	0.20	96.40
DS64	PP-M	POT	36.05	3.97	13.19	17.32	0.14	13.79	0.96	0.05	0.17	9.67	0.67	0.21	95.85
DS64	PP-M	POT	36.66	4.01	12.76	16.42	0.13	14.41	0.69	0.02	0.14	9.99	0.68	0.22	95.79
DS64	PP-M	POT	36.68	4.00	12.76	16.32	0.14	14.30	0.91	0.01	0.16	9.76	0.74	0.22	95.63
DS64	PP-M	POT	36.69	3.96	12.93	16.45	0.12	14.15	0.87	0.01	0.15	9.82	0.81	0.19	95.78
DS64	PP-M	POT	36.38	4.01	12.92	16.33	0.11	14.27	0.99	0.08	0.13	9.81	0.82	0.19	95.65
DS64	PP-M	POT	36.22	3.91	12.72	16.29	0.12	14.11	0.89	0.13	0.14	9.70	0.65	0.24	94.79
DS64	PP-M	POT	36.80	3.79	12.90	16.54	0.11	14.37	0.41	0.00	0.15	10.04	0.72	0.20	95.69
DS64	PP-M	POT	36.74	3.39	13.05	15.91	0.13	15.16	0.81	0.00	0.18	10.01	0.64	0.20	95.90
DS64	PP-M	POT	37.09	3.54	12.76	15.88	0.10	15.25	0.22	0.00	0.21	10.15	0.71	0.19	95.76
DS64	PP-M	POT	36.90	3.47	12.96	15.84	0.13	15.11	0.51	0.00	0.18	9.96	0.71	0.21	95.63
DS64	PP-M	POT	36.02	3.56	13.16	15.95	0.15	15.40	0.75	0.05	0.21	8.91	1.27	0.19	95.03
DS64	PP-M	POT	36.56	3.88	12.95	16.52	0.15	14.41	0.59	0.03	0.19	10.05	0.75	0.22	95.93
DS64	PP-M	POT	36.58	3.68	12.81	15.93	0.15	15.15	0.52	0.00	0.17	10.16	0.63	0.22	95.68
DS65	PP-M	POT	37.32	4.36	12.94	14.80	0.09	15.26	0.24	0.08	0.18	9.58	0.73	0.21	95.42
DS65	PP-M	POT	37.10	4.41	13.16	14.72	0.12	14.88	0.44	0.09	0.17	9.37	0.76	0.19	95.05
DS65	PP-M	POT	37.17	4.24	13.18	14.89	0.10	15.10	0.76	0.08	0.18	9.05	0.75	0.20	95.35
DS65	PP-M	POT	36.91	4.33	13.09	14.38	0.09	14.94	0.66	0.12	0.16	9.00	0.79	0.17	94.26
DS65	PP-M	POT	37.30	3.98	13.97	13.75	0.09	15.00	0.79	0.10	0.21	9.08	1.01	0.15	94.96
DS65	PP-M	POT	37.16	4.74	13.64	14.40	0.09	15.12	1.05	0.30	0.19	9.30	0.80	0.24	96.62
DS65	PP-M	POT	37.08	4.16	13.12	14.93	0.09	15.40	0.50	0.17	0.16	8.88	0.72	0.19	95.05
DS65	PP-M	POT	36.68	4.25	13.17	14.91	0.11	15.35	0.66	0.08	0.20	9.04	0.80	0.22	95.07
DS65	PP-M	POT	37.35	4.15	13.19	15.01	0.13	15.03	0.55	0.16	0.19	8.63	0.81	0.17	94.98
DS65	PP-M	POT	36.74	4.55	13.04	14.90	0.14	14.84	0.63	0.26	0.19	9.09	0.70	0.23	94.97
DS65	PP-M	POT	38.31	4.00	13.35	12.81	0.09	15.95	0.19	0.15	0.17	9.30	1.04	0.19	95.07

Sample #	Rock/Type		SiO_2	TiO_2	Al_2O_3	FeO	MnO	MgO	BaO	CaO	Na_2O	K_2O	F	Cl	Total
DS65	PP-M	POT	37.32	4.51	13.22	14.64	0.11	15.20	0.69	0.09	0.19	9.33	0.77	0.20	95.90
DS65	PP-M	POT	37.32	4.36	12.94	14.80	0.09	15.26	0.24	0.08	0.18	9.58	0.73	0.21	95.42
DS65	PP-M	POT	37.10	4.41	13.16	14.72	0.12	14.88	0.44	0.09	0.17	9.37	0.76	0.19	95.05
DS65	PP-M	POT	37.17	4.24	13.18	14.89	0.10	15.10	0.76	0.08	0.18	9.05	0.75	0.20	95.35
DS65	PP-M	POT	36.91	4.33	13.09	14.38	0.09	14.94	0.66	0.12	0.16	9.00	0.79	0.17	94.26
DS65	PP-M	POT	37.30	3.98	13.97	13.75	0.09	15.00	0.79	0.10	0.21	9.08	1.01	0.15	94.96
DS65	PP-M	POT	37.16	4.74	13.64	14.40	0.09	15.12	1.05	0.30	0.19	9.30	0.80	0.24	96.62
DS65	PP-M	POT	37.08	4.16	13.12	14.93	0.09	15.40	0.50	0.17	0.16	8.88	0.72	0.19	95.05
DS65	PP-M	POT	36.68	4.25	13.17	14.91	0.11	15.35	0.66	0.08	0.20	9.04	0.80	0.22	95.07
DS65	PP-M	POT	37.35	4.15	13.19	15.01	0.13	15.03	0.55	0.16	0.19	8.63	0.81	0.17	94.98
DS65	PP-M	POT	36.74	4.55	13.04	14.90	0.14	14.84	0.63	0.26	0.19	9.09	0.70	0.23	94.97
DS65	PP-M	POT	38.31	4.00	13.35	12.81	0.09	15.95	0.19	0.15	0.17	9.30	1.04	0.19	95.07
DS65	PP-M	POT	37.32	4.51	13.22	14.64	0.11	15.20	0.69	0.09	0.19	9.33	0.77	0.20	95.90
DS165	DRB-S	POT	36.99	3.40	14.57	16.22	0.07	14.58	0.44	0.00	0.21	10.25	0.80	0.24	97.37
DS165	DRB-S	POT	36.19	3.50	14.34	16.58	0.05	13.70	0.67	0.00	0.23	10.05	0.71	0.27	95.93
DS165	DRB-S	POT	36.71	3.55	14.32	16.27	0.07	14.23	0.42	0.00	0.23	10.11	0.77	0.31	96.61
DS165	DRB-S	POT	36.30	3.48	14.62	16.22	0.05	13.95	0.38	0.02	0.20	10.23	0.80	0.27	96.13
DS165	DRB-S	POT	36.85	3.35	14.36	16.29	0.05	14.57	0.40	0.00	0.23	10.05	0.79	0.27	96.80
DS165	DRB-S	POT	36.53	3.24	14.58	16.49	0.06	13.99	0.32	0.01	0.15	10.43	0.81	0.30	96.48
DS165	DRB-S	POT	37.14	3.13	14.27	16.63	0.05	14.19	0.15	0.03	0.08	10.37	0.81	0.28	96.72
DS165	DRB-S	POT	37.00	3.55	14.22	16.78	0.06	14.24	0.59	0.00	0.22	10.33	0.79	0.29	97.65
DS165	DRB-S	POT	37.17	3.15	14.34	16.55	0.04	14.66	0.61	0.01	0.23	10.06	0.85	0.32	97.54
DS165	DRB-S	POT	36.97	3.29	14.54	16.64	0.06	14.22	0.81	0.02	0.21	9.93	0.80	0.29	97.38
DS165	DRB-S	POT	37.12	3.17	14.38	16.29	0.06	14.60	0.46	0.00	0.19	10.23	0.88	0.34	97.28
DS165	DRB-S	POT	36.98	3.22	14.09	16.90	0.06	13.98	0.34	0.00	0.15	10.55	0.81	0.29	96.96
DS165	DRB-S	POT	36.55	3.03	14.30	17.01	0.06	14.68	0.45	0.03	0.23	9.61	0.83	0.30	96.65
DS165	DRB-S	POT	36.94	3.24	14.68	16.53	0.04	14.58	0.74	0.00	0.23	9.97	0.78	0.32	97.66
DS165	DRB-S	POT	36.92	3.12	14.53	16.32	0.05	14.52	0.49	0.01	0.21	10.20	0.84	0.30	97.07
DS165	DRB-S	POT	36.95	3.08	14.55	16.60	0.07	14.60	0.67	0.00	0.22	10.01	0.85	0.33	97.50
DS165	DRB-S	POT	36.79	3.22	14.20	16.43	0.06	14.27	0.55	0.04	0.19	10.07	0.89	0.33	96.60
DS165	DRB-S	POT	37.02	3.21	14.14	16.69	0.05	14.22	0.50	0.01	0.17	10.27	0.81	0.30	97.00
DS165	DRB-S	POT	37.03	2.84	14.40	16.72	0.05	14.92	0.93	0.02	0.17	9.83	0.87	0.32	97.67
DS165	DRB-S	POT	36.70	2.93	14.16	16.48	0.06	14.56	0.96	0.01	0.22	10.06	0.86	0.37	96.92
DS165	DRB-S	POT	36.89	2.87	14.44	16.64	0.07	14.51	1.00	0.01	0.17	9.89	0.94	0.31	97.26
DS165	DRB-S	POT	36.97	3.05	14.17	16.14	0.04	14.32	0.66	0.02	0.19	10.08	0.90	0.33	96.41
DS165	DRB-S	POT	37.96	2.59	14.28	16.06	0.09	14.43	0.13	0.04	0.06	10.64	0.96	0.28	97.05
DS165	DRB-S	POT	37.21	3.17	14.30	16.36	0.03	14.20	0.70	0.01	0.19	10.08	0.81	0.29	96.93
DS165	DRB-S	POT	36.73	3.39	14.63	16.86	0.06	13.55	1.07	0.00	0.13	10.06	0.76	0.31	97.15
DS165	DRB-S	POT	37.07	3.20	14.55	16.36	0.05	13.78	1.08	0.00	0.20	9.79	0.75	0.28	96.72
DS165	DRB-S	POT	36.97	3.14	14.63	16.31	0.05	13.90	1.13	0.00	0.23	9.91	0.80	0.31	96.98
DS165	DRB-S	POT	36.79	3.29	14.42	16.54	0.04	13.95	1.39	0.03	0.17	9.98	0.84	0.27	97.30
DS165	DRB-S	POT	37.08	3.11	14.39	16.53	0.04	14.08	1.15	0.00	0.22	9.87	0.82	0.31	97.19
DS165	DRB-S	POT	37.08	3.16	14.55	16.35	0.05	13.82	0.54	0.02	0.15	10.11	0.78	0.25	96.47
DS165	DRB-S	POT	37.22	2.91	14.20	16.26	0.07	14.39	1.15	0.00	0.19	9.95	0.91	0.29	97.11
DS165	DRB-S	POT	37.11	2.94	14.09	16.15	0.04	14.43	1.14	0.00	0.19	9.94	0.93	0.32	96.80
DS165	DRB-S	POT	37.12	2.99	14.38	16.62	0.04	14.47	0.81	0.00	0.20	9.99	0.84	0.29	97.34
DS165	DRB-S	POT	37.31	2.91	14.20	16.18	0.05	14.84	0.80	0.00	0.21	10.17	0.94	0.30	97.44
DS165	DRB-S	POT	37.48	2.62	14.44	16.15	0.05	14.82	0.30	0.00	0.21	10.11	0.87	0.27	96.89
DS165	DRB-S	POT	37.10	2.90	14.46	16.16	0.04	14.58	0.97	0.00	0.18	10.12	0.90	0.27	97.23
DS165	DRB-S	POT	35.91	3.02	13.97	16.36	0.03	13.71	0.97	0.04	0.18	9.73	0.76	0.31	94.59
DS165	DRB-S	POT	36.53	3.17	14.11	16.62	0.07	14.09	1.31	0.00	0.23	9.90	0.74	0.32	96.71

Sample #	Rock/Type		SiO_2	TiO_2	Al_2O_3	FeO	MnO	MgO	BaO	CaO	Na_2O	K_2O	F	Cl	Total
DS165	DRB-S	POT	36.78	3.10	14.24	16.53	0.06	14.30	1.06	0.05	0.19	9.96	0.80	0.37	97.02
DS165	DRB-S	POT	36.82	2.88	14.22	16.28	0.06	14.16	0.60	0.02	0.16	9.95	0.80	0.35	95.88
DS165	DRB-S	POT	36.93	3.10	14.14	16.44	0.07	14.47	0.57	0.02	0.21	10.02	0.74	0.33	96.61
DS165	DRB-S	POT	36.81	3.14	14.26	16.42	0.04	14.35	1.07	0.02	0.21	9.70	0.76	0.28	96.68
DS165	DRB-S	POT	36.74	2.73	14.12	16.05	0.05	14.93	0.57	0.03	0.23	9.80	0.72	0.27	95.89
DS165	DRB-S	POT	36.88	2.66	14.30	15.83	0.04	15.10	0.35	0.01	0.18	10.40	0.79	0.30	96.44
DS165	DRB-S	POT	37.03	2.82	14.20	16.07	0.05	14.95	0.47	0.01	0.24	10.15	0.75	0.27	96.63
DS165	DRB-S	POT	36.56	2.82	14.12	16.02	0.05	14.79	0.56	0.01	0.22	9.91	0.76	0.28	95.71
DS165	DRB-S	POT	37.25	2.72	14.30	16.05	0.05	14.92	0.53	0.02	0.15	10.08	0.78	0.30	96.76
DS165	DRB-S	POT	36.88	2.90	14.16	16.06	0.05	15.12	0.51	0.01	0.23	10.10	0.83	0.28	96.71
DS165	DRB-S	POT	36.93	3.25	14.36	16.31	0.04	14.80	0.64	0.02	0.26	9.95	0.71	0.30	97.19
DS165	DRB-S	POT	37.14	3.27	14.52	16.09	0.06	14.60	0.49	0.02	0.13	10.24	0.74	0.25	97.19
DS165	DRB-S	POT	37.21	3.05	14.42	16.44	0.06	14.58	0.71	0.01	0.23	10.09	0.74	0.28	97.45
DS165	DRB-S	POT	37.38	3.03	13.86	15.86	0.06	14.92	0.35	0.09	0.24	10.23	0.79	0.30	96.70
DS165	DRB-S	POT	36.41	3.46	14.20	16.83	0.05	13.93	1.02	0.00	0.24	9.76	0.68	0.34	96.56
DS165	DRB-S	POT	34.99	2.77	13.64	14.12	0.02	14.33	0.37	0.00	0.26	9.12	0.87	0.25	90.31
DS165	DRB-S	POT	36.90	3.30	14.32	16.67	0.05	14.11	0.86	0.00	0.25	9.84	0.61	0.30	96.89
DS165	DRB-S	POT	36.81	3.54	14.47	16.80	0.03	13.92	1.07	0.01	0.25	9.77	0.69	0.34	97.33
DS165	DRB-S	POT	37.02	3.18	14.30	16.42	0.04	14.46	0.79	0.00	0.24	9.93	0.71	0.28	97.01
DS165	DRB-S	POT	36.85	3.29	14.47	16.63	0.04	14.32	0.54	0.01	0.20	10.13	0.62	0.31	97.06
DS165	DRB-S	POT	37.06	2.96	14.22	16.34	0.05	14.44	0.47	0.01	0.19	10.24	0.75	0.29	96.63
DS165	DRB-S	POT	37.12	3.02	14.01	15.95	0.06	14.67	0.52	0.02	0.21	10.16	0.74	0.29	96.37
DS165	DRB-S	POT	36.80	2.93	13.83	16.04	0.08	14.70	0.55	0.00	0.20	10.20	0.73	0.30	95.99
DS165	DRB-S	POT	36.21	2.93	13.75	16.25	0.07	14.82	0.52	0.00	0.24	9.75	0.77	0.32	95.23
DS165	DRB-S	POT	36.81	2.92	13.72	16.01	0.08	14.60	0.57	0.00	0.21	9.96	0.71	0.23	95.48
DS165	DRB-S	POT	36.82	2.87	13.85	15.73	0.08	14.58	0.45	0.02	0.20	9.91	0.72	0.32	95.17
DS165	DRB-S	POT	36.76	2.96	14.08	16.31	0.08	14.58	0.41	0.01	0.16	9.86	0.72	0.28	95.85
DS165	DRB-S	POT	37.26	2.65	13.78	15.65	0.06	14.78	0.31	0.00	0.13	10.29	0.78	0.31	95.60
DS165	DRB-S	POT	37.27	2.88	13.77	16.00	0.08	14.93	0.33	0.02	0.23	10.26	0.74	0.29	96.42
DS165	DRB-S	POT	37.36	2.99	13.98	16.10	0.09	15.11	0.30	0.02	0.22	10.05	0.75	0.26	96.85
DS165	DRB-S	POT	36.94	2.87	14.32	16.02	0.06	14.73	0.69	0.01	0.24	9.85	0.72	0.30	96.39
DS165	DRB-S	POT	36.90	2.80	14.39	15.87	0.09	14.73	0.53	0.02	0.16	10.34	0.65	0.29	96.43
DS165	DRB-S	POT	37.05	2.74	13.86	15.93	0.06	15.10	0.55	0.03	0.22	10.01	0.76	0.24	96.15
DS165	DRB-S	POT	36.49	3.56	13.78	16.42	0.07	14.30	0.41	0.00	0.20	10.26	0.79	0.27	96.15
DS165	DRB-S	POT	36.50	3.48	13.92	16.14	0.08	14.26	0.56	0.00	0.21	10.17	0.73	0.26	95.94
DS165	DRB-S	POT	36.85	3.33	13.82	16.27	0.09	14.45	0.46	0.00	0.21	10.32	0.77	0.27	96.46
DS165	DRB-S	POT	36.55	3.37	14.18	16.36	0.09	14.34	0.44	0.00	0.19	10.23	0.75	0.27	96.38
DS165	DRB-S	POT	36.96	3.68	13.94	17.01	0.08	13.63	0.20	0.00	0.17	10.39	0.73	0.25	96.68
DS165	DRB-S	POT	37.04	3.75	14.07	16.44	0.08	13.80	0.47	0.02	0.22	10.19	0.66	0.28	96.66
DS165	DRB-S	POT	36.75	3.48	14.16	16.02	0.07	14.22	0.65	0.01	0.23	10.18	0.73	0.27	96.39
DS165	DRB-S	POT	36.55	3.50	14.03	16.37	0.09	14.29	0.26	0.00	0.21	10.42	0.69	0.30	96.35
DS165	DRB-S	POT	37.04	3.35	14.11	16.35	0.09	14.45	0.46	0.00	0.21	10.25	0.73	0.27	96.93
DS165	DRB-S	POT	37.17	3.62	14.25	16.89	0.08	13.86	0.25	0.00	0.13	10.20	0.74	0.26	97.07
DS165	DRB-S	POT	37.09	3.60	14.24	16.52	0.06	14.24	0.52	0.00	0.18	9.75	0.73	0.26	96.81
DS165	DRB-S	POT	37.13	3.44	14.54	16.24	0.06	14.39	0.43	0.00	0.23	9.87	0.71	0.27	96.93
DS165	DRB-S	POT	36.90	3.45	14.79	16.25	0.07	13.88	0.81	0.00	0.24	9.85	0.68	0.27	96.84
DS165	DRB-S	POT	36.74	3.44	14.78	16.14	0.05	14.02	0.81	0.00	0.20	9.68	0.74	0.25	96.47
DS165	DRB-S	POT	36.58	3.64	14.82	16.25	0.06	13.69	0.75	0.00	0.18	9.89	0.71	0.29	96.49
DS165	DRB-S	POT	36.89	3.26	14.88	15.96	0.07	14.05	0.37	0.00	0.22	10.02	0.71	0.24	96.31
DS165	DRB-S	POT	36.70	3.48	14.95	16.39	0.07	13.66	1.06	0.00	0.20	9.55	0.73	0.26	96.70
DS165	DRB-S	POT	37.22	3.33	14.87	15.97	0.08	14.22	0.55	0.00	0.20	9.90	0.73	0.25	96.95

Sample #	Rock/Type		SiO_2	TiO_2	Al_2O_3	FeO	MnO	MgO	BaO	CaO	Na_2O	K_2O	F	Cl	Total
DS133	DRB-S	POT	37.45	2.76	14.32	15.08	0.12	16.00	0.41	0.02	0.13	9.67	0.33	0.33	96.39
DS133	DRB-S	POT	37.35	2.95	14.26	15.25	0.10	16.02	0.44	0.00	0.18	9.72	0.36	0.33	96.74
DS133	DRB-S	POT	37.57	2.78	14.30	15.98	0.11	15.42	0.41	0.00	0.15	9.78	0.35	0.31	96.94
DS133	DRB-S	POT	37.02	2.64	14.36	15.57	0.12	15.95	0.46	0.05	0.17	9.51	0.37	0.32	96.29
DS133	DRB-S	POT	36.81	3.03	14.17	15.21	0.09	15.59	0.46	0.10	0.16	9.31	0.35	0.27	95.34
DS133	DRB-S	POT	36.66	2.91	14.37	15.25	0.09	15.61	0.43	0.13	0.11	9.05	0.30	0.29	94.99
DS133	DRB-S	POT	36.50	3.04	13.91	15.00	0.09	15.60	0.37	0.18	0.14	9.06	0.29	0.33	94.31
DS133	DRB-S	POT	36.68	2.39	14.25	15.40	0.10	15.78	0.41	0.12	0.11	9.29	0.32	0.28	94.93
DS133	DRB-S	POT	36.11	2.83	14.26	15.69	0.09	15.16	0.31	0.25	0.06	8.58	0.36	0.19	93.70
DS133	DRB-S	POT	36.31	2.76	14.56	15.97	0.09	15.09	0.32	0.18	0.07	9.87	0.34	0.26	95.61
DS133	DRB-S	POT	36.50	2.82	14.34	15.34	0.09	15.73	0.43	0.00	0.16	9.69	0.34	0.31	95.53
DS133	DRB-S	POT	36.71	2.78	14.07	15.58	0.07	15.50	0.42	0.02	0.15	9.58	0.36	0.29	95.29
DS133	DRB-S	POT	36.66	2.58	14.36	15.35	0.08	15.94	0.38	0.02	0.17	9.48	0.37	0.34	95.50
DS133	DRB-S	POT	37.32	3.01	14.42	15.27	0.08	15.78	0.49	0.02	0.13	9.84	0.37	0.30	96.79
DS133	DRB-S	POT	37.23	2.11	14.77	15.50	0.09	15.63	0.38	0.04	0.15	9.59	0.58	0.36	96.10
DS133	DRB-S	POT	37.31	2.06	14.69	15.20	0.09	15.76	0.35	0.03	0.14	9.79	0.61	0.31	96.01
DS133	DRB-S	POT	37.09	2.09	14.73	15.26	0.09	15.84	0.48	0.06	0.17	9.56	0.62	0.34	95.99
DS133	DRB-S	POT	37.08	1.98	14.63	15.44	0.10	15.47	0.37	0.07	0.14	9.73	0.57	0.34	95.60
DS133	DRB-S	POT	37.22	2.05	15.03	15.55	0.11	15.35	0.24	0.07	0.08	10.00	0.55	0.32	96.25
DS133	DRB-S	POT	36.31	3.00	14.55	16.09	0.09	15.02	0.64	0.05	0.19	9.39	0.57	0.36	95.94
DS133	DRB-S	POT	36.44	3.00	14.61	16.05	0.11	15.02	0.62	0.07	0.22	9.51	0.58	0.33	96.25
DS133	DRB-S	POT	36.75	3.18	14.62	16.25	0.10	14.92	0.64	0.06	0.22	9.43	0.55	0.32	96.73
DS133	DRB-S	POT	36.80	2.87	14.53	16.24	0.11	15.13	0.77	0.09	0.18	9.44	0.58	0.34	96.74
DS133	DRB-S	POT	36.75	2.67	14.44	15.94	0.10	15.18	0.60	0.08	0.15	9.61	0.60	0.32	96.10
DS147	PP-S	POT	37.56	3.27	13.30	16.90	0.14	15.18	0.33	0.02	0.10	9.61	0.57	0.34	97.01
DS147	PP-S	POT	36.94	3.38	13.38	16.84	0.12	14.60	0.43	0.03	0.12	9.74	0.51	0.32	96.11
DS147	PP-S	POT	37.56	3.11	13.11	16.01	0.12	15.33	0.17	0.01	0.14	9.58	0.57	0.33	95.72
DS147	PP-S	POT	37.51	3.17	13.50	16.89	0.13	14.91	0.33	0.03	0.10	9.77	0.54	0.31	96.89
DS147	PP-S	POT	38.35	3.25	13.27	16.51	0.11	15.46	0.22	0.00	0.15	9.69	0.61	0.30	97.58
DS147	PP-S	POT	38.11	3.16	13.26	17.05	0.14	15.36	0.20	0.05	0.14	9.35	0.56	0.30	97.37
DS147	PP-S	POT	37.17	3.10	13.04	16.88	0.14	14.95	0.20	0.11	0.11	9.28	0.48	0.28	95.46
DS147	PP-S	POT	37.43	3.21	13.45	17.37	0.13	14.97	0.24	0.00	0.12	9.78	0.50	0.30	97.22
DS147	PP-S	POT	37.87	3.18	13.25	17.20	0.13	14.93	0.22	0.03	0.14	9.68	0.48	0.36	97.18
DS147	PP-S	POT	37.31	3.07	13.40	17.12	0.14	14.94	0.24	0.07	0.13	9.35	0.49	0.28	96.26
DS147	PP-S	POT	35.52	3.88	13.76	17.88	0.17	13.84	1.25	0.04	0.15	9.43	0.43	0.40	96.46
DS147	PP-S	POT	35.80	3.83	13.53	17.85	0.14	13.79	0.86	0.02	0.14	9.62	0.49	0.35	96.13
DS147	PP-S	POT	35.74	3.83	13.88	17.70	0.12	13.94	0.91	0.03	0.15	9.62	0.47	0.31	96.42
DS147	PP-S	POT	35.93	3.59	13.80	17.48	0.12	14.25	0.45	0.04	0.15	9.66	0.46	0.34	96.01
DS147	PP-S	POT	36.87	3.36	13.78	17.27	0.14	14.46	0.30	0.03	0.14	9.76	0.49	0.31	96.62
DS147	PP-S	POT	36.09	3.83	13.87	17.75	0.15	14.05	1.02	0.00	0.13	9.60	0.52	0.36	97.06
DS147	PP-S	POT	36.18	3.80	13.73	17.86	0.17	13.93	1.20	0.01	0.14	9.53	0.47	0.34	97.09
DS147	PP-S	POT	37.11	3.65	13.31	17.18	0.14	14.55	0.39	0.00	0.12	9.72	0.49	0.31	96.70
DS147	PP-S	POT	36.89	3.70	13.67	17.68	0.13	14.45	0.82	0.01	0.12	9.61	0.48	0.35	97.61
DS147	PP-S	POT	36.89	3.54	13.40	17.71	0.15	14.32	0.34	0.01	0.12	9.59	0.48	0.35	96.61
DS147	PP-S	POT	36.89	3.90	13.67	17.59	0.16	13.98	0.73	0.00	0.11	9.50	0.47	0.28	97.01
DS147	PP-S	POT	37.08	3.85	13.64	17.50	0.18	14.06	0.65	0.00	0.13	9.63	0.46	0.30	97.21
DS147	PP-S	POT	35.81	4.29	13.85	18.17	0.15	13.43	1.43	0.01	0.15	9.15	0.46	0.34	96.95
DS147	PP-S	POT	36.77	4.03	13.54	17.49	0.12	13.93	0.54	0.03	0.14	9.47	0.47	0.31	96.57
DS147	PP-S	POT	37.23	3.53	13.58	17.22	0.15	14.08	0.35	0.02	0.09	9.66	0.52	0.30	96.45
DS147	PP-S	POT	36.66	3.14	13.31	17.28	0.14	14.58	0.21	0.01	0.13	9.54	0.53	0.30	95.53
DS147	PP-S	POT	36.46	3.22	13.10	17.08	0.11	14.73	0.21	0.00	0.13	9.53	0.55	0.32	95.14

Sample #	Rock/Type		SiO_2	TiO_2	Al_2O_3	FeO	MnO	MgO	BaO	CaO	Na_2O	K_2O	F	Cl	Total
DS147	PP-S	POT	36.83	3.20	13.24	17.07	0.11	14.71	0.14	0.09	0.11	9.30	0.54	0.31	95.35
DS147	PP-S	POT	37.45	3.02	13.27	17.44	0.13	14.42	0.16	0.00	0.11	9.64	0.54	0.35	96.23
DS147	PP-S	POT	37.37	3.19	13.30	17.54	0.11	14.42	0.25	0.00	0.12	9.81	0.51	0.30	96.63
DS147	PP-S	POT	37.21	3.31	13.24	17.29	0.13	14.84	0.20	0.00	0.12	9.59	0.56	0.31	96.48
DS147	PP-S	POT	37.42	3.26	13.24	16.93	0.10	15.00	0.15	0.00	0.11	9.73	0.52	0.25	96.43
DS147	PP-S	POT	37.27	3.08	13.06	17.17	0.12	14.69	0.19	0.07	0.14	9.58	0.56	0.33	95.96
DS147	PP-S	POT	37.67	3.26	13.00	16.72	0.12	15.10	0.23	0.00	0.11	9.63	0.59	0.35	96.45
DS147	PP-S	POT	36.83	3.26	13.53	17.70	0.13	14.47	0.20	0.01	0.11	9.65	0.52	0.28	96.40
DS147	PP-S	POT	37.04	3.15	13.65	17.70	0.14	14.65	0.35	0.00	0.10	9.54	0.54	0.31	96.88
DS147	PP-S	POT	37.24	3.08	13.70	17.35	0.13	14.83	0.33	0.01	0.13	9.68	0.48	0.35	97.02
DS147	PP-S	POT	37.41	3.14	14.03	17.48	0.13	14.44	0.45	0.00	0.12	9.44	0.47	0.31	97.15
DS147	PP-S	POT	37.62	3.30	13.51	17.61	0.15	14.74	0.34	0.00	0.13	9.69	0.50	0.32	97.62
DS147	PP-S	POT	37.27	3.04	13.70	17.57	0.13	14.62	0.50	0.00	0.13	9.60	0.52	0.32	97.10
DS147	PP-S	POT	37.46	3.02	13.44	16.93	0.13	15.07	0.27	0.07	0.06	9.40	0.54	0.33	96.41
DS147	PP-S	POT	38.70	2.97	12.98	16.27	0.11	15.70	0.28	0.00	0.07	9.48	0.66	0.26	97.14
DS147	PP-S	POT	37.98	3.12	13.13	16.78	0.13	15.08	0.26	0.00	0.09	9.64	0.57	0.28	96.74
DS147	PP-S	POT	37.95	3.10	13.19	16.76	0.11	15.29	0.34	0.02	0.08	9.70	0.59	0.32	97.14
DS147	PP-S	POT	37.86	3.11	13.47	17.75	0.13	14.95	0.38	0.04	0.09	9.58	0.57	0.32	97.93
DS106	DRB-S	POT	37.41	2.81	14.01	15.88	0.06	15.55	0.35	0.00	0.17	10.03	1.08	0.28	97.10
DS106	DRB-S	POT	37.00	2.93	13.72	16.18	0.09	15.28	0.45	0.03	0.18	9.86	1.02	0.26	96.51
DS106	DRB-S	POT	37.01	2.99	13.57	16.10	0.07	15.12	0.50	0.00	0.18	9.84	1.07	0.30	96.22
DS106	DRB-S	POT	38.28	2.86	12.76	15.11	0.07	15.79	0.10	0.02	0.22	9.83	1.21	0.26	95.93
DS106	DRB-S	POT	37.12	3.21	13.61	15.81	0.09	15.11	0.36	0.00	0.21	9.99	1.02	0.33	96.34
DS106	DRB-S	POT	36.49	3.12	14.05	16.42	0.07	14.77	0.09	0.02	0.18	10.05	0.99	0.26	96.03
DS106	DRB-S	POT	36.29	3.04	14.09	16.33	0.09	14.49	0.14	0.02	0.22	10.02	0.89	0.27	95.43
DS106	DRB-S	POT	36.17	3.08	14.25	16.73	0.09	14.40	0.12	0.00	0.21	10.07	0.88	0.26	95.83
DS106	DRB-S	POT	36.90	3.04	13.83	16.53	0.07	14.72	0.04	0.01	0.16	10.10	0.94	0.24	96.14
DS106	DRB-S	POT	37.66	3.07	13.28	15.59	0.08	15.16	0.12	0.01	0.15	10.02	1.10	0.26	95.97
DS106	DRB-S	POT	37.79	2.99	13.56	15.43	0.08	15.50	0.16	0.02	0.19	10.00	1.10	0.23	96.53
DS106	DRB-S	POT	37.18	3.13	13.99	15.94	0.07	14.96	0.10	0.01	0.16	10.06	1.01	0.26	96.38
DS106	DRB-S	POT	37.87	3.26	13.26	15.80	0.07	15.51	0.16	0.03	0.16	9.91	1.10	0.26	96.87
DS106	DRB-S	POT	37.44	3.17	13.86	16.10	0.07	15.06	0.07	0.02	0.12	10.20	1.00	0.23	96.85
DS106	DRB-S	POT	37.18	3.43	13.60	16.09	0.08	14.55	0.07	0.08	0.16	10.09	1.01	0.24	96.09
DS106	DRB-S	POT	37.16	3.14	14.12	15.78	0.08	15.10	0.48	0.02	0.21	9.94	0.91	0.26	96.76
DS106	DRB-S	POT	36.42	3.16	14.29	16.27	0.07	14.38	1.09	0.03	0.20	9.38	0.86	0.30	96.02
DS106	DRB-S	POT	37.12	3.19	14.01	16.07	0.06	14.84	0.46	0.01	0.21	9.85	0.85	0.30	96.56
DS106	DRB-S	POT	36.95	3.03	14.46	15.71	0.08	14.65	0.70	0.01	0.23	9.72	0.93	0.28	96.28
DS106	DRB-S	POT	37.03	2.78	14.20	15.82	0.10	15.07	0.54	0.01	0.20	9.71	1.01	0.28	96.25
DS106	DRB-S	POT	37.12	3.61	14.75	15.02	0.09	14.74	0.83	0.01	0.19	9.23	0.81	0.22	96.22
DS106	DRB-S	POT	36.82	3.43	14.93	14.86	0.09	14.56	1.05	0.00	0.20	9.25	0.78	0.26	95.84
DS106	DRB-S	POT	36.58	3.06	15.15	14.70	0.09	14.72	0.98	0.01	0.24	9.38	0.87	0.24	95.57
DS106	DRB-S	POT	36.74	3.48	15.04	14.89	0.09	14.37	0.97	0.00	0.22	9.35	0.87	0.25	95.83
DS106	DRB-S	POT	36.82	3.42	15.01	14.86	0.13	14.68	1.02	0.00	0.20	9.34	0.85	0.24	96.14
DS106	DRB-S	POT	36.89	3.25	15.18	15.41	0.10	14.37	0.94	0.01	0.21	9.26	0.91	0.25	96.33
DS106	DRB-S	POT	36.66	3.19	15.01	15.40	0.11	14.37	0.92	0.00	0.19	9.40	0.96	0.23	95.97
DS106	DRB-S	POT	37.18	3.30	14.95	15.27	0.09	14.47	0.72	0.00	0.18	9.57	0.94	0.25	96.46
DS106	DRB-S	POT	37.07	3.14	14.81	15.17	0.10	14.56	0.77	0.01	0.19	9.37	0.90	0.25	95.90
DS106	DRB-S	POT	36.13	4.18	15.10	15.47	0.11	14.73	0.54	0.03	0.16	9.03	0.96	0.19	96.18
DS106	DRB-S	POT	36.49	3.79	15.29	15.99	0.11	13.62	1.38	0.00	0.23	9.32	0.73	0.26	96.86
DS106	DRB-S	POT	36.66	3.64	15.34	15.90	0.11	13.91	1.21	0.00	0.20	9.39	0.78	0.27	97.03
DS106	DRB-S	POT	36.58	3.79	15.48	15.79	0.10	14.00	1.38	0.00	0.22	9.25	0.81	0.27	97.28

Sample #	Rock/Type		SiO_2	TiO_2	Al_2O_3	FeO	MnO	MgO	BaO	CaO	Na_2O	K_2O	F	Cl	Total
DS106	DRB-S	POT	36.28	3.76	15.26	15.87	0.09	13.62	1.23	0.01	0.23	9.27	0.79	0.27	96.28
DS106	DRB-S	POT	36.37	3.73	15.26	15.92	0.08	13.79	1.36	0.00	0.21	9.36	0.82	0.30	96.78
DS106	DRB-S	POT	37.05	3.00	15.29	15.14	0.11	14.70	0.76	0.06	0.21	9.40	1.06	0.25	96.50
DS106	DRB-S	POT	36.77	3.03	15.16	15.06	0.10	14.62	0.86	0.03	0.17	9.47	0.96	0.24	96.00
DS106	DRB-S	POT	36.98	3.65	14.90	15.59	0.11	14.56	1.02	0.02	0.21	9.44	1.10	0.29	97.35
DS106	DRB-S	POT	36.81	2.84	15.43	15.06	0.10	14.50	1.00	0.04	0.19	9.24	1.04	0.27	96.02
DS106	DRB-S	POT	37.07	2.88	15.30	14.85	0.12	14.85	0.62	0.08	0.17	9.24	1.04	0.21	95.93
DS106	DRB-S	POT	36.95	3.45	14.60	15.34	0.07	14.82	0.70	0.00	0.19	9.66	1.00	0.23	96.53
DS106	DRB-S	POT	36.93	3.44	14.72	15.00	0.07	14.75	0.73	0.00	0.20	9.52	1.09	0.22	96.15
DS106	DRB-S	POT	36.80	3.58	14.80	14.79	0.09	14.35	0.58	0.00	0.19	9.49	0.93	0.24	95.41
DS106	DRB-S	POT	37.25	3.37	14.52	14.60	0.09	14.91	0.43	0.01	0.14	9.67	1.01	0.26	95.78
DS106	DRB-S	POT	37.20	3.36	14.65	15.25	0.08	14.75	0.78	0.00	0.18	9.67	0.99	0.24	96.68
DS106	DRB-S	POT	36.77	3.42	15.48	14.64	0.08	14.25	0.95	0.02	0.23	9.75	0.85	0.24	96.26
DS106	DRB-S	POT	36.18	3.84	15.73	15.16	0.09	13.68	1.50	0.00	0.22	9.38	0.81	0.24	96.43
DS106	DRB-S	POT	36.85	3.41	15.95	14.70	0.10	14.21	0.57	0.01	0.14	9.99	0.88	0.23	96.60
DS106	DRB-S	POT	36.82	3.08	15.81	14.40	0.07	14.29	0.55	0.04	0.20	9.68	0.84	0.19	95.58
DS106	DRB-S	POT	37.08	3.36	15.33	13.88	0.10	14.53	0.56	0.01	0.18	9.79	0.88	0.20	95.48
DS106	DRB-S	POT	36.77	3.84	15.16	15.52	0.09	14.16	1.41	0.02	0.20	9.15	0.76	0.26	96.96
DS106	DRB-S	POT	36.54	3.92	15.18	15.68	0.09	14.15	1.50	0.00	0.17	9.47	0.83	0.25	97.36
DS106	DRB-S	POT	36.69	3.67	14.93	15.40	0.07	14.23	1.10	0.03	0.19	9.40	0.81	0.21	96.34
DS106	DRB-S	POT	36.69	3.83	15.21	15.25	0.06	14.30	1.08	0.00	0.20	9.54	0.86	0.24	96.83
DS106	DRB-S	POT	36.81	3.79	14.79	14.97	0.08	14.27	1.19	0.02	0.19	9.35	0.89	0.27	96.18
DS113	PP-M	POT	36.83	4.21	12.95	17.40	0.09	14.39	0.94	0.00	0.16	9.68	0.57	0.23	97.15
DS113	PP-M	POT	37.13	4.17	13.20	17.24	0.10	14.37	0.73	0.00	0.14	9.61	0.53	0.20	97.15
DS113	PP-M	POT	36.82	4.11	13.23	17.22	0.08	14.28	0.75	0.00	0.21	9.57	0.80	0.20	96.86
DS113	PP-M	POT	37.11	4.30	13.18	17.43	0.09	13.93	0.61	0.00	0.16	9.43	0.70	0.21	96.81
DS113	PP-M	POT	36.92	3.89	12.80	16.74	0.08	14.98	0.29	0.00	0.11	9.75	0.48	0.22	96.00
DS113	PP-M	POT	37.04	3.99	13.18	17.00	0.10	14.36	0.88	0.01	0.17	9.07	0.63	0.26	96.35
DS113	PP-M	POT	36.45	4.04	13.22	17.05	0.07	14.34	0.79	0.00	0.17	8.87	0.63	0.21	95.53
DS113	PP-M	POT	36.36	3.98	13.32	17.39	0.09	14.18	0.84	0.01	0.16	9.15	0.63	0.21	96.01
DS113	PP-M	POT	36.64	4.14	13.31	17.41	0.10	13.89	0.55	0.02	0.19	9.18	0.57	0.19	95.89
DS113	PP-M	POT	36.65	4.04	13.21	17.13	0.07	14.17	0.97	0.00	0.17	9.10	0.62	0.24	96.05
DS113	PP-M	POT	36.68	4.25	13.28	17.29	0.10	13.95	0.70	0.00	0.19	8.90	0.68	0.22	95.90
DS113	PP-M	POT	36.75	4.27	13.16	16.69	0.12	14.41	1.03	0.00	0.16	9.00	0.64	0.21	96.13
DS113	PP-M	POT	37.03	4.28	13.29	17.14	0.11	14.22	0.71	0.01	0.17	9.14	0.55	0.17	96.55
DS113	PP-M	POT	37.02	4.38	13.55	17.20	0.09	13.60	0.42	0.00	0.22	9.36	0.75	0.19	96.40
DS113	PP-M	POT	36.89	4.29	13.15	17.38	0.11	14.10	0.72	0.01	0.14	9.12	0.53	0.19	96.37
DS113	PP-M	POT	36.77	4.06	13.20	16.96	0.09	14.32	0.61	0.00	0.18	9.04	0.60	0.23	95.76
DS113	PP-M	POT	37.20	3.98	13.17	16.76	0.10	14.82	0.64	0.00	0.17	9.14	0.51	0.21	96.41
DS113	PP-M	POT	36.42	4.18	13.32	17.92	0.13	13.61	0.88	0.01	0.20	9.03	0.71	0.22	96.28
DS113	PP-M	POT	37.13	4.20	13.04	17.46	0.11	14.26	0.37	0.00	0.16	9.09	0.55	0.21	96.28
DS113	PP-M	POT	36.69	4.41	13.19	16.75	0.12	14.56	1.02	0.02	0.17	8.91	0.53	0.20	96.31
DS113	PP-M	POT	36.77	4.11	13.32	17.35	0.09	14.09	0.54	0.00	0.19	9.18	0.70	0.21	96.20
DS113	PP-M	POT	36.87	4.05	13.35	16.76	0.11	14.75	0.46	0.03	0.17	9.29	0.62	0.21	96.37
DS113	PP-M	POT	36.85	3.90	13.03	16.68	0.08	14.72	0.29	0.00	0.17	9.31	0.65	0.23	95.59
DS113	PP-M	POT	36.86	3.99	13.30	17.28	0.09	14.24	0.39	0.02	0.20	9.16	0.66	0.27	96.12
DS113	PP-M	POT	36.43	4.38	13.20	17.51	0.07	14.01	0.48	0.00	0.15	9.28	0.55	0.21	95.98
DS122	DRB-S	POT	35.77	4.28	15.01	16.76	0.06	13.25	2.70	0.06	0.25	8.33	0.72	0.22	97.06
DS122	DRB-S	POT	35.78	4.44	14.74	16.88	0.05	13.07	2.92	0.04	0.24	8.25	0.71	0.27	97.04
DS122	DRB-S	POT	35.75	4.25	14.84	16.71	0.08	13.47	2.11	0.07	0.26	8.53	0.75	0.25	96.68
DS122	DRB-S	POT	36.53	3.08	15.15	16.40	0.06	14.11	0.26	0.08	0.21	9.27	0.72	0.22	95.75

Sample #	Rock/Type		SiO_2	TiO_2	Al_2O_3	FeO	MnO	MgO	BaO	CaO	Na_2O	K_2O	F	Cl	Total
DS122	DRB-S	POT	36.72	3.55	14.67	16.61	0.06	13.80	0.69	0.06	0.23	9.12	0.69	0.29	96.13
DS122	DRB-S	POT	37.64	3.06	14.10	16.24	0.06	14.88	0.17	0.06	0.18	9.60	0.88	0.27	96.70
DS122	DRB-S	POT	37.31	3.01	13.79	15.92	0.04	15.19	0.18	0.07	0.18	9.19	0.85	0.26	95.59
DS122	DRB-S	POT	38.81	2.81	13.53	15.98	0.05	15.23	0.11	0.06	0.15	9.25	0.99	0.27	96.76
DS122	DRB-S	POT	38.28	2.89	13.72	15.47	0.07	15.28	0.20	0.04	0.20	9.28	0.92	0.27	96.15
DS122	DRB-S	POT	36.54	2.84	13.76	16.16	0.06	14.97	0.09	0.33	0.14	8.16	0.74	0.18	93.60
DS122	DRB-S	POT	37.81	2.92	13.64	15.45	0.06	15.39	0.16	0.02	0.17	9.30	0.84	0.29	95.64
DS122	DRB-S	POT	38.46	2.85	13.38	14.98	0.04	15.97	0.09	0.00	0.16	9.34	0.94	0.20	95.97
DS122	DRB-S	POT	37.94	2.90	13.44	15.24	0.04	15.60	0.13	0.00	0.14	9.25	1.03	0.24	95.45
DS122	DRB-S	POT	37.05	3.10	14.01	15.71	0.06	14.95	0.29	0.00	0.21	9.19	0.87	0.24	95.26
DS122	DRB-S	POT	37.97	2.74	13.74	15.26	0.02	15.43	0.14	0.02	0.16	9.34	0.98	0.23	95.56
DS122	DRB-S	POT	36.49	3.67	14.78	16.06	0.04	14.00	1.24	0.01	0.24	9.10	0.80	0.23	96.27
DS122	DRB-S	POT	36.97	3.61	14.76	16.05	0.07	14.24	0.99	0.05	0.25	8.97	0.88	0.25	96.64
DS122	DRB-S	POT	36.63	3.65	14.74	16.05	0.07	14.25	1.13	0.00	0.25	9.04	0.85	0.20	96.47
DS122	DRB-S	POT	36.91	3.22	14.65	15.97	0.06	14.28	0.67	0.02	0.24	9.44	0.84	0.26	96.14
DS122	DRB-S	POT	36.93	2.96	15.06	15.87	0.07	14.28	0.25	0.00	0.22	9.49	0.85	0.22	95.79
DS122	DRB-S	POT	37.45	3.00	14.05	16.18	0.09	15.16	0.34	0.08	0.20	9.46	0.89	0.22	96.69
DS122	DRB-S	POT	37.24	3.08	14.39	16.12	0.06	14.98	0.24	0.07	0.19	9.42	0.84	0.25	96.46
DS122	DRB-S	POT	37.00	2.94	14.27	16.31	0.09	14.64	0.30	0.11	0.20	9.28	0.80	0.24	95.77
DS122	DRB-S	POT	37.93	3.01	13.54	15.55	0.05	15.48	0.12	0.06	0.21	9.46	0.95	0.23	96.14
DS122	DRB-S	POT	37.76	3.01	13.96	16.12	0.07	15.11	0.30	0.13	0.22	9.44	0.83	0.27	96.82
DS122	DRB-S	POT	37.16	2.82	13.96	16.06	0.10	15.17	0.17	0.10	0.12	9.33	0.88	0.26	95.70
DS122	DRB-S	POT	37.42	2.93	13.60	15.72	0.10	15.20	0.15	0.04	0.15	9.39	0.91	0.25	95.42
DS122	DRB-S	POT	37.06	2.90	14.05	15.74	0.12	15.18	0.22	0.14	0.17	9.40	0.94	0.27	95.73
DS122	DRB-S	POT	37.51	2.96	13.92	15.59	0.06	15.25	0.14	0.06	0.19	9.54	0.91	0.23	95.92
DS122	DRB-S	POT	37.51	2.66	14.01	15.81	0.09	15.27	0.16	0.07	0.15	9.53	0.95	0.23	95.98
DS122	DRB-S	POT	37.36	1.97	14.48	14.58	0.09	16.50	0.13	0.04	0.22	9.68	1.02	0.22	95.80
DS122	DRB-S	POT	37.67	1.92	14.43	14.41	0.07	16.49	0.13	0.02	0.22	9.48	1.07	0.22	95.64
DS122	DRB-S	POT	37.55	1.97	14.45	14.49	0.09	16.16	0.15	0.05	0.24	9.43	1.04	0.20	95.34
DS122	DRB-S	POT	37.41	2.49	13.88	15.18	0.10	16.20	0.18	0.03	0.22	9.52	1.05	0.22	96.00
DS122	DRB-S	POT	37.27	2.60	14.07	15.15	0.07	15.82	0.12	0.07	0.24	9.66	1.04	0.22	95.83

Abbreviations: DRB = Dawson Range batholith; PP = Patton porphyry; M (magmatic) = Biotite of magmatic origin; S (secondary) = Biotite inferred to have precipitated from a hydrothermal fluid; LA = Biotite in least-altered rock; PR = Biotite in a propylitic-altered rock; PH = Biotite in a phyllic-altered rock; POT = Biotite in a potassic-altered rock.

Appendix IV

Oxygen isotope data from potassic-stage quartz veins of the Casino occurrence.

Sample#	Mineral Type	$\delta^{18}O$ (per mil) SMOW
Casino		
	Potassic	
DS106	Quartz	9.5
DS140	Quartz	9.4
DS146	Quartz	11.3
DS147	Quartz	10.8